INVESTIGATION OF THE LOW LYING ENERGY LEVELS IN ^{56}Fe, ^{75}As and ^{156}Gd WITH A DUAL-PARAMETER ENERGY TIME SPECTROMETER

Aziz Mahmoud Shaban

B.Sc., M.Sc.

A Thesis Submitted for the Degree of

Doctor of Philosophy

in the

University of London

Physics Department
Bedford College
London
1980.

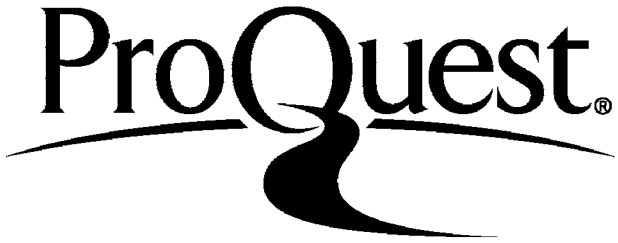

ABSTRACT

The gamma-ray transitions from the states populated in ^{56}Fe, ^{75}As and ^{156}Gd by the decay of ^{56}Co, ^{75}Se and ^{156}Eu were investigated using six Ge(Li) detectors and an intrinsic Ge detector.

Coincidence studies were undertaken with a Dual-Parameter Energy-Time Spectrometer employing a fast-plastic scintillator detector and two large volume Ge(Li) detectors.

The energies and intensities of measured gamma-rays were determined. The lifetime of energy levels in the n sec. range belonging to ^{75}As and ^{156}Gd were measured. The level schemes were constructed; log ft values, transition multipolarities, spins and parities were deduced. Different shell-model calculations were discussed and compared with experimental results.

CONTENTS Page No.

LIST OF FIGURES

CHAPTER I

INTRODUCTION

1.1 General

In low energy physics there are many ways one can study the structure of the nucleus. But, by far, gamma-ray spectroscopy offers the most comprehensive means of investigating the decay scheme of the nucleus.

The development of the Ge(Li) (lithium-drifted germanium) detector with an energy resolution, which is vastly superior to that of the high efficiency NaI(Tℓ) gamma-ray detector, allows the possibility of detection of many close lying (energy levels) and weak intensity gamma-ray transitions.

This improvement in gamma-ray spectroscopy has resulted in the need to develop the supporting electronics both for energy and timing measurements. In fact, use of fast pulse amplifiers, processors, time-pickoffs and megachannel capacity analog-to-digital converters have been reported [1-3]. With the availability of integrated circuits and microprocessors, hard-wired multichannel analysers are slowly being replaced by minicomputers offering flexibility in the operation of the system. The use of a dual-parameter data collection system in the Energy-Time coincidence measurements offers enormous advantages over the conventional fast-slow coincidences system for use in decay scheme, lifetime and angular correlation studies.

In the present work, investigations were made of the decay schemes of ^{56}Fe, ^{75}As and ^{156}Gd including some level-lifetime measurements in ^{75}As and ^{156}Gd, by measuring the gamma-ray transitions using Ge(Li) and plastic scintillator detectors operated in singles and coincidence modes.

Some theoretical considerations related to the present work are given in the rest of this chapter. Chapters 2 and 3 describe the calibration techniques and experimental details. The details of the decay of ^{56}Co,

^{75}Se and ^{156}Eu are reported in Chapters 4, 5 and 6 respectively.

1.2 Neutron activation and second order reactions

When a material is irradiated in a nuclear reactor a number of processes can take place. Neutrons are captured by the nuclei of the target element and the product nuclei may themselves capture additional neutrons. The rate of build-up of the required radioisotope is a result of these factors, so that the activity in transformations per second A is given by[4)]

$$A = \frac{N_o \sigma_1 \phi \lambda_1}{\lambda_1 + \sigma_2 \phi - \sigma_1 \phi} (e^{-\sigma_1 \phi t} - e^{-(\lambda_1 + \sigma_2 \phi)t}) \qquad (1.1)$$

where N_o is the number of target nuclei originally present, σ_1 and σ_2 are the neutron capture cross-sections of the target and product nuclei respectively, ϕ is the effective neutron flux (n cm^{-2} sec^{-1}), λ is the decay constant of the produced radioisotope and t is irradiation time. For a low neutron flux reactor and a small σ_2 the specific activity becomes:

$$S = \frac{0.6 \phi \sigma}{3.7 \times 10^{10} W} (1 - e^{-0.693\ t/\tau}) \quad Ci\ g^{-1} \qquad (1.2)$$

where W is the target atomic weight and τ is the half life of the product radioisotope.

When a high neutron flux is used and the resulting isotope has a short half-life (order of minutes) together with the daughter nuclei having a high capture cross-section, a second order reaction takes place, which can be represented by the reaction:

$$\underset{[1]}{{}^{A}_{z}X(n,\gamma)\ {}^{A+1}_{z}X} \xrightarrow{\beta^-} \underset{[3]}{{}^{A+1}_{z+1}X(n,\gamma)\ {}^{A+2}_{z+1}X} \qquad (1.3)$$

$$\underset{[2]}{{}^{A+1}_{z}X} \downarrow$$

$${}^{A+1}_{z}X(n,\gamma)\ {}^{A+2}_{z}X$$

The rates of nuclide transformation in (1.3) are described[5-8] by the following system of differential equations:

$$\frac{dN_1}{dt} = -N_1 \phi \sigma_1$$

$$\frac{dN_2}{dt} = N_1 \phi \sigma_1 - \lambda_2 N_2 - N_2 \phi \sigma_2$$

$$\frac{dN_3}{dt} = F_2 \lambda_2 N_2 - N_3 \phi \sigma_3$$

$$\frac{dN_4}{dt} = N_3 \phi \sigma_3 - \lambda_4 N_4 - N_4 \phi \sigma_4$$

where N_1, N_2, N_3 and N_4 are the number of nuclei of elements 1-4 respectively. Similarly, for the capture cross-sections σ_1, σ_2, σ_3 and σ_4, F_2 is the fraction of disintegration. These equations can be solved in the classical way, but the solution for N_3 is laborious and for N_4 is even more tedious, so it is more simple to use directly the Bateman-Rubinson solution.

$$\Lambda_1 = \phi \sigma_1$$

$$\Lambda_2 = \lambda_2 + \phi \sigma_2$$

$$\Lambda_3 = \phi \sigma_3 \quad , \text{ and}$$

$$\Lambda_4 = \lambda_4 + \phi \sigma_4 \ .$$

Using this notation the solution for N_4 gives

$$N_4 = N_1 \phi^2 \sigma_1 \sigma_3 F_2 \lambda_2 \sum_{i=1}^{i=4} C_i \exp(-\Lambda_i t) \qquad (1.4)$$

where

$$F_2 = 1$$

$$C_1 = \frac{1}{(\Lambda_2 - \Lambda_1)(\Lambda_3 - \Lambda_1)(\Lambda_4 - \Lambda_1)} ,$$

$$C_2 = \frac{1}{(\Lambda_1 - \Lambda_2)(\Lambda_3 - \Lambda_2)(\Lambda_4 - \Lambda_2)} ,$$

$$C_3 = \frac{1}{(\Lambda_1 - \Lambda_3)(\Lambda_1 - \Lambda_3)(\Lambda_4 - \Lambda_3)} , \quad \text{and}$$

$$C_4 = \frac{1}{(\Lambda_1 - \Lambda_4)(\Lambda_2 - \Lambda_4)(\Lambda_3 - \Lambda_4)} .$$

The Bateman-Rubinson equations are tedious to solve by hand and often lead to a loss in significance in performing the summations of the exponential terms $C_i \exp(-\Lambda_i t)$. For this reason the aid of computer double precision is highly desirable, so that Eq.(1.4) accurately gave the number of active nuclei, which was particularly useful in calculating the ^{156}Eu activity (Chapter 6).

1.3 Gamma-ray transitions

The emission of electromagnetic radiation by a nucleus has been adequately treated theoretically by a semi-classical approach which describes the electromagnetic radiation source in terms of an oscillating distribution of electric charges, i.e. the electromagnetic radiation is caused by changes in the physical state of the moving charges and current density distributions, which act as the source of the field. The process is by far the best understood of all the emission processes.

The charges and current density distributions can be expanded into multipole moments, and the properties and characteristics of the emitted radiations depend on the dominant multipole term or terms in the interaction between the field and the source.

The theoretical treatment of the emission process is very lengthy, but well documented and detailed in such works as Blatt and Weisskopf[9] from which the results are quoted.

Gamma-ray transitions are classified according to the total angular momentum, L, carried by the multipole. For a nuclear transition between an initial state, i, and a final state, f, having nuclear spins of I_i and I_f respectively, it has been shown that a momentum selection rule applies which limits the permitted range of multipolarities. This is given in vectorial relations as $I_i - I_f = \underline{L}$ which implies

$$|I_i - I_f| \leq L \leq (I_i + I_f) . \qquad (1.5)$$

In addition, a distinction is made between electric (EL) and magnetic (ML) multipoles according to the parity associated with the electromagnetic radiation. This depends on the parities of the two nuclear states involved. Electric multipole radiation of order L has parity as $\pi_i\pi_f = (-1)^L$, and for magnetic multipole $\pi_i\pi_f = (-1)^{L+1}$. Although Equ.(1.5) suggests a series of values for L for a given I_i and I_f, the radiation emitted is usually limited to the lowest one or two orders permitted, as the probability of emission decreases rapidly with increasing L when the condition $R << \lambda$ is satisfied [R is the nuclear radius and λ the wavelength of the radiation]. In addition, the relative probability of emission of magnetic multipole radiation is considerably smaller than that of electric multipole radiation of the same order. The transitions usually encountered have $L =: |I_i - I_f|$, or $L =: |I_i - I_f|$ with an admixture of $L = |I_i - I_f| + 1$.

The simplest model used to describe a nucleus is the independent particle model. This assumes very weak coupling between the individual nucleous, so that in a gamma-ray transition only a single nucleon experiences a change in its quantum state. This nucleon moves in a central potential due to the other nucleons, and makes requested transitions from a state of angular momentum L to a state of zero angular momentum.

The transition probabilities for the emission of gamma radiation of of frequency w during this change, T(EL) and T(ML), can be calculated on

this basis and in generalizations is[10]

$$T(L;\ I_i \to I_f) = \sum_{\mu, m_f} T(L, \mu;\ I_i\ m_i \to I_f\ m_f)$$

$$= \frac{8\pi(L+1)}{L\,[(RL+1)!!]^2}\ \frac{1}{\hbar}\left(\frac{w}{c}\right)^{2L+1} B(L, I_i \to I_f) \qquad (1.6)$$

where the quantity

$$B(L;\ I_i \to I_f) \equiv \sum_{\mu, m_f} |\ < I_f\ m_f\ |\ M(L,\mu)\ |\ I_i\ m_i\ >\ |^2 \qquad (1.7)$$

is called the reduced transition probability. While the transition probability depends on the transition energy, being related to E^{2L+1}, the reduced transition probability does not depend on energy, but is the squared transition matrix element (M). It is, therefore, convenient to convert T(L) into B(L). Usually B(EL) is expressed in units of e^2R^{2L} and B(ML) in units of $\mu_N^2\ R^{2L-2}$; and numerically[10],

$$B(EL) = 4.57 \times 10^{-20} \times \frac{L[(2L+1)!!]^2}{8\pi(L+1)} \cdot \left(\frac{197}{E(\text{in MeV})}\right)^{2L+1} \times [T(EL) \text{ in } \text{sec}^{-1}]$$

$$\text{in } e^2\ \text{fm}^{2L} \text{ units} \qquad (1.8)$$

$$B(ML) = 4.15 \times 10^{-20} \times \frac{L[(2L+1)!!]^2}{8\pi\ (L+1)} \cdot \left(\frac{197}{E(\text{in MeV}}\right)^{2L+1}$$

$$\times\ [T(ML) \text{ in } \text{sec}^{-1}] \text{ in } \mu_N^2\ \text{fm}^{2L-2} \qquad (1.9)$$

The use of (1.8) and (1.9) gives the relations

$$T(E1) = 1.59 \times 10^{15}\ E^3\ B(E1),$$

$$T(E2) = 1.22 \times 10^{9}\ E^5\ B(E2), \text{ and}$$

$$T(M1) = 1.76 \times 10^{13}\ E^3\ B(M1)$$

which are needed for use in Chapters 4 and 6.

1.4 Internal conversion process and theoretical considerations

The internal conversion process provides one of the most effective methods of assigning spin and parity quantum numbers to the low-lying

nuclear states. In many cases it gives the definitive information for constructing a decay scheme.

When a nucleus is in an excited state for which the excitation energy is insufficient for nuclear particle emission, the de-excitation will proceed predominantly by either a gamma-ray emission or the nuclear excitation will be transferred to one of the orbital electrons resulting in the ejection from the atom of this electron. The latter process is referred to as internal conversion. The branching ratio, giving the number of conversion electrons per second (Ne) to the number of photons detected per second (Nq), is the internal conversion coefficient

$$\alpha = \frac{Ne}{Nq} \tag{1.10}$$

The emitted electrons will appear as a line spectrum in a magnetic spectrometer, so that a given γ-ray transition can convert in a number of possible atomic shells. If an atomic electron in a K orbit is ejected, the internal conversion coefficient is written $\alpha(K)$.

The internal conversion theory is formulated with the aid of two basic assumptions[11]. The first makes use of perturbation theory. The nucleus is coupled to the electromagnetic field and the electron is similarly coupled. Therefore, the nuclear and electron systems may exchange, acting as quanta, resulting in the transition: nucleus excited + bound electron → nucleus in ground state + electron in continuum[12]. The Nq calculation done by Green[13] used first order perturbation theory, while for the calculation of Ne, second order perturbation theory is needed, and the following results are obtained:

$$Nq = 8 \pi a k \zeta_n \left| \int d\tau_N \, \underline{J_N} . \underline{A^*_{LM}} \right|^2 \tag{1.11}$$

$$Ne = 2 \pi a^2 \zeta_e \left| \int d\tau_N \int d\tau_e \, (\underline{J_N} . \underline{J_e} - \varrho_N \varrho_e) \, \frac{e^{ik|r_N - r_e|}}{|r_N - r_e|} \right|^2 \tag{1.12}$$

where a is the fine structure constant, $\underline{J_N}$ and $\underline{J_e}$ are transition current

densities for the nucleon and electron respectively. Also $\mathcal{Q}_N$ and $\mathcal{Q}_e$ are transition charge densities. ζ_N is a sum over final and average over initial nuclear substates. ζ_e contains, in addition to these operations, a sum over final electron states and a sum over magnetic quantum numbers of the initial states. The integration symbol over the nuclear coordinates is also meant to involve a sum over nucleons. A_{LM} is the standing wave vector potential of the appropriate 2^L pole (L multipole order given by Eq.(1.5) and $M = M_i - M_f$, the change in magnetic quantum numbers in the nuclear transition. The Ne (Eq.(1.12)) in fact depends very much on whether the electron will be kept outside the nuclear region ($r_e > R$) or whether the finite magnitude of R is clearly considered. In the first case the expansion of the Green's function[14] in (1.12) yields standing waves in r_N and outgoing waves in r_e and, as is well known, the nuclear matrix element which finally appears in (1.12) is identical to that in (1.11). In this approximation then, the conversion coefficient does not depend on nuclear structure, but it still depends on nuclear parameters in the sense that, besides L and $\Delta\pi$ which are provided by the nucleus the gamma-ray transition $k = (E_i - E_f)/\hbar c$ is also an important factor.

The internal conversion coefficient calculations given by Rose et al.[15], Sliv and Bond[16], Church and Weneser[17], provide very useful comparisons with the experimental internal conversion coefficient in order to determine the multipolarity of the different transitions.

1.5 Nuclear shell model

For many years the main objective of the shell model was to interpret the magic numbers. As more developments were introduced, it was found that this model was able to explain many other nuclear properties beside the magic numbers. By introducing a deformed potential as in the Nilsson model[18], the motions between the single particle and collective degrees of freedom can be correlated.

There are various versions of the shell model, notably the extreme single particle model, the single particle model and the independent particle model, all of which possess a common property, that is, the particles in the nucleus are assumed to move in a mean potential independent of each other. Essentially, in the extreme single particle model, the properties of the nucleus are assumed to be attributed to the single unpaired nucleon. With the single particle model the nucleus is visualised as consisting of filled shells that contain the maximum number of neutrons and protons permitted by the Pauli exclusion principle, and unfilled shells containing the remaining numbers of nucleons.

The single particle estimate of gamma transition probability provides a crude but useful estimate of the order of magnitude of this quantity. Furthermore, the single particle estimates constitute convenient units, in which the experimentally observed properties can be expressed. Within the framework of the single particle model, the reduced transition probability can be expressed as

$$B(EL) = \frac{(1.2)^{2L}}{4\pi} \left\{ \frac{3}{L+3} \right\}^2 A^{2L/3} \; e^2 \; (fm)^{2L} \qquad (1.13)$$

and

$$B(ML) = \frac{10}{11} \; [1.2]^{2L-2} \left\{ \frac{3}{L+2} \right\}^2 A^{(2L-2)/3} \; N_N^2 \; (fm)^{2L-2} \qquad (1.14)$$

These expressions, which are normally referred to as Weiss Kopf-estimates[19], are independent of the energy of the nuclear states involved in the transition.

1.6 The collective effect

The experimental discoveries of large nuclear quadrupole moments in the regions away from closed shells noted by Townes et al.[20] and Goldhaber et al.[21] in their study of E2 transition probabilities led to significant developments of the shell model. Rainwater et al.[22] noted that if the nuclei are assumed to be deformed so that they have permanent non-spherical shapes (spheroidal shapes) the many particles in the nucleus

can give large values of the electric quadrupole moments. As more experimental information is obtained, the regularities observed in even-even nuclei are becoming more obvious. In the region of $150 < A < 185$ and $A > 225$, these regularities are the especially simple ones characteristic of rotational spectra[23], and are explained with great accuracy by the Bohr-Mottelson strong coupling collective model[24]. In those nuclei outside these regions, experimental regularities characteristic of vibrational spectra are observed, and it can be summarized as follows.

The ratio of the energy of second to first excited states is about 2, varying from about 1.5 near the magic numbers to about 2.5 far from them. Those nuclei that have either closed neutron shells or closed proton shells have the ratio less than 2 and have the spin sequence 0^+, 2^+, 4^+ as shown by French et al.[25]. As the values of Z or N move away from the magic numbers, a second spin-two level moves close to the spin-four level and comes below the four level as indicated by van Patter[26]. In this region the above ratio increases from about 1.5 to a value of about 2.2 or 2.3 while the energy of the first excited state decreases. In the vibrational or near harmonic region the ratio is about 2.2 with the energy of the second 2^+ level being slightly lower than that of the 4^+ level for most cases. As the rotational region is approached a different trend is noted. The ratio becomes larger, reaching a value of $10/3$ in the rotational region, and the energy of the second 2^+ level again moves higher than the energy of the 4^+ level.

The E2 gamma-ray transitions between neighbouring levels are greatly enhanced so that the crossover transition from the second excited state to the ground state is much smaller, in general, than the transition from the second to the first excited state. In addition the ratio of M1 to E2 is often less than one in the transitions between the two levels with $I = 2$.

1.7 Core excitations

The collective approach to the theoretical problem would be unrealistic were it considered alone. The effect of particle excitations as well as internuclear forces have to be taken into account. In other words, a unified description in terms of the weak coupling models[27-29] would be more appropriate. This means that the particles are coupled to the vibrating core to produce the collective effect, so that the Hamiltonian can be separated into four parts:

$$H = H_c + H_{int} + H_{12} + H_{sp} \tag{1.15}$$

where H_c is the Hamiltonian for the core vibration, H_{sp} is the usual single particle model Hamiltonian, H_{int} describes the interaction between the particle and the core and H_{12} appears only when two particles are coupled to the core and represents then the two-body interaction. Many forms of H_{int} have been used to describe the coupling between the particle and the core, and usually only quadrupole-quadrupole interactions are considered[30,31]. Sometimes it is advantageous to express H_{int} in terms of $H_{p\text{-core}}$ and $H_{n\text{-core}}$ as have been used by McGrory et al.[32] in their calculation for state on ^{56}Fe. Also, the idea of coupling nucleons to the core has been used by Ogawa et al.[33]. These Hamiltonian representations are natural within the framework of Bohr and Mottelson's collective model, which is very useful to evaluate the H_{int} from the experimental observed quantities of the neighbouring even-even nuclei.

The theoretical calculations based on the assumptions and considerations discussed in Sections 5, 6 and 7 produce different sets of data which are compared with the experimental results in Chapters 4 and 6.

CHAPTER II

EXPERIMENTAL ARRANGEMENT

2.1 Singles spectra measurements and Ge(Li) detectors specification

During the course of this work, different types of gamma-ray spectra have been taken using six true-coaxial Ge(Li) detectors and a Ge(I) detector; their efficiencies, equivalent volumes and measured performance characteristics are listed in Table (2.1). Each of these detectors are equipped with cooled FETs low noise preamplifiers. The output signals were fed into a spectroscopy amplifier Ortec (Model No. 472) whose shape time constant value of 2 μ sec indicated a good signal-to-noise ratio. These signals fed through a Northern Scientific ADC (Model 626) into a Northern Scientific memory unit (Model No. 630) and pulse height spectra were recorded in 4096 channels. The block diagram of the experimental pulse height recording system used is shown in Fig. (2.1).

Low isotope activities were used with a source-to-detector distance of 25 cm. The avoidance of a short source-to-detector distance enabled the total counting rates to be kept below 2,000 S^{-1} so that the pile-up effects were minimised and the coincidence summing corrections suggested by Detertin and Schötzig [34] need not be applied.

Singles spectra measurements in the energy region of E_α > 100 keV were made by using detectors 2, 4, 6 and 7; detector 3 was also useful for the measurements in the energy region <100 keV.

2.2 Energy and efficiency calibration

The energy calibration was done using the chemical standards sources [35], consisting of the sources ^{57}Co, ^{60}Co, ^{88}Y, ^{133}Ba and ^{137}Cs. The uncertainties in their calibrated energies were taken from Ref. 36-38).

Essentially the uncertainties in energy determination can be attributed to two main sources, the listed calibration uncertainty and

No	Detector	Approximate Volume	Relative Efficiency	Resolution (keV) @ 1.33 MeV	Photopeak/Compton @ 1.33 MeV
1	Ne - Ge(Li)	25 cc	4%	3.9	20
2	Ne - Ge(Li)	35 cc	6%	2.8	28
3	Princeton Ge(I)	200mm^2 x 5 mm		225; 500 eV*	
4	Princeton Ge(Li)	42 cc	8%	1.8	36
5	Harshow Ge(Li)	~ 70 cc	11%	2.4	35
6	Ortec Ge(Li)	60 cc	10%	2.2	30
7	Ortec Ge(Li)	70 cc	12%	1.9	38

Table (2.1) The measured performance characteristics of the detectors used during the course of this work.

* The FWHM for 5.9 keV and 122 keV gamma ray lines respectively.

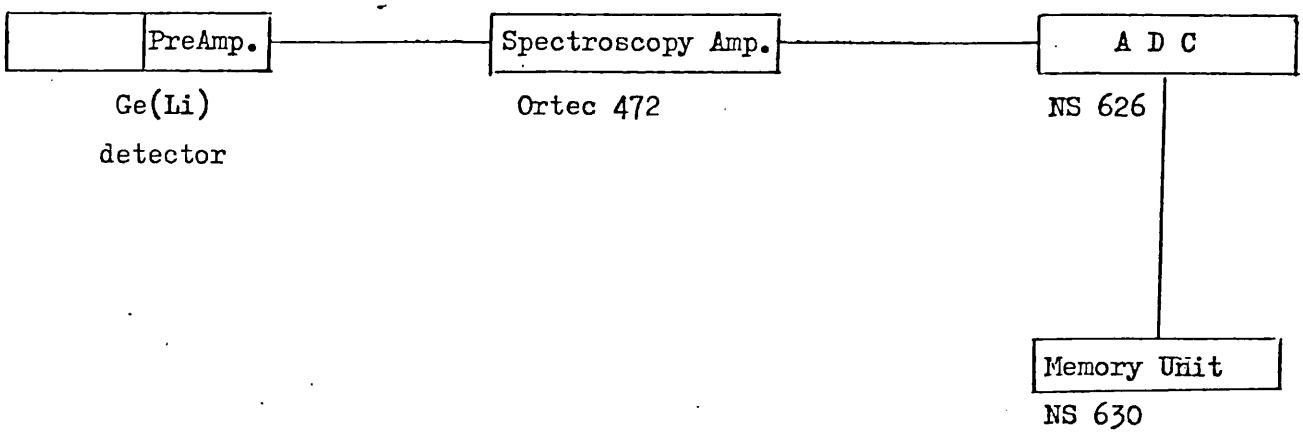

Fig.(2.1) Block diagram of the pulse height system

TABLE (2.2)

Details of the gamma-ray calibration sources

Table (2.2a)

Nuclide	Calibration Energy(keV)	Intensity Number of γ-rays per 100 disintegrations
^{133}Ba	81.0	34.7
^{57}Co	121.97	87.7
^{57}Co	136.33	12.2
^{133}Ba	302.87	18.3
^{133}Ba	356.03	62.3
^{133}Ba	383.87	8.9
^{137}Cs	661.6	85.3
^{88}Y	898.0	91.4
^{60}Co	1173.1	99.9
^{60}Co	1332.4	100.0
^{88}Y	1836.1	99.4

Table (2.2b)

Nuclide	Calibration Energy E (kev)	Reference Energy R (kev)	Intensity Ratio I(E)/I(R)
^{56}Mn	2112.8	1810.7	0.537
^{38}Cl	2166.8	1642.0	1.316
^{24}Na	2753.6	1368.4	0.986
^{88}Rb	3218.0	898.1	0.0176
^{49}Ca	4071.0	3083.0	0.0868

that arisis from the experimental measurement which was mainly due to the ADC nonlinearity.

The energy calibration was determined by a least-squares fit to an n-th degree polynomial to the γ-ray energies from the several standard sources. The peak positions for this fit were corrected for spectrometer nonlinearity as measured with a precision pulser. The nonlinearity correction was ± 0.55 channels over 90% of the ADC range. The non-linearity correction was estimated to give between 0.05 and 0.1 channels uncertainty in determining the photopeak centroid and was folded into the peak position error. A third order polynomial was found to give the best fit. This led to errors assigned in the energies, as determined by the Program SAMPO[39,40], ranging from 50 eV for the most intense gamma-ray transitions, to 0.8 keV for the weak high-energy transition.

The efficiency curve for the intensity determination was constructed using gamma-ray sources over the energy range from 81.0 keV to 4.071 MeV. Up to 1.84 MeV the chemical standards sources set, whose details are given in Table (2.2a), was used. The calibration was extended to higher energies (4.1 MeV) by using the five isotopes ^{56}Mn, ^{38}Cl, ^{24}Na, ^{88}Rb and ^{49}Ca, which were prepared using the University of London Reactor irradiation facilities. Table (2.2b) gives details of these five isotopes, where the first column gives the energies of prominent gamma-rays used as calibration points, the second column represents the reference photopeak energies and the last column indicates the photopeaks intensity ratios for each of these isotopes which were taken from Ref. 41-43).

The efficiency ε of a Ge(Li) detector was taken as a function of the energy E to be [40]:

$$\varepsilon = P_1 [E^{P_2} + P_3 \exp (P_4 E)], \qquad (2.1)$$

and the parameters P_1, P_2, P_3 and P_4 were found by a least-squares

minimisation procedure carried out by the program SAMPO [39,40], modified to run on the University of London CDC-6600 Computer. The efficiency curve fitted with a χ^2 of (1%) as a function of energy given by Eq.(2.1), is shown in Fig. (2.2) for the most efficient detector, No. 7. Fig.(2.2a) shows the absolute efficiency as a function of energy over the full energy range, and Fig.(2.2b) shows the expected linearity when plotted as a function of log E in the range from 800 keV to 4 MeV. Fig.(2.3) shows the efficiency curve as a function of energy for the detector No. 6 for energy range <2 MeV. The efficiency-energy relationships for detectors Nos. 1, 2 and 4 were very similar to those shown in Figs. (2.2) and (2.3) with the exception of lower efficiency values for E > 1 MeV. The Harshow detector (No. 5) shows an identical curve to that of detector (No. 7) shown in Fig.(2.2).

2.3 Compton Suppression Spectrometer

The Compton suppression system belonging to the University of London Reactor Center, consisted of the detector No. 5 and a 20 cm. diameter x 20 cm. long NaI(Tℓ) crystal viewed by four photomultipliers. A photopeak to Compton ratio of 270:1 for the 1.33 MeV ^{60}Co gamma-ray photopeak was obtained using a dual sum Ortec (Model 433Á) unit and a Harshow (NC26) time analyser. The block diagram of the Compton Suppression system used is shown in Fig.(2.4): The spectra taken using this spectrometer were particularly important for those isotopes in which there were several low intensity gamma-ray lines located in the Compton scattering region.

2.4 The fast-slow coincidence system

The devising of a nuclear decay scheme by gamma-gamma coincidence studies is particularly useful when the coincidence is signified by time correlation. This can be arranged by fast-slow coincidence system whose block diagram is shown in Fig.(2.5).

The pulses from the gating and spectrum Ge(Li) detectors (detectors

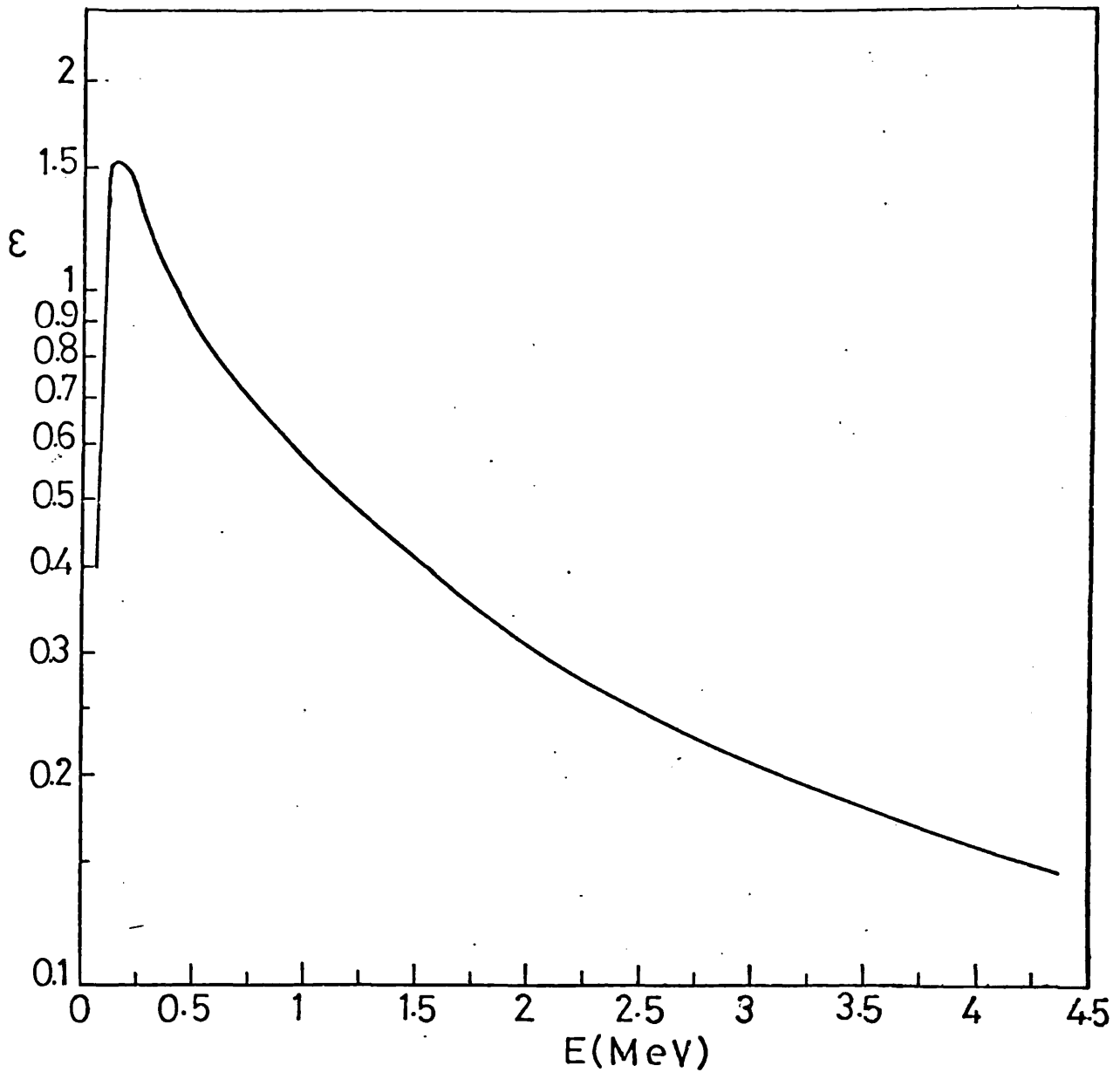

Fig(2.2a) The absolute efficiency-energy relationship for the 12% efficient detector

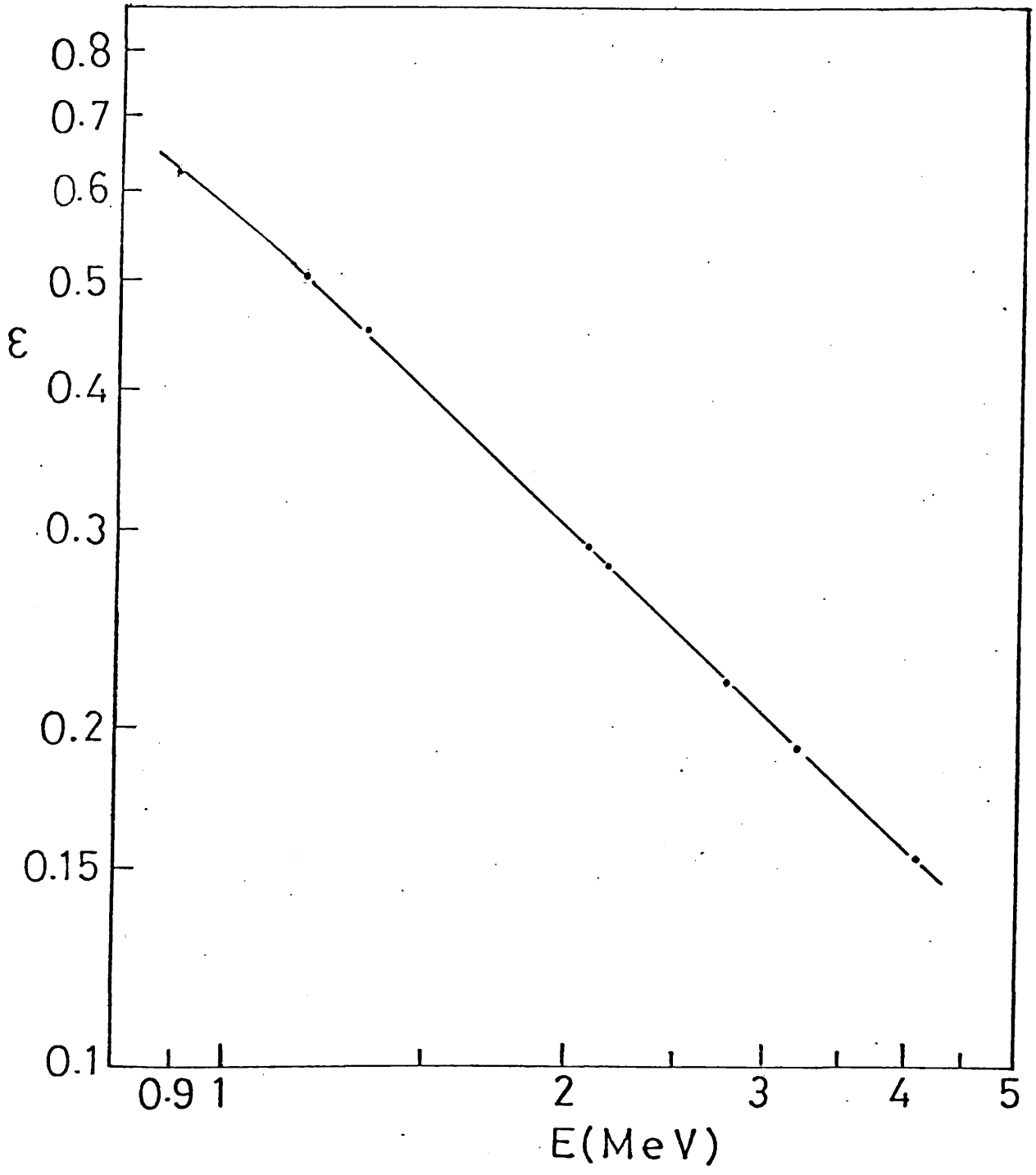

Fig(2.2b) The absolute efficiency-energy relationship for the 12% efficient detector

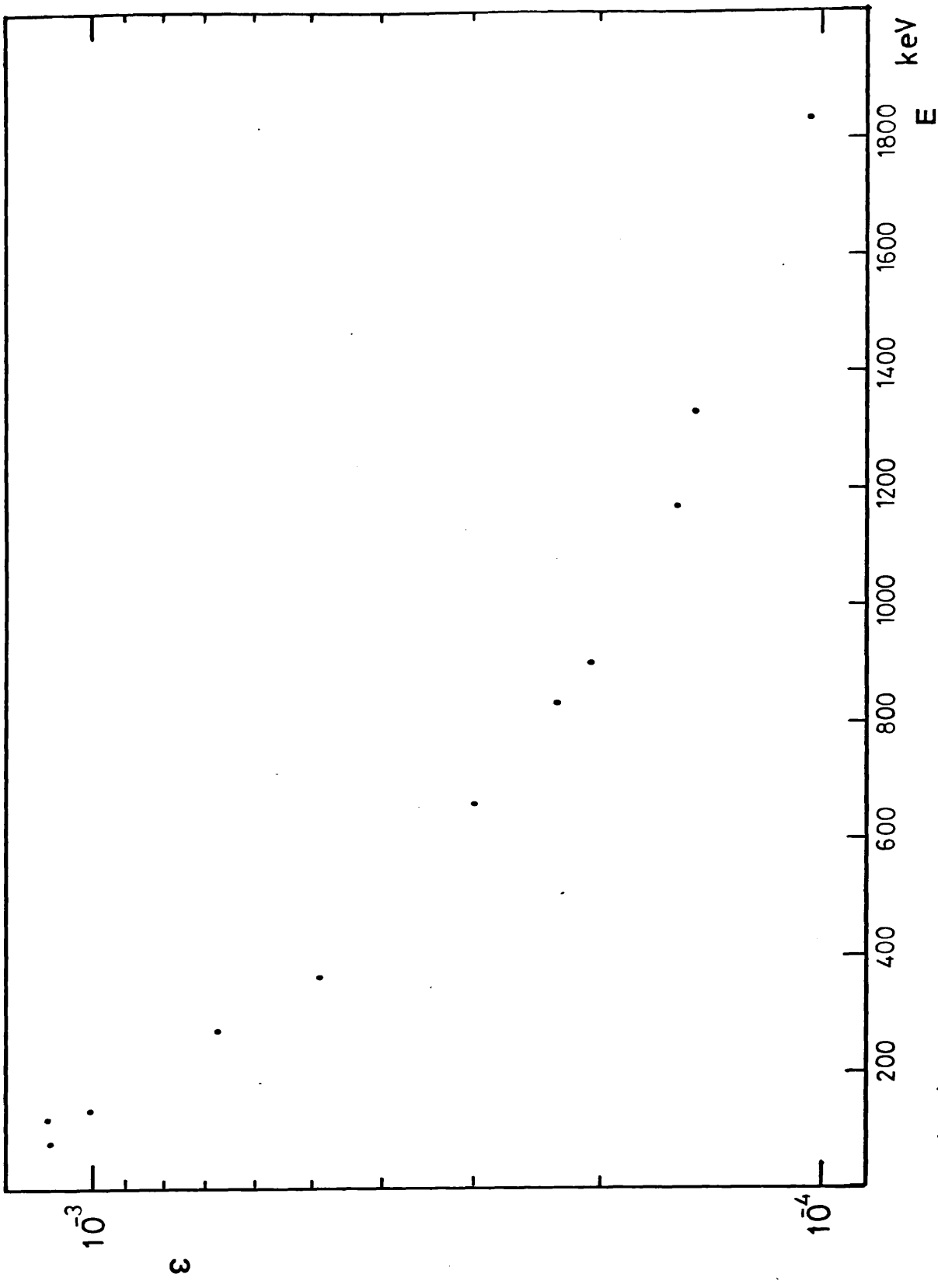

Fig(2.3) The absolute efficiency-energy relationship for the 10% efficient detector

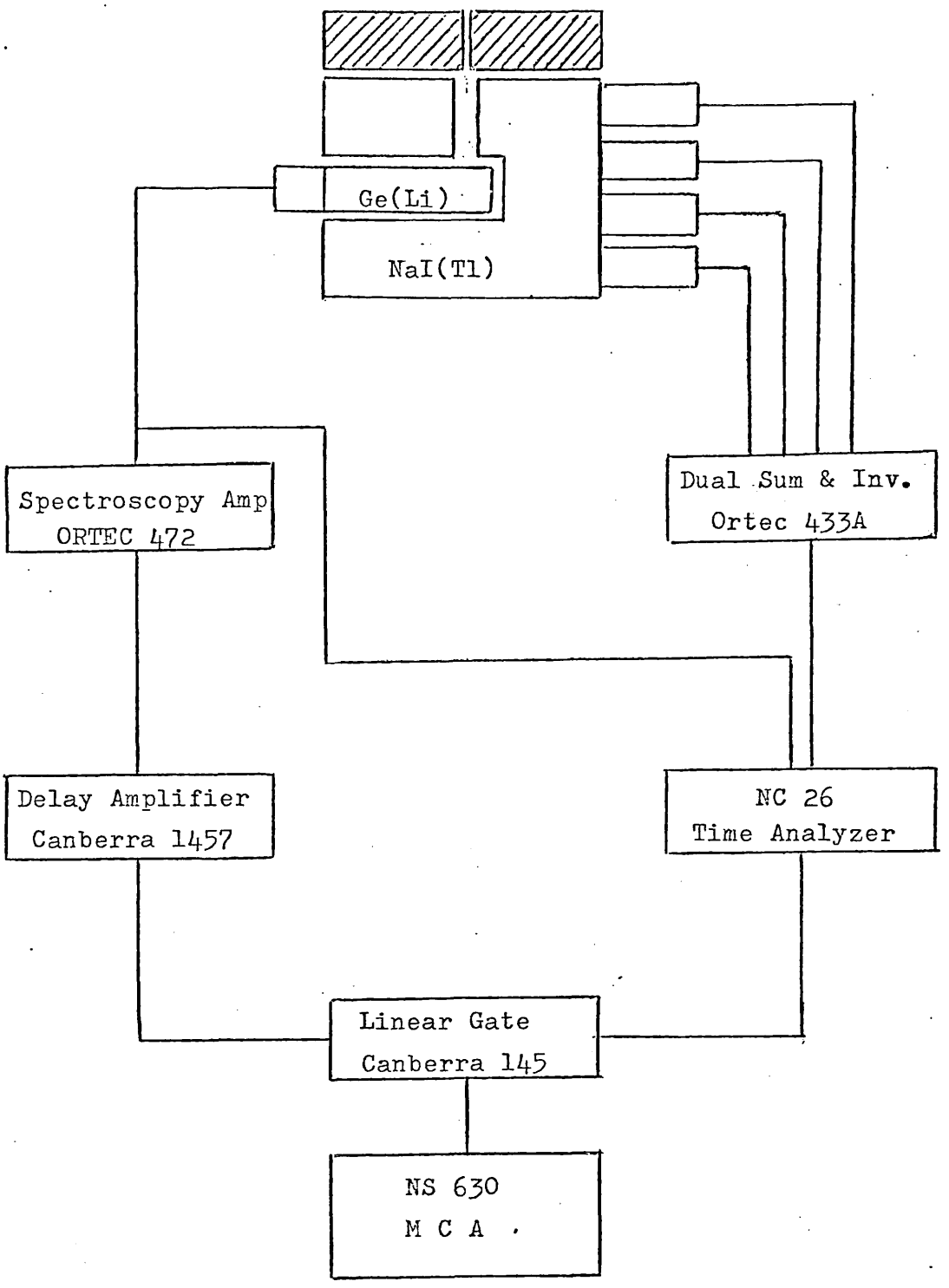

Fig.(2.4) Block diagram of the Compton suppression spectrometer

Nos.2 and 6 respectively) were fed into charge sensitive preamplifiers with cooled FETs; their outputs were fed into two Ortec 454 timing filter amplifiers (TFA) so that the manipulations of pulse shapes and pulse amplification can be made, then through two Ortec 463 constant fraction discriminators (CFD), each operated in Ge(Li) shaping mode. The pulses from the gating detector (No. 2) were used to start the time-to-pulse-height converter (TPHC), and the pulses from the second arm were used to stop the (TPHC), whose output-amplitude gives a time distribution for the events in the two detectors within the (TPHC) range of 0.05 μ sec.

The accuracy of any coincidence experiment depends on this time distribution as a timing correlation for the coincidence gate (i.e. the resulting spectrum in coincidence with certain gamma-ray gate will be for these gamma-rays detected by both gating and spectrum detectors within the system time resolution or the FWHM of the TPHC time distribution); this time distribution can be seriously affected by the contribution from undesired events. These events generally arise from chance coincidences and coincidence with background under the gating peak interval. Chance coincidences depend on the resolving time τ (or the system resolution which in the same time is the fast part resolution); it is in fact the FWHM of the timing peak for the (TPHC) time distribution which is strongly affected by time walk and jitter noises in the electronics. The time information derived from the detector to (TPHC) can be followed briefly as follows, when the detector signals trigger the discriminator at fixed threshold by different rise time due to different locations of the interactions points in the detector crystal, this leads to walk effect in the discriminator response called time walk. If the two pulses triggering the discriminators have different amplitude this will lead to the same effect (time walk).

Theoretical and experimental investigations on the time walk and the

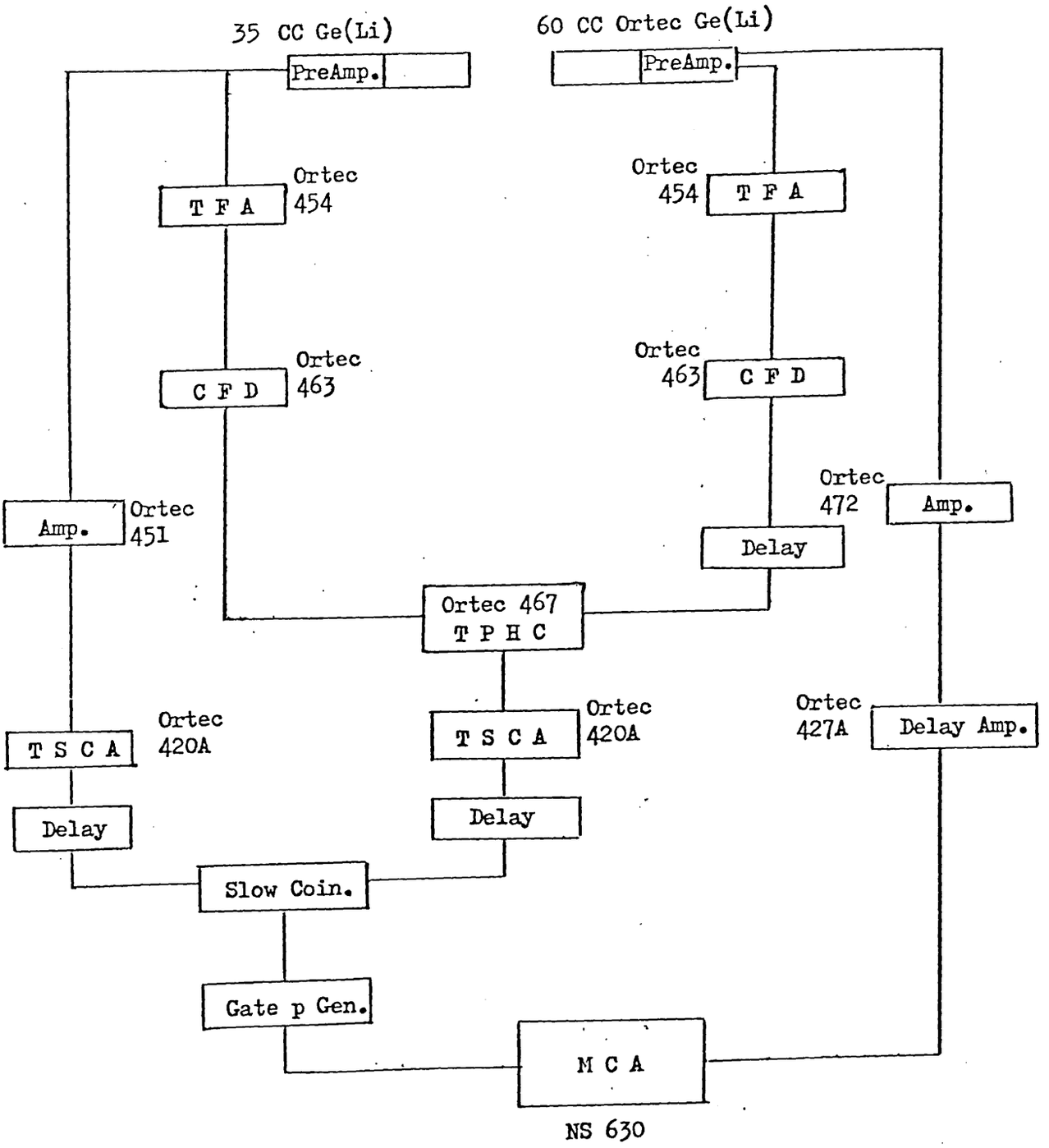

Fig. 2.5 Block diagram of
The Fast-Slow Coincidence System

different types of timing discriminator modes of Braunsfurth et al.[44], Gedck et al.[45] and Bengston et al.[46] have revealed that for pulses having constant amplitude the rise times at a certain fraction ranges from 10% to 20% of the pulse height. This method called constant fraction timing mode offers considerable advantages by reducing the time walk effect, and an improvement in the time resolution of 20% to 30% was obtained by Maier et al.[47] over that using leading edge timing mode.

The presence of noise signals superimposed on the real signals can also cause accidental coincidence (chance coincidence) due to uncertainty in the time signals. This is called jitter and can appear as the main source of inaccuracy when the effect of time walk is considerably reduced. In this case the constant fraction discriminator level was adjusted at a value just above the level of the noise signals (0.1 volt was a suitable adjustment) in order to reduce the jitter contribution into the timing distribution of the (TPHC) output, and hence the accuracy of the coincidence experimental results. More details of the timing problems will be discussed in section (3.6).

The (TPHC) output was discriminated by a timing single channel analyser (TSCA) Ortec 420A, whose window was adjusted on the timing peak which represented the true coincidence event, another TSCA (Ortec 420A) being used to give a gating photopeak at certain selected windows. The two TSCA outputs fed into an Elscint slow coincidence unit through μ sec delays. The output of this coincidence unit opened the (NS630) Multichannel analyser gate to record pulse height spectra from the spectrum detector which were in coincidence with the selected photopeak gate.

CHAPTER III

THE DUAL-PARAMETER ENERGY-TIME SPECTROMETER

3.1 General

For most of the current research on the energy level properties of nuclei, in particular those involving coincidence arrangements, multi-parameter systems are found to be very efficient and capable of giving more information than a conventional coincidence system.

A Dual-Parameter Energy-Time Spectrometer has a 4096 by 4096 coincident gamma-gamma spectra from two Ge(Li) detectors stored in a large capacity magnetic tape. Timing information from one of these Ge(Li) detectors and a fast plastic detector stored in an MCA memory was found to be sufficient for the requirements of this work. A block diagram of the Dual-Parameter Energy-Time Spectrometer is shown in Fig.(3.1). The energy part is discussed in Section (3.2) and the lifetime part is discussed in Section (3.3).

The performance characteristics of the two Ge(Li) detectors used as spectrum and gating detectors were given in Table(2.1). These two detectors were placed at 90^{o} to one another to minimize detector-to-detector Compton scattering.

The gating detector (No. 6) timing signals were used as the stop for the TPHC of the lifetime spectrometer while the start pulses were taken from a NE102 (1" x 1") plastic scintillator detector. Care was taken in the geometry of these detectors. The angle between them was fixed all the time at 180^{o} in order to minimize the error which could be injected due to the influence of perturbations of the angular correlation of the measured cascade as reported by Baverstam and Hojeberg[48]. A view of the experimental arrangement of the Dual-Parameter Energy-Time Spectrometer is shown in Fig.(3.2).

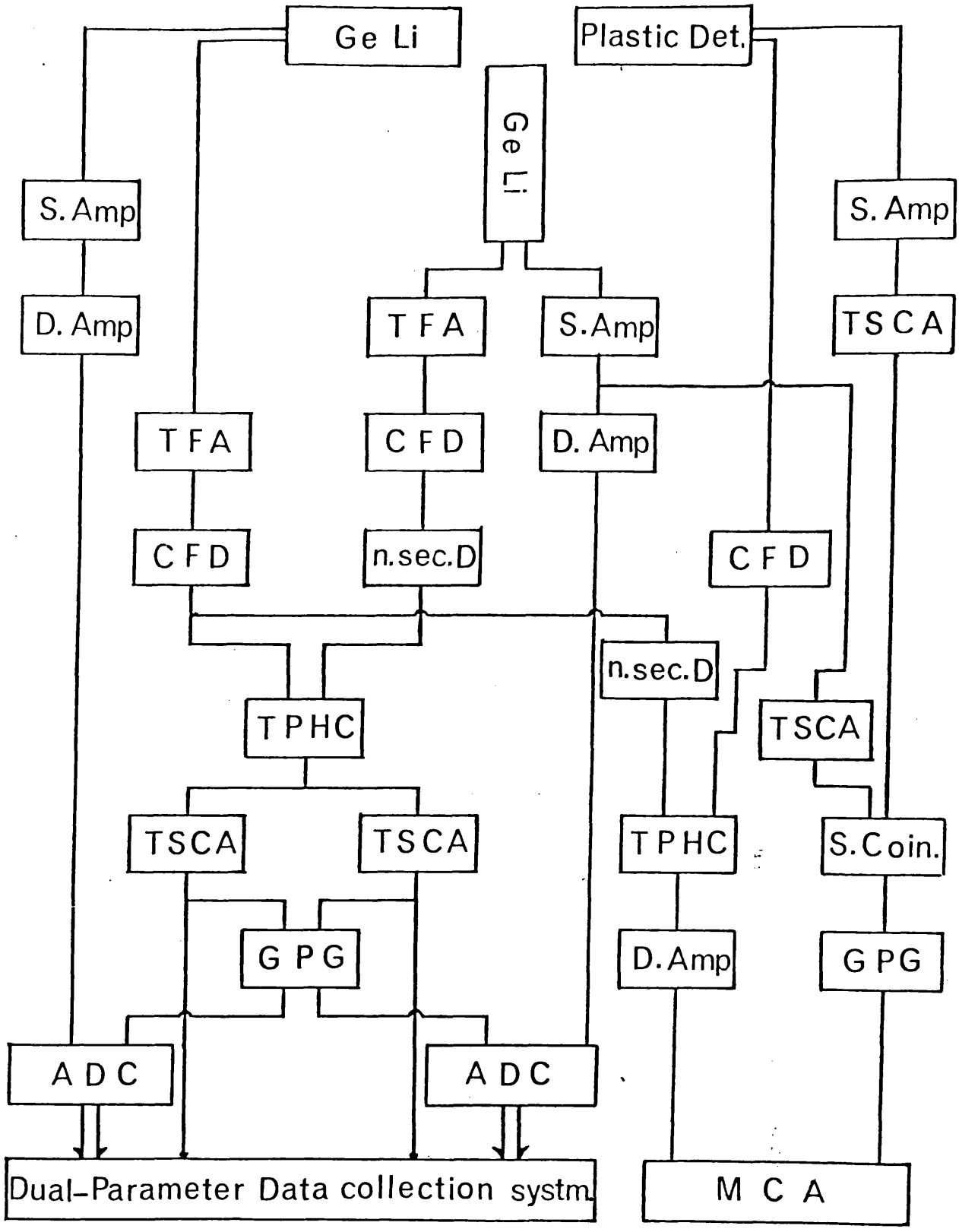

Fig.(3.1) Block diagram of the Dual-Parameter Energy-Time spectrometer

Fig.(3.2) A view of the experimental arrangement of the Dual-Parameter Energy-Time Spectrometer.

3.2 Description and operation of the Dual-Parameter Data Collection System

The system used a simple dual-parameter interface between the coincidence section and the magnetic tape storage and is called the write interface. Another dual-parameter interface is used as the interface between the magnetic tape transport and the memory unit and is called the read interface. The block diagram of the whole system is shown in Fig.(3.3).

The circuit diagram of the write interface is shown in Fig.(3.4). Initially the system should be cleared by the master reset. The master and ordinary reset components consist of monastables (M) 2, 3, 4 and NOR gates 2 and 3. This clear operation resets flip-flops (F) 1, 2, 3, 4, 5, 6 and clears counters (C) 1, 2, 3 and also enables the ADCs. The F1 reset enables the NAND gate 1. This will allow incoming events to trigger monostable (M1). The delay on this monostable is the time required for a complete digital conversion by the ADCs of the analysed pulse. When the conversion in both ADCs are completed, the triple input NAND gate 1 gives an output that set F1 which inhibits NAND gate 1. After that no further pulses can then be accepted by the system. The output from the triple NAND gate 1 is at the same time furnished to NAND gates 2 and 3. While a total event is being processed, F3 will then be in a high state and NAND gate 3 will give an output while NAND gate 2 will be inhibited.

The output of the triple NAND gate 1 is also used to trigger monostable 2. The output of this monostable signals the start of the entire coding process and at the termination of the delay on this monostable all F/Fs, counters and ADCs will be reset, ready to analyse a new event.

The second part of the write interface functions to drive the processed event to the tracks on the magnetic tape transport however the event processed output is furnished to a NAND gate 4. If the magnetic tape

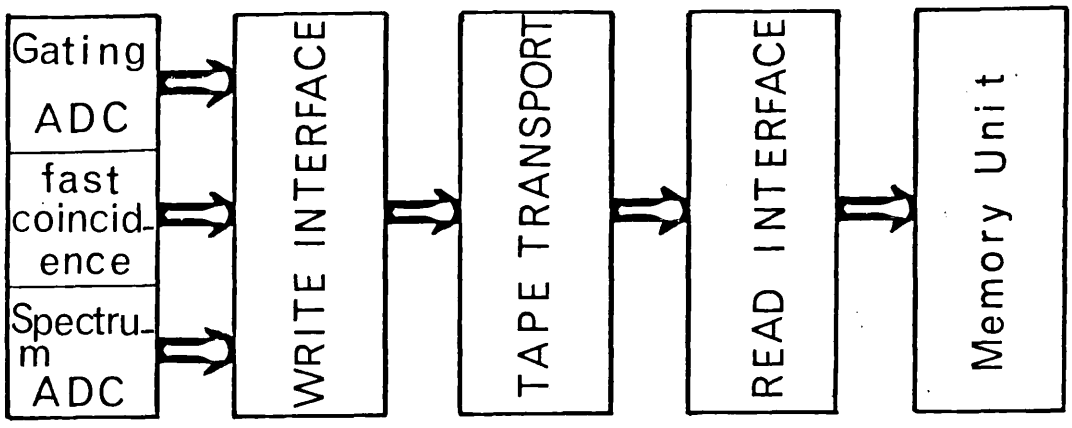

Fig.(3.3) Block diagram of the dual-parameter data collection system

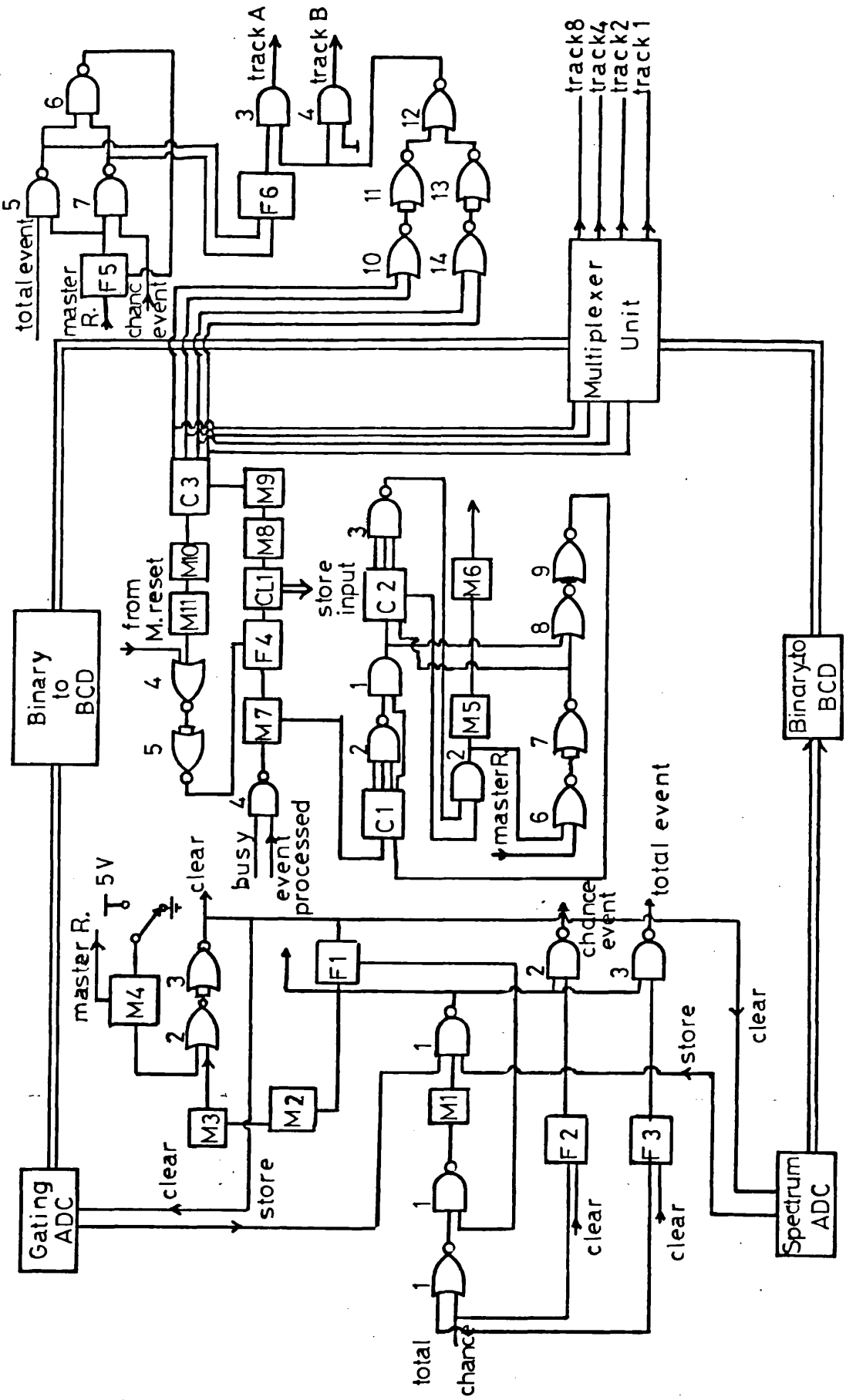

Fig (3.4) The circuit diagram of the write interface

transport is not busy, then it will trigger monostable 7. Output of this monostable then sets F4 and enables clock 1. The latter will act as the store input data clock to the buffer and is also the input to counter 3 (C3). Meanwhile, monostables 10 and 11 together with NOR gates 4 and 5 will help to reset F4 and stop (C3) after nine pulses. The pulses from (C3) denoted as A, B, C and D are then passed to the multiplexer units to facilitate changing the BCD addresses from the binary-to-BCD converter units into serial form. The data from the multiplexer are then connected to the input of the respective tracks 1, 2, 4 and 8 on the buffer of the magnetic tape recorder.

The final part of the circuit, comprising counters 1 and 2, triple input NAND gates 2 and 3, AND gates 1 and 2, NOR gates 6, 7, 8 and 9 and monostables 5 and 6 all act as a counter of 225. When the counter reaches this value of 225, a write data block pulse is initiated and the system is dead, while the transfer of data takes place from the buffer onto the magnetic tape. Meanwhile, the two NAND gates 5 and 7 remain high when F5 is in a reset state. When either a total or a chance coincidence signal is being processed either NAND gate 5 or NAND gate 7 gives an output provided F5 is reset. This output is then passed via NAND gate 6 to F5 which gets set and in turn closes back NAND gates 5 and 7. The output of F6 will be high or low if a total or chance coincidence has been accepted respectively. At this stage, counter 3 outputs A, B, C and D are all at low levels. Combinations of NOR gates 10, 11, 12, 13 and 14 cause the output of gate 12 to be high. Accordingly, AND gate 3 gives a high level for total coincidence event and a low level for chance coincidence event on track A. The output of AND gate 4 which is the B track, is always in a high state, so that we have writing the total coincidence tag word as 000011 onto the tracks 1248 AB respectively, and for the chance coincidence tag word as 000001 onto the tracks 1248 AB respectively.

The read interface circuit diagram is shown in Fig.(3.5). In this interface shift-register was used to convert the serial data back to parallel form suitable for the NS630 memory unit. The outputs of the shift register that correspond to addresses from the gating ADC are wired to the comparator units. The upper and lower level comparators for the 10^2 position only are shown in the Fig.(3.5). The actual interface contains 8 comparators - two each for 10^3, 10^2, 10^1 and 1 positions. The remaining outputs of the register are addresses of the spectrum ADC. These are presented to the BCD-to-binary converters which are in turn connected to the NS630 memory unit. The front panel switch on the read interface unit determines whether we want to collect a total or a chance spectrum. In case of the total spectrum, this is indicated by a pulse on track A of the tag word. A switch selected to total position ensures that the AND gate 1 goes high when the pulse on track A and the read data clock are present simultaneously. The AND gate 1 then sets F1 which enables the shift register. Data on tracks 1, 2, 4 and 8 are then read into the shift registers whenever a read data clock is present at the corresponding inputs of the shift registers. After the tag word both tracks A and B are zero, so that the shift registers remain enable and counter 1 will begin to count till eight. Then, after a short delay determined by monostable 3, F1 is reset and this will in turn inhibit the shift register.

At this time all outputs at the shift registers are in steady states enabling the comparators to compare input data (from the shift registers) with levels set on two thumbwheel switches (acting as lower and upper level windows). If the data falls within the preselected window thresholds, output of NOR gate 2 will go high. Meanwhile, the delay on monostable 3 will change the state of AND gate 6 which sets F2. The output of this F/F causes the memory unit to store the addresses from BCD-to-binary converter. When the store process is completed, a clear signal from the

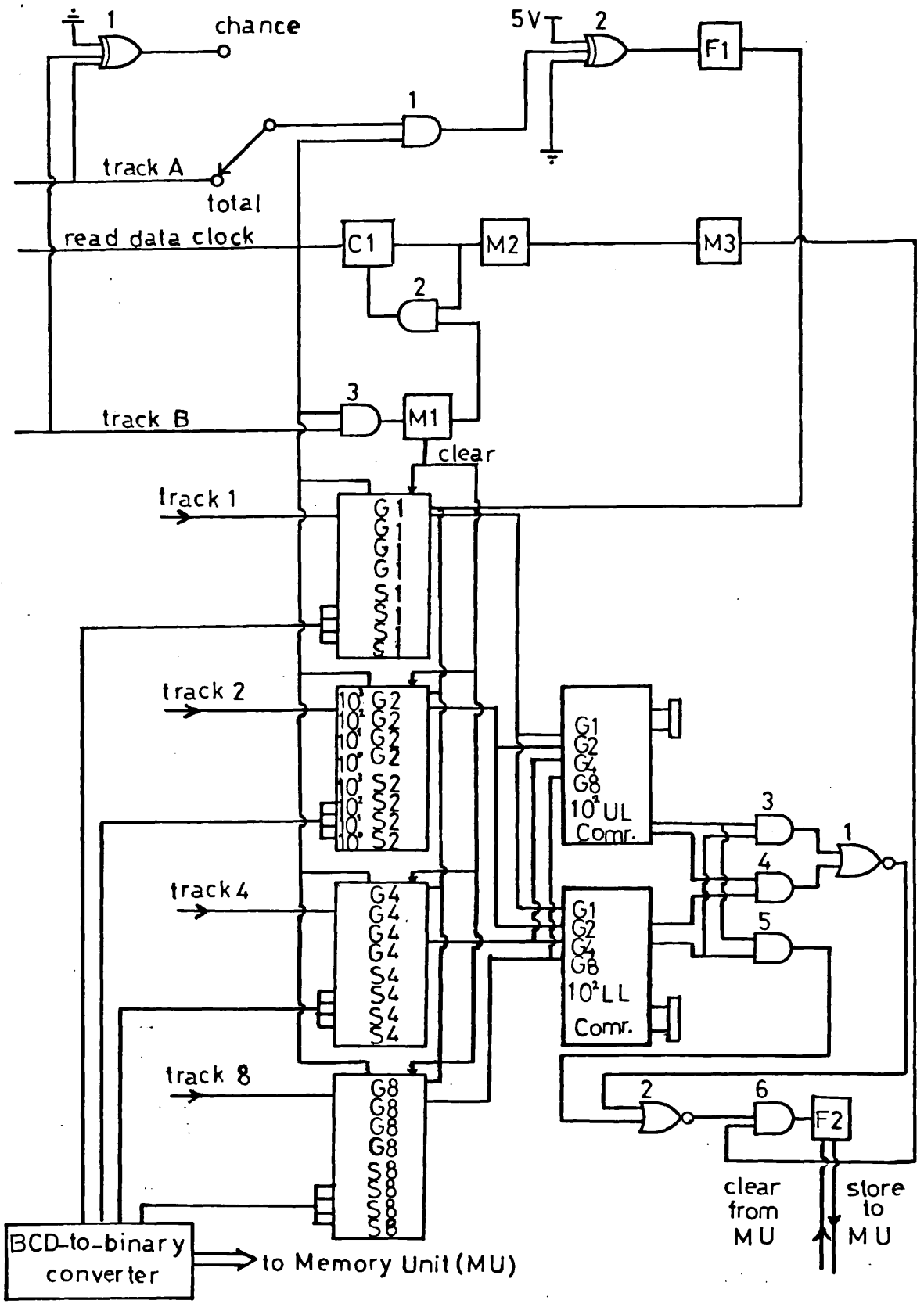

Fig.(3.5) The read interface circuit diagram

MCA is generated which resets F2 back to its original state. If the data falls outside the preselected window, gate 6 will not change the state of F2, and the addresses will remain at the comparators and BCD-to-binary units until another coincidence event (consisting of nine words) is detected for another analysis. The actual circuit of the store cycle, binary-to-BCD converter, multiplexer cycle, total-chance indicator multiplexer, write magnetic tape control, BCD-to-binary converter, select gate, total-chance, shift register and read magnetic tape control units are given in reference[50] together with Operating and Service Manual for each unit, and for the whole system.

3.3 The lifetime spectrometer

A typical electronic system used to process the signals from two detectors for time measurements makes use of constant fraction circuits to derive standard pulses from the detector signals which then carry the time information to the time difference unit (TPHC, or the fast coincidence unit). A TPHC gives an output pulse whose amplitude is proportional to the time difference between the arrival of the timing pulse from plastic scintillator detector (start detector) and the arrival of the timing pulse from the Ge(Li) detector (the stop detector). The absolute magnitude of this time difference is unimportant in assessment of the performance of the system; the criterion necessary to judge the system is the spread of the time difference with respect to time, i.e. the FWHM of the timing spectrum of two prompt gammas, which is called the system timing resolution τ or the system lifetime.

A block diagram for the fast-part of the system is shown in Fig.(3.6). The start detector is a 1" x 1" NE102 plastic scintillator connected to an RCA8575 fast photomultiplier, with an Ortec (265) base. The EHT applied was 2.2 kV (-ve polarity), which produced anode pulses of 7 volts and 1.9 n.sec. rise time for the ^{60}Co gamma rays, and dynode pulses of 7 n.sec.

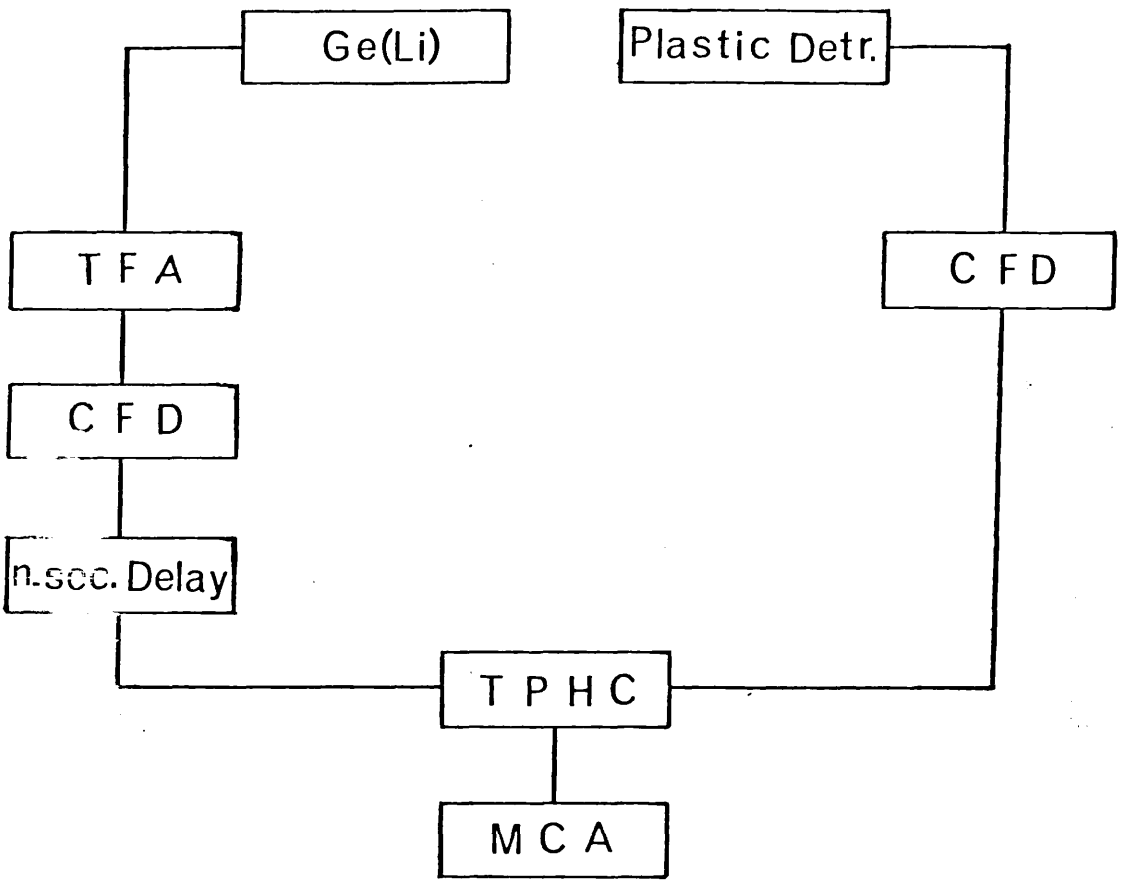

Fig.(3.6) Block diagram for the fast-part of the lifetime spectrometer

rise time. The stop detector is a large volume ($\simeq$ 60 cc) Ge(Li) detector of 10% efficiency, whose preamplifier output was fed into a timing filter amplifier (TFA) to shape the very long-tailed pulses suitably for the timing constant fraction discriminator, whose output was connected to the stop input of the TPHC after a n.sec. delay unit. The plastic (fast) detector dynode output and the Ge(Li) detector preamplifier output form the energy condition on the timing spectrum. This was done by driving those two output pulses to two spectroscopy amplifiers and using two timing single channel analysers. The TSCA windows were adjusted on the measured cascade (gamma rays feed one energy level and another gamma ray makes a transition from this level to a lower level) as start and stop. The outputs of these two (TSCAs) go to a slow coincidence unit whose output opens the gate for the timing spectrum to be recorded in the multichannel analyser.

3.4 Timing measurement problems and timing calibration

The time spectrum is simply a time distribution as measured with a TPHC, due to the statistical spread of emission times of the photons corresponding to the transitions. In the case of two prompt gamma rays, the arrival of non-related signals will generate an output signal which is indistinguishable from a true coincidence event (N_t). The relationships between the number of such chance coincidences per unit time N_c and N_t is given by A. Wapstra[51]:

$$N_t/N_c = I/2\tau N$$

where

I is the coincidence intensity

N is source strength

τ is system resolution

I is outside our control for a given detection system, but N can be minimized and

a few microcuries of source activity were found to be suitable. To minimize the resolving time in order to yield a given statistical accuracy on the true coincident counts the nature of events occurring in the detector and the means whereby the signals are processed in the electronics need to be carefully looked at. The time behaviour of a scintillation counter can be appraised by considering the current pulse available at the anode and is given[52] by

$$I(t) = \frac{R}{\tau - \tau_1} \left(e^{-t/\tau} - e^{-t/\tau_1}\right)$$

where τ is decay time constant of the scintillator

τ_1 is the rise time constant of the photomultiplier

R is the total number of photoelectrons per scintillation.

Thus it is desirable to use high gain photomultiplier tubes and small decay time constant scintillators such as the RCA 8575 photomultiplier with an NE102 plastic scintillator.

The statistical nature of the light emission in the scintillator, the conversion of this light (fluorescence and luminescence) into electrons by the photomultiplier sensitive cathodes, and also the secondary emission of the photomultiplier dynodes causes jitter in the output signal with respect to the time, so that the discrimentor level of the CFD receiving these pulses should be adjusted above the signal noise level (0.1 vol.).

The Ge(Li) detector (stop detector) has different timing characteristics, but in general the N_2 liquid cooled FETs of the preamplifier minimized considerably the jitter noise. On the other hand, the rise times of semiconductor detector signals is a function of the detector geometry and also dependent on the locations of the gamma-ray point of interaction in the Ge(Li) detector element. This can lead to two pulses having the same amplitude but different rise times for the same γ-ray energy which leads to time walk in the time discriminator. While the same effect

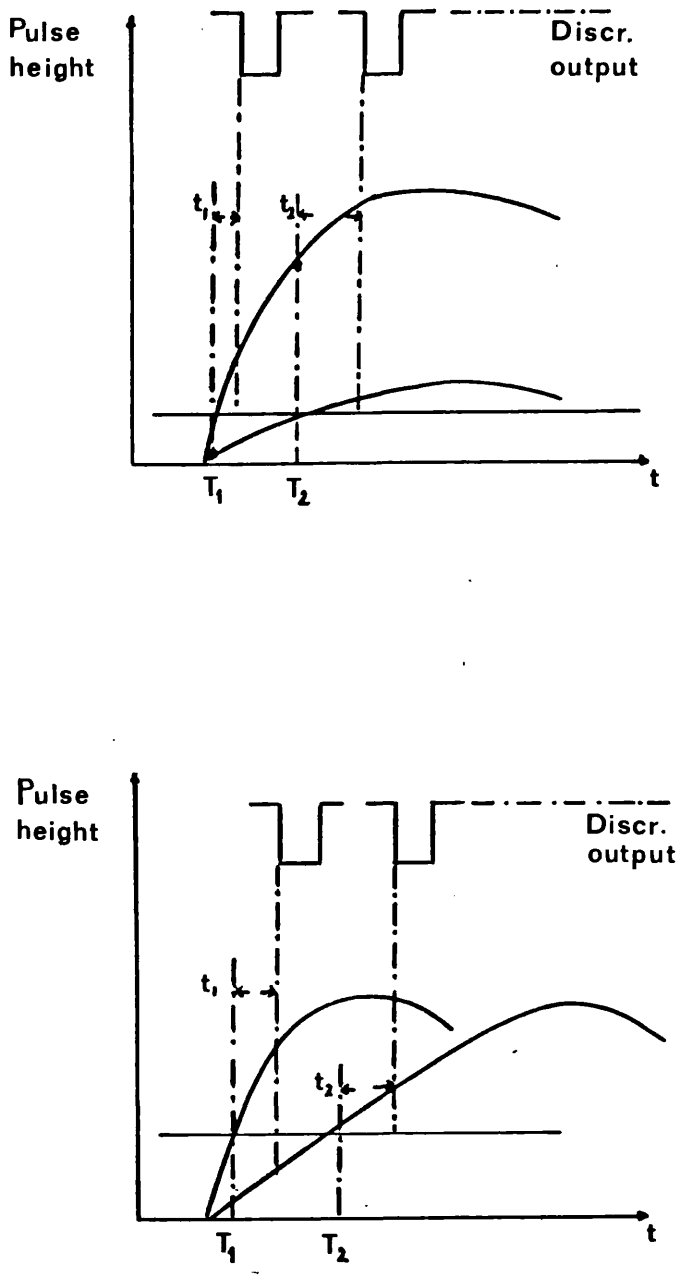

Fig.(3.7) The origins of timing walk in the output discriminator

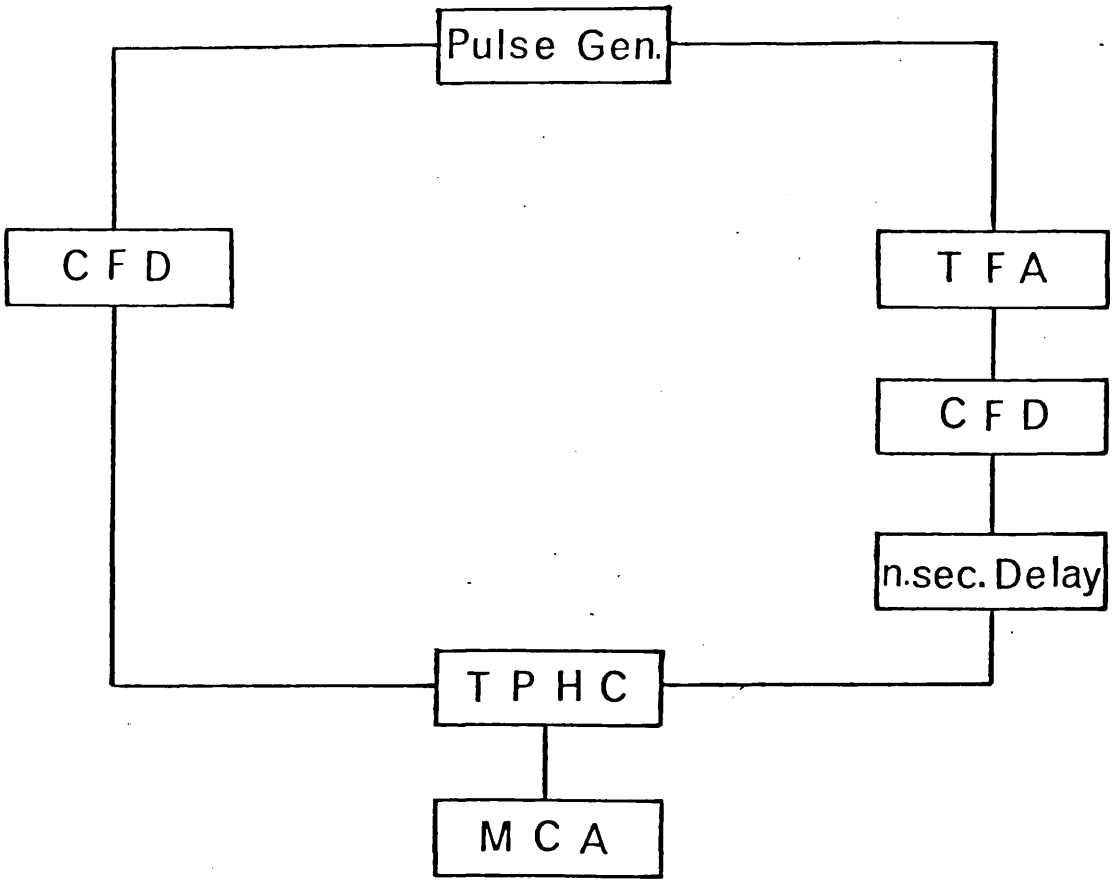

Fig.(3.8) Block diagram of multichannel analyzer time calibration set up

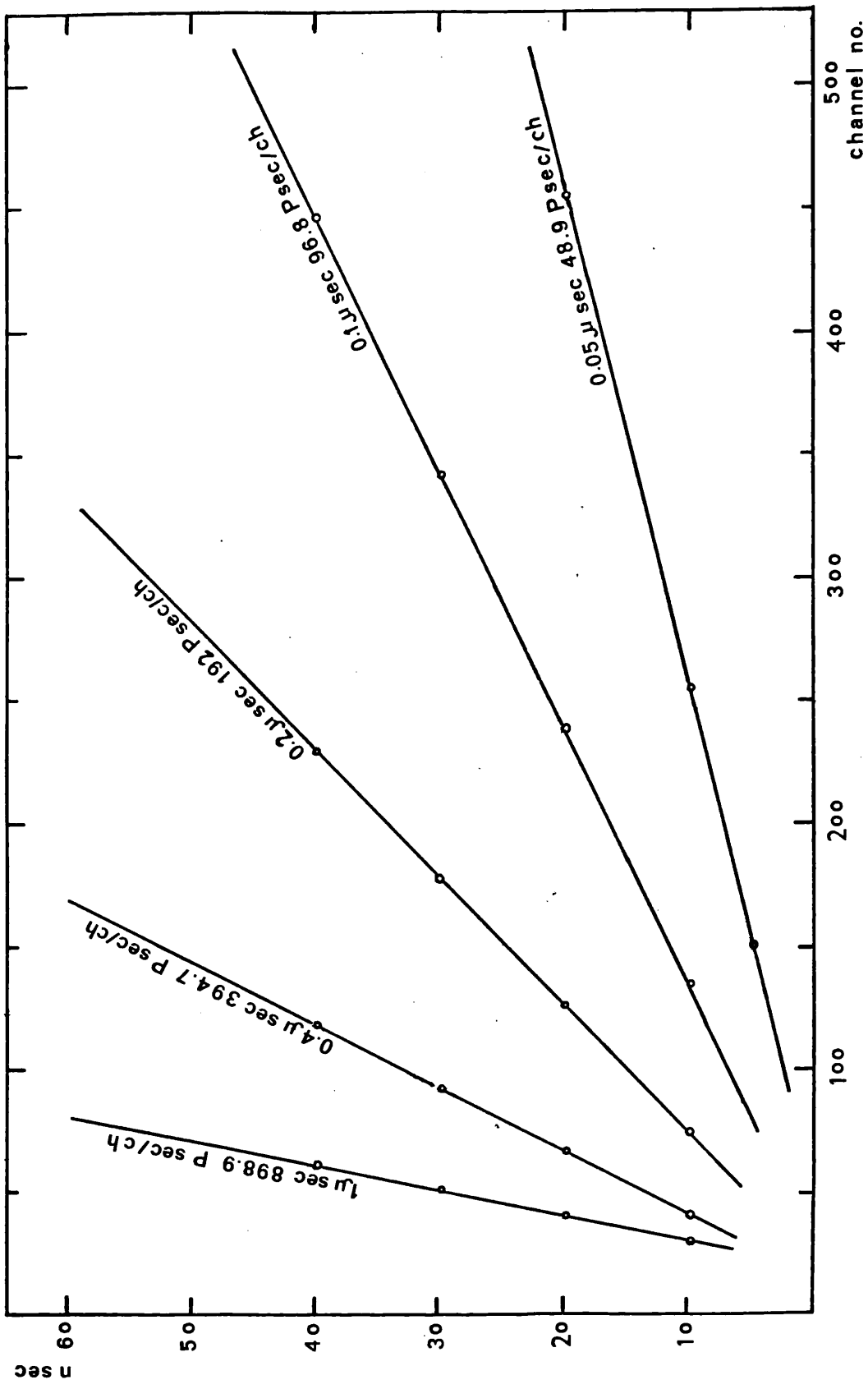

Fig(3.9) The time calibration of the MCA for different TPHC ranges

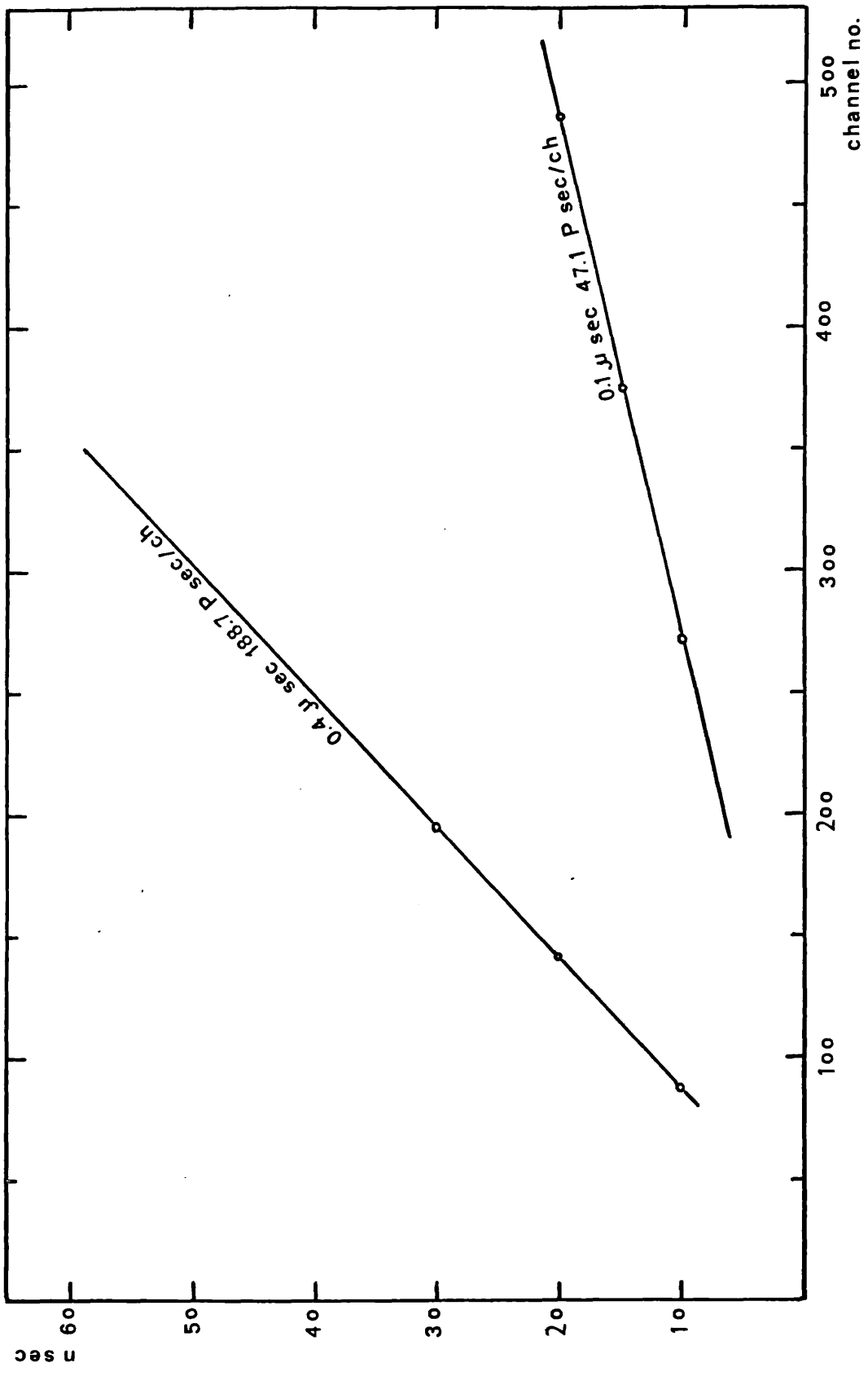

Fig(3.10) The time calibration for different ADC conversion gain

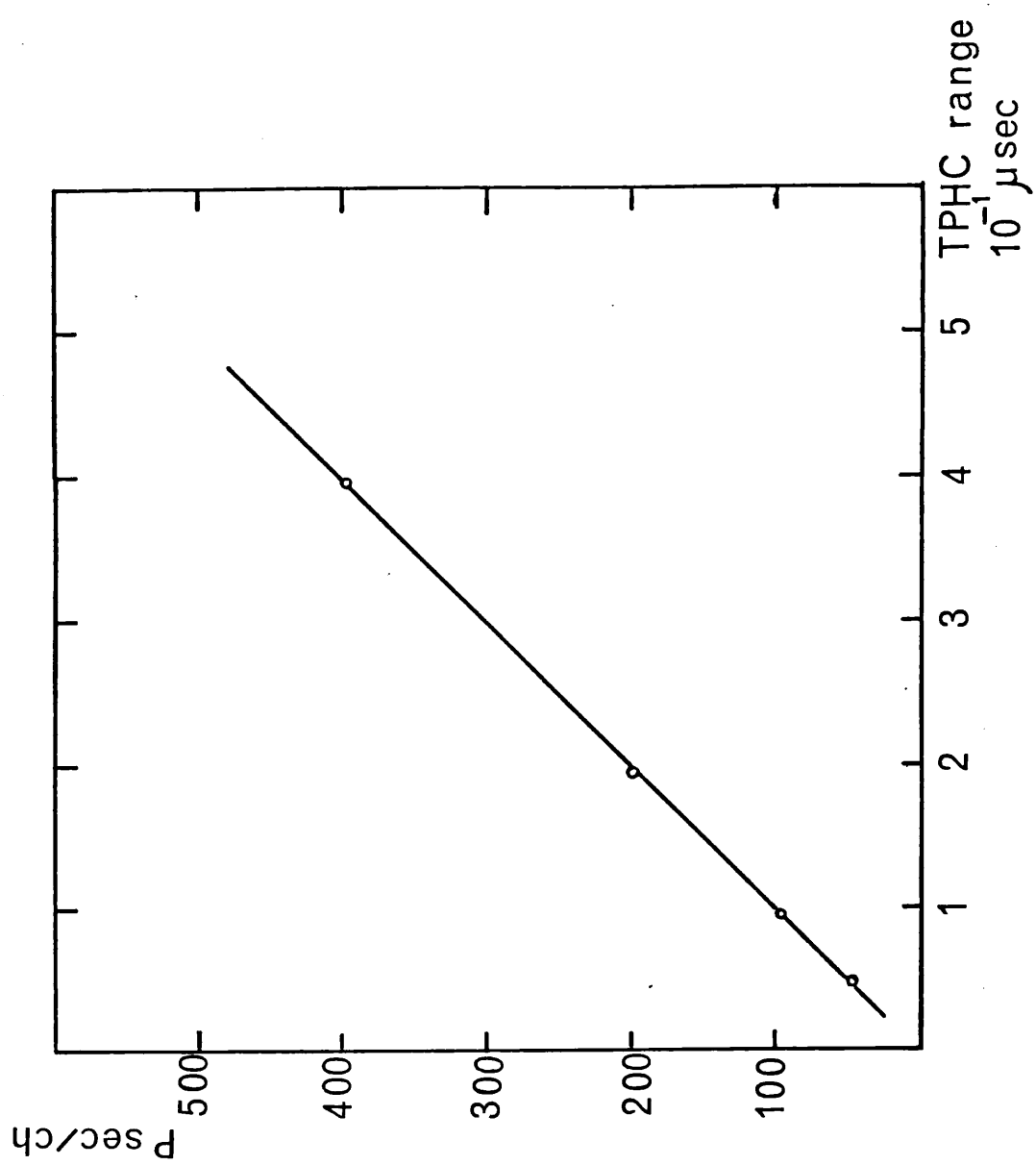

Fig(3.11) The calibration-TPHC range relationship

observed for signals having different amplitudes is mainly due to the scintillation detector (start detector), Fig.(3.7) shows the origins of timing walk in the output discriminator of fixed threshold due to different types of pulses. The answer, of course, for this type of inaccuracy is the constant fraction timing mode discriminator which triggered all the time for its discriminator threshold at 20% from the pulse height, and reduced so much the time walk effect. The Ortec 473A constant fraction discriminator is designed with a shaping mode switch to make it useful for both fast-plastic and Ge(Li) inputs. In the case of Ge(Li) shaping mode there is an automatic slow-rise-time rejection function in the discriminator, which results in superior timing with some loss in efficiency. However, the use of an Ortec 454 timing filter amplifier shapes pulses for optimizing the signal to noise ratio as suitable for use with the 473A CFD. This combination was used successfully without losing the Ge(Li) efficiency in the stop arm.

The time calibration of the multichannel analyser was performed using the set-up shown in Fig.(3.8), a precision pulse generator being used in this set-up. Fig.(3.9) shows the time calibration of the M.C.A. for different TPHC ranges, while Fig.(3.10) shows the time calibration at different A.D.C. conversion gains. The expected linearity of the calibration TPHC range relationship is shown in Fig.(3.11).

3.5 Performance of the system

The performance of the system can be tested by measuring the coincidence spectra of the well established coincidence relations of ^{110}Ag gamma-rays and the lifetime of the positron from ^{22}Na annihilated in a Lucite sample in a separate measurement. The γ-γ coincidence measurements were performed with detector 6 and 7; the former was used as the gating detector and the lifetime stop detector. The start detector was the plastic detector as described in Section (3.3). The

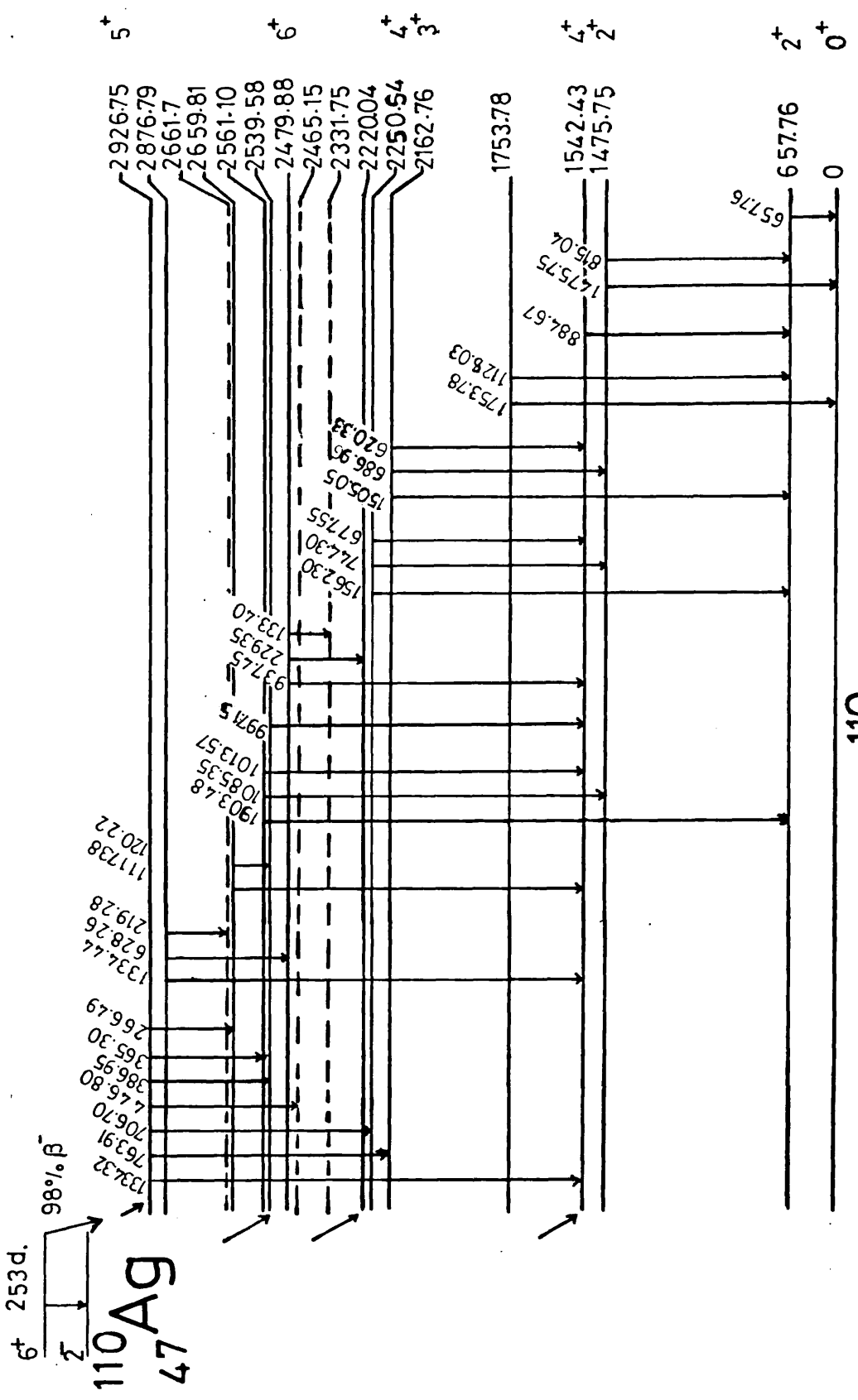

Fig(3.12) The ^{110}Cd level scheme

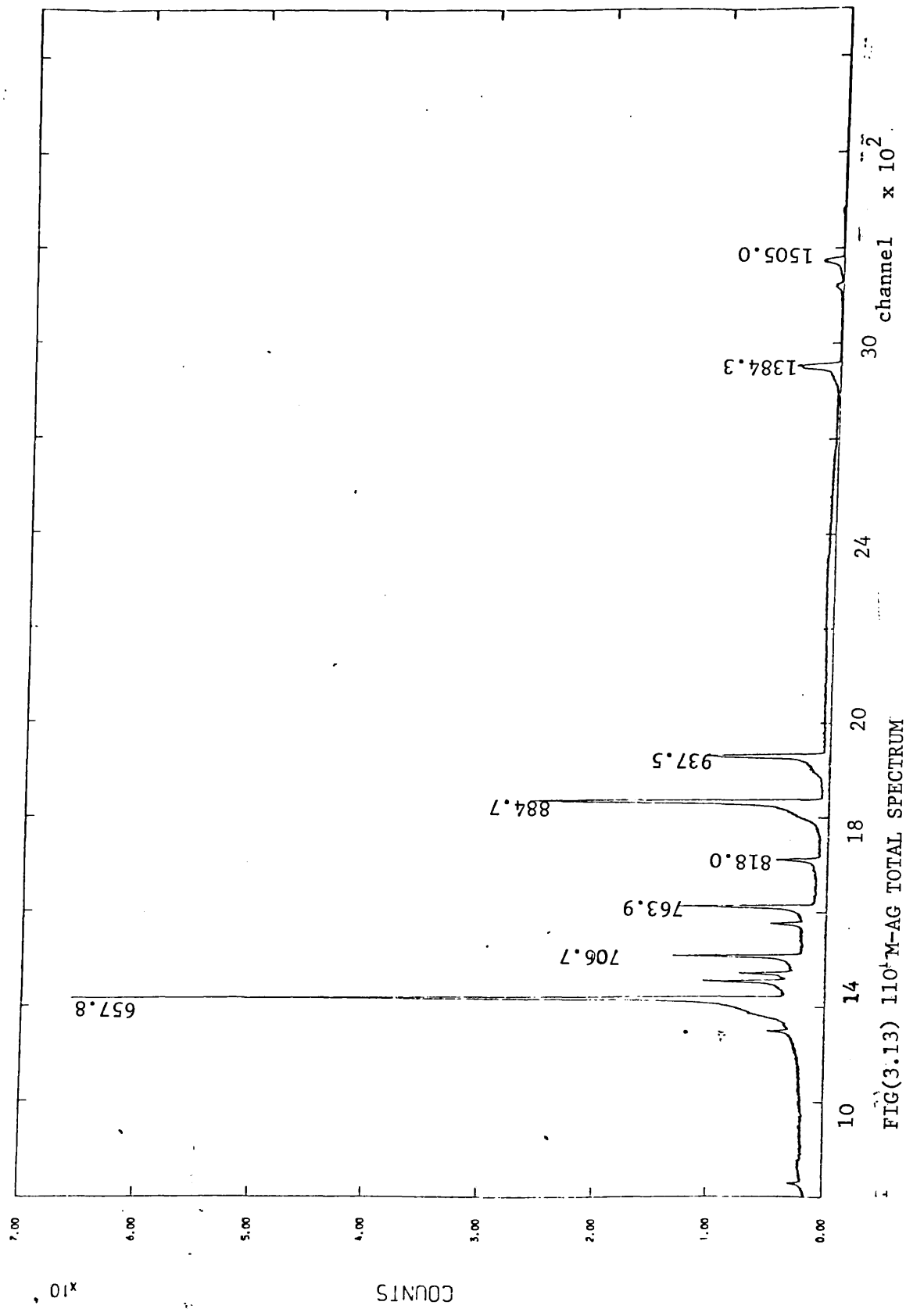

FIG(3.13) 110^{t}M-AG TOTAL SPECTRUM

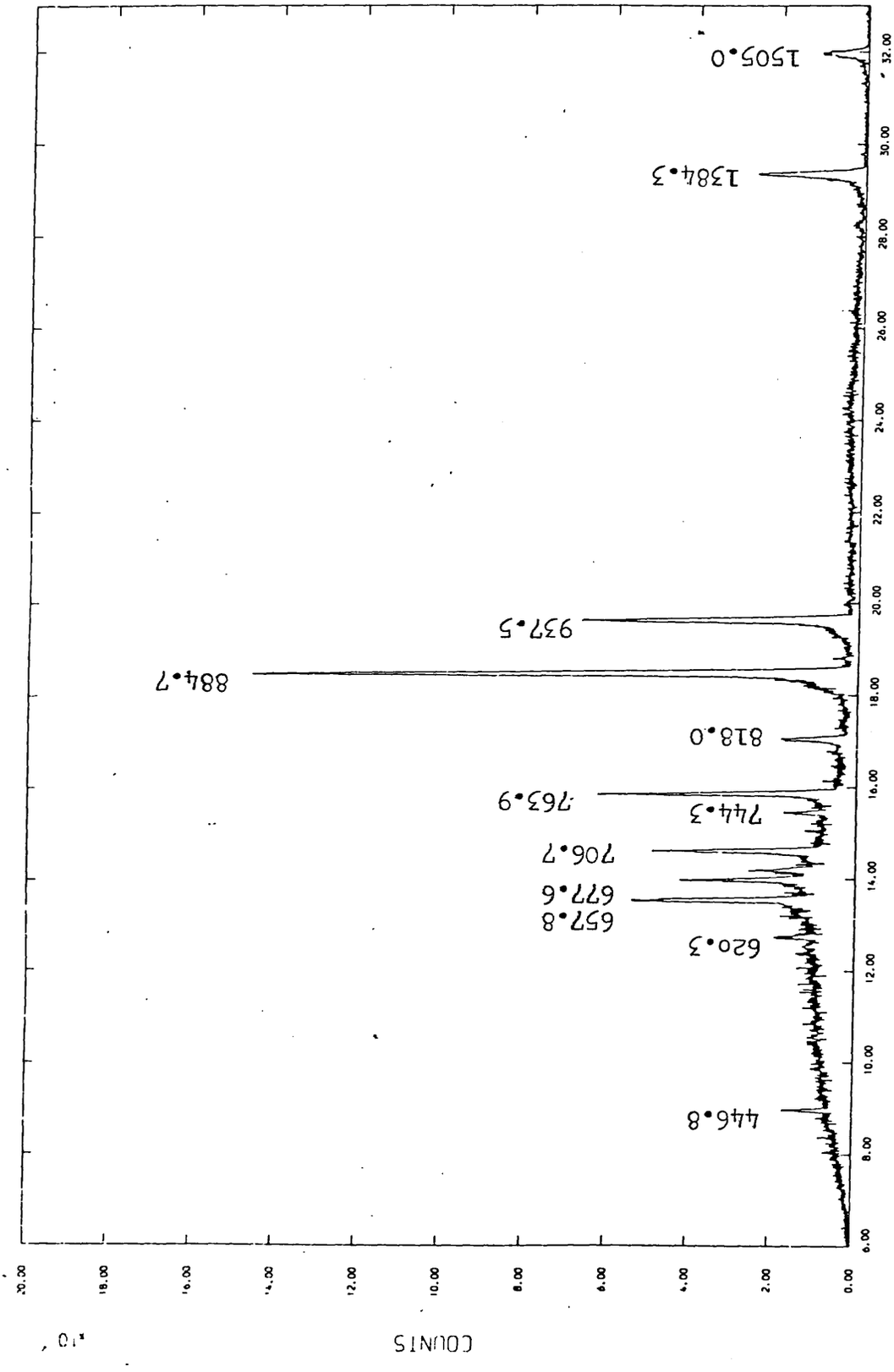

FIG(3.14) UNCORRECTED SPECTRUM OF 110M-AG IN COINCIDENCE WITH 658 KEV

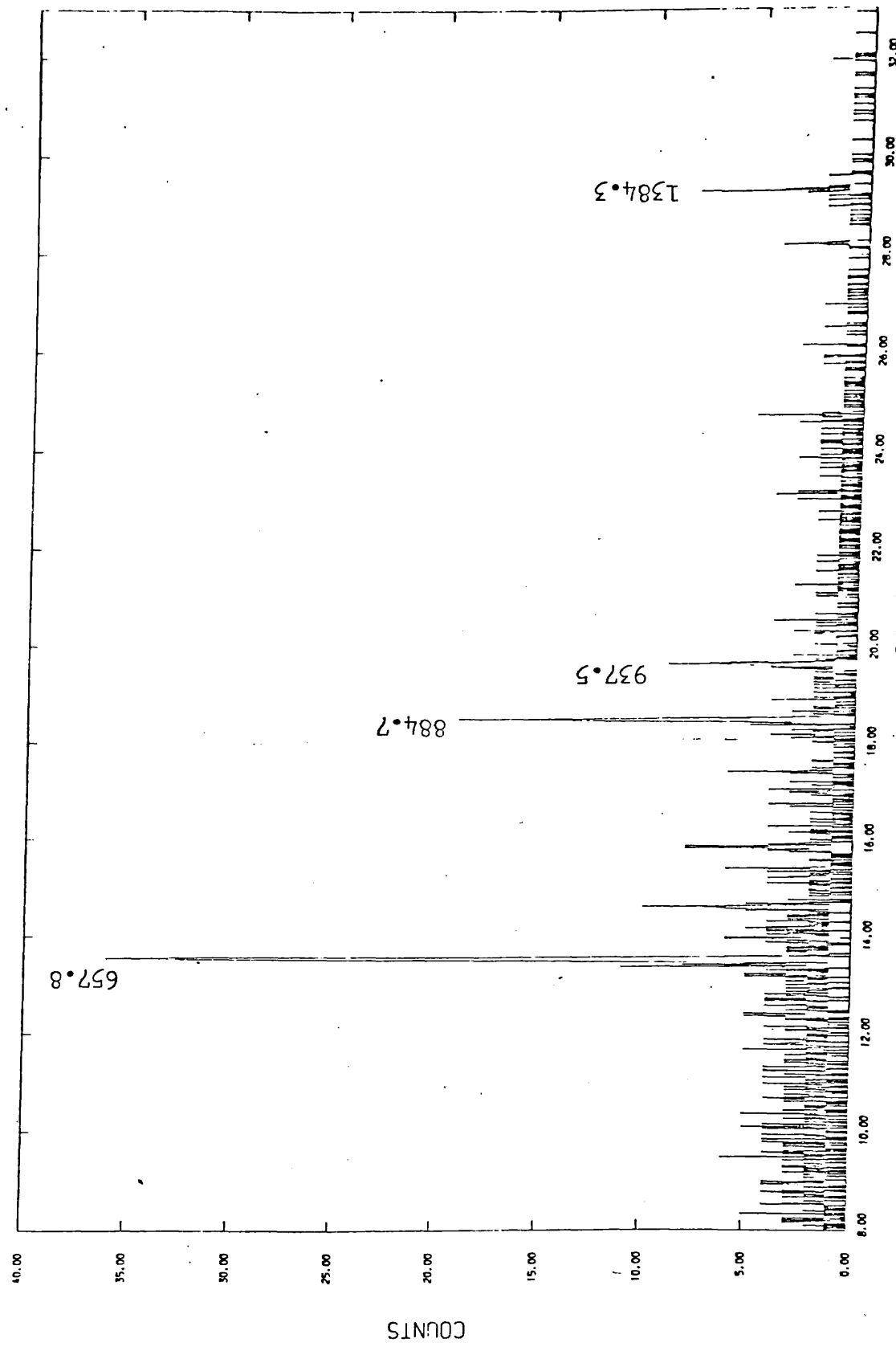

FIG(3.15) CHANCE SPECTRUM OF 110M-AG IN COINCIDENCE WITH 658. KEV

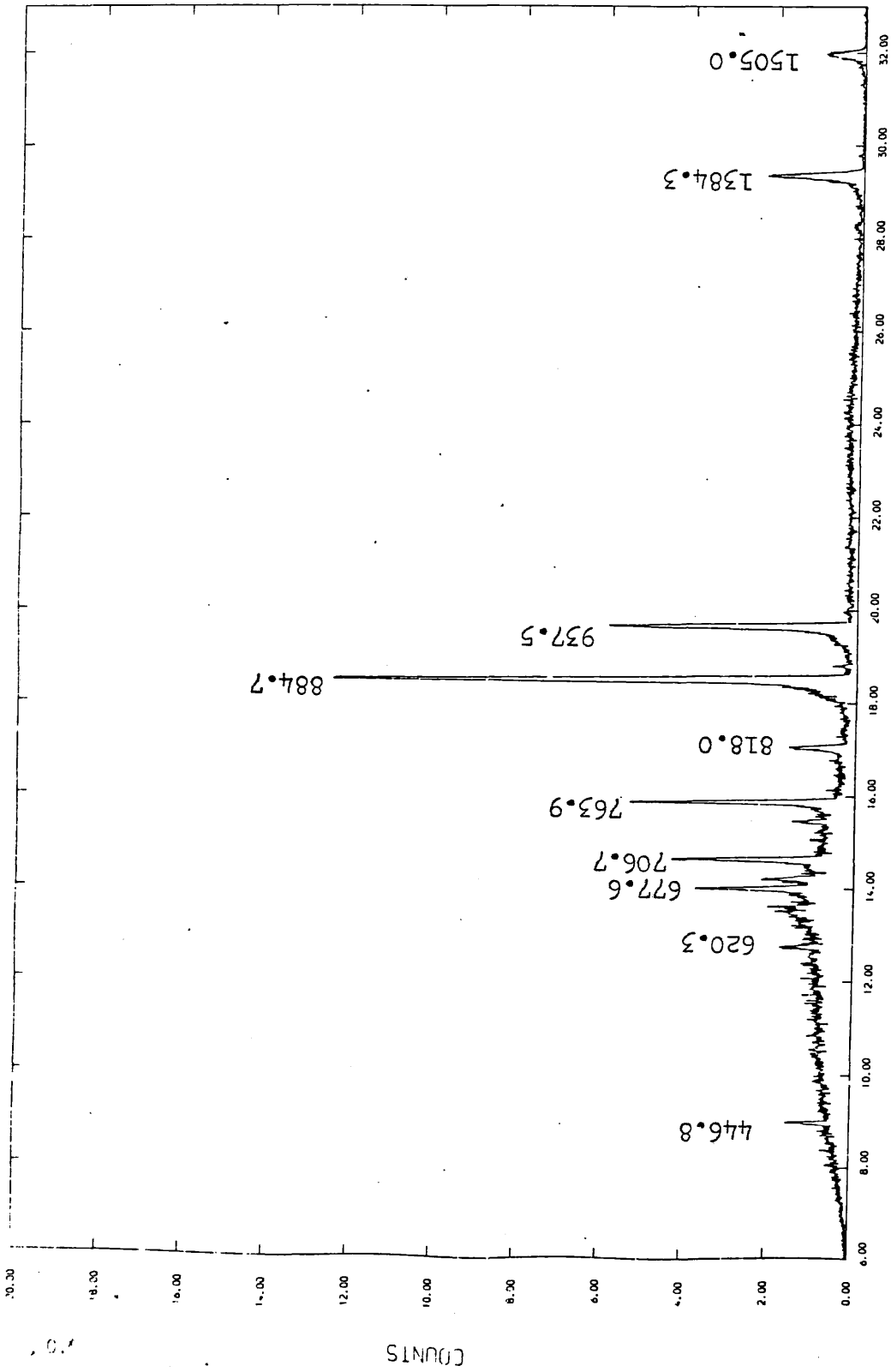

FIG.(3.16) CORRECTED SPECTRUM OF 110M-AG IN COINCIDENCE WITH 658 KEV

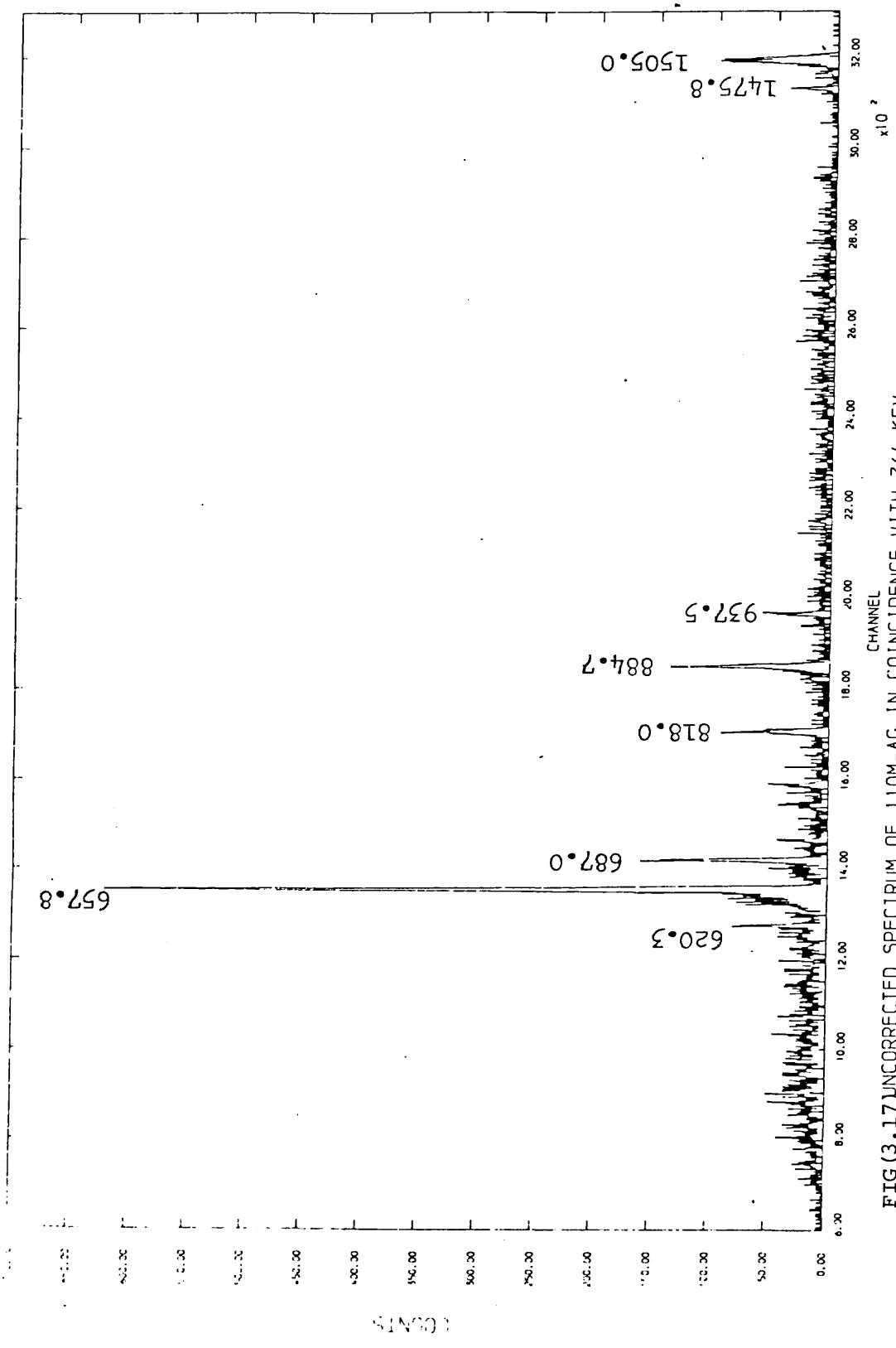

FIG(3.17)UNCORRECTED SPECTRUM OF 110M-AG IN COINCIDENCE WITH 764 KEV

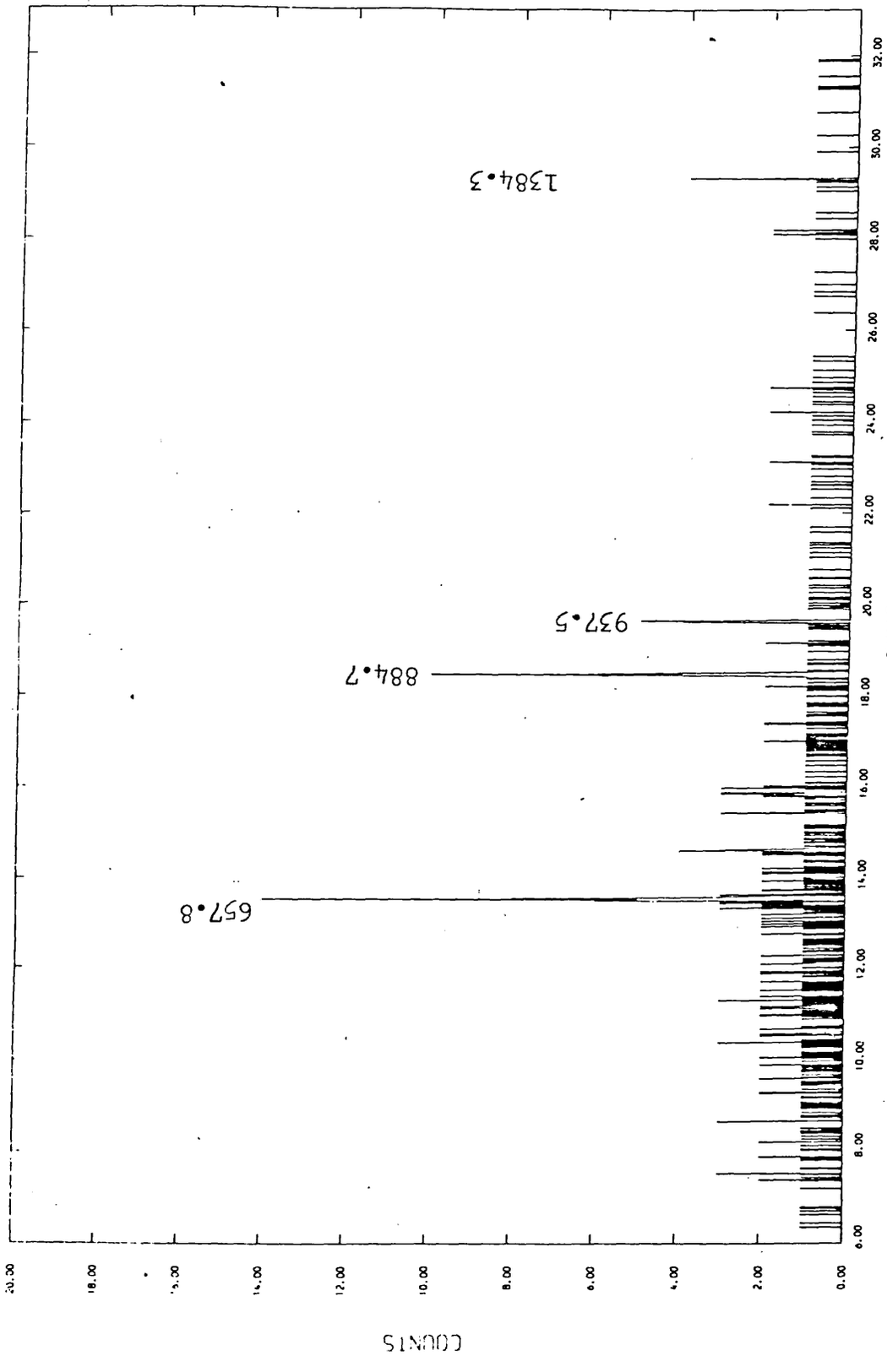

FIG(3.18) CHANCE SPECTRUM OF 110M-AG IN COINCIDENCE WITH 764 KEV

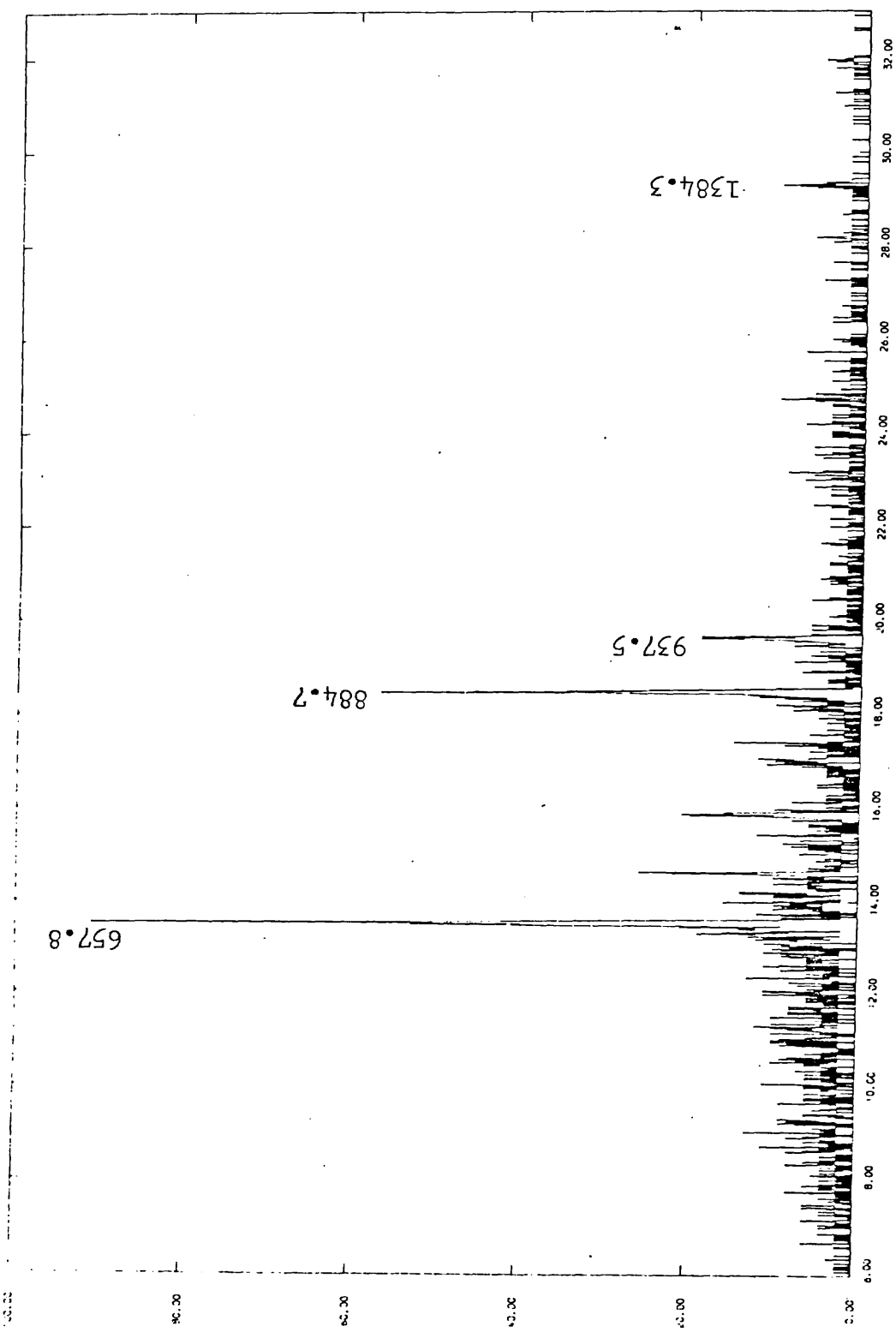

FIG(3.19) BACKGROUND SPECTRUM OF 110M AG IN COINCIDENCE WITH 764 KEV

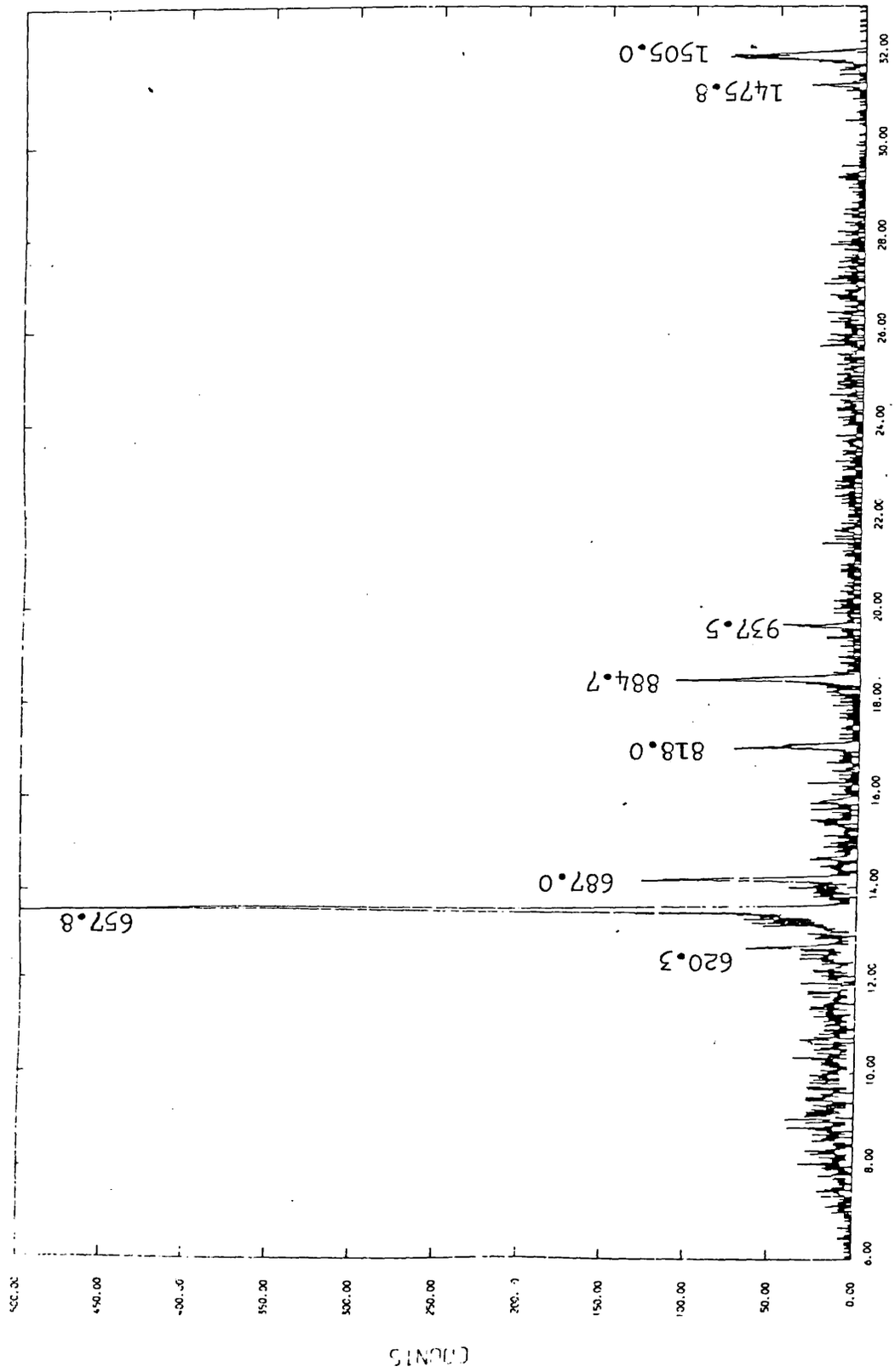

FIG(3.2o) CORRECTED SPECTRUM OF 110M-AG IN COINCIDENCE WITH 764 KEV

Energy (keV)	Singles Intensity	Intensity	
		658 keV	764 keV
446.80 (3)	3.46 (13)	26.5 (15)	
620.33 (3)	2.81 (7)	29.1 (20	64.1 (24)
657.76 (3)	100		515.8 (110)
677.59 (4)	10.8 (3)	148.3 (59)	
686.96 (3)	6.65 (18)	46.2 (2)	129.9 (39)
706.70 (4)	16.57 (39)	126.0 (62)	
744.30 (3)	4.74 (11)	22.7 (9)	
763.91 (3)	21.57 (64)	222.6 (60)	
818.04 (4)	7.24 (24)	100	100
884.67 (4)	73.88 (196)	816.4 (201)	86.9 (85)
937.45 (5)	34.22 (77)	422.6 (176)	7.6 (11)
1384.32 (5)	25.09 (38)	211.1 (38)	
1475.75 (5)	4.18 (61)		39.1 (20
1504.95 (7)	12.99 (62)	79.4 (31)	299.9 (80)
1562.10 (6)	1.18 (59)	49.6 (10)	

Table (3.1) The relative intensities of spectrum in coincidence with 658 keV and 764 keV compared with the single intensities.

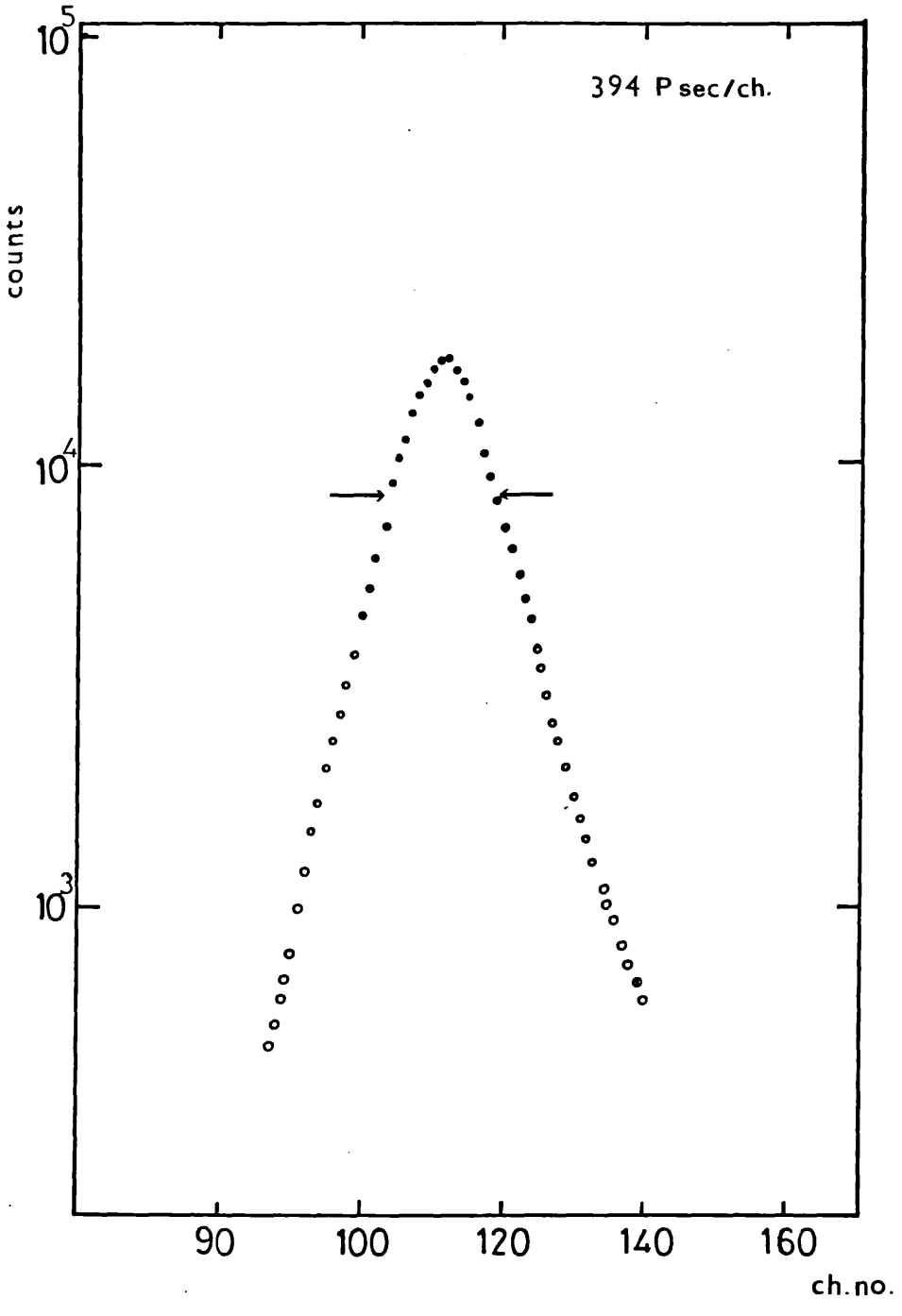

Fig(3.21) ^{60}Co prompt lifetime spectrum

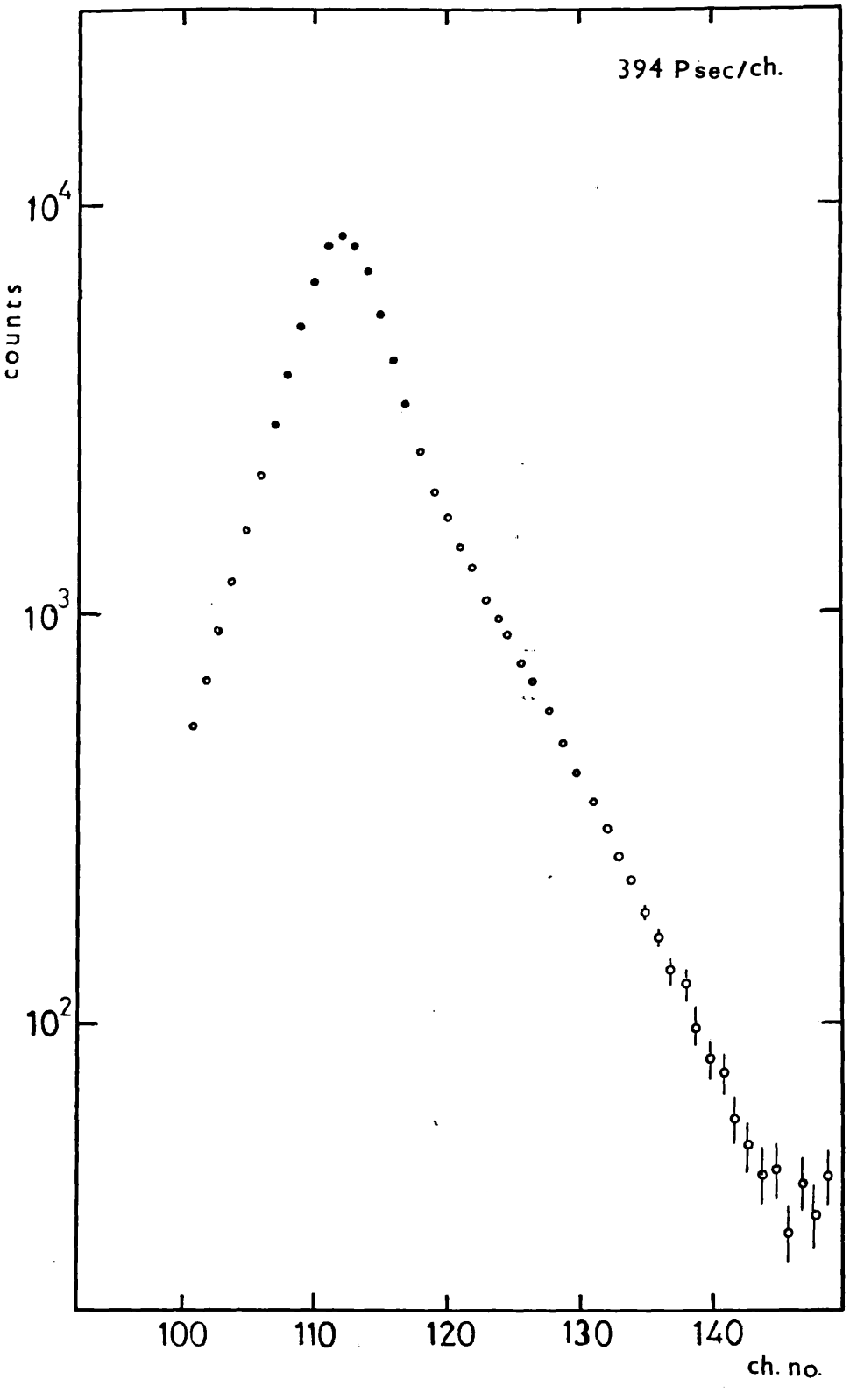

Fig(3.22)Positron lifetime in Lucit sample

Present work	Fisi et al.[54]	Groseclose et.al[55]	Wilson et al.[56]
1.87 ± 0.05	1.55 ± 0.01	1.91 ± 0.04	1.7 ± 0.2

Table(3.2) The positron lifetime in Lucite sample compared with the previous measurements (values are in n.sec.)

^{110}Cd decay scheme given by Thein[53] is shown in Fig.(3.12), the coincidence results measurements are shown in Fig.(3.13) to Fig.(3.20). Table (3.1) shows the analysis of these coincidence spectra, where the coincidence relative intensities have been arbitrarily normalised to the 818 keV gamma-ray intensity.

In this Table it is clear that peaks that are truly in coincidence have intensities which appear greater than their singles intensities, which explains very well the feature of the decay scheme shown in Fig.(3.12).

The lifetime spectrometer time resolution measured using the prompt gamma-rays of ^{60}Co is shown in Fig.(3.21) and FWHM of 5.8 ± 0.2 n.sec. was obtained; the measurements were performed at room temperature and for an M.C.A. calibration of 394.7 p.sec./ch. The time spectrum obtained from the positron annihilation in the Lucite sample is shown in Fig.(3.22). The performance of the timing system can be compared with previous measurement in Table (3.2). The measured value of 1.87 ± 0.05 n.sec. is in good agreement with those of Groxeclose et al.[55] and Wilson et al.[56] within the quoted errors, but it is higher than the value reported by Fisi et al.[54] by about six times the quoted errors.

CHAPTER IV

DECAY OF ^{56}Co

The ^{56}Co nucleus decay with a half-life of 78.8 days[57] by β^+, EC to the stable even-even nucleus ^{56}Fe. In the past, many experimental investigations[58-67] have been carried out, the relative intensities of some 44 gamma-ray transitions following the decay of ^{56}Co being widely required for calculations of the Ge(Li) detector's efficiency, in particular in the energy range up to 3.5 MeV. In the last 10 years few experimental investigations of the ^{56}Fe level scheme have been done, and only one experiment on the electromagnetic properties of the gamma-ray transitions has been carried out.

The present work has reinvestigated the energy level scheme of ^{56}Fe by measuring its gamma-ray transitions following the decay of ^{56}Co by means of Ge(Li) detectors arranged in singles and coincidence modes; the coincidence measurements being advantageously made using a dual-parameter data collection system. This chapter will survey previous work, report the results of the investigation on the decay of ^{56}Co and discuss the analyses of different types of spectra.

4.1 Previous investigations

Early investigations of the level scheme of ^{56}Fe from the decay of ^{56}Co and ^{56}Mn employing NaI(Tℓ) detectors arranged in singles and coincidence modes, have been reported (in 1959) by Kienle et al.[58], who proposed a simple ^{56}Fe level scheme of 10 levels and 17 gamma-ray transitions. Since then extensive and detailed studies of ^{56}Co decay using Ge(Li) detectors and NaI(Tℓ) were carried out by Kerm[59], Camp et al.[60], Gehrke et al.[61], Hautala et al.[62], McCallum et al.[63], Taylor et al.[64], Armitage et al.[65], Agarmal et al.[66] and Hofmann[67].

The relative intensity measurements for the calibration of Ge(Li) detectors have been carried out by Kerm[59], Camp et al.[60] and Gehrke

et al.[61]. The most recent work of Hantala et al.[62] provides a valuable comparison with that of McCallum et al.[63], both employing the known decay scheme of (P, γ) reaction resonances. McCallum et al.[63] endeavoured to prove the existence of systematic errors of more than 10% in the intensities of the higher energy gamma-rays, greater than 2 MeV, but Hautala et al.[62] were able to point out some defects of their work in connection with the construction of the efficiency curve. McCallum et al.[63] suggest the correction factor

$$F(E) = 1 \qquad E < 2$$

$$= 1.053 - 0.079\ E + 0.036\ E^2, \quad 2 \leq E \leq 5$$

where E is the gamma-ray energy in MeV, deduced from a comparison with published intensity values for both ^{56}Co[68] and ^{66}Ga[69] which leads to an overestimation when applied to ^{56}Co alone.

The gamma-gamma-directional correlation measurements of Taylor et al.[64] which leads to a proposed level scheme for ^{56}Fe gave no evidence to support the existence of the 2657 keV transition, but a level at 4447 keV was suggested for the first time.

The extensive studies of Armitage et al[65] from the $^{56}Fe(n,n'\gamma)$ and $^{56}Fe\ (p,n)^{56}Co$ reactions employing γ-γ directional correlation led to a proposed level scheme of 18 gamma ray transitions between 11 Energy levels. Agarwal et al[66] used NaI(Tℓ)- Ge(Li) detectors in the same technique provided a level scheme of 21 gamma ray transitions between 13 levels. In all the last mentioned γ-γ directional correlation measurements Multipole mixing ratios were measured for the most intense transitions.

The most recent experimental studies on the even-even ^{56}Fe nucleus using the same technique were performed by Hofman[67] in 1974, several weak γ-rays from the transition in ^{56}Fe were confirmed and added to the decay scheme; the 674.7 and 2657.4 keV gamma-rays were observed in his

work shown up in his proposed level scheme. In addition, he proposed a β^+,EC feeding of the level at 3600.3 keV. The resulting 44 gamma ray-transition level scheme was the last suggested and no more studies of this decay scheme have been carried out since.

Sher et al[70] proposed a level scheme of 23 γ-ray transitions between 14 levels in (1968) based on γ-γ coincidence measurements using a NaI(Tℓ) detector together with a small volume (0.85cc) Ge(Li) detector. No subsequent γ-γ coincidence measurements have been made in the intervening 12 years during which time the performance of Ge(Li) detectors have been greatly improved.

Pettersson et al[71] using magnetic spectrometer techniques on the decay of ^{56}Co measured K-electron intensities I(k) for 18 gamma-ray transitions. The values of I(k) obtained in ref. 71 for the γ-ray transitions at 3009.6 and 3451.2 keV showed very large discrepancies from those reported more recently by Metskvarishili et al[72].

As ^{56}Co is a very important calibration source, the high effficiency high resolution Ge(Li) detectors were used in γ-γ coincidence measurements to further establish the relative intensities of the gamma rays from the decay of ^{56}Co. This enabled a more realistic comparison of results to be made with the recent γ-γ directional correlation studies. Detailed investigations could then be undertaken of the ^{56}Fe energy level scheme.

4.2 Singles Spectra

Singles Spectra over the energy range from 200 keV up to 4 MeV were measured using the detectors Nos.6 and 7, and detector No.5 was used to give the Compton suppression spectrum in the lower energy region. The spectra taken using the suppression spectrometer were very useful as there were several low intensity gamma-ray lines located in the Compton scattering region from high intensity photopeak, these low energy low intensity transition photopeaks being shown in Fig.(4.1). The Compton

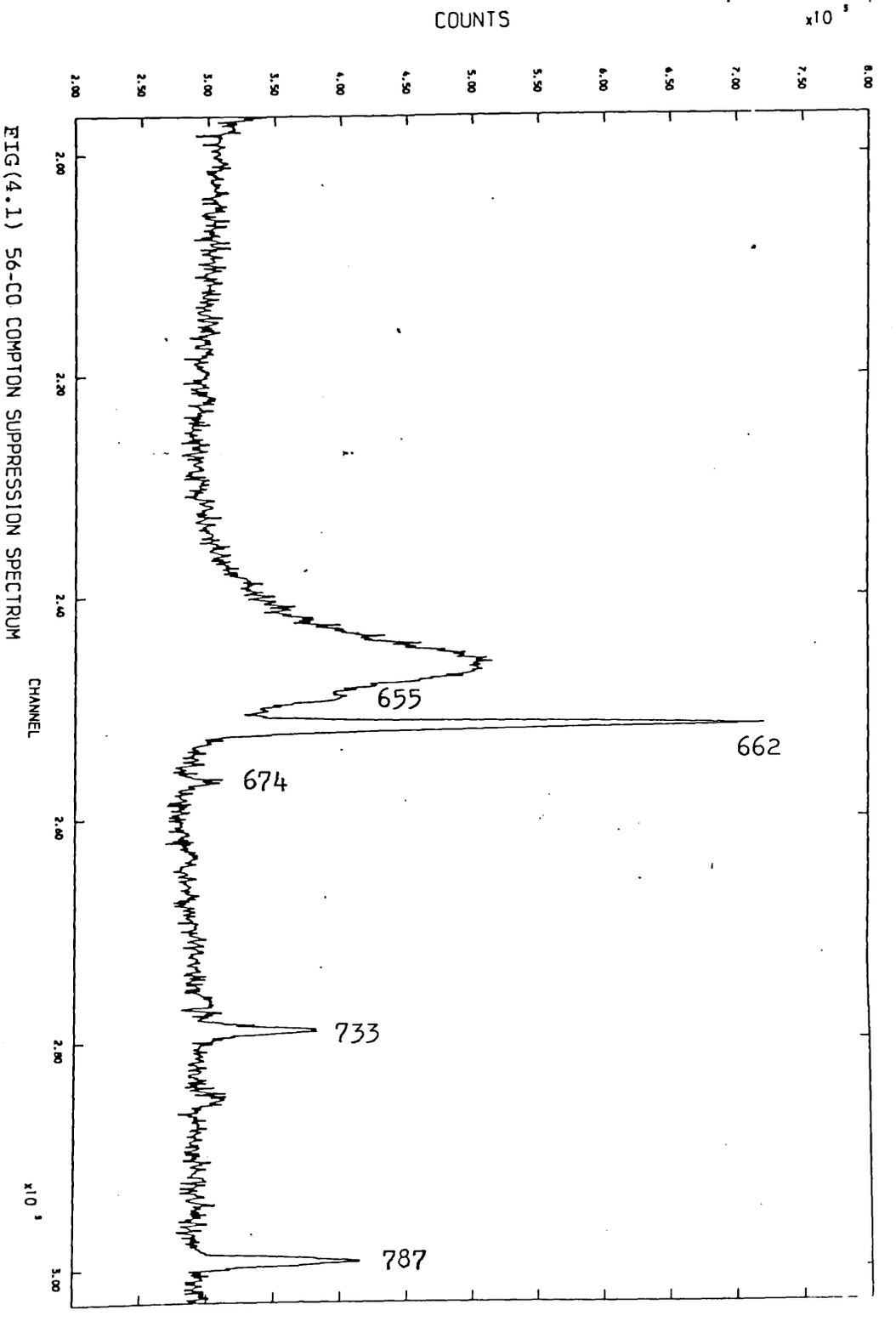

FIG(4.1) 56-CO COMPTON SUPPRESSION SPECTRUM

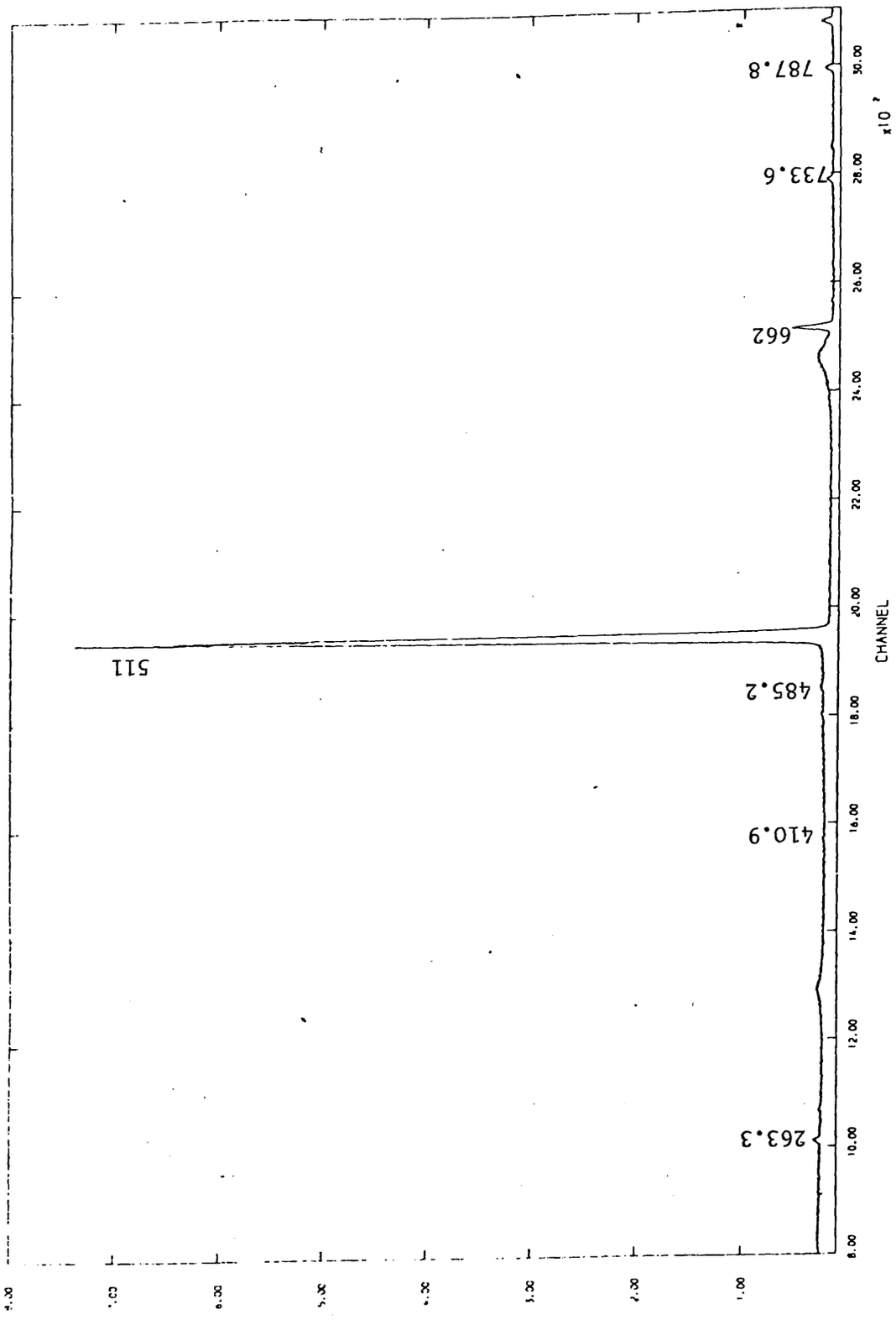

FIG(4.2) COMPTON SUPPRESSION FOR GAMMA-RAY UP TO 0.8 MEV

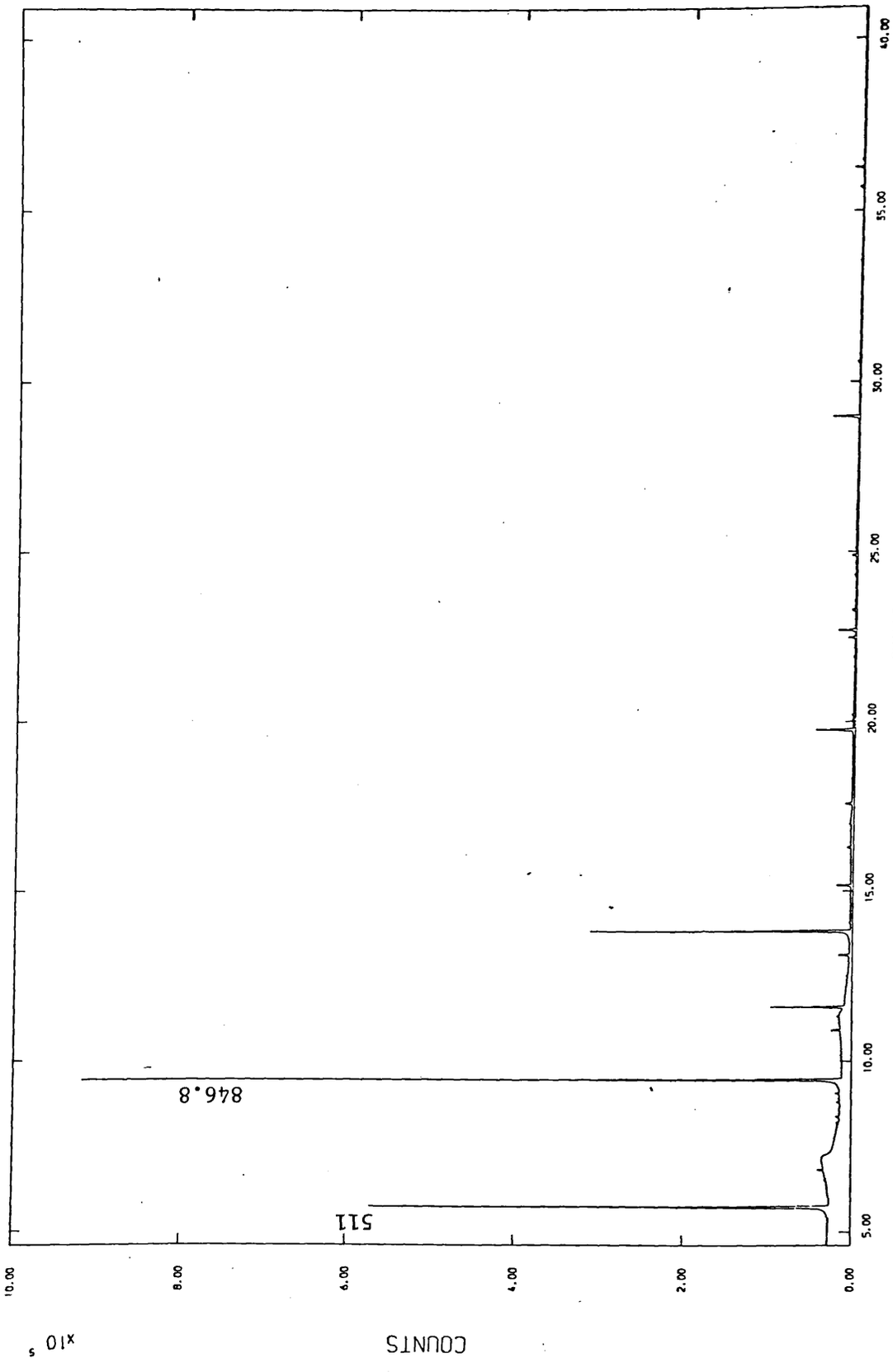

FIG(4.3a) 56-CO SINGLE SPECTRUM 0.12 DETECTOR

FIG(4.3b) EX-SITU SINGLE SPECTRUM 0.12 DETECTOR

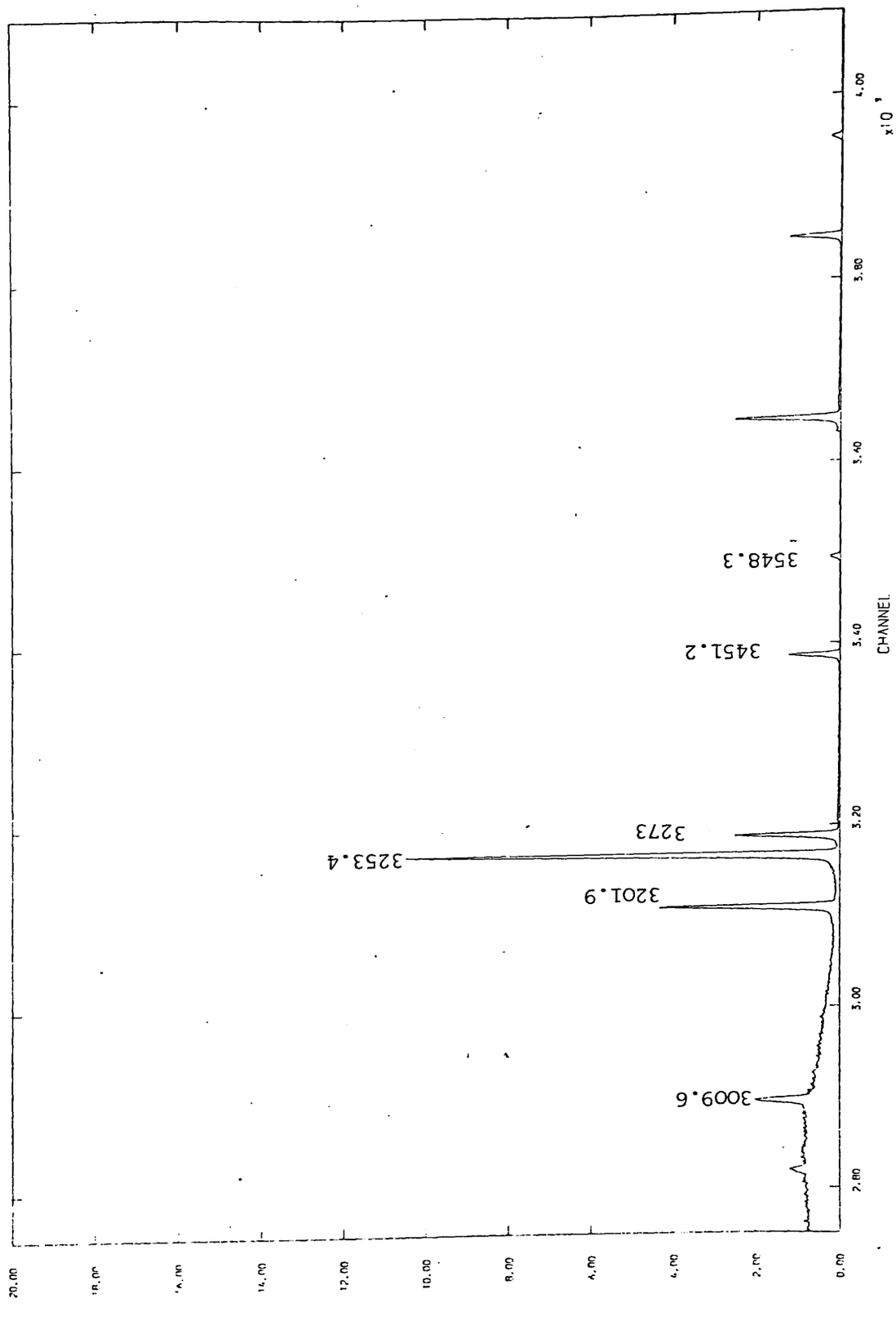

FIG(4.3c) 56-CO SINGLE SPECTRUM 0.12 DETECTOR

Table (4.1) Energies of gamma-ray emitted in the decay of ^{56}Co.

Present work *	Ref. (73)	Ref. (60)	Ref. (70)
263.34 (7)		263.40 (10)	
410.94 (10)		411.37 (8)	
485.2 (6)		486.53 (11)	
655.0 (2)			
674.7 (4)			
733.6 (1)		733.70 (15)	732.2 (5)
787.77 (4)		787.86 (7)	788.6 (5)
846.76 (1)	846.764 (6)	846.78 (6)	846.6 (5)
896.55 (6)		896.55 (20)	
977.39 (9)		977.46 (6)	977.7 (6)
996.48 (6)		997.30 (16)	
1037.84 (1)	1037.844 (4)	1037.83 (7)	1037.6 (5)
1089.31 (7)		1089.00 (24)	
1140.52 (18)		1140.25 (10)	
1160.0 (4)		1160.05 (16)	
1175.10 (2)	1175.099 (8)	1175.13 (8)	1175.3 (5)
1198.77 (6)		1198.75 (20)	
1238.28 (3)	1238.287 (6)	1238.28 (4)	1238.0 (5)
1272.20 (6)		1272.15 (60)	
1335.56 (4)		1335.53 (8)	
1360.21 (1)	1360.206 (6)	1360.22 (7)	1359.8 (5)
1442.65 (8)		1442.71 (8)	
1462.28 (4)		1462.30 (12)	
1640.38 (18)		1640.50 (13)	
1771.35 (6)	1771.350 (15)	1771.49 (6)	1771.4 (5)
1810.72 (11)	1810.722 (17)	1810.40 (50)	1810.7 (5)

Table (4.1) Energies of gamma-ray emitted in the decay of ^{56}Co, continued (2)

Present work *	Ref.(73)	Ref.(60)	Ref.(70)
1963.71 (14)	1963.714 (12)	1963.94 (6)	1963.4 (5)
2015.18 (18)	2015.179 (11)	2015.36 (3)	2015.3 (6)
2035.76 (7)	2034.759 (11)	2034.92 (6)	2034.9 (6)
2113.11 (6)	2113.107 (12)	2113.80 (15)	2112.8 (5)
2212.92 (5)	2212.921 (10)	2213.10 (15)	2213.0 (5)
2276.09 (20)		2276.30 (16)	
2373.71 (11)		2373.65 (40)	
2523.0 (24)		2523.80 (20)	
2598.46 (2)	2598.460 (10)	2598.58 (8)	2598.4 (5)
3009.59 (9)	3009.596 (17)	3010.20 (23)	3009.8 (5)
3201.95 (4)	3201.954 (14)	3202.30 (16)	3202.3 (5)
3253.42 (6)	3253.417 (14)	3253.60 (16)	3253.6 (5)
3272.99 (8)	3272.998 (14)	3273.25 (16)	3273.1 (5)
3369.97 (11)		3369.60 (30)	
3451.15 (6)	3451.154 (13)	3451.55 (20)	3451.3 (6)
3548.27 (18)		3548.05 (20)	3548.2 (6)
3600.85 (30)		3600.60 (40)	
3611.8 (50)		3611.60 (40)	

* The uncertainties (bracketed) are variations in the last digits of the best value. For example, 846.76(1) may be written as 846.76 ± 0.01 keV

Energy (keV)	Intensity related to I(847) = 1000				
	Present Work	Ref.(62)	Ref.(67)	Ref.(63)	Ref.(65)
263.34	0.22 ± 0.04		0.20 ± 0.06		
410.94	0.31 ± 0.04		0.25 ± 0.09		
485.2	0.69 ± 0.07		0.7 ± 0.02		
655.0	0.38 ± 0.08				
674.7	0.38 ± 0.07		0.3 ± 0.1		
733.6	1.95 ± 0.14	1.43 ± 0.13	1.65 ± 0.08		
787.77	3.2 ± 0.07	3.4 ± 0.3	2.9 ± 0.3	3.3 ± 0.3	
846.76	1000	1000	1000	1000	1000
896.55	0.63 ± 0.06	0.77 ± 0.1	0.62 ± 0.06		
977.39	14.1 ± 0.2	13.8 ± 0.4	13.7 ± 0.04	14.5 ± 0.7	11 ± 1
996.48	0.92 ± 0.14	1.7 ± 0.14	1.7 ± 0.5		
1037.84	141.1 ± 1.9	135.0 ± 2	142.4 ± 1.4	133.4 ± 2.5	96 ± 6
1089.31	0.5 ± 0.07	0.6 ± 0.2	0.7 ± 0.2		
1140.52	1.25 ± 0.06	1.17 ± 0.13	1.3 ± 0.02		
1160.0	0.74 ± 0.08	0.8 ± 0.1	0.78 ± 0.07		
1175.10	23.0 ± 0.32	21.1 ± 1.0	22.5 ± 1.1	21.2 ± 1.2	19 ± 2
1198.77	0.4 ± 0.1	0.44 ± 0.08	0.28 ± 0.09		
1238.28	684.7 ± 8.7	651.0 ± 4	676.4 ± 6.8	686.0 ± 4	696.0 ± 35
1272.20	0.38 ± 0.06	0.35 ± 0.04	0.22 ± 0.03		
1335.56	1.28 ± 0.06	1.2 ± 0.2	1.2 ± 0.12		
1360.21	43.2 ± 0.6	42.4 ± 1.5	43.5 ± 1.2	42.7 ± 0.4	46 ± 3
1442.65	1.73 ± 0.07	1.95 ± 0.1	1.77 ± 0.09		

Table (4.2) Relative intensities of the gamma-rays in the decay of ^{56}Co

Energy (keV)	Intensity related to I(847) = 1000				
	Present Work	Ref. (62)	Ref. (67)	Ref. (63)	Ref. (65)
1462.28	0.91 ± 0.13		0.65 ± 0.12		
1640.38	0.62 ± 0.07	0.5 ± 0.1	0.63 ± 0.06		
1771.35	155.0 ± 4.0	152.6 ± 1.5	157.8 ± 1.6	157.2 ± 2.2	162 ± 10
1810.72	6.29 ± 0.13	5.9 ± 0.3	6.3 ± 0.3		
1963.71	7.19 ± 0.15	7.0 ± 0.2	7.1 ± 0.3	7.0 ± 0.3	9 ± 2
2015.18	31.82 ± 0.66	29.7 ± 0.3	30.95 ± 0.31	29.8 ± 0.5	39 ± 3
2034.76	81.4 ± 1.7	76.4 ± 0.6	79.5 ± 0.8	77.7 ± 2.0	82 ± 5
2113.11	3.75 ± 0.14	3.4 ± 0.2	3.7 ± 0.2	3.8 ± 0.1	3 ± 1
2212.92	4.2 ± 0.2	3.9 ± 0.2	3.6 ± 0.2		
2276.09	1.17 ± 0.09	1.5 ± 0.2	1.28 ± 0.08		
2373.71	0.97 ± 0.12	0.5 ± 0.06	0.59 ± 0.12		
2523.0	0.79 ± 0.11	0.84± 0.09	0.44 ± 0.1		
2598.46	174.0 ± 3.8	171.9 ± 1.5	168.5 ± 1.7	175.1 ±2.0	187 ± 11
2657.4	< 0.05	0.29± 0.04	0.16 ± 0.05		
3009.59	8.4 ± 0.4	10.5 ± 0.3	9.8 ± 0.9	9.9 ± 0.5	9 ± 5
3201.95	30.3 ± 0.7	32.4 ± 0.3	30.3 ± 0.3	33.6 ± 0.5	30 ± 2
3253.42	76.0 ± 1.5	79.7 ± 1.1	73.9 ± 0.75	81.2 ± 0.9	71 ± 4
3272.99	18.15 ± 0.36	18.4 ± 0.3	17.55 ± 0.18	18.2 ± 0.4	13 ± 1
3369.97	0.11 ± 0.02	0.1 ± 0.01	0.08 ± 0.02		
3451.15	9.0 ± 0.2	9.5 ± 0.2	8.9 ± 0.4	9.6 ± 0.2	8 ± 1
3548.27	1.96 ± 0.06	1.96± 0.05	1.78 ± 0.09	2.0 ± 0.1	1 ± 1
3600.85	0.15 ± 0.02	0.12± 0.03	0.16 ± 0.02		
3611.80	0.10 ± 0.02	0.05± 0.02	0.08 ± 0.02		

Table (4.2) continued. Relative intensities of the gamma-rays in the decay of ^{56}Co

suppression spectrum for gamma ray energies less than 0.8 MeV is also shown in Fig.(4.2).

The detector efficiencies detailed in section (2.2) and singles spectra have been measured using the set up discussed in section (2.1). Singles spectrum for the gamma-ray following the decay of ^{56}Co measured by the 12% efficient detector is shown in Fig.(4.3).

The data collected were analyzed with the program SAMPO[39,40] on the University of London CDC 6600 computer as described in section (2.2). The measured energies of the gamma-ray transitions are listed in Table (4.1) together with recently published values. The relative intensities of the 44 gamma-ray transitions measured following the decay of ^{56}Co compared with the recently published intensity values are given in Table (4.2).

4.3 Coincidence results

Coincidence experiments were performed with two large-volume detectors (Nos. 6 and 7) coupled to the 4096 X 4096 Dual-Parameter Data collection system (experimental details in Chapter 3). The coincidence data written on 6 magnetic tapes were analyzed at a later time after the data collection, by setting the digital windows on a particular region of interest in the spectrum from the 10% efficient detector. In the decay of ^{56}Co the coincidence relationships could be thoroughly investigated using 9 prominent gamma-rays in the energy range from 788 keV to 3.2 MeV. The ^{56}Co total spectrum is shown in Fig.(4.4). The Coincidence spectra corrected for chance and background coincidences are shown in Figs.4(5-13). A summary of the coincidence results is given in Table (4.3). The gamma ray gates which are necessary to establish the features of the ^{56}Fe level scheme are listed in the first row. The observation of a gamma-ray in the spectrum in coincidence with a gating

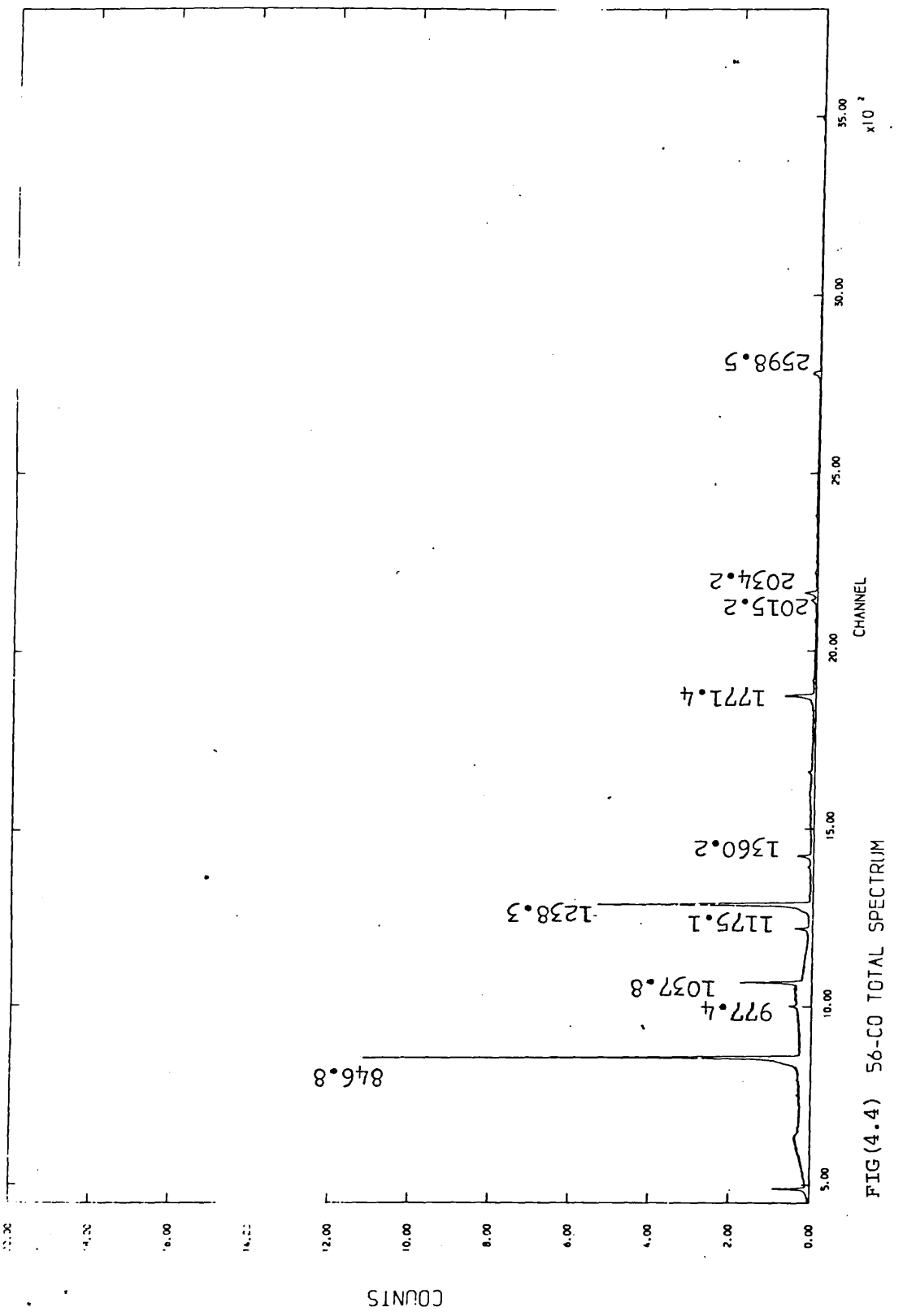

FIG(4.4) 56-CO TOTAL SPECTRUM

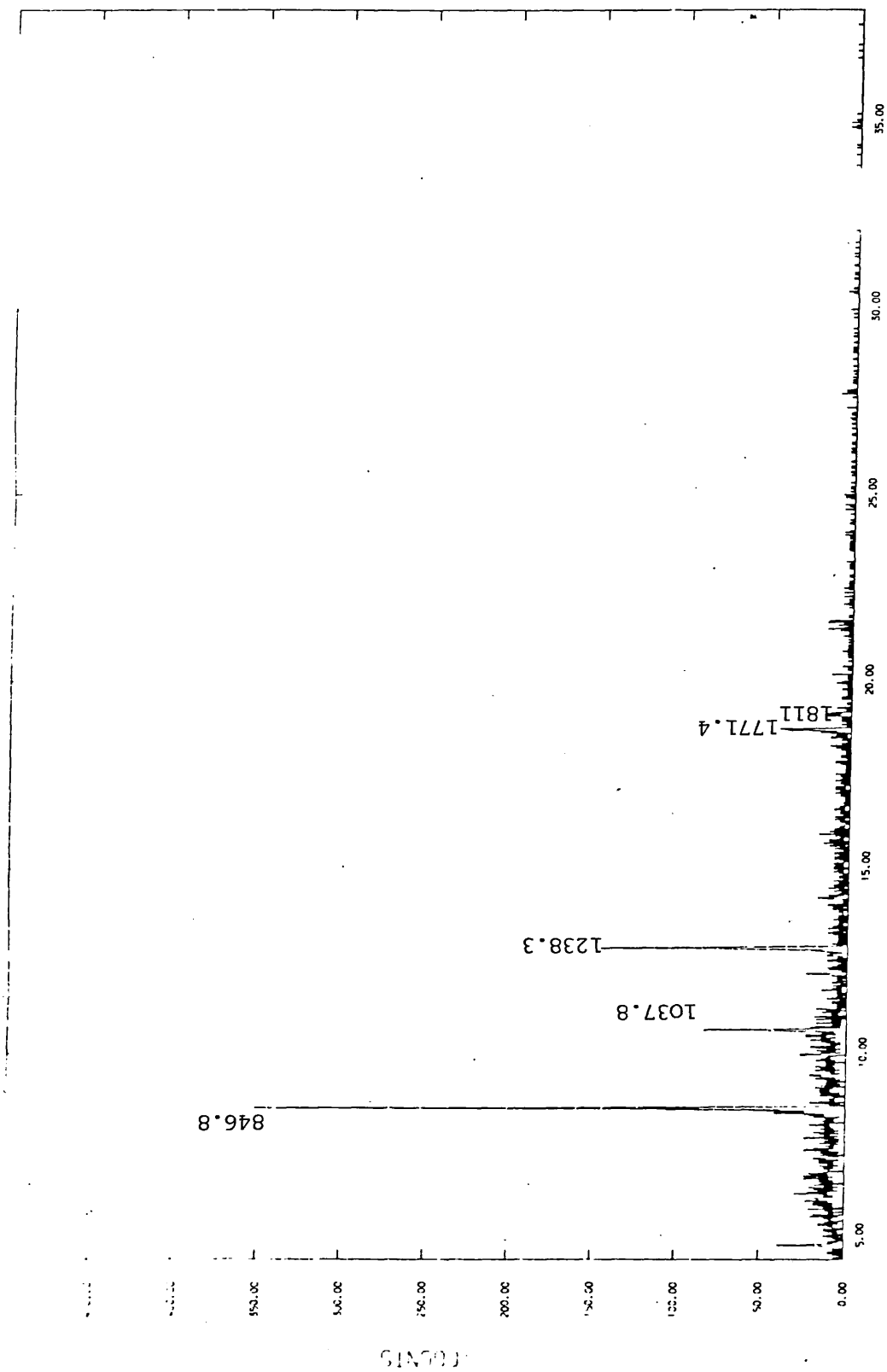

FIG(4.5) SPECTRUM OF 56- CO IN COINCIDENCE WITH 788 KEV

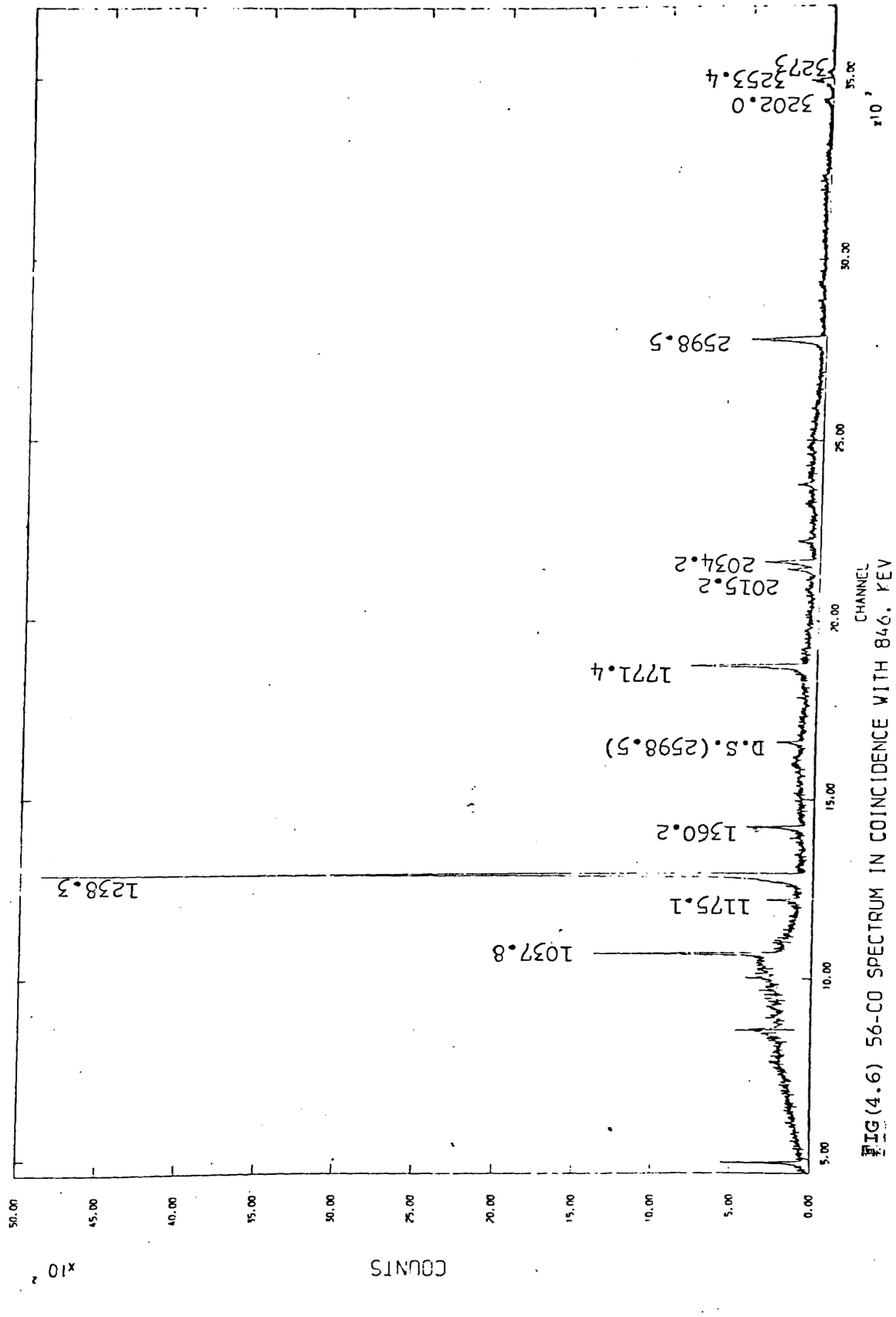

FIG (4.6) 56-CO SPECTRUM IN COINCIDENCE WITH 846. KEV

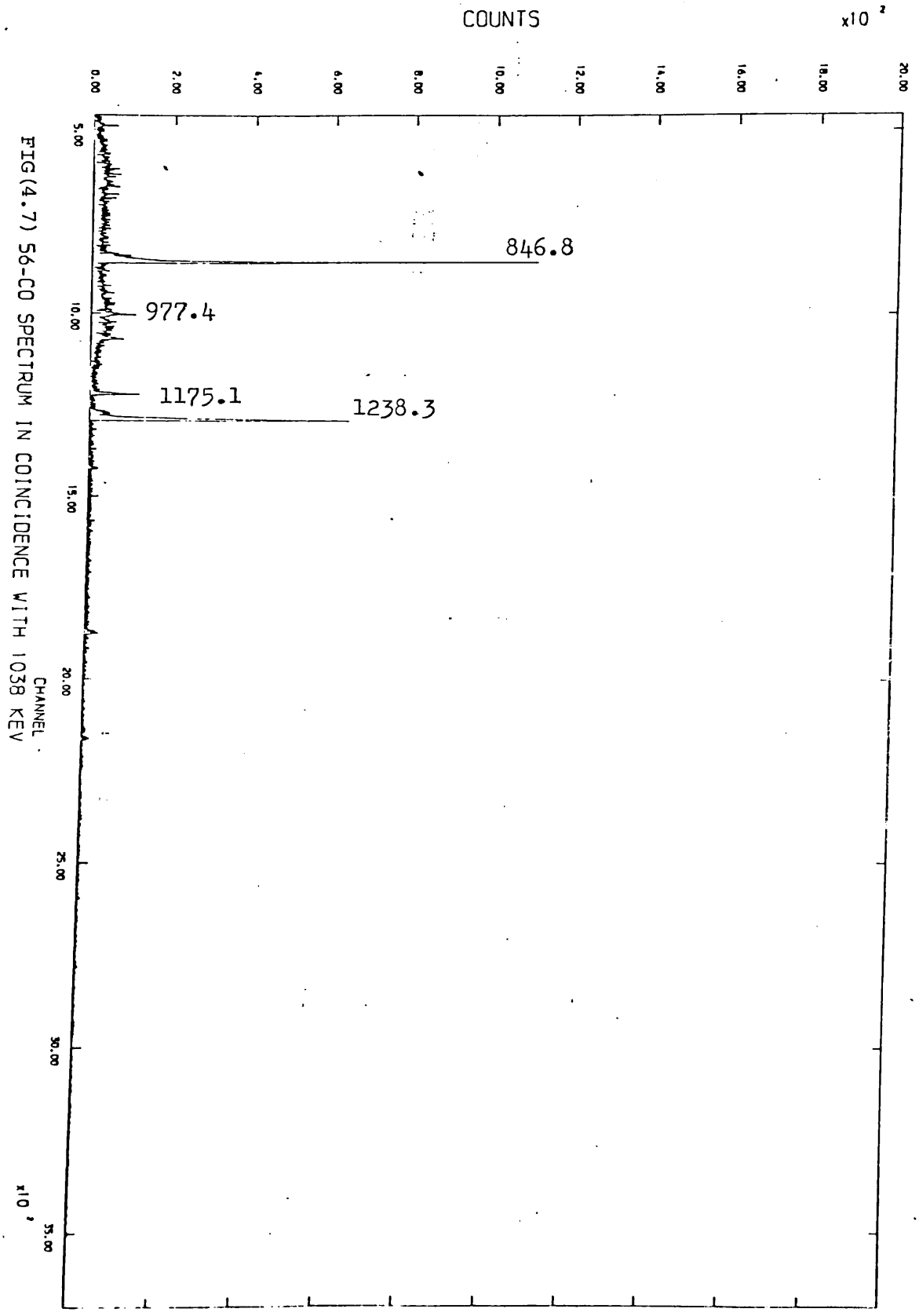

FIG(4.7) 56-CO SPECTRUM IN COINCIDENCE WITH 1038 KEV

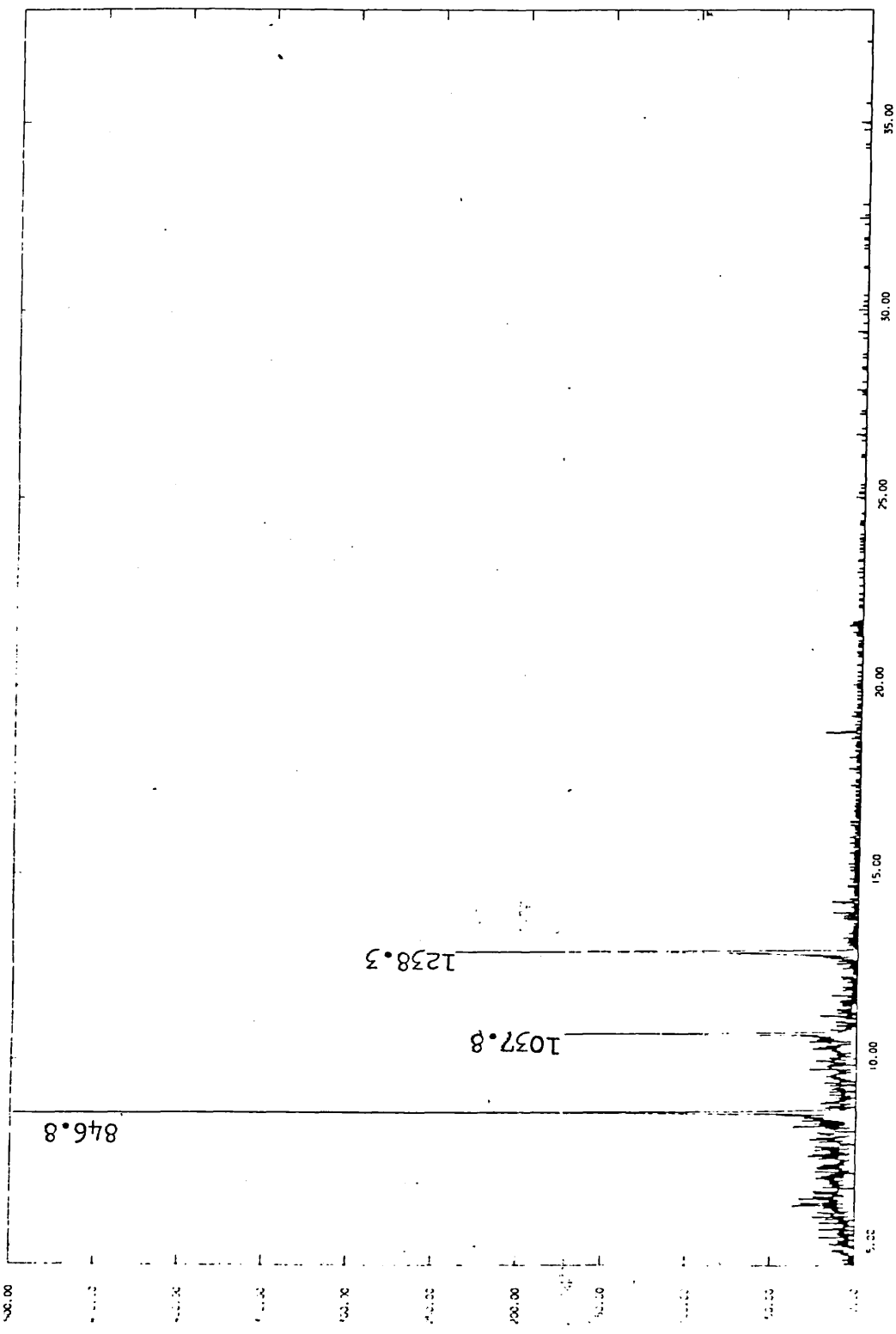

FIG(4.8) SPECTRUM OF 56- CO IN COINCIDENCE WITH 1175 KEV

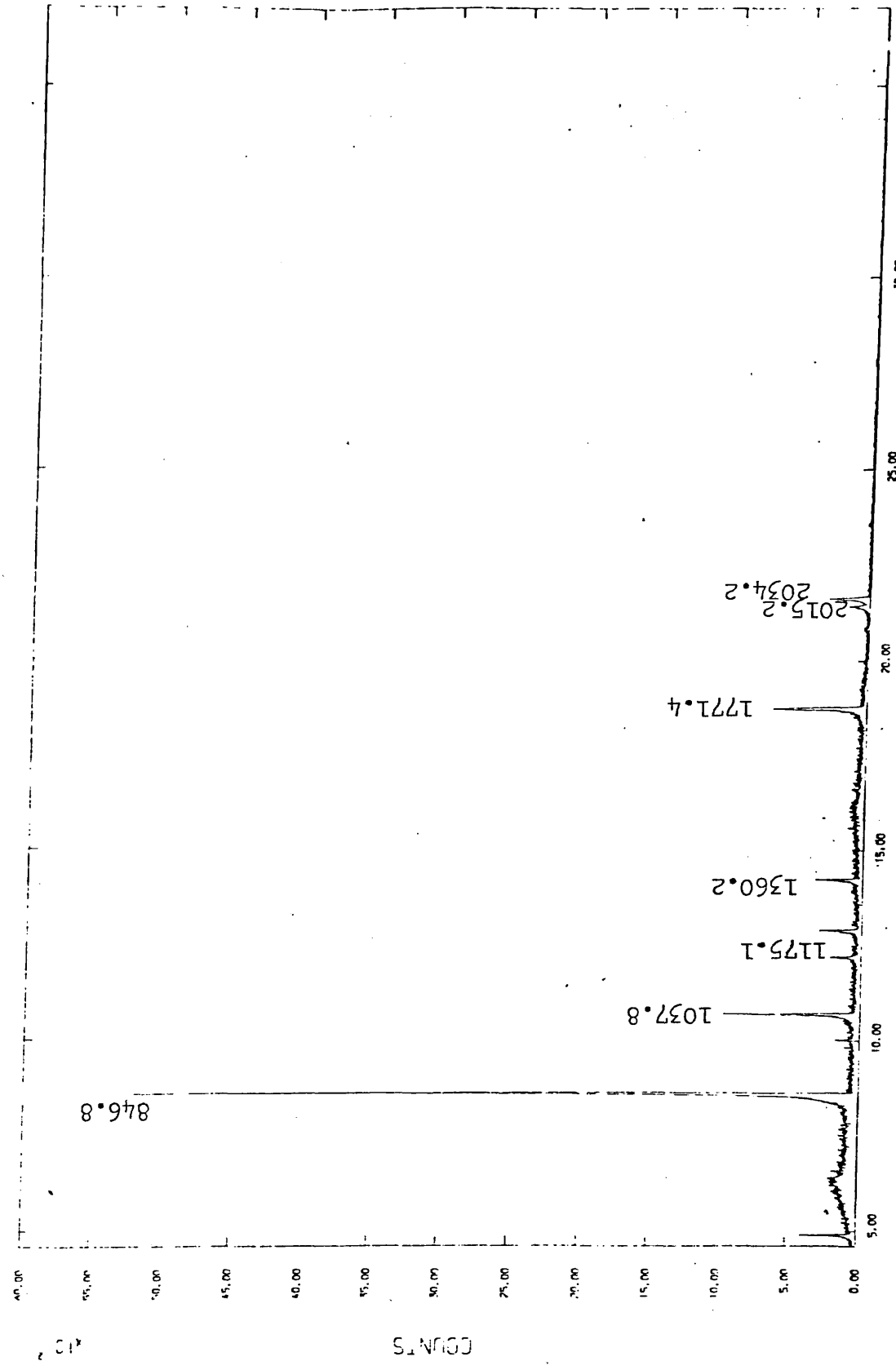

FIG(4.9) 56-CO SPECTRUM IN COINCIDENCE WITH 1238 KEV

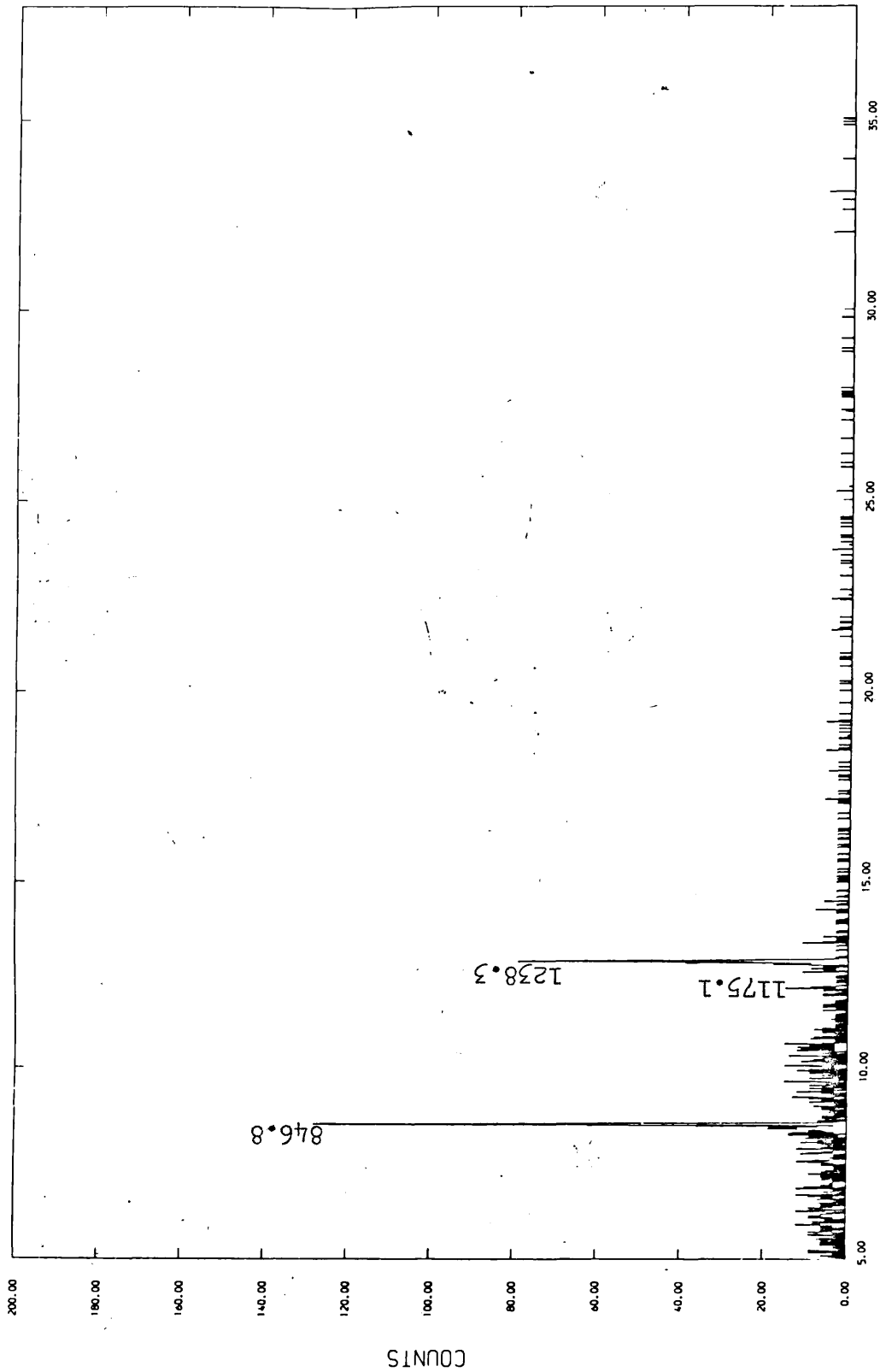

FIG(4.10) SPECTRUM OF 56- CO IN COINCIDENCE WITH 1335 KEV

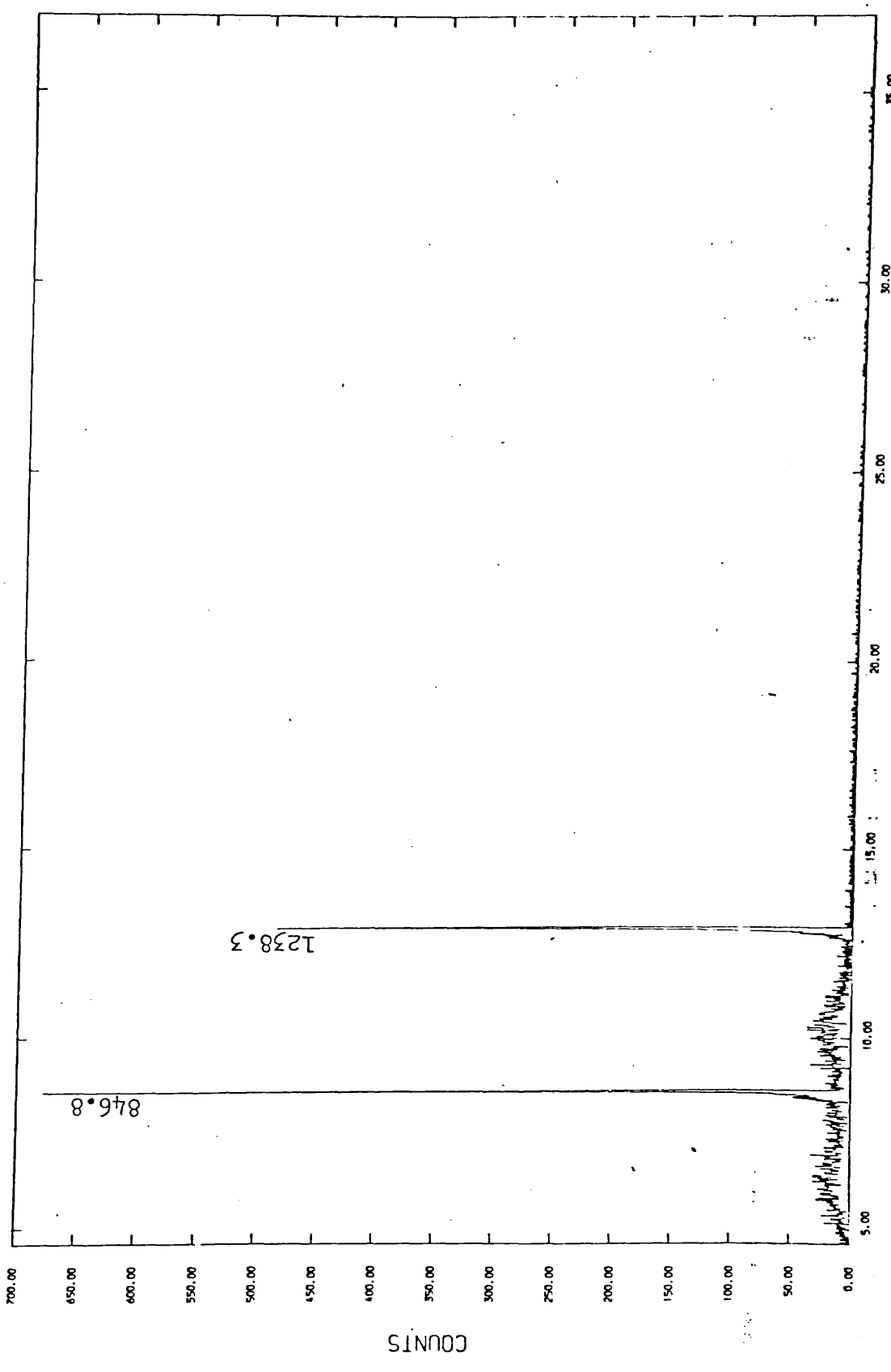

FIG(4.11) 56-CO SPECTRUM IN COINCIDENCE WITH 1771 KEV

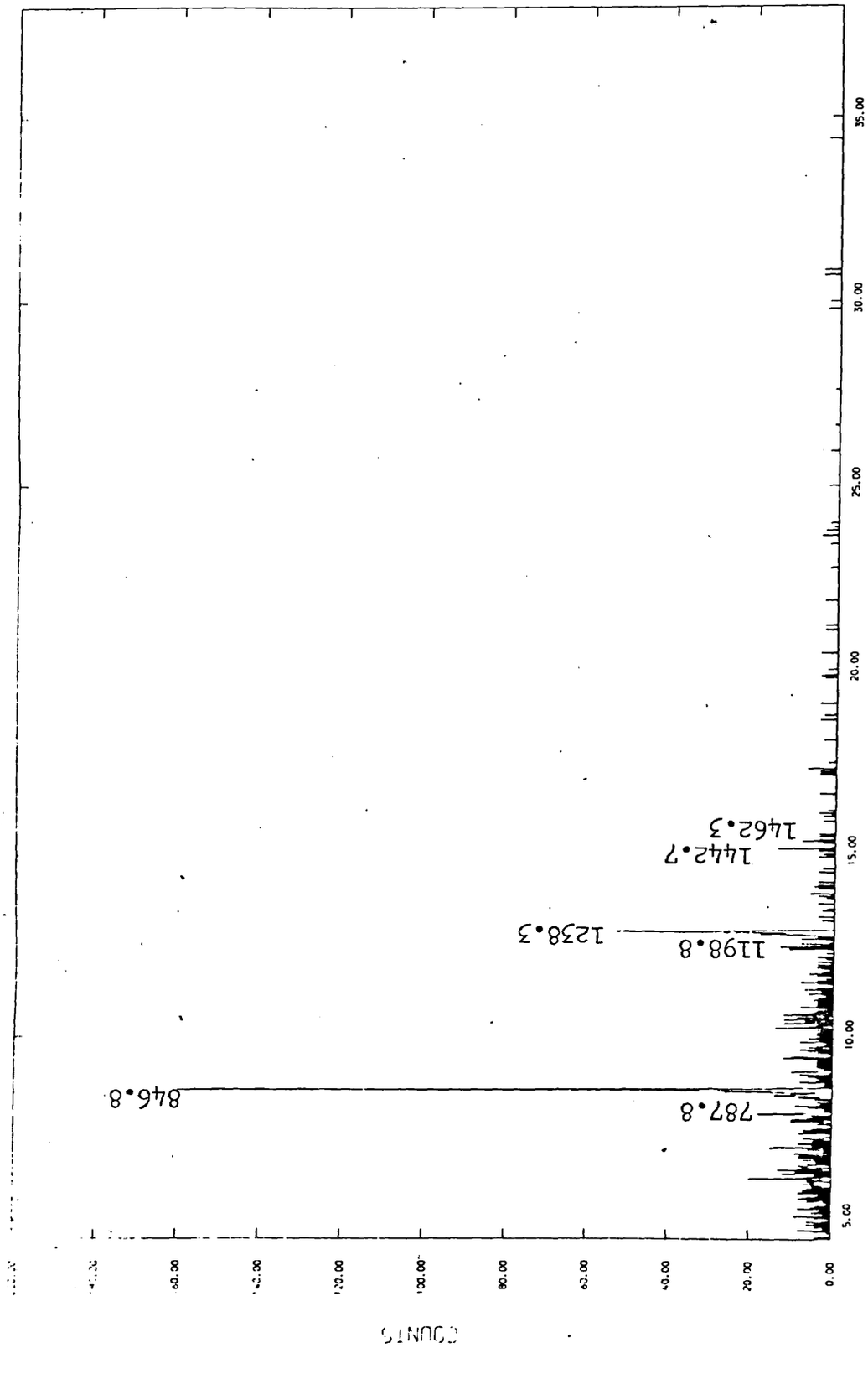

FIG(4.12) SPECTRUM OF 56- CO IN COINCIDENCE WITH 1810 KEV

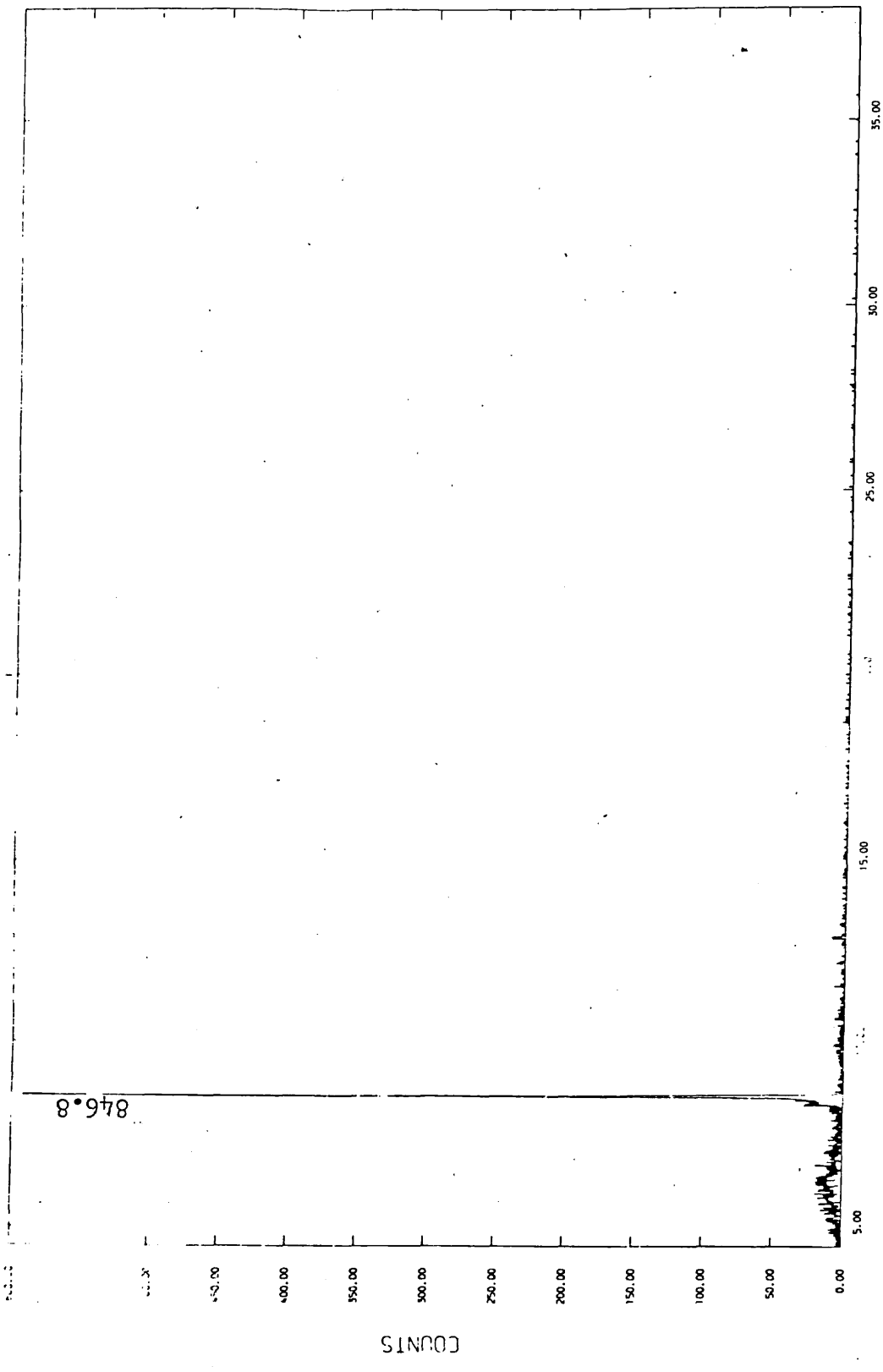

FIG(4.13a SPECTRUM OF 56-Co IN COINCIDENCE WITH 2598 KEV

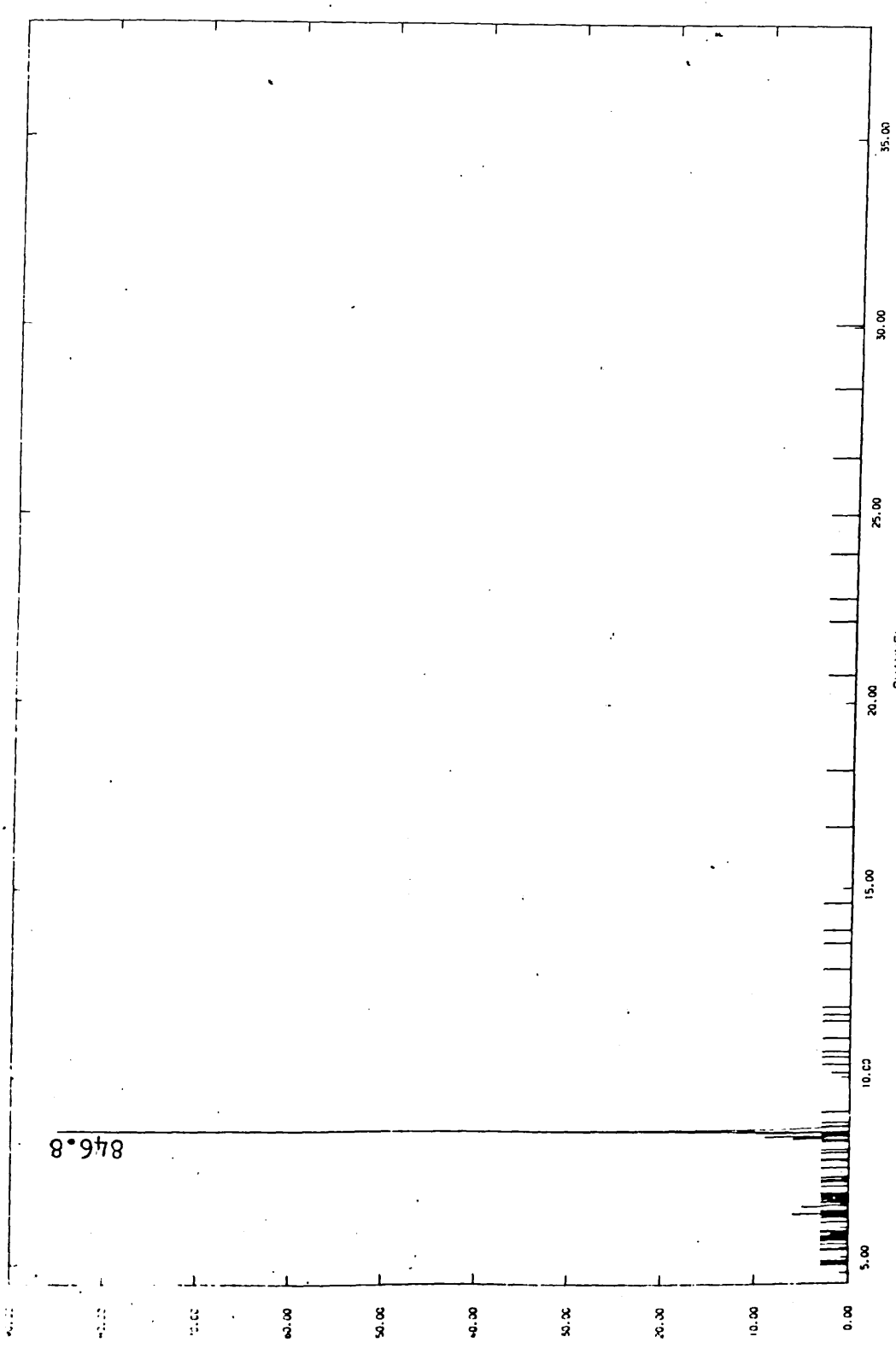

FIG(4.13b SPECTRUM OF 56- CO IN COINCIDENCE WITH 3202 KEV

E_γ \ Gate (keV)	768	846	1038	1175	1238	1335	1771	1810	2034	2113	2598	3202
263.34							P					
410.94												
485.2			S									
655.0											W	
674.7												
733.6												
787.77								VS				
846.77	S		VS	S	VS	S	S	VS	S	S	VS	VS
896.55										P		
977.39			P									
996.48			P									
1037.85	W			VS		VS	VW					
1089.31										P		
1140.52										W		
1160.00										W		
1175.09												
1198.77								S				
1238.28	W	VS		S		S	VS	S	VS	VW		
1272.2												
1335.56				VS								
1360.20				W								
1442.62								S				
1462.28								W				
1640.38								VW				
1771.33	W			W								
1810.72	VS	VS										
1963.71												
2015.18	W											
2034.76	W											
2113.10		S			VW							
2212.92												
2276.09		S										
2373.71												
2523.0		W										
2598.46		VS										
2657.4												
3009.59		VS										
3201.96		VS										
3253.42		VS										
3273.00		VS										
3369.97												
3451.15		S										
3548.27		S										
3600.85		S										
3611.8		S										

Table (4.3) A summary of coincidence results

gamma-ray is indicated in the Table by one of the following entries: VS, S, W, VW or P. These entries give the strength of the observed gamma-ray relative to the other gamma-rays in the coincidence spectrum and they represent Very Strong, Strong, Weak, Very Weak and Probable, respectively. The last entry (P) represents a coincidence relationship which, within the error limits of the coincidence data is probable, yet not conclusive. Table (4.4) gives the mean energy level values from the energysum relation.

4.4 Decay scheme and spin-parity assignments

Based on the coincidence results and energy sum relations the decay scheme of ^{56}Fe was obtained and is shown in Fig.(4.14). The log ft values, spin and parity assignments, together with the β^+ energies and its feeding branching ratios for each level are given in Table (4.5). The log ft was evaluated using the Mozkowaki[74] monograms. The β^+ Q value of 4567.9 keV used was taken from ref.[75]. The experimental K-shell internal-conversion coefficients $\alpha(K)$ for transitions in ^{56}Fe are compared with the theoretical values corresponding to E1, E2 and M1 multipolarity in Table (4.6a). The experimental $\alpha(K)$ values were calculated using the γ-ray intensities reported here (Table 4.2) and the K-electron intensities I(K) of Pettersson et al[71]. The theoretical results were taken from Rose[76] for transitions <1 MeV and from Trusov[77] for transitions above 1 MeV. Table (4.6b) shows a comparison with $\alpha(K)$ calculated from the more recent I(K) values of Meskvarishvili et al.[72] indicating very large discrepancies for both the 3009.6 and 3451.2 keV transitions and indicates a (M1/E2) multipolarity.

The Table (4.3) shows that most of the gamma-rays are in coincidence with the 846.8 keV gamma-rays. This result is to be expected because the spin of the ground state of the ^{56}Co nucleus as given by Auble[78] is 4^+

Table (4.4) Energy sum relations

Energy of transition (keV)	Energy Sum (keV)	Energy level (keV)
846.76		846.76
846.76 + 1238.28	2085.04	2085.04
1810.72 + 846.76	2657.48	2657.48
2113.11 + 846.76	2959.87	2959.87
1037.84 + 1238.28 + 846.76	3122.88	3122.88
2276.17 + 846.76	3211.88	
3369.97	3369.97	3369.95
2523.17 + 846.76	3369.93	
2598.46 + 846.76	3445.22	3445.22
1360.21 + 1238.28 + 846.76	3445.25	
787.72 + 1810.72 + 846.76	3445.20	
410.94 + 2598.46 + 846.76	3856.16	3856.36
485.2 + 3359.97	3856.17	
733.6 + 1037.84 + 1238.28 + 846.76	3856.48	
896.55 + 2113.11 + 846.76	3856.42	
1198.97 + 1810.76 + 846.76	3856.49	
1771.35 + 1238.28 + 846.76	3856.39	
3009.59 + 846.76	3856.35	

Table (4.4) continued (2)

Energy of transition (keV)	Energy Sum (keV)	Energy level (keV)
1089.31 + 2113.11 + 846.76	4049.18	4048.71
1963.21 + 1238.28 + 846.76	4048.25	
3201.95 + 846.76	4048.71	
655.0 + 2598.46 + 846.76	4100.22	
977.39 + 2276.09 + 846.76	4100.24	4100.22
1140.52 + 2113.11 + 846.76	4100.39	
1442.65 + 1810.72 + 846.76	4100.14	
2015.18 + 1238.28 + 846.76	4100.24	
3253.42 + 846.76	4100.18	
263.34 + 411.2 + 2598.46 + 846.76	4119.76	4119.78
674.7 + 2598.46 + 846.76	4119.92	
996.48 + 2276.09 + 846.76	4119.33	
1462.28 + 1810.72 + 846.76	4119.76	
2034.76 + 1238.28 + 846.76	4119.80	
1160.10 + 2113.11 + 846.76	4119.97	
3272.99 + 846.76	4119.75	
1175.10 + 1037.84 + 1238.28 + 846.76	4297.98	4297.97
1640.38 + 1810.72 + 846.76	4297.98	
2212.94 + 1238.28 + 846.76	4297.98	
3451.15 + 846.76	4297.91	

Table (4.4) continued (3)

Energy of transition (keV)	Energy Sum (keV)	Energy level (keV)
1272.2 + 1037.84 + 1238.28 + 846.76	4395.03	4395.03
3548.27 + 846.76	4395.03	
3600.82 + 846.76	4447.58	4447.58
1335.56 + 1037.84 + 1238.28 + 846.76	4458.38	4458.56
2373.7 + 1238.28 + 846.76	4458.74	
3611.8 + 846.76	4458.56	

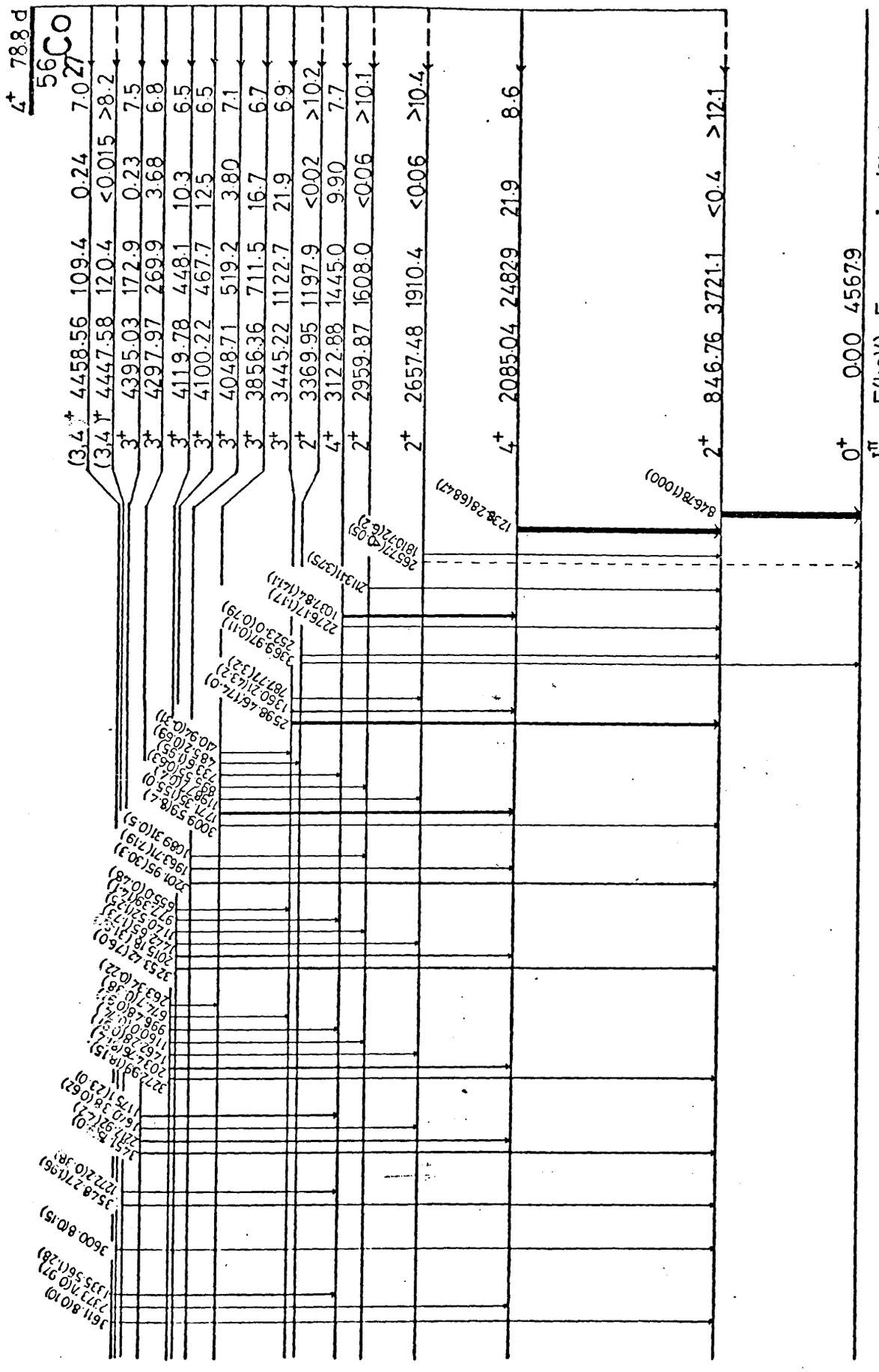

Fig(4.14) The ^{56}Fe level scheme

Energy level (leV)	ΣI_γ feed	ΣI_γ decay	B.R.	E^+EC	log ft	J^π
846.76	99.6	100	< 0.4	3721.1	>12.1	2^+
2085.04	46.59	68.47	21.9	2482.9	8.6	4^+
2657.48	0.56	0.62	< 0.06	1910.4	>10.4	2^+
2959.87	0.315	0.375	0.06	1608.0	10.1	2^+
3122.88	4.38	14.28	9.90	1445.0	7.7	4^+
3369.95	0.069	0.09	< 0.02	1197.9	> 0.2	2^+
3445.22	0.069	22.04	21.9	1122.7	6.9	3^+
3856.36	0.02	16.72	16.7	711.5	6.7	2^+
4048.71	-	3.799	3.80	519.9	7.1	3^+
4100.22	-	12.52	12.5	467.7	6.5	3^+
4119.78	-	10.27	10.3	448.1	6.5	3^+
4297.97	-	3.682	3.68	269.9	6.8	3^+
4395.03	-	0.0234	0.23	172.9	7.5	4^+
4447.58	-	0.015	< 0.015	120.4	> 8.2	3^+, 4^+
4458.56	-	0.235	0.24	109.4	7.0	3^+, 4^+

Table (4.5) Deduced spins and parities of levels in ^{56}Fe from the available information.

E_γ (keV)	$I_i^{\pi_i} \rightarrow I_f^{\pi_f}$	Experimental $\alpha(K) \times 10^4$	Theoretical $\alpha(K)$			Adopted Multipolarity
			E1	E2	M1	
733.6	$3^+ \rightarrow 4^+$	2.51 (54)	1.30	3.78	2.58	M1
787.77	$3^+ \rightarrow 2^+$	2.66 (26)	1.18	3.08	2.28	M1/E2
846.76	$2^+ \rightarrow 0^+$	2.6	1.22	2.60	1.97	E2
977.39	$3^+ \rightarrow 4^+$	1.39 (5)	0.81	1.88	1.45	M1
1037.84	$4^+ \rightarrow 4^+$	1.33 (10)	0.72	1.66	1.30	M1
1175.10	$3^+ \rightarrow 4^+$	0.94 (21)	0.57	1.22	0.99	M1
1238.29	$4^+ \rightarrow 2^+$	1.012 (18)	0.518	1.048	0.915	E2
1360.21	$3^+ \rightarrow 4^+$	0.764 (16)	0.445	0.902	0.768	M1
1771.35	$3^+ \rightarrow 4^+$	0.472 (18)	0.270	0.480	0.460	M1/E2
1963.71	$3^+ \rightarrow 4^+$	0.389 (17)	0.248	0.430	0.388	M1
2015.18	$3^+ \rightarrow 4^+$	0.389 (20)	0.236	0.405	0.374	M1/E2
2034.76	$3^+ \rightarrow 4^+$	0.372 (13)	0.232	0.400	0.370	M1
2598.46	$3^+ \rightarrow 2^+$	0.260 (8)	0.168	0.264	0.248	M1/E2
3009.60	$3^+ \rightarrow 2^+$	0.262 (72)	0.136	0.212	0.200	M1/E2
3201.95	$3^+ \rightarrow 2^+$	0.209 (11)	0.127	0.189	0.183	M1/E2
3253.42	$3^+ \rightarrow 2^+$	0.195 (9)	0.124	0.186	0.178	M1/E2
3273.00	$3^+ \rightarrow 2^+$	0.191 (17)	0.122	0.181	0.176	M1/E2
3451.15	$3^+ \rightarrow 2^+$	0.113 (20)	0.114	0.167	0.164	E1

(a) Comparison with theory

E_γ (keV)	$\alpha(K) \times 10^4$	
	I(K) from [71]	I(K) from [72]
2598.46	0.260 (8)	0.260
3009.60	0.262 (72)	0.174 (29)
3201.95	0.209 (11)	0.206 (22)
3253.42	0.195 (9)	0.186 (19)
3273.00	0.191 (17)	0.185 (19)
3451.15	0.113 (20)	0.143 (16)

(b) Dependence on experimental K-electron intensities

Table (4.6) K-shell internal-conversion coefficients

and therefefore the β^+, EC decay will primarily populate levels with spins and parities 3^+ or 4^+. Levels of such high spin would be expected to decay primarily to the 2^+ first excited state rather than decay to the even-even ground state ^{56}Fe nucleus of 0^+ spin parity.

The coincidence between the 3600.8 keV and the 846.8 keV gamma-rays would suggest a level in ^{56}Fe at 4447.6 keV which was not shown in the decay scheme proposed by Hofmann[67], but he had suggested the level at 3600.8 as a β^+, EC fed level, decaying to the ground state by the 3600.8 keV transition. This level of 4447.6 was previously suggested in the level scheme proposed by Taylor et al[64] based on their results from γ-γ directional correlation measurements, but no definite evidence for its existence was forthcoming so the origin of the 3600.8 keV gamma-ray line was not certain.

A new 655.0 keV gamma-ray seen for the first time in this work in singles and Compton spectra is located as shown in Fig.(4.1) in the Compton edge of the major gamma-ray peak of 846.8 keV, so that the relative intensity of this transition could not be calculated by SAMPO except only in Compton suppression spectrum; however, the γ-ray was placed in the decay scheme arising from the gamma-transition between the (3^+) 4100.22 keV level and the (3^+) 3445.22 keV level.

The 2085.04 keV level (log ft = 8.6) is observed to decay to the 846.76 keV (2^+) level via the 1238.28 keV transition which appears to be a pure (E2) transition so that the established spin and parity assignment of 4^+ is verified.

The 2657.48 keV level (log ft >10.4) is observed to decay to the 846.76 keV (2^+) level by the 1810.72 keV transition. This level is mainly fed by the 787.65 keV (M1/E2) transition and the possibility of β^+, EC feeding is very poor so that the probable value of spin-parity is 2^+.

The γ-ray transition of 2657.7 keV from this level to the 0^+ ground state level is not seen in the coincidence spectrum, or in any of the singles spectra. Additional data taken using a Compton suppression spectrometer in a special investigation to look for this transition did not show any evidence at more than 5×10^{-5} relative to the intensity of the 846.76 keV line.

The 2959.87 keV level (log ft = 10.1) is established from the strong coincidence between the 846.76 keV gamma-ray arising by a pure (E2) transition from the first excited state to the ground state and the 2113.11 keV gamma-ray from this level to the first excited state. The log ft value suggests a spin parity assignment of 2^+.

The gamma-ray seen at 1037.85 keV suggests an M1 transition between the 3122.88 keV level (log ft = 7.7) and the second excited 4^+ state at 2085.04 keV and provides a spin-parity assignment of either 4^+ or 3^+ for the former level, but the calculated log ft value clearly indicates a spin-parity of 4^+.

The 3445.22 keV level (log ft = 6.9) is established from the strong coincidence between the 846.76 keV gamma ray and the 2598.54 keV gamma-ray in an (M1/E2) transition. The 1360.22 keV (M1) transition from this level to the 4^+ 2085.04 keV level and the log ft value verify the established spin parity assignment of 3^+.

The 3856.36 keV level (logft= 6.7) is established from the coincidence between the 3009.6 keV and the 846.7 keV gamma-rays from another coincidence between the 1171.4 keV and 1238.3 keV gamma-rays. The gamma-rays of 733.6, 1771.5 and 3009.6 keV from the level cause transitions to the levels at 3122.8, 2085 and 846.7 keV respectively, which appear to be M1 transitions so the spin parity assignment of the 3856.36 keV level is taken to be 3^+.

The energy level at 4100.22 keV (log ft = 6.5) yields pure (M1) transitions of 977.5 keV and 3253.63 keV to the 3122.88 keV (4^+) and 846.8

keV (2^+) levels respectively, which suggests a spin parity assignemnt of 3^+.

The 4297.97 keV level (log ft = 6.8) decays by an apparent E1 gamma-ray transition to the 846.8 keV (2^+) level leading to a spin-parity assignment of 3^- which is in agreement with Pettersson et al[71]. However, as is seen from table (4.7b), the work of Metskvarishvili et al[72] leads to a different value for $\alpha(K)$, which indicates an (M1/E2) multipolarity, and suggests a spin parity assignment of 3^+. Also, the gamma-ray transition of 1175.1 keV from this level to the 3122.88 keV (4^+) level appears to be a pure (M1) transition which leads to a spin-parity assignment of 3^+. It is therefore suggested that a spin of 3, with an even parity is the most probable for the log ft value of 6.8 of this level.

4.5 Shell-model structure of the collective states

The Shell-model calculation of ^{56}Fe by Horie and Ogama[33] based on $(\pi\ f_{7/2})^{-2}$ $(\nu\ p_{3/2},\ f_{5/2},\ P_{1/2})^{2}$ configuations outside the ^{56}Ni core give a valuable comparison with these experimental results. Also the extended shell-model calculations to the high-spin state by McGrory and Raman[32]) assuming an inert ^{48}Ca core represent a different set of theoretical B(E2) and branching ratio values for the comparison. The experimental energy levels of ^{56}Fe together with the calculated levels are shown in Fig.(4.15). The experimental and calculated Branching ratios are shown in Table (4.7), where the third column of this Table represents the Branching ratios determined from the results reported here and the fourth column, the theoretical values of Ogawa et al[33], while the last column is theoretical values from Bendjaballa et al[79].

The reduced transition probability of electric Quadrupole transitions (the excited state lifetime τ_{ex} were taken from the Table of Isotopes 1978

$J^{\pi}_i \rightarrow J^{\pi}_f$	E_γ (keV)	Exp.B.R.%	Theo.B.R.% Ref(33)	Theo.B.R.% Ref(79)
$2^+_1 \rightarrow 0^+_g$	846.76	100		100
$4^+_2 \rightarrow 4^+_1$	1037.84	99.18 ± 0.18		≃ 100
$4_1 \rightarrow 2^+_1$	1238.28	100	100	100
$2^+_2 \rightarrow 0^+_g$	2657.7		1	
$2^+_2 \rightarrow 2^+_1$	1810.72	100	99	
$2^+_3 \rightarrow 2^+_1$	2113.11	100	96	
$2^+_4 \rightarrow 0^+_g$	3369.97	12.2 ± 0.2	4	
$2^+_4 \rightarrow 2^+_1$	2523.0	87.8 ± 0.9	96	

Table (4.7) Experimental and theoretical branching ratios

$J^{\pi}_i \rightarrow J^{\pi}_f$	E_γ	Exp B(E2)	Theor.(1) Ref.(32)	Theor.(2) Ref. (32)	Theor.(3) Ref.(33)
$2^+_1 \rightarrow 0^+_g$	846.76	298 ± 59	360	176	179
$4^+_1 \rightarrow 2^+_1$	1238.28	408 ± 85	457	224	234

Table (4.8) Experimental and theoretical reduced transition probability of electric quadrupole transition in μ_n^2 fm^4

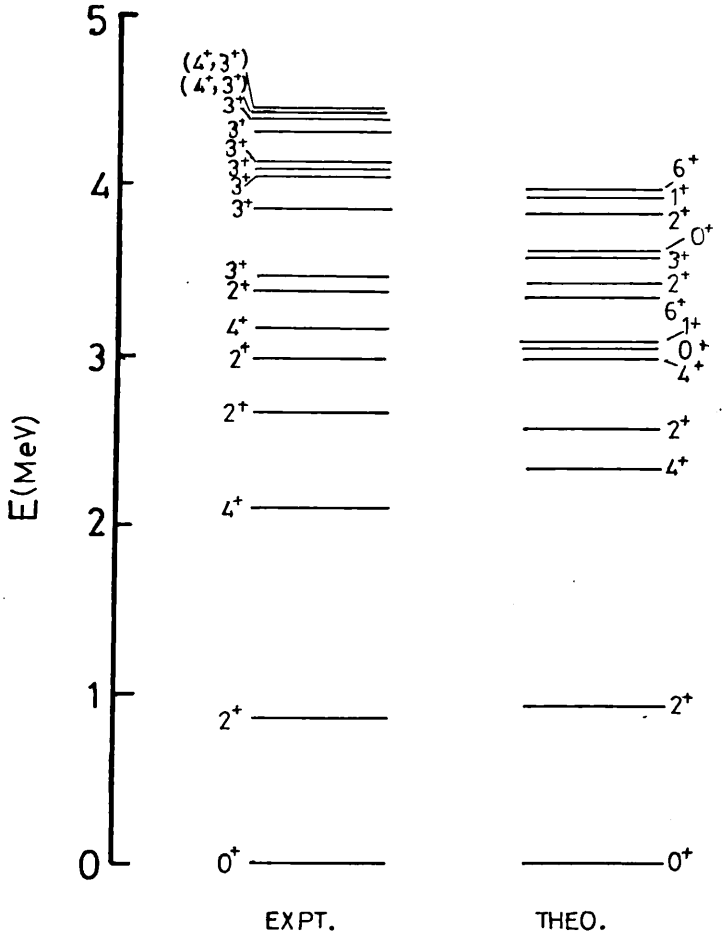

Fig(4.15) ^{56}Fe energy levels

in the p sec range[80]) are compared with the theoretical values in Table (4.8).

4.6 Conclusions

The level scheme of ^{56}Fe has been investigated with Ge(Li) detectors using a dual-parameter data collection system for γ-γ coincidence measurements. Support is found for the five transitions reported by Hofmann[67] and not observed by Hautala[62]. Of these, the relative intensities at the four lowest energies of 263.3, 410,9, 485.2 and 674.7 keV, the last proposed for the first time by Hofmann[67], are in very good agreement.

A comparison of the relative intensity measurements of the gamma-rays from the decay of the important calibration standard source of ^{56}Co with those of Hautala et al.[62], based on (p, γ) reactions, does not show a systematic high variation for energies above 2.5 MeV, as might have been expected from the work of McCallum and Coote[63], but would rather indicate this possibility between 1.5 and 2.5 MeV, as do the results of Hofmann. A new 655.0 keV gamma-ray was found to fit energetically between the levels at 4100.22 keV and the level at 3445.22 keV, and no evidence was found for the transition of 2657.4 keV. The spin-parity assignment and energy levels of ^{56}Fe based on the transition energy values, transition multipolarity assignments, and log ft values show good agreement with shell-model calculation by Ogawa et al.[33] based on $(\pi\ f_{7/2})^{-2}\ (\nu\ P_{3/2},\ f_{5/2},\ P_{1/2})^{2}$ configurations outside the ^{56}Ni core. The experimental branching ratios and reduced transition probabilities for electric quadrupoles show good agreement with those produced by McGrory and Raman[32] from shell-model calculation based on an inert ^{48}Ca core.

CHAPTER V

DECAY OF ^{75}Se

Since the discovery of the ^{75}Se isotope by Cowart et al.[81] many investigations have been carried out on this nucleus. The ^{75}Se nucleus decays by electron capture to the excited state of ^{75}As with a half-life of 120.4 days[82]. The yield nucleus of ^{75}As has an odd proton number (33) and an even neutron number (42) which is well removed from neutron and proton closed shells. Thus a simple shell model treatment of this nucleus does not provide a satisfactory description of the established experimental energy level values and their decay properties. The most successful theoretical models for this nucleus have been developed by Imanishi et al.[83] and Schölz et al.[84]. For this isotope the first lifetime measurements could be made with the full operation of the Dual-Parameter Energy-Time Spectrometer.

5.1 Previous investigations

Early investigations on the decay of ^{75}Se by Mathilde et al.[85], Edwards et al.[86], Grigoriev et al.[87] and Jahn et al.[88] employing a β-ray spectrometer, obtained most of the main gamma-ray modes by measurement of their internal conversion intensities which can indicate the multipolarities of these transitions. The work of Edwards et al.[86], Varma et al.[89] and Venngopala Rao et al.[90] on the gamma-ray spectra using NaI(Tℓ) scintillation detectors revealed the main transitions but no confirmation of the 24 keV and 81 keV transitions was given. These two transitions were suggested by β-ray spectrometer investigations. The use of Ge(Li) detectors by Raeside et al.[91] and Paradellis et al.[92] revealed some evidence for the 24 keV, 81 keV, 373 keV and 468 keV gamma-ray transitions. Robinson et al.[93] in his Coulomb excitation investigation on ^{75}As, suggested gamma-rays at 308 keV, 293 keV and

374 keV. The work of Pratt et al.[94] supported the suggested transition at 469.4 and 821.7 keV, but no evidence for any of the other gamma-rays suggested by Robinson et al.[93]. The most recent ^{75}Se investigations and last ^{75}As level scheme studies from the decay of ^{75}Se were performed by Thomas and Thomas[95] and no evidence was found for the transition of 373.8 keV, 468.8 keV and 821.7 keV more than 5×10^{-3}, 2×10^{-3} and 2×10^{-3} relative intensities respectively. A 14.9 keV gamma-ray was suggested to fit energetically between the level at 279.5 keV and level at 264.6 keV.

Neither Campbell[96] nor Puri and Shahota[97] in their low-energy gamma-ray spectrum studies of ^{75}Se using Si(Li) detectors had found support for the 14.9 keV transition.

5.2 Experimental considerations and singles spectra

Radioactive sources of ^{75}Se were made by the neutron reaction ^{74}Se (n,γ) ^{75}Se; the neutron capture in 10 mg. metal selenium (abundance of 87% for ^{74}Se) was done using the University of London Reactor irradiation facilities. Irradiation of one sample in a neutron flux of 2×10^{12} n cm^{-2} sec^{-1} for 36 hours gave a ^{75}Se activity of 10.9 μ Ci, and also irradiation of another sample for 10 hours gave a ^{75}Se isotope having an activity of 3 μ Ci.

Different singles spectra were taken using detectors Nos. 1, 2, 7 and No. 3 of Table (2.1). The detector efficiencies were detailed in Section (2.2) and the singles spectrum pulse recording system has been discussed in Section (2.1).

The singles spectra measurements in the energy region of $E_\gamma > 100$ keV used the first three detectors, and the Compton suppression spectrum also usefully employed detector No. 5 in the region of $E_\gamma > 100$ keV where several weak gamma-ray transitions were confirmed. This spectrum is shown in Fig.(5.1).

The part of the spectrum $E_\gamma < 100$ keV was measured by a small volume

FIG(5.1)

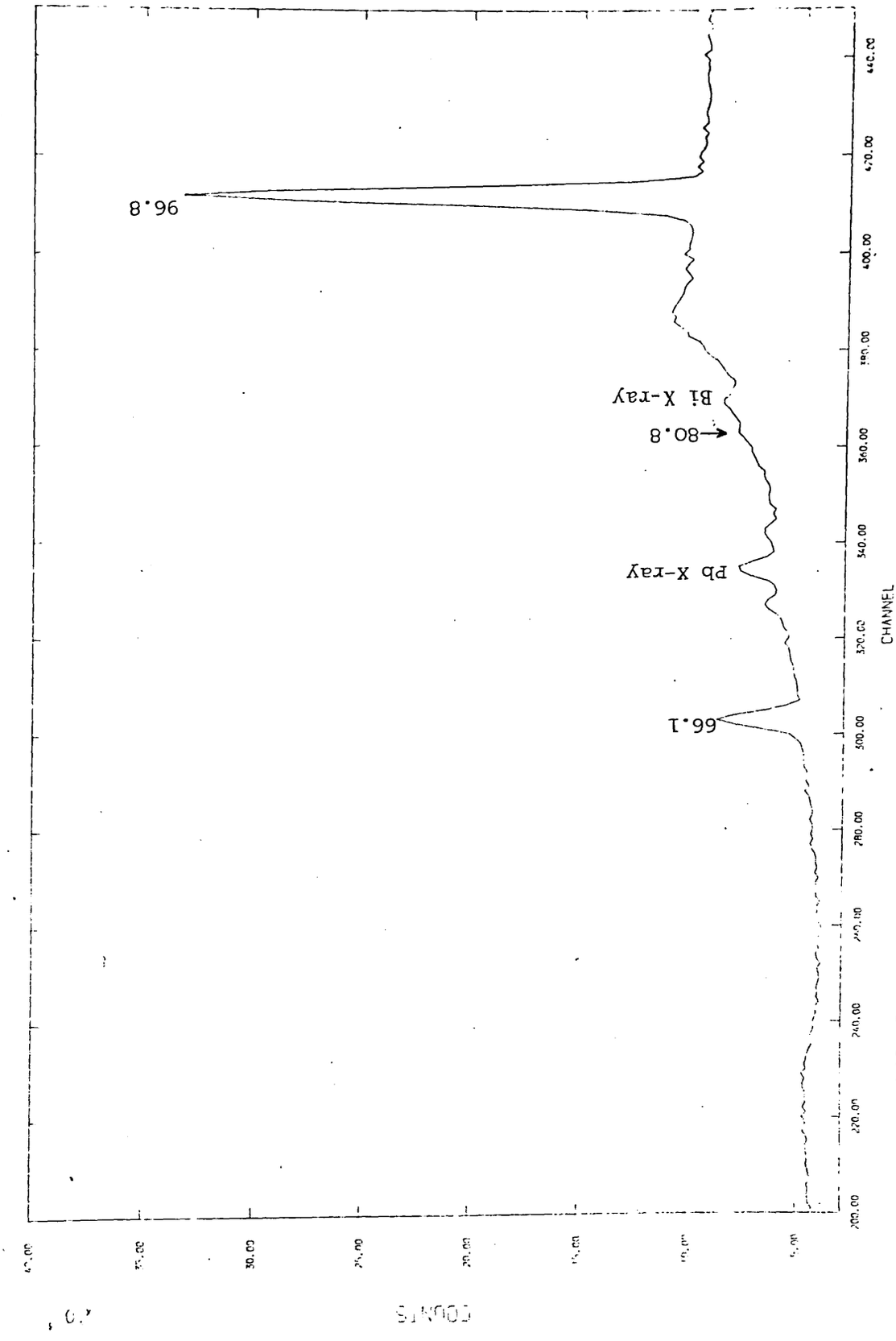

FIG. (5.2) SPECTRUM (ENERGY RANGE <100 KEV)

Present Work		Relative Intensities		
Energy (keV)	Relative Int.	Ref. (95)	Ref. (92)	Ref. (90)
14.9	< 0.01	0.34 (6)		
24.3 (2)	0.38 (5)	0.63 (6)	0.44 (6)	
66.10 (20)	16.6 (5)	15.0 (15)	17.2 (4)	16.4 (5)
80.8 (1)	0.18 (4)	0.11 (3)		
96.78 (10)	52.7 (8)	54.0 (40)	51.2 (10)	53.3 (16)
121.01 (8)	263.5 (40)	267 (30)	277 (5)	278 (8)
135.94 (18)	257.5 (160)	259 (70)	950 (18)	949 (200)
198.73 (12)	25.5 (4)	25.9 (20)	23.8 (7)	22.8 (5)
264.83 (14)	1000	1000	1000	1000
279.71 (12)	423.4 (73)	421 (8)	420 (8)	430 (9)
303.98 (17)	22.1 (37)	21.1 (30)	21.9 (7)	23.9 (5)
400.74 (17)	190.3 (35)	180 (4)	204 (5)	223 (50)
419.11 (55)	0.20 (1)	0.17 (3)	0.23 (2)	0.32 (6)
468.25 (13)	0.09 (2)		0.10 (5)	
572.34 (3)	0.52 (5)	0.48 (5)	0.63 (2)	0.64 (1)
618.8 (6)	0.073 (3)	0.059 (7)	0.075 (2)	0.078 (2)
821.8 (8)	0.039 (12)			

Table (5.1) Energies and relative intensities of γ-rays emitted in the decay of ^{75}Se (relative to γ-ray of 264.6 keV = 1000)

Ge(I) detector No. 3 Table (2.1). This detector was calibrated for energy and efficiency using the gamma-ray reference sources ^{241}Am and ^{57}Co supplied by the Radiochemical Centre, Amersham. The relative intensities were given by Ellis[98] and Auble[99]. This detector was used specially in the low energy region of interest to look for the 14.9, 24.4 and 80.8 keV gamma-ray transitions. The spectrum taken by this detector is shown in Fig.(5.2).

The energies and relative intensities as measured for the gamma-ray transition following the decay of ^{75}Se are given in Table (5.1) for comparison with previous workers' results.

5.3 Coincidence studies

The coincidence studies of the gamma-ray transitions from this isotope were done in the early stages of the present work using a fast-slow coincidence system (Section 2.4). These results were confirmed later; also more coincidence studies were done, using the more efficient dual-parameter data collection system. After all the coincidence data were written on the magnetic tapes the gating peaks were selected, and by setting the digital windows on these gating peaks and their immediate background the coincidence relations were investigated; the background and chance coincidence events were subtracted from each coincidence spectrum. The total coincidence ^{75}Se spectrum is shown in Fig.(5.3). The coincidence spectra for the prominent gamma-rays which are necessary to establish the features of the level scheme of ^{75}As are shown in Figs. (5.4-5.8). A summary of the coincidence results derived from these spectra is given in Table (5.2).

5.4 The lifetime measurement

The ^{75}As energy levels of 199 keV and 401 keV have lifetimes in the nano-sec. range, so that simultaneous measurements for the lifetimes together with the gamma-gamma coincidence were performed using the dual-

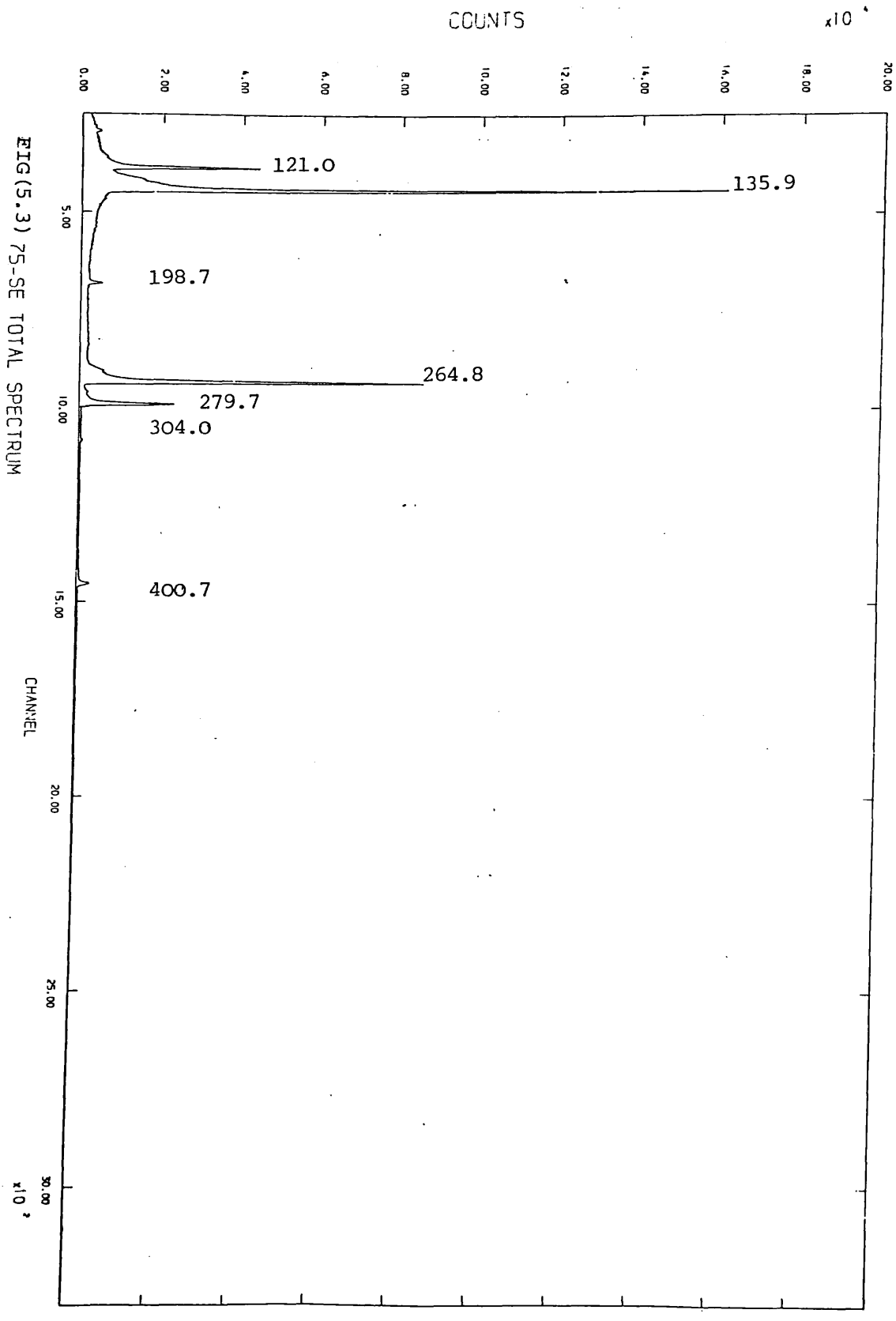

FIG(5.3) 75-SE TOTAL SPECTRUM

FIG(5.4) SPECTRUM OF 75-SE IN COINCIDENCE WITH 198.6 KEV GAMMA-RAY

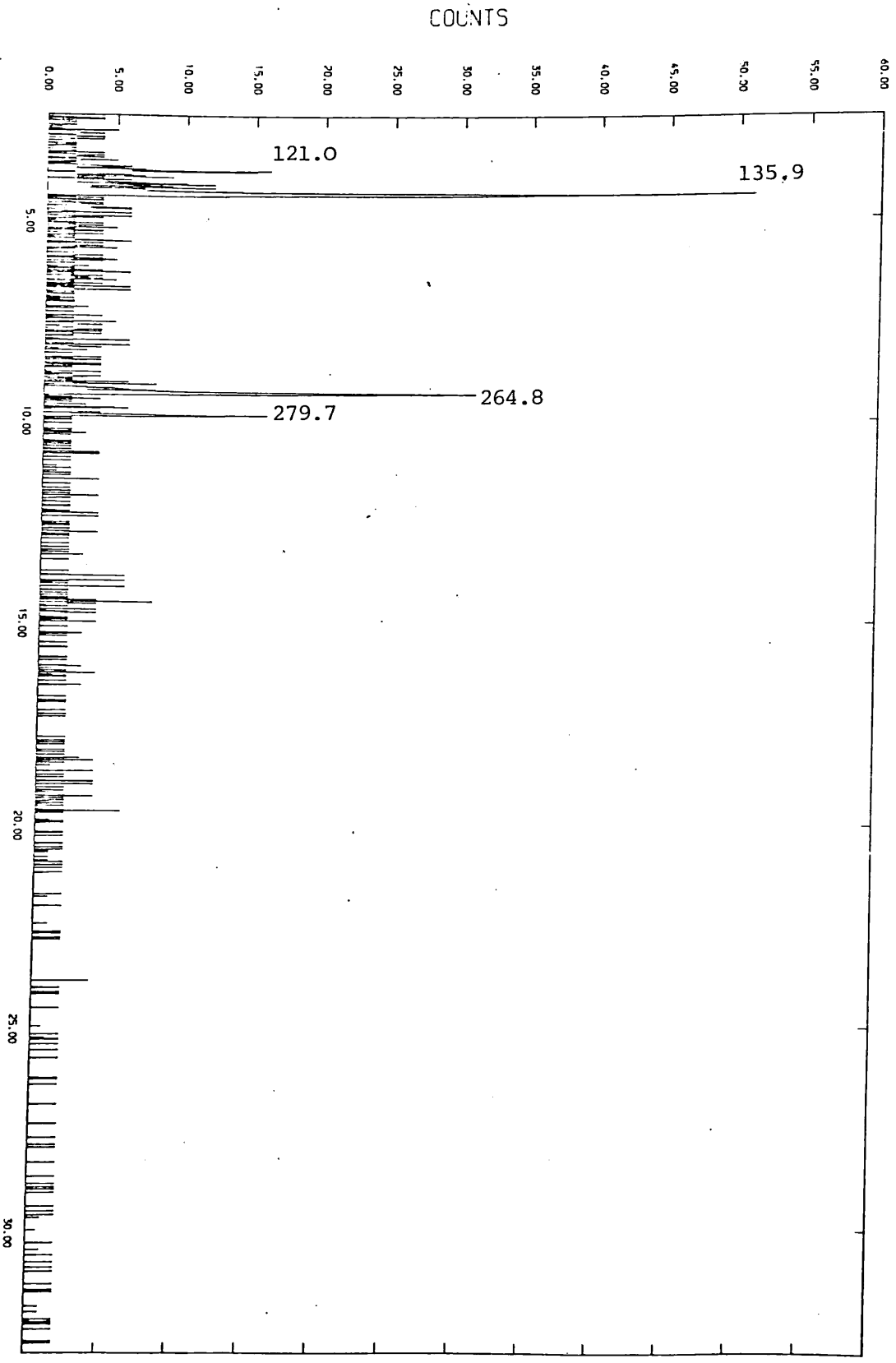

FIG(5.5)SPECTRUM OF 75-SE IN COINCIDENCE WITH 303.9 KEV GAMMA-RAY

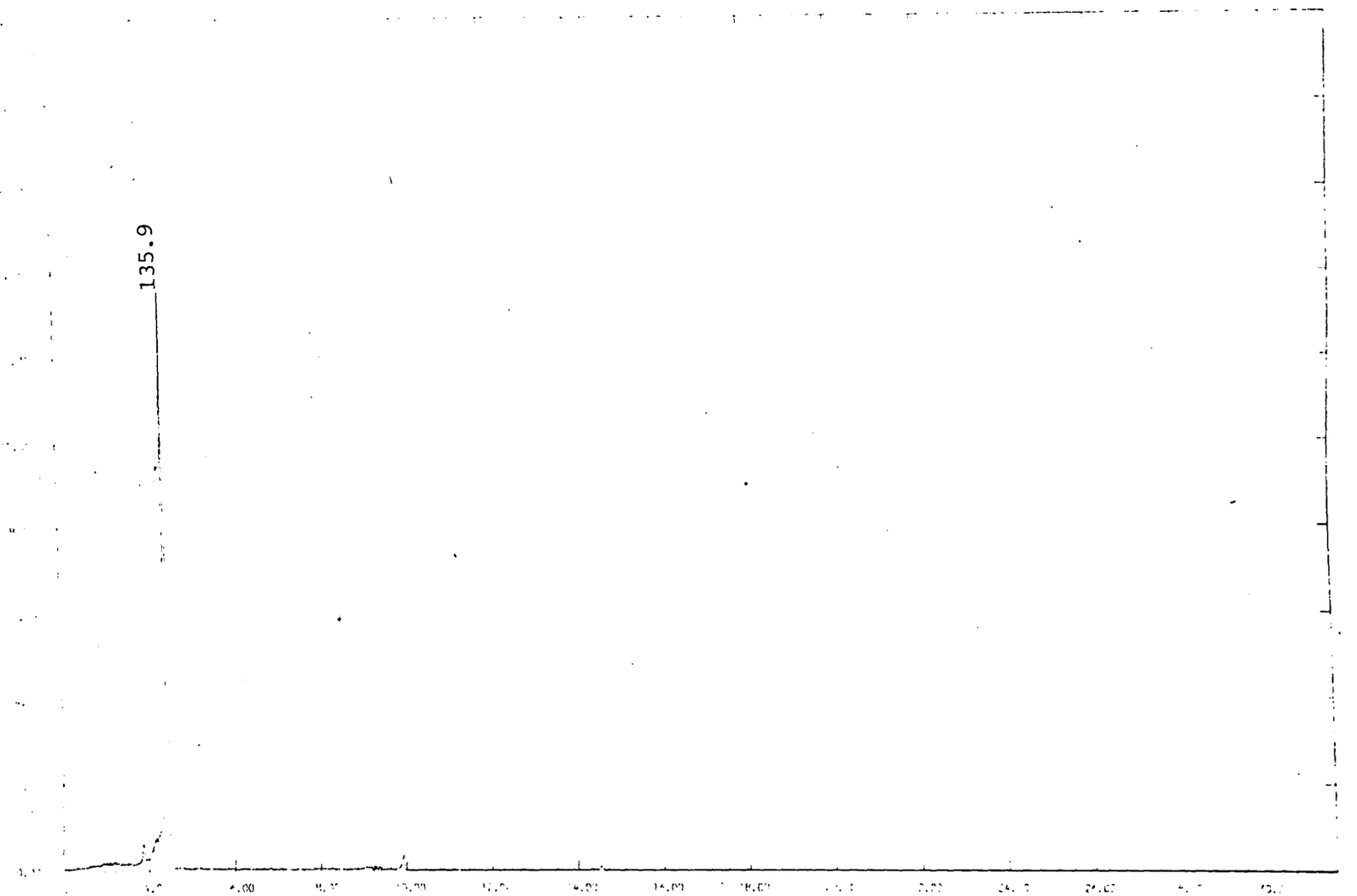

FIG(5.6) [illegible] SE-75 [illegible] 264 KEV

FIG(5.7)

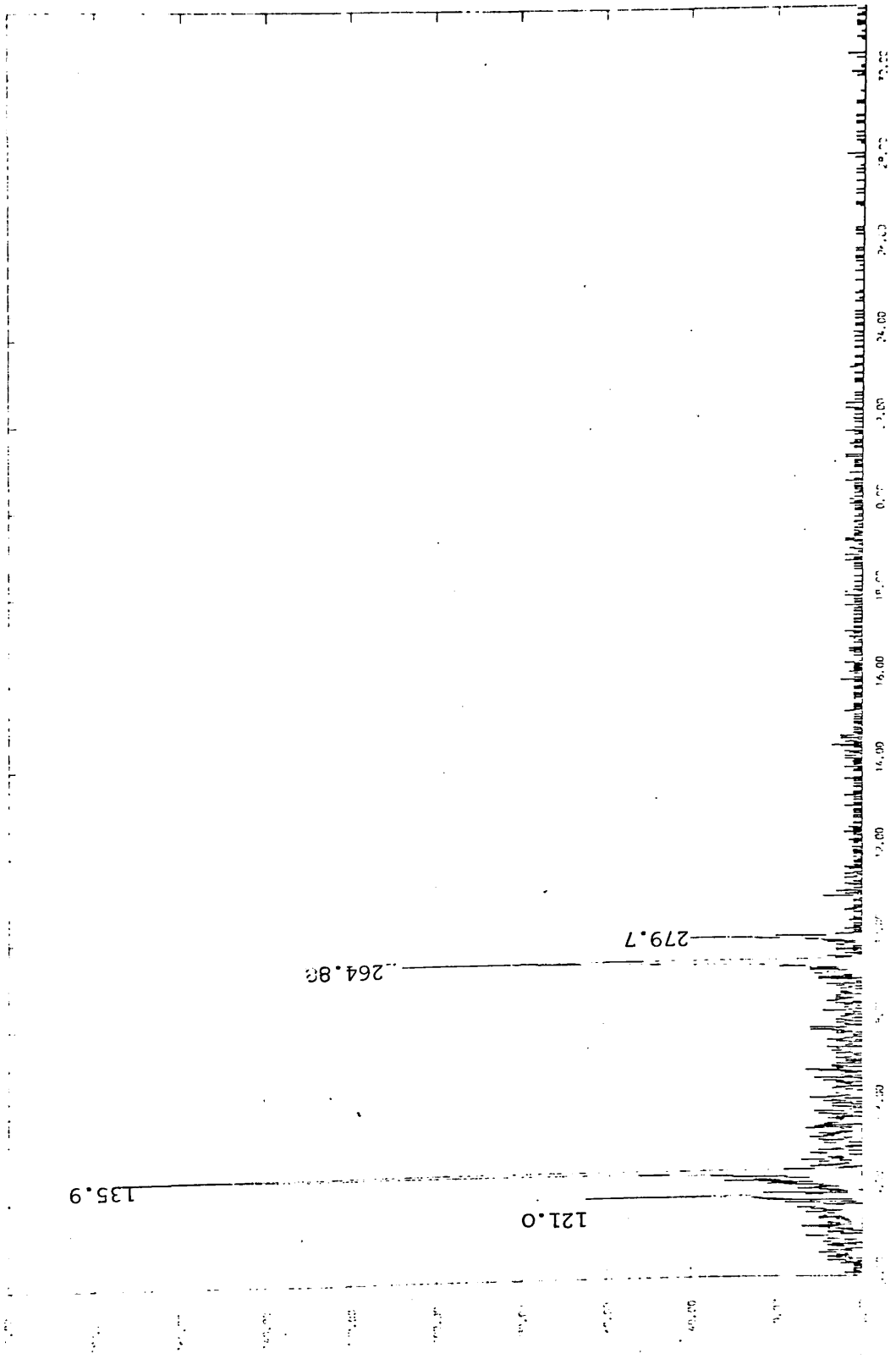

FIG(5.8) SPECTRUM OF 75-SE IN COINCIDENCE WITH 400. KEV

Gate (keV) / E_γ	198.7	264.8	279.7	304.0	400.7
96.8					
121.0	VW		VS	W	W
135.9	S	VS	VW	W	W
198.7		VW			
264.8	VW		VW	W	VW
279.7	P			S	VW
304.0					
400.7			P		
419.1	S				
468.3					
572.3					
618.8					
821.8					

Table (5.2) A summary of the coincidence results

parameter energy-time spectrometer (described in Chapter 3). The lifetimes of these levels were previously measured and provided a good test for the dual-parameter energy-time spectrometer.

Care was taken with the system stability as long runs were needed to collect enough data, noteably for the 199 keV level measurement, where the start and stop energy gates were the Compton edge of ≈70 keV and 198 keV photopeak respectively. The 198 keV photopeak taken from the gating (stop Ge(Li)) detector is a very well-defined peak but a weak transition, so that continuous counting for approximately four weeks was needed.

The analyses of the lifetime spectra were done using the slope method[100]. The experimental errors were small (< 2.8%) due to the completely linear response of the time-to-pulse height converter (Section 3.4) for a wide range of approximately 20 n sec.

The 198 keV and 401 keV levels lifetime spectra are shown in Fig.(5.9) and Fig.(5.10) respectively. The results of the lifetime measurements together with those of previous workers for time measurements on ^{75}As levels are given in Table (5.3).

The lifetime of the 400.8 keV level shows good agreement with the value reported by Ref.[103] and also Ref.[104]. The 199.7 keV level lifetime value is in good agreement with those reported by Refs.[103] and [105].

5.5 Decay scheme and discussion

The gamma-ray energies, relative intensities and their coincidence relationship were used to construct the level scheme of ^{75}As from the decay of ^{75}Se shown in Fig.(5.11). The energy sum relation for the energy level evaluation is given in Table (5.4). The EC energies were determined from the level energies obtained by considering the Q-value of 864.8 keV taken from Ref.[101]. The EC feeding branching ratios to ^{75}As levels were calculated from the decay fraction for the gamma-ray

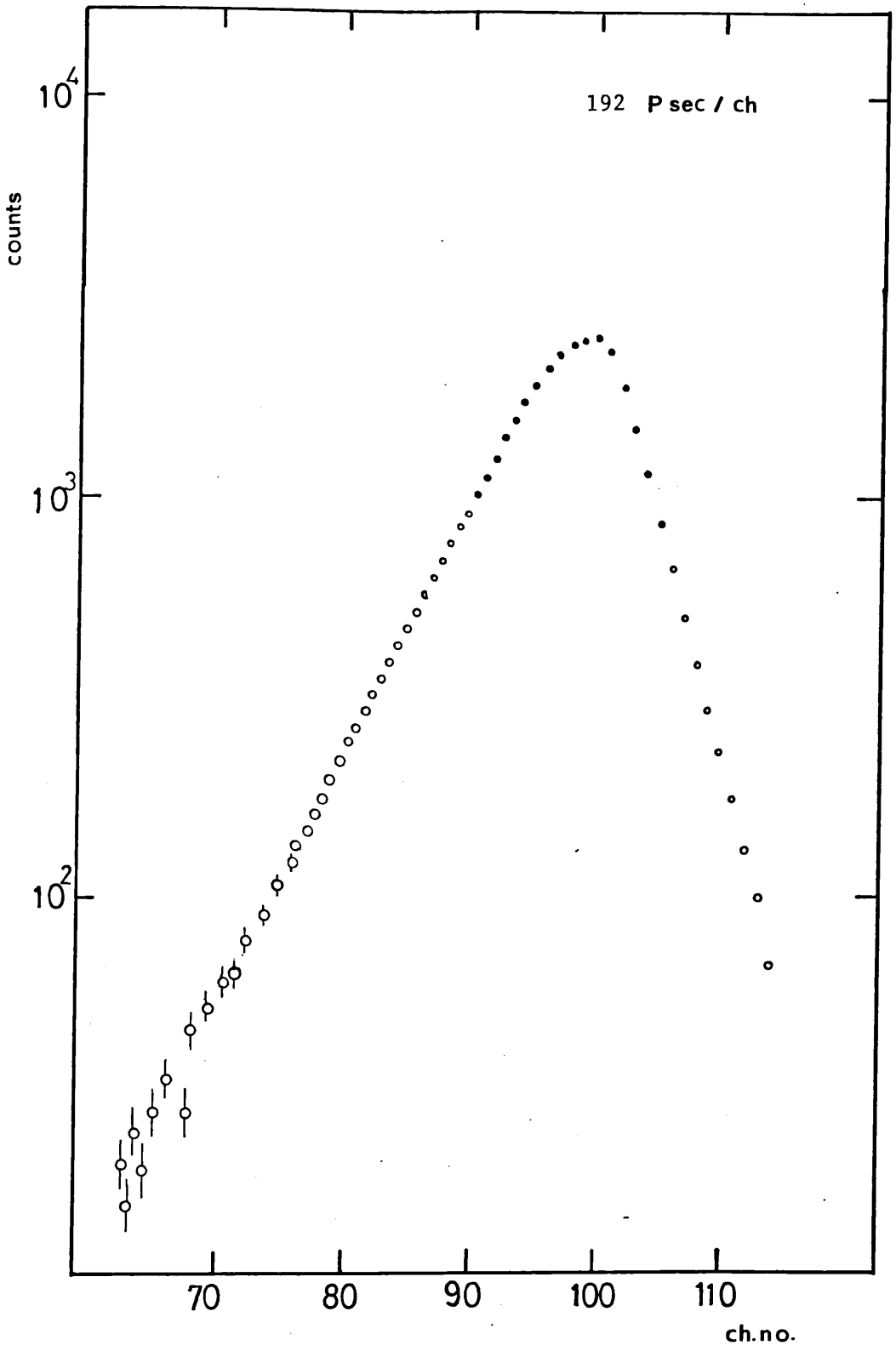

Fig(5.9) The 199 keV level lifetime spectrum

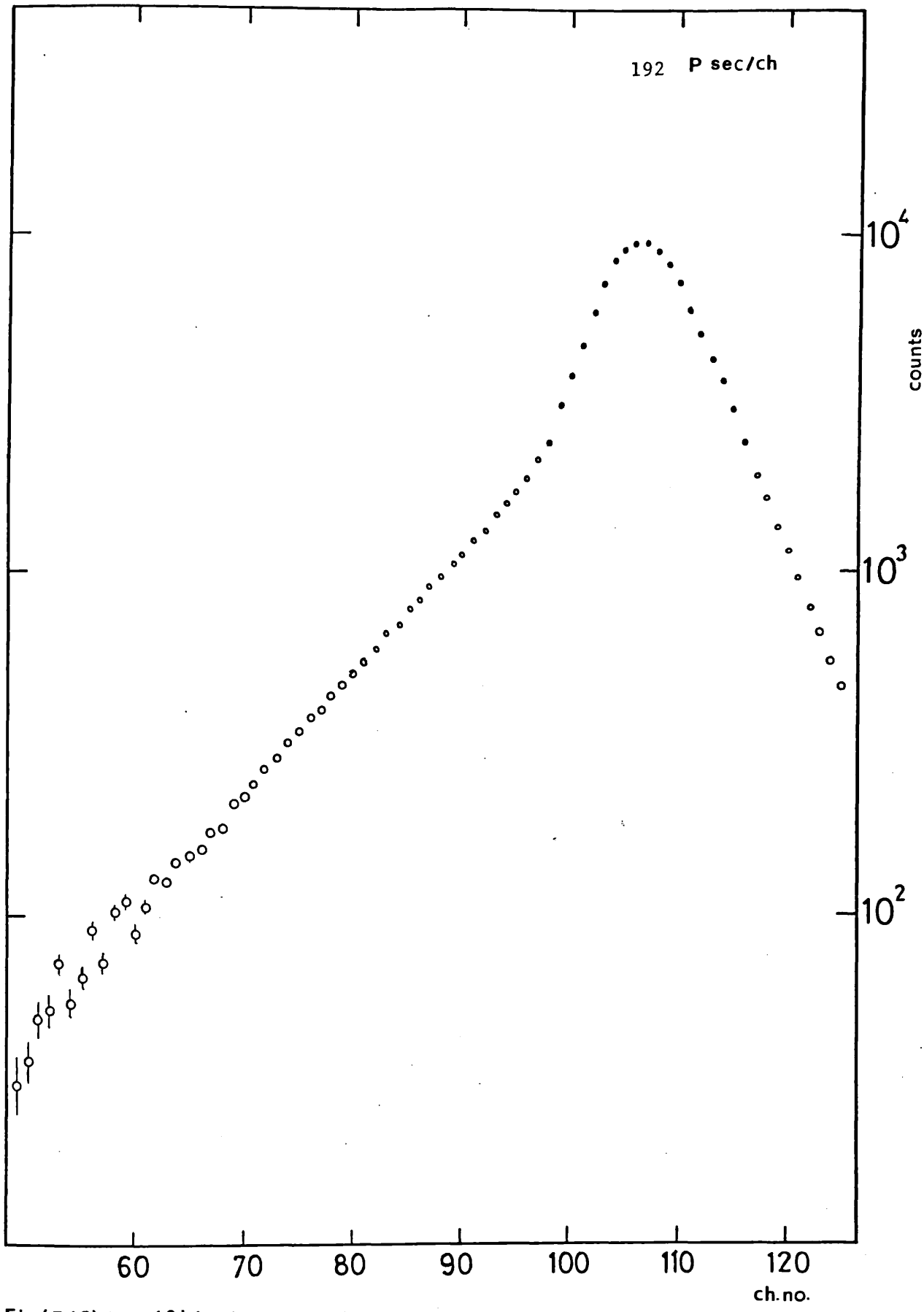

Fig (5.10) Tl e 401 keV level lifetime spectrum

Energy level (keV)	Present Work	Ref. (103)	Ref. (104)	Ref. (105)
199.73	0.89 ± 0.19	0.87 ± 0.03		0.9 ± 0.1
400.75	1.68 ± 0.19	1.67 ± 0.14	1.60 ± 0.10	

Table (5.3) Lifetimes for levels in 75 As (values are in n.sec.)

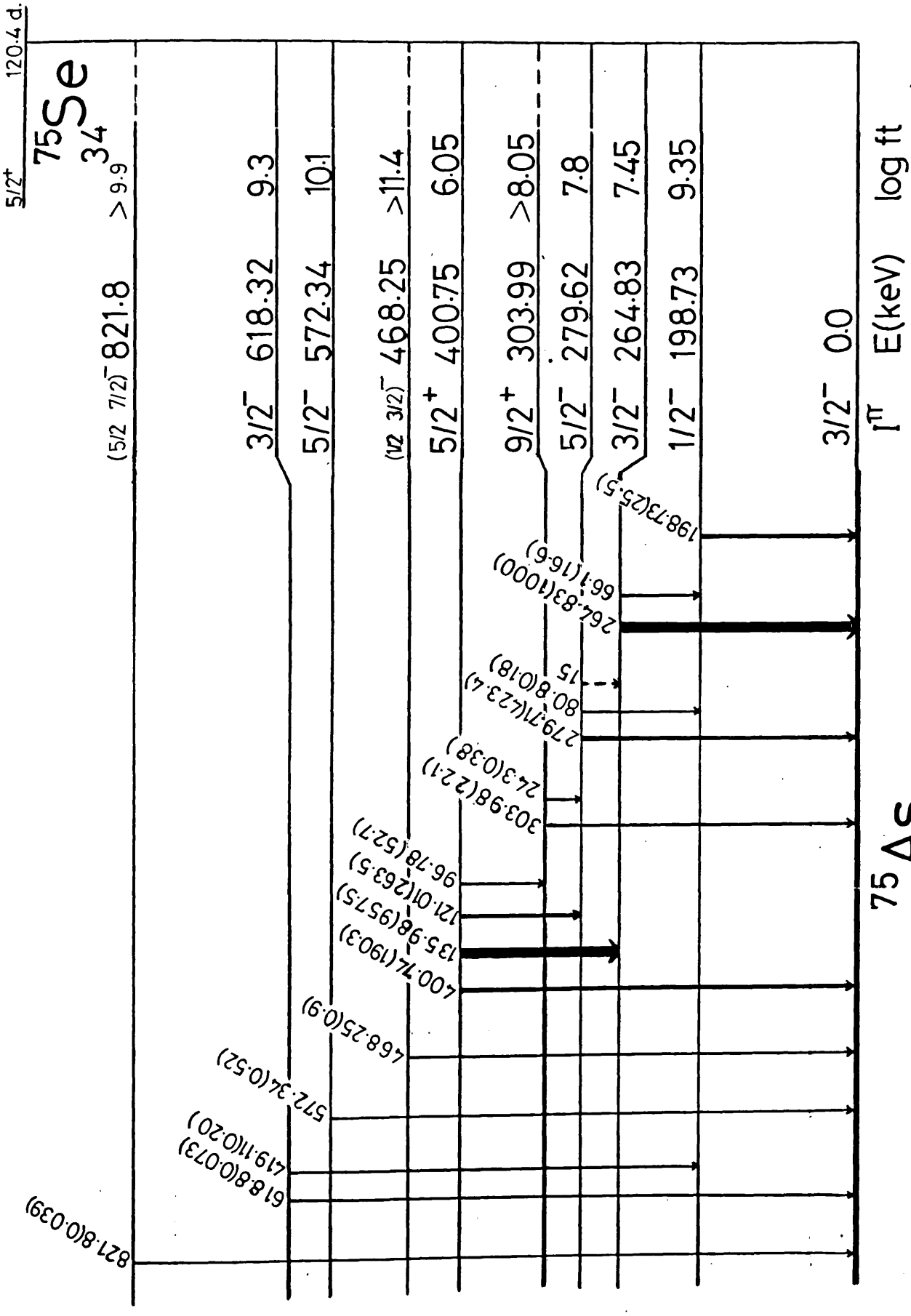

Fig(5.11) ^{75}As level scheme

Table(5.4) The energy sum relationships

Energy of transition (keV)	Energy Sum (keV)	Energy level (keV)
198.73		198.73
264.83		264.83
198.73 + 66.10	264.83	
279.71		279.62
198.73 + 80.8	279.53	
303.98		303.98
279.71 + 24.3	304.01	
400.74		400.75
264.83 + 135.94	400.77	
279.71 + 121.01	400.72	
303.98 + 96.78	400.76	
468.25		468.25
572.34		572.34
618.8		618.3
419.11 + 198.73	617.84	
821.8		821.8

transition following the decay of ^{75}Se, the internal conversion coefficients used were taken from Edwards et al.[86]. The log ft and spin and parity assignments together with the EC energies and its feeding branching ratios for each level are given in Table (5.5). The experimental K-shell conversion coefficients $\alpha(K)$ for transition in ^{75}As are compared with the theoretical values corresponding to E1, E2 and M1 multipolarity in Table (5.6). Using the K-electron intensities I(K) of Edwards et al.[86] and the gamma-ray intensities of Table (5.1) the experimental $\alpha(K)$ values were calculated. The $\alpha(K)$ theoretical values were taken from Rose[76]. The spin-parity of $5^+/_2$ for the ^{75}Se ground state were taken from Ref.[102].

The 198.7 keV level (log ft = 9.35) is observed to decay to the ground state ($3/_2^-$) by the 198.7 keV transition which is mainly (M1) transition (84%[102]) so that the established spin and parity assignment of $\frac{1}{2}^-$ is verified.

The 264.8 keV level (log ft = 7.45) is mainly fed by the (E1) 136.0 keV transition, and 98% decayed to the ($3/_2^-$) ground state by the 264.8 keV (M1) transition so that the spin parity assignment of ($3/_2^-$) is in good agreement with the log ft value.

The 279.6 keV level (log ft = 7.8) is observed to decay to the first excited state ($1/_2^-$) by the 80.8 keV transition which is pure (E2)[95] transition, so that the established spin and parity assignment of ($5/_2^-$) is verified. No evidence has been found for the 14.9 keV transition from this level to the 264.6 keV level.

The 303.9 keV level (log ft > 8.) is observed to decay to the ($3/_2^-$) ground state by the 303.9 keV (E3) transition. This level is mainly fed by the 96.8 keV (E2) transition and the possibility of EC feeding is very poor so that the possible value of spin-parity is $9^+/_2$.

The 400.8 keV level (log ft = 6.05) is established from the strong coincidence between the 264.8 keV gamma-ray transition arising from the

Energy level (keV)	ΣI_γ feed	ΣI_γ decay	B.R.%	E_{EC} (keV)	log ft	J^π *
198.73	16.8	25.5	0.1	662.2	9.35	$1/2^-$
264.83	957.5	1016.6	4.9	600.2	7.45	$3/2^-$
279.62	263.9	423.6	2.9	585.3	7.8	$5/2^-$
303.99	52.7	22.5	<0.3	560.9	> 8.05	$9/2^+$
400.75	-	1464.0	88.2	464.2	6.05	$5/2^+$
468.25	-	0.09	<0.005	396.1	>11.4	$1/2^-, 3/2^-$
572.34	-	0.05	<0.003	292.5	>10.1	$5/2^-$
618.32	-	0.27	<0.015	247.2	> 9.3	$3/2^-$
821.8	-	0.039	<0.0018	43.0	> 9.95	$7/2^-, 5/2^-$

Table (5.5) Summary of the level properties in ^{75}As

* Spins and parities deduced from the all available information.

E_γ (kev)	$I_i^\pi \rightarrow I_f^\pi$	Experimental $\alpha(K) \times 10^3$		Theoretical $\alpha(K) \times 10^3$			Adopted Multipolarity
				El	E2	Ml	
66.1	$^3/_2^- \rightarrow {}^1/_2^-$	353	(40)	284	2004	298	Ml/E2
96.8	$^5/_2^+ \rightarrow {}^9/_2^+$	856	(74)	63.8	778.2	79.9	E2
121.0	$^5/_2^+ \rightarrow {}^5/_2^-$	40.6[a]		36.9	378.5	46.6	El
135.9	$^5/_2^+ \rightarrow {}^3/_2^-$	24.0[a]		26.3	269.9	31.8	El
198.7	$^1/_2^- \rightarrow {}^3/_2^-$	17.3	(18)	7.98	48.8	11.8	Ml/E2
264.8	$^3/_2^- \rightarrow {}^3/_2^-$	6.0	(5)	3.48	15.9	6.2	Ml
279.7	$^5/_9^- \rightarrow {}^3/_2^-$	7.6	(8)	2.98	13.2	5.2	Ml/E2
3040.0	$^9/_2^+ \rightarrow {}^3/_2^-$	46.6	(61)	2.48	11.4	4.42	E3[b]
400.7	$^5/_2^+ \rightarrow {}^3/_2^-$	1.12	(11)	1.17	4.42	2.29	El

Table (5.6) Experimental and theoretical K-shell conversion coefficient.

(a) The conversion coefficients were normalized to the 121.0 keV and 135.9 keV to be pure El transition.

(b) The theoretical $\alpha(K)$ for 304 keV transition is 45.9×10^{-3} for the E3 multipolarity.

second excited state to the ground state and the 136.0 keV (E1) gamma-ray transition from this level the $(3/2^-)$ 264.8 keV level which leads to spin-parity assignment of $(5/2^+)$. Also, the log ft value clearly indicates no change in the spin-parity of the ^{75}Se ground state of $(5/2^+)$.

The 468.3 keV level (log ft > 11.4) is observed to decay to the $(3/2^-)$ ground state by the 468.9 keV gamma-ray transition, the log ft value showing that there are possible spin values of $1/2$ or $3/2$ with odd parity.

The EC fed energy level at 572.3 keV (log ft > 10.1) yields a M1 transition (87% $M1^{102}$) to the $(3/2^-)$ ground state so that the spin-parity assignment of $(5/2^-)$ is verified.

The 618.3 keV level (log ft = 9.3) is established from the strong coincidence between the 198.7 keV gamma-ray transition and the 419.1 gamma-ray (M1) from this level to the $(1/2^-)$ 198.7 keV level, and also it is observed to decay to the ground state via the 618.8 keV gamma-ray transition. The established spin and parity assignment of $(3/2^-)$ is verified.

The EC fed energy level at 821.8 (log ft > 9.9) is observed to decay to the ground state via the 821.8 keV gamma-ray transition. The possible values of spin are $5/2$ or $7/2$ with odd parity assignment.

5.6 Conclusions

The decay scheme of ^{75}As has been investigated using Ge(Li) detectors arranged in singles and coincidence modes. The detailed study of ^{75}Se has confirmed the presence of two gamma-rays of 24 keV and 81 keV previously suggested and has supported their positions in the decay scheme. But no support for the 14.9 keV gamma-ray was found. The strong evidence for the 821.8 keV transition supports the existance of a level at 821.8 keV. The lifetimes of the 199 keV and 401 keV levels measured values of 0.89 and 1.68 respectively and show good agreement with the previous measurements. The gamma-rays fitted nine excited states and the spins and parities of these levels were deduced.

CHAPTER VI

PROPERTIES OF ^{156}Gd LEVELS POPULATED IN THE DECAY OF ^{156}Eu

6.1 Previous investigations

Studies of the nuclear structure of the strongly deformed nuclei of ^{156}Gd through the decays of ^{156}Eu and ^{156}Tb have been made. Since the early ^{156}Gd level scheme investigations by Ewan et al.[106] there has been a very limited amount of high resolution data available from experiments investigating the decay of ^{156}Eu. These included the investigations of Peek et al.[107], and Bower et al.[108]. The only extensive studies of the ^{156}Gd level scheme from the ^{156}Eu decay, employing Ge(Li) detectors have been done by Kluk et al.[109].

The higher spin states of ^{156}Gd have been studied through neutron-capture experiments[110-115] and from the decay[116-119] of ^{156}Tb which has a ground state spin-parity of 3^-.

The γ-γ directional correlation measurements of Hamilton et al.[120] for several cascades in ^{156}Gd determined the M1 admixtures of several transitions.

The β-ray spectrometer measurement of the conversion electrons in the decay of ^{156}Eu carried out by Peek et al.[107] provided data for 29 γ-rays and enabled a 10 level ^{156}Gd level scheme to be constructed.

The most recent gamma-gamma coincidence work of Kluk et al.[109] led them to propose a level scheme of 84 gamma-ray transitions between 26 excited states. Seven of these levels have been proposed for the first time. Another 11 gamma-ray transitions were seen in their work, but there was no clear cut answer for placement in their proposed level scheme. This experiment was performed using a dual-parameter data collection system employing Ge(Li) detectors.

The most recent β-ray magnetic spectrometer experiment has been done by H. Yamada et al.[121], and the internal conversion coefficients of 47

gamma-ray transitions from the decay of ^{156}Eu were deduced. Their results were used as a basis to construct a 19 level and 50 gamma-ray ^{156}Gd energy level scheme.

It is clear that there are not many studies of the decay of ^{156}Eu, mainly because of the need for high flux reactors and the requirement for enriched ^{154}Sm targets in order to obtain the ^{156}Eu activity via a second order reaction. Also, only one set of high resolution data was available due to a lack of advanced electronics, high resolution detectors and multiparameters systems. However, from the available data, it seems that the proposed ^{156}Gd level scheme is insufficient and also the outstanding gamma-rays not placed in the ^{156}Gd level scheme clearly indicate the need for reinvestigation of the decay of ^{156}Eu.

6.2 Experimental considerations and singles spectra

Radioactive sources of ^{156}Eu were made up by the second order neutron reaction:

$$^{154}Sm\ (n,\gamma)\ ^{155}Sm \xrightarrow[22\ min]{\beta\ decay}\ ^{155}Eu\ (n,\gamma)\ ^{156}Eu$$

Samarium oxide powder enriched in ^{154}Sm to 98.9% of about 1 mg was irradiated in the PLUTO Reactor of the Isotope Production Unit (Harwell) at a flux of 2×10^{14} n cm^{-2} sec^{-1} for four hours to give a ^{156}Eu isotope having activity of 20 μCi with 30 μCi of ^{155}Eu activity. The ^{156}Eu nucleus decays with a halflife of 15.19 days[124] to the stable even-even nucleus of ^{156}Gd. More details about the second order reaction activation are given in Section (1.2).

The ^{155}Eu gamma-ray are all of low energy and they did not interfere with the ^{156}Eu spectra. However, the adjusted lower level discriminator of the ADCs just above the 105 keV was enough to eliminate the ^{155}Eu photopeaks from the measured singles and coincidence spectra. This also enabled the count rate in each case to be keep below 2000 sec^{-1}.

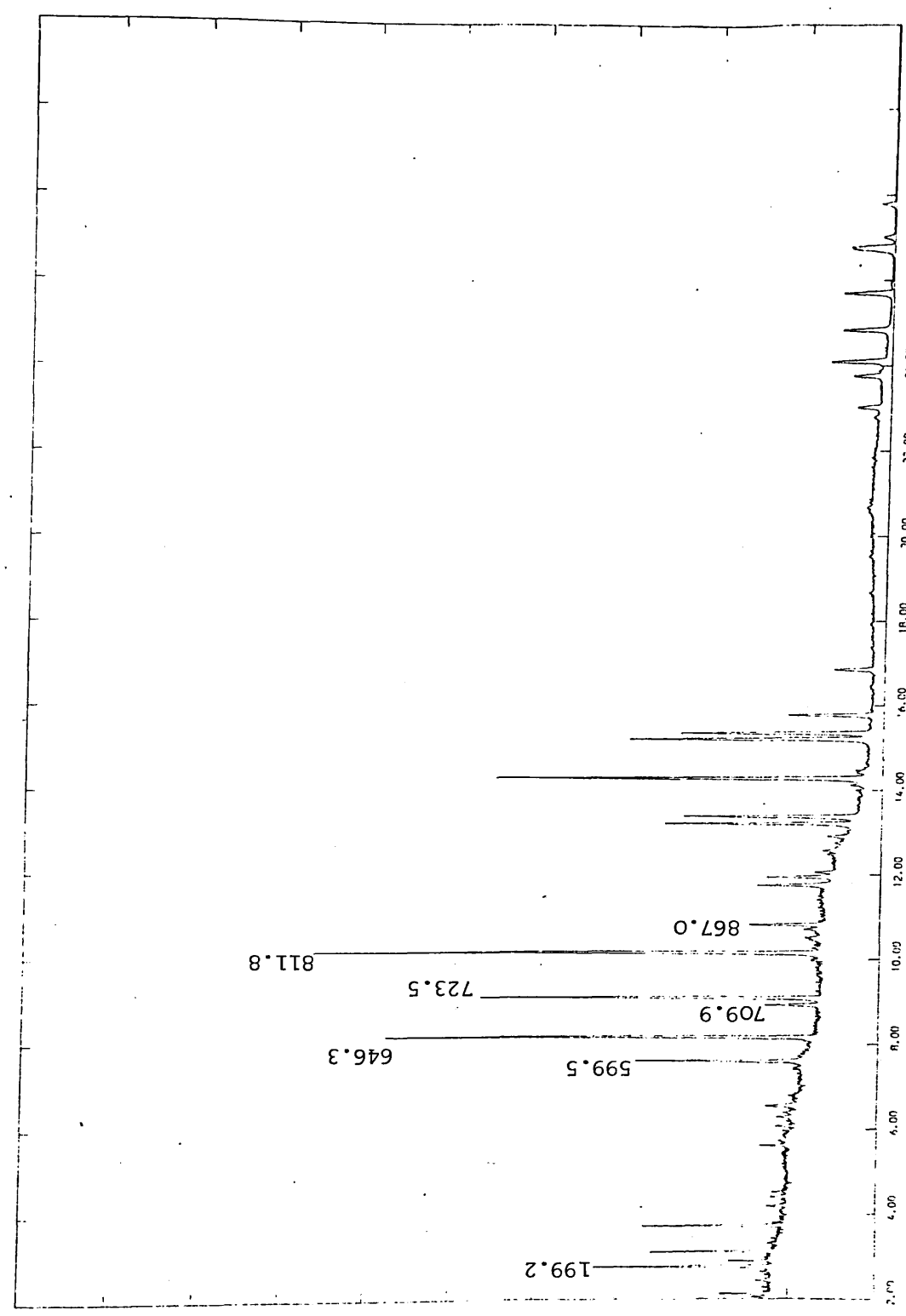

FIG. (6.11a) SINGLES SPECTRUM OF [illegible] FROM 0.12 EFFICIENCY DETECTOR

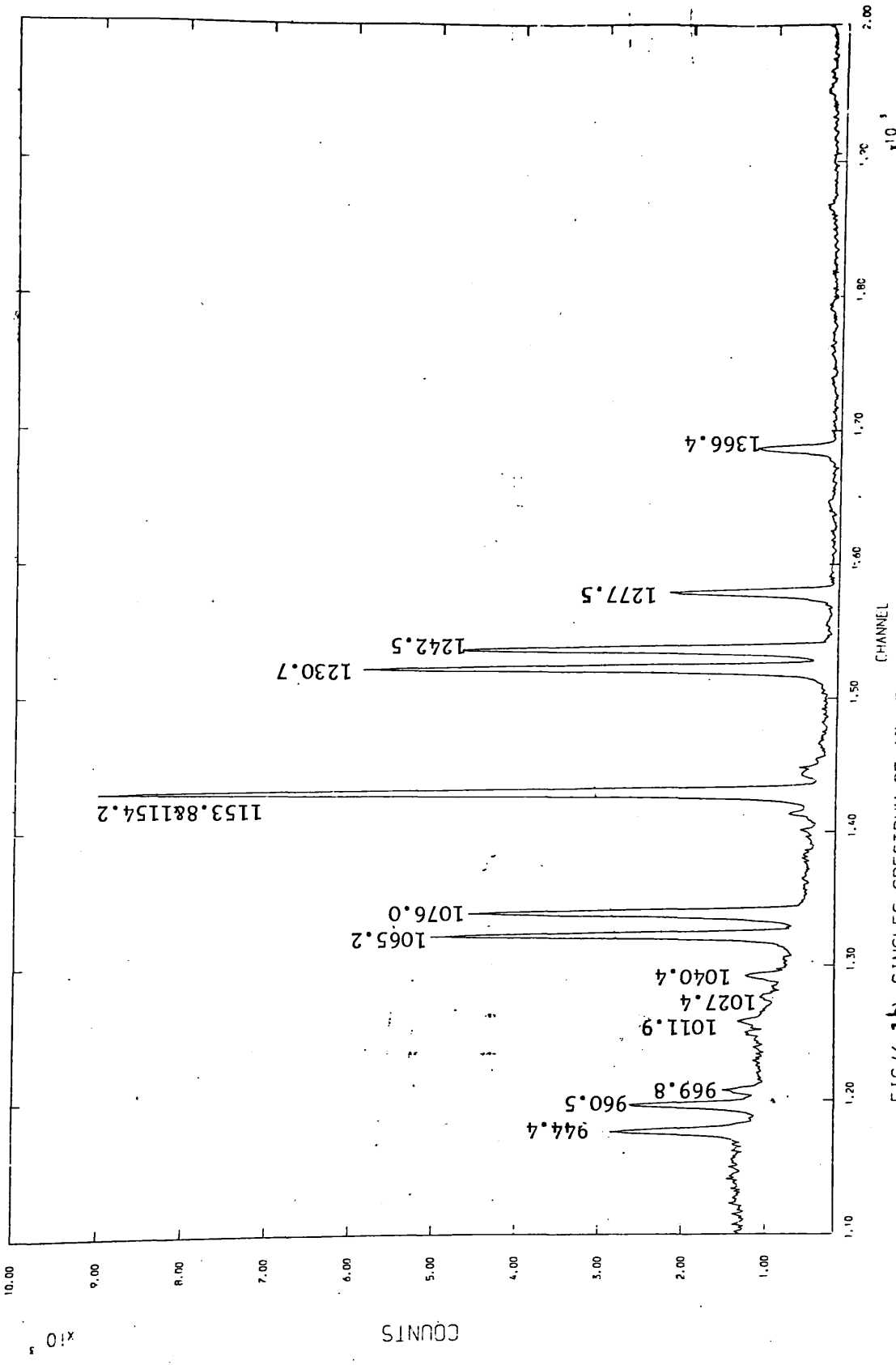

FIG(6.1b) SINGLES SPECTRUM OF 152-EU FROM A LEFFICIENT DETECTOR

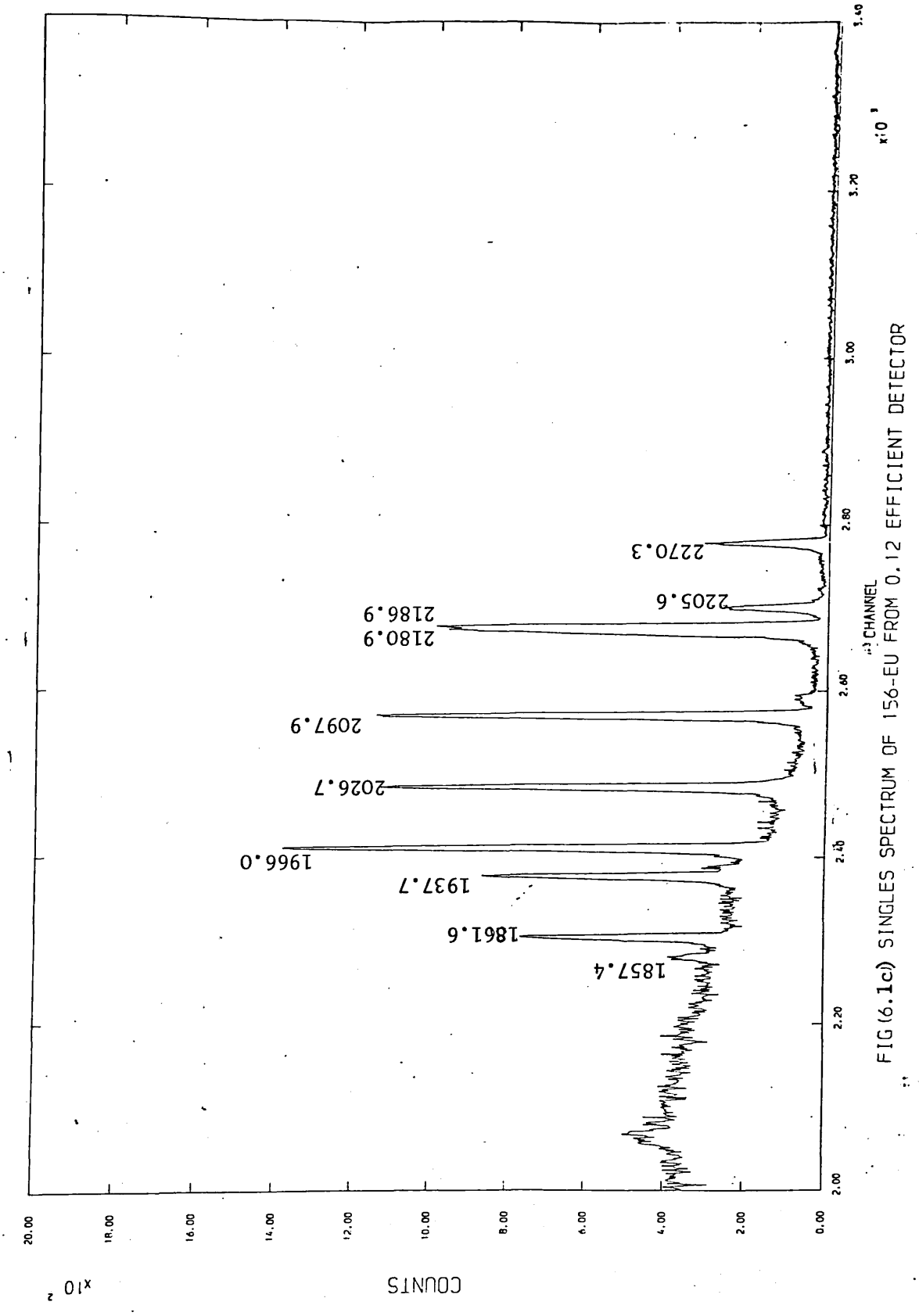

FIG (6.1c) SINGLES SPECTRUM OF 156-EU FROM 0.12 EFFICIENT DETECTOR

Singles spectra over the energy range from 110 keV up to 2.5 MeV were measured using detectors Nos. 6 and 7, and detector No. 5 was used to give the Compton suppression spectrum in the same energy region. The detector efficiencies detailed in Section (2.2), and singles spectra have been measured using the set-up discussed in Section (2.1). The singles spectrum for the gamma-rays following the decay of ^{156}Eu measured by the 12% efficient detector is shown in Fig. (6.1 a-c). The ^{156}Eu Compton suppression spectrum is shown in Fig. (6.2 a-c). The data collected were analyzed with the program SAMPO[39,40] on the University of London CDC 6600 Computer. The energy of the transitions above 0.5 MeV are compared with previously measured values in Table (6.1), and the relative intensities of all 91 gamma-ray transitions measured following the decay of ^{156}Eu are compared with the recently published values in Table (6.2). In the first column of this Table is given the measured gamma-ray transition energies; those below 0.5 MeV were taken from Ref.(109). The rest of the columns give the measured and previous workers' measured values of the relative intensities.

From the 91 γ-rays given in Table (6.2) by Kluk et al.[109], the 11 gamma-rays remained unplaced in the ^{156}Gd level scheme. They suggest 4 of these, at 335.7, 348.3, 354.2 and 554.7 keV, could be placed in their level scheme on the basis of energy fit, but they chose not to do so because their low intensity did not provide a clear-cut interpretation in the coincidence data. For the remaining 7 γ-ray transitions no explanation was given.

In order to identify these transitions reported by previous workers as γ-rays emitted in the decay of ^{156}Eu, several singles spectra have been measured at equal intervals of time for about 4 weeks to determine the halflife for each of these 11 transitions, on the basis of the change in the peak area (the peak area calculation in most of the cases by the program SAMPO . Table (6.3) shows the measured halflife for each of

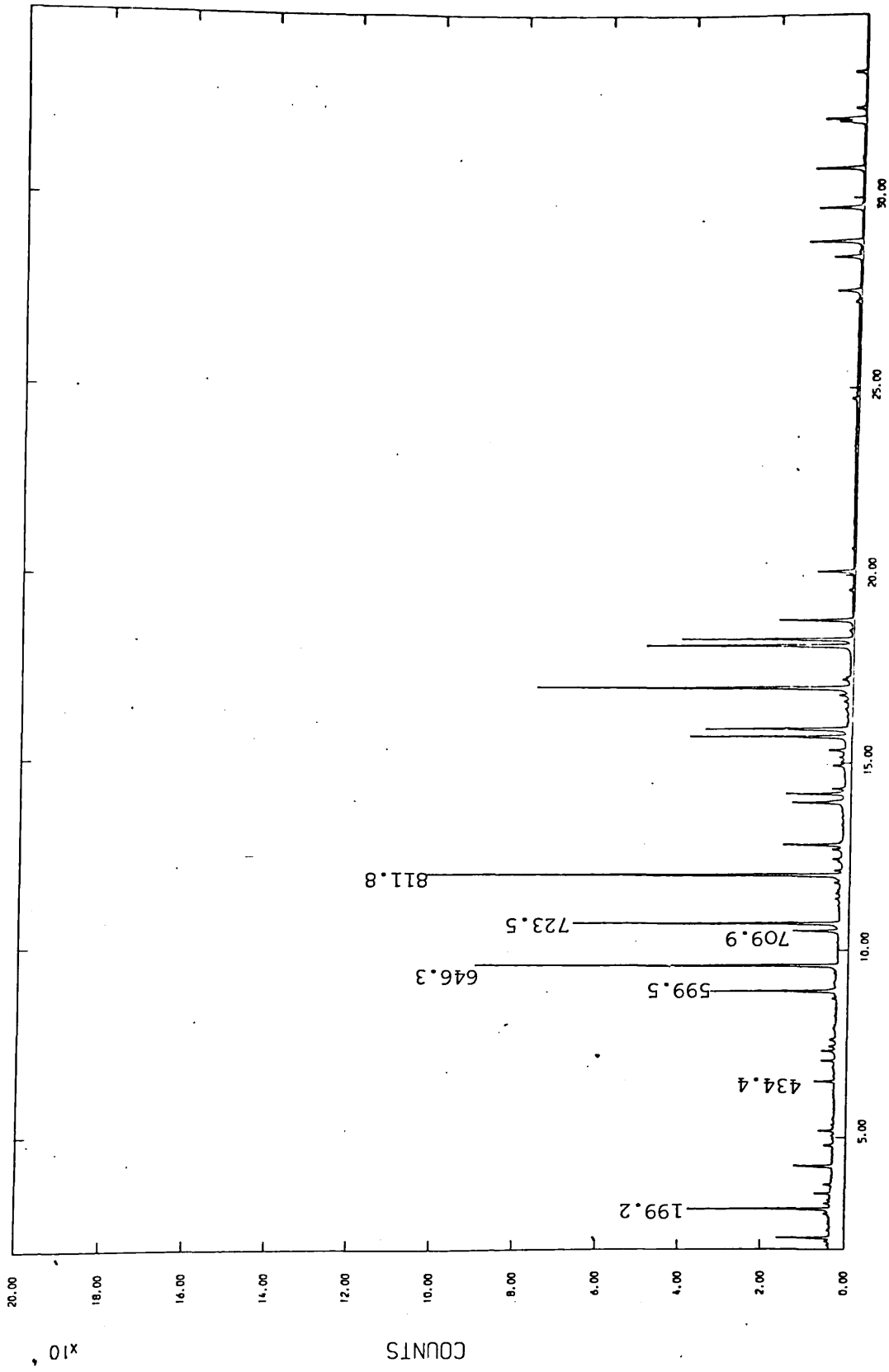

FIG. (6.2) COMPTON SUPPRESSION SPECTRUM OF 156-EU

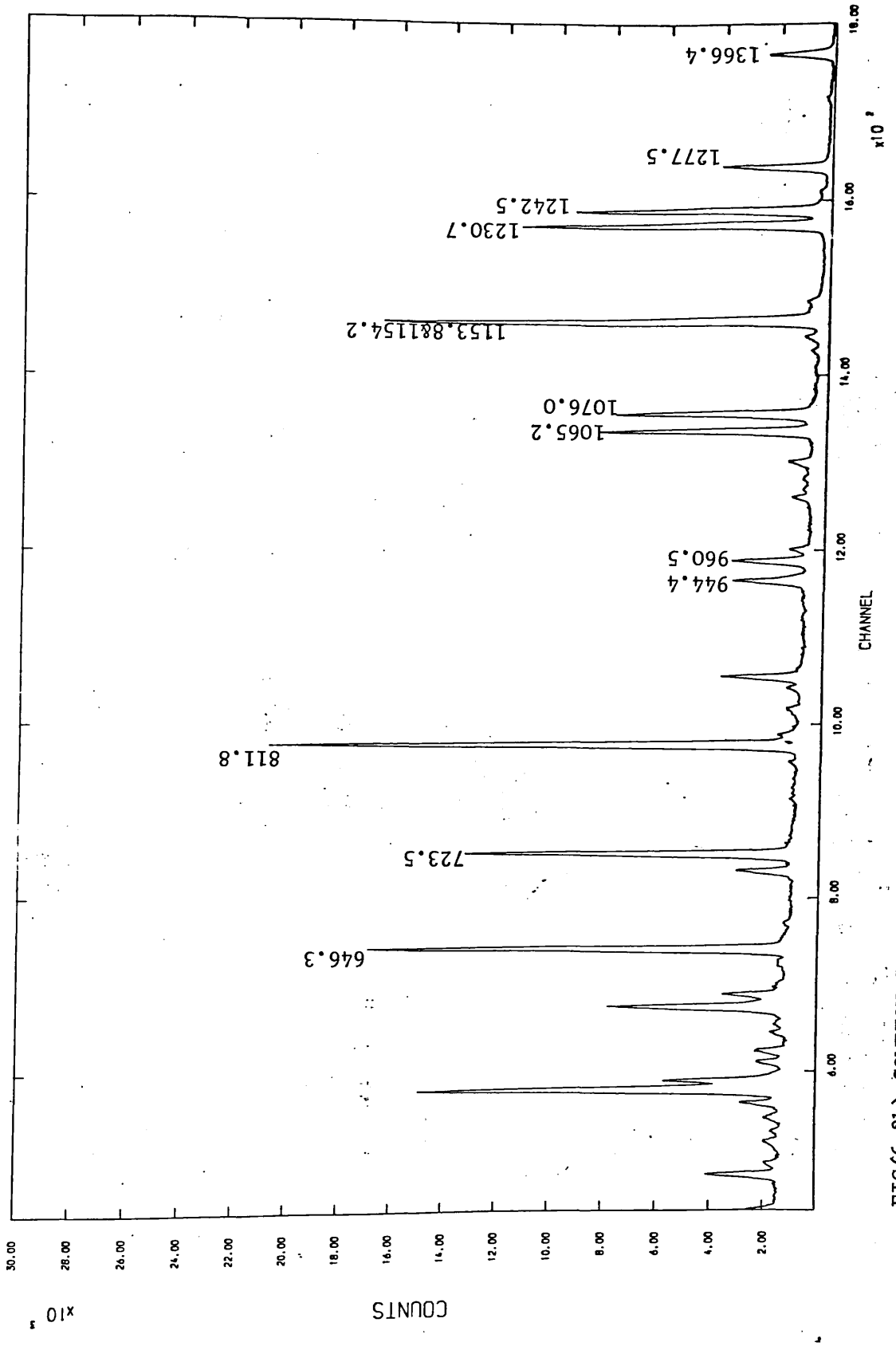

FIG(6.2b) COMPTON SUPPRESSION SPECTRUM OF 156-EU

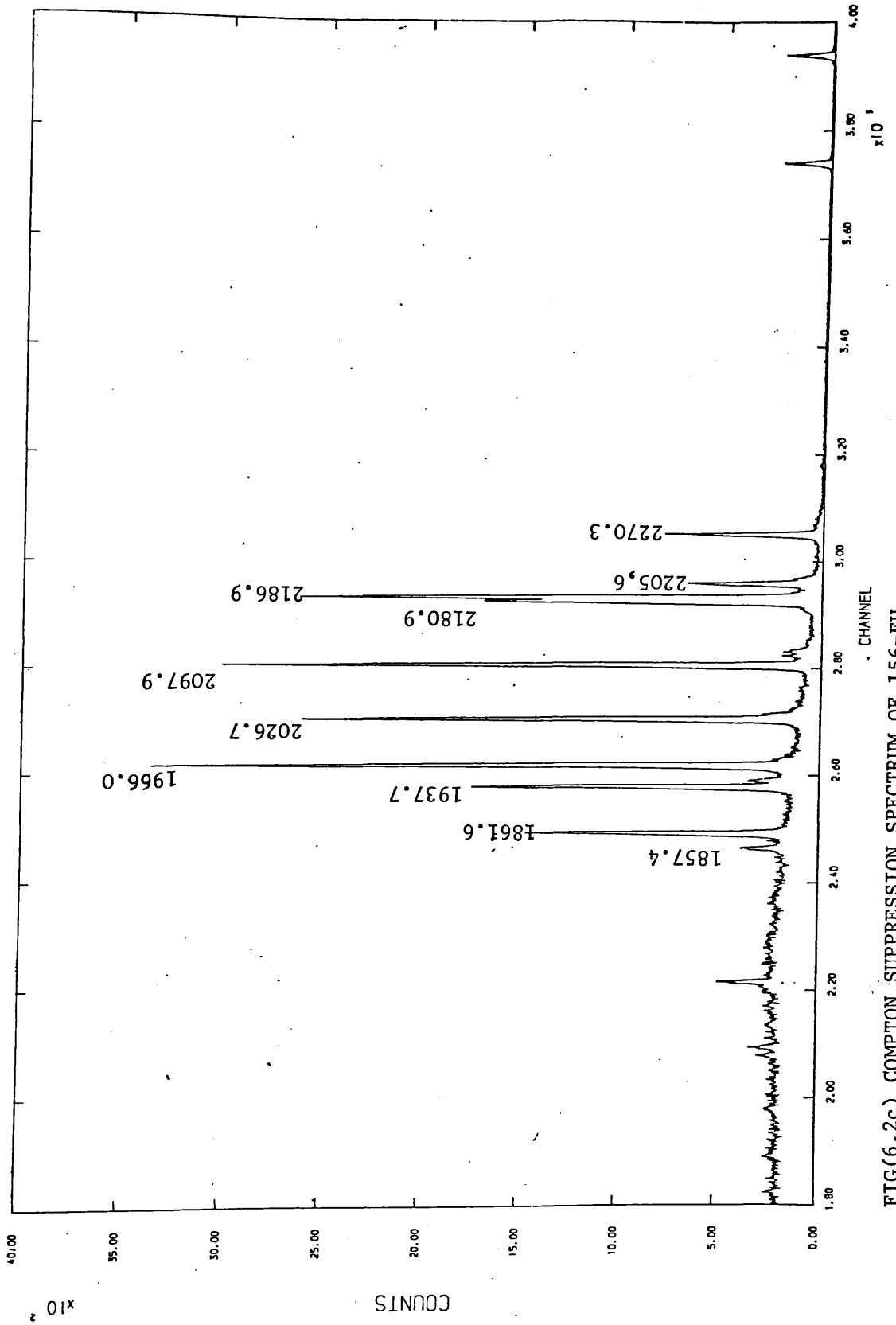

FIG(6.2c) COMPTON SUPPRESSION SPECTRUM OF 156-EU

Table (6.1) Energies of Gamma-Rays from the Decay of ^{156}Eu

Present Work	Kluk et al.[109]	Ref (126)
554.69 (8)	554.66 (6)	
585.99 (9)	585.90 (6)	
599.53 (5)	599.47 (5)	599.43 (8)
632.78 (6)	632.79 (8)	
646.29 (4)	646.29 (5)	646.23 (8)
707.18 (8)	707.1 (2)	
709.86 (5)	709.86 (5)	709.85 (12)
723.48 (5)	723.47 (5)	723.44 (9)
768.49 (7)	768.56 (7)	768.3 (2)
784.32 (8)	784.14 (10)	
797.65 (6)	797.73 (6)	797.67 (10)
811.75 (6)	811.77 (5)	811.73 (7)
820.37 (7)	820.36 (7)	820.32 (12)
836.57 (6)	836.52 (7)	836.4 (12)
839.08 (2)	839.0 (2)	
841.11 (10)	841.16 (10)	841.1 (3)
858.35 (6)	858.36 (12)	858.2 (2)
865.99 (8)	865.98 (12)	
867.01 (8)	867.01 (8)	866.98 (10)
872.49 (8)	872.39 (9)	
903.61 (10)	903.62 (10)	
916.41 (9)	916.4 (4)	
928.34 (4)	928.8 (4)	
944.43 (7)	944.35 (7)	944.06 (8)
947.43 (15)	947.46 (18)	
960.50 (8)	960.50 (8)	960.41 (9)
961.09 (36)	961.0 (6)	
969.82 (6)	969.83 (6)	969.80 (12)

Table (6.1) Energies of Gamma-Rays from the Decay of ^{156}Eu, continued (2)

Present Work	Kluk et al.[109]	Ref (126)
1011.87 (5)	1011.87 (5)	1011.8 (1)
1018.42 (10)	1018.50 (10)	
1027.38 (9)	1027.39 (8)	1027.50 (12)
1037.38 (48)	1037.43 (43)	
1040.42 (7)	1040.44 (7)	1040.4 (1)
1065.19 (5)	1065.14 (5)	1065.08 (8)
1075.98 (28)	1075.99 (20)	1075.19 (10)
1079.17 (5)	1079.16 (5)	1079.19 (8)
1101.70 (11)	1101.80 (11)	
1115.48 (7)	1115.78 (7)	
1129.49 (8)	1129.47 (7)	1129.30 (12)
1140.46 (5)	1140.51 (5)	1140.5 (1)
1153.84 (7)	1153.47 (7)	1153.72 (8)
1154.15 (17)	1154.09 (7)	
1155.95 (30)	1155.95 (30)	1158.88 (10)
1164.22 (13)	1164.2 (3)	1164.81 (12)
1169.12 (5)	1169.12 (5)	1168.94 (12)
1187.28 (8)	1187.3 (5)	
1220.50 (11)	1220.50 (11)	
1230.71 (8)	1230.71 (6)	1230.66 (8)
1242.47 (5)	1242.42 (5)	1242.47 (8)
1258.08 (7)	1258.03 (7)	1258.3 (3)
1277.46 (6)	1277.43 (5)	1277.50 (8)
1366.42 (5)	1366.41 (5)	1366.44 (8)
1626.05 (4)	1625.29 (14)	
1682.14 (7)	1682.10 (12)	1681.10 (15)

Table (6.1) Energies of Gamma-Rays from the Decay of ^{156}Eu, continued (3)

Present Work	Kluk et al.[109]	Ref (126)
1857.37 (6)	1857.42 (11)	1857.20 (15)
1876.97 (5)	1877.03 (15)	1876.91 (10)
1937.74 (11)	1937.71 (11)	1937.66 (12)
1946.36 (8)	1946.34 (13)	1945.90 (15)
1965.98 (10)	1965.95 (12)	1965.91 (10)
2026.73 (11)	2026.65 (11)	2026.68 (10)
2032.51 (12)	2032.51 (12)	2031.57 (20)
2097.93 (12)	2097.70 (11)	2097.57 (15)
2110.77 (12)	2110.52 (13)	2110.64 (20)
2116.78 (13)	2116.49 (13)	2116.46 (15)
2170.95 (18)	2170.86 (20)	
2180.89 (12)	2180.91 (12)	2181.05 (10)
2186.91 (9)	2186.71 (11)	2186.82 (10)
2205.56 (13)	2205.38 (13)	2205.57 (10)
2211.85 (9)	2211.83 (12)	2211.85 (12)
2270.17 (6)	2269.90 (12)	2269.85 (10)
2293.19 (5)	2293.40 (12)	2292
2300.8 (2)	2301.0 (2)	2301
2344.32 (47)	2344.3 (7)	
2361.3 (1)	2361.2 (3)	2361

Table (6.2) Relative Intensities of Gamma-Rays from the Decay of ^{156}Eu

Energy * (keV)	Relative Intensities		
	Present work	Kluk et al.[109]	Ref.(126)
88.95 (5)	870 (90)	870 (90)	4651 (232)
138.7 (2)	0.76 (13)	0.81 (9)	
160.2 (2)	1.23 (9)	1.06 (11)	
190.16 (8)	2.25 (27)	1.70 (16)	51.1 (90)
199.19 (5)	79.2 (31)	76. (4)	60.4 (22)
215.7 (2)	2.36 (30)	1.3 (3)	
244.7 (3)	5.39 (26)	0.9 (3)	
281.4 (2)		0.8 (2)	
290.49 (15)	5.22 (32)	0.9 (2)	
317.30 (9)	7.77 (25)	6.5 (4)	
335.69 (11)	2.51 (18)	1.05 (14)	
348.27 (9)	2.05 (18)	1.4 (2)	
354.2 (9)	1.80 (19)	1.5 (2)	
434.40 (9)	23.72 (63)	21.2 (11)	23.7 (23)
472.70 (6)	17.6 (4)	14.1 (8)	17.7 (18)
490.34 (6)	16.5 (9)	17.5 (12)	17.7 (20)
494.90 (15)	1.4 (8)	1.6 (7)	
498.88 (6)	7.39 (60)	6.0 (7)	
554.69 (8)	2.93 (24)	2.3 (5)	
585.99 (5)	7.20 (35)	6.5 (6)	
599.53 (15)	210.7 (45)	217 (11)	217 (22)
632.78 (6)	3.89 (6)	3.6 (6)	
646.29 (4)	649.9 (99)	650 (33)	651 (56)
707.18 (8)	6.08 (64)	4.2 (14)	
709.86 (5)	87.4 (22)	88 (5)	93 (9)
723.48 (5)	559.7 (86)	558 (28)	558 (46)

Table (6.2) Relative Intensities of Gamma-Rays from the Decay of ^{156}Eu continued (2)

Energy * (keV)	Relative Intensities		
	Present work	Kluk et al.[109]	Ref. (126)
768.49 (7)	7.34 (56)	8.6 (9)	9.3 (17)
784.32 (8)	4.67 (50)	4.0 (7)	
797.65 (6)	11.99 (46)	10.6 (13)	9.3 (14)
811.75 (6)	1000	1000	1000
820.37 (7)	14.8 (16)	15.4 (10)	16.2 (18)
836.57 (6)	7.73 (49)	8.6 (11)	11.1 (21)
839.08 (2)	3.1 (9)	3.2 (8)	
841.11 (10)	20.9 (6)	23.3 (16)	22.7 (21)
858.35 (6)	20.4 (9)	12.1 (12)	27.9 (18)
865.99 (8)	17.3 (4)	15.3 (30)	
867.01 (8)	137.2 (25)	135 (14)	155.3 (88)
872.49 (8)	4.86 (107)	3.2 (7)	
903.61 (10)	3.68 (26)	3.1 (8)	
916.41 (9)	3.95 (31)	4.0 (20)	
928.34 (4)	2.69 (29)	2.4 (8)	
944.43 (7)	139 (59)	134 (8)	247.4 (12)
947.43 (15)	31.2 (18)	30 (9)	
960.50 (8)	149 (10)	149 (13)	164.6 (80)
961.0 (6)a	17. (1)	15 (3)	
969.82 (61)	36.8 (16)	37.2 (18)	39 (2)
1011.87 (5)	34.2 (8)	32.7 (20)	55.8 (71)
1018.42 (10)	9.44 (73)	7.8 (9)	
1027.38 (9)	13.6 (6)	11.5 (10)	39. (4)
1037.38 (48)	1.89 (5)	3.4 (6)	
1040.42 (7)	53.4 (12)	51. (3)	55. (4)
1065.19 (5)	542.9 (138)	503 (25)	548.8 (323)
1075.98 (28)	34. (8)	36. (6)	247.2 (281)

Table (6.2) Relative Intensities of Gamma-Rays from the Decay of ^{156}Eu

continued (3)

Energy * (keV)	Relative Intensities		
	Present work	Kluk et al.[109]	Ref. (126)
1079.17 (5)	518.5 (89)	423 (25)	483.7 (198)
1101.70 (11)	5.38 (30)	3.6 (11)	
1115.48 (7)	8.18 (82)	5.5 (80)	
1129.49 (7)	16.8 (5)	13.9 (12)	17.7 (61)
1140.46 (5)	31.4 (7)	28.5 (19)	31.6 (37)
1153.84 (7)	699 (18)	686 (67)	1302 (86)
1154.15 (17)[a]	517 (22)	506 (45)	
1155.95 (30)	15. (3)	13.5 (20)	
1164.2 (3)	6.1 (7)	5.8 (9)	162. (29)
1169.12 (5)	29.9 (31)	28.2 (20)	32 (28)
1187.88 (8)	2.14 (31)	1.5 (7)	
1220.50 (11)	1.8 (6)	1.7 (6)	
1230.71 (8)	871.6 (211)	838 (42)	897.6 (668)
1242.47 (5)	720.4 (190)	691 (34)	734.8 (789)
1258.08 (7)	10.5 (3)	9.5 (9)	9.3 (9)
1277.46 (5)	317.4 (61)	303 (15)	330.2 (89)
1366.42 (5)	174.6 (36)	170 (9)	186 (32)
1626.05 (4)	4.41 (35)	3.4 (7)	
1682.14 (7)	27.1 (12)	27.6 (20)	43.2 (39)
1857.37 (6)	25.56 (66)	24.5 (17)	33 (4)
1876.97 (5)	161.6 (27)	162 (8)	153.5 (99)
1937.74 (11)	205.9 (35)	201 (10)	206.9 (105)
1946.38 (8)	18.2 (8)	18.2 (13)	12.5 (18)
1965.98 (10)	410.2 (69)	402 (21)	454.9 (199)
2026.73 (11)	332.9 (73)	339 (17)	392.6 (321)

Table (6.2) Relative Intensities of Gamma-Rays from the Decay of ^{156}Eu

continued (4)

Energy * (keV)	Relative Intensities		
	Present work	Kluk et al.[109]	Ref.(126)
2032.51 (12)	11.9 (11)	12.5 (11)	45.6 (23)
2097.93 (12)	403.3 (65)	398 (20)	547.9 (40)
2110.77 (12)	8.86 (57)	8.2 (8)	16.3 (19)
2116.78 (13)	12.4 (6)	12.1 (8)	17.6 (9)
2121.3	$< 10^{-5}$	0.48 (16)	
2170.95 (18)	4.8 (8)	5.3 (5)	
2180.89 (12)	224 (4)	233 (12)	423.7 (606)
2186.91 (9)	364.4 (61)	353 (18)	630.2 (612)
2205.56 (13)	83.2 (29)	92 (5)	175.8 (121)
2211.85 (9)	8.9 (7)	9.3 (6)	20.4 (55)
2255.	$< 10^{-5}$	0.62 (12)	
2259	$< 10^{-5}$	1.71 (17)	
2270.17 (6)	106.7 (21)	106.0 (53)	247.9 (87)
2293.19 (5)	2.19 (13)	2.4 (2)	
2300.8 (2)	0.87 (10)	0.96 (16)	
2344.32 (47)	0.21 (9)	0.25 (6)	
2361.3 (1)	1.54 (9)	1.77 (17)	

a - Energies determined from the energy difference.

* - The uncertainties (bracketed) are variations in the last digits of the best values. For example, 811.75 (6) may be written as 811.75 ± 0.06.

Energy (kev)	Half-life $\tau_{\frac{1}{2}}$ days	Comment
215.7	15.54 (30)	
244.7	46.2 (5)	Gamma-ray not from the decay of ^{156}Eu.
281.4		No evidence more than 2×10^{-5} relative to the refrence peak
290.49	44.6 (31)	Gamma-ray not from the decay of ^{156}Eu.
335.69	2.48 (25)	Gamma-ray not from the decay of ^{156}Eu.
348.27	15.5 (20)	^{156}Eu gamma-ray transition to fit energetically $1715.17(0^+) \rightarrow 1366.42(1^-)$
354.20	15.21 (19)	^{156}Eu gamma-ray transition to fit energetically $2300.80(1^\pm) \rightarrow 1946.34(1^-)$.
494.90	14.21 (98)	^{156}Eu gamma-ray transition to fit energetically $1771.17(2^+) \rightarrow 1276.23(3^-)$.
554.69	4.33 (30)	Gamma-ray not from the decay of ^{156}Eu.
1187.28	18.0 (36)	^{156}Eu gamma-ray transition to fit energetically $1276.23(3^-) \rightarrow 88.95(2^+)$.
2110.77	41.1 (41)	Gamma-ray not from the decay of ^{156}Eu.

Table (6.3) Gamma-ray not identified by the previous workers.

these 11 gamma-rays, only 5 of which have the same halflife [15.19d] as ^{156}Eu within the quoted experimental errors.

The gamma-ray at 215.7 keV appears as a well-defined peak in all singles spectra taken. The halflife of 15.54 ± 0.30 days gives a clear indication that the gamma-ray comes from the decay of ^{156}Eu, but it cannot be placed in between any of the 27 excited states proposed for the ^{156}Gd level scheme as deduced in these studies. This transition would suggest a new level, but there was no clear supporting evidence in the coincidence data, nor were other γ-transitions observed which would support the existence of such a level.

6.3 Coincidence results

The coincidence data written on four magnetic tapes were analyzed at a later time after the data collection from two large-volume Ge(Li) detectors (Nos. 6 and 7 of Table (2.1)), by the Dual-Parameter Data Collection system (experimental details in Chapter 3). The analysis of the coincidence data was done by setting the digital windows on a particular region of interest (representing the gating photopeak) in the spectrum from the 10% efficient detector. In the decay of ^{156}Eu the coincidence relationships were investigated using 10 prominent gamma-rays in the energy range from 599 keV to 1682 keV.

The coincidence spectra corrected for chance and background coincidences are shown in Fig. (6 (3-13)). The ^{156}Eu total spectrum is shown in Fig. (6.3). A summary of the coincidence results is given in Table (6.4). The gamma-ray gates which are necessary to establish the features of the ^{156}Gd level scheme are listed in the first row. The observation of a gamma-ray in the spectrum in coincidence with a gating gamma-ray is indicated in this Table by one of the following entries: VS, S, W, VW or P. These entries give the strength of the observed gamma-ray relative to the other gamma-rays in coincidence spectrum and they

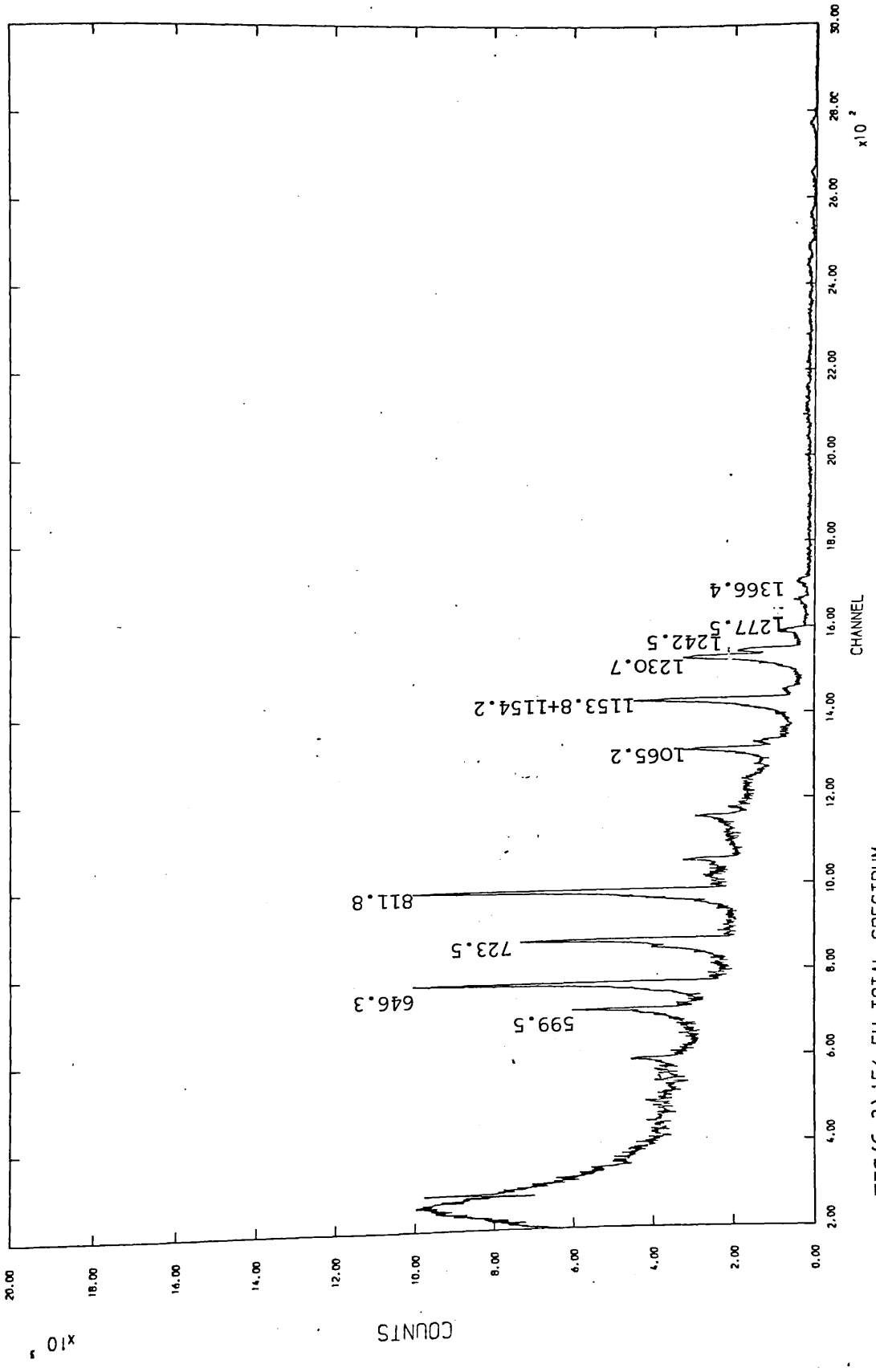

FIG(6.3) 156-EU TOTAL SPECTRUM

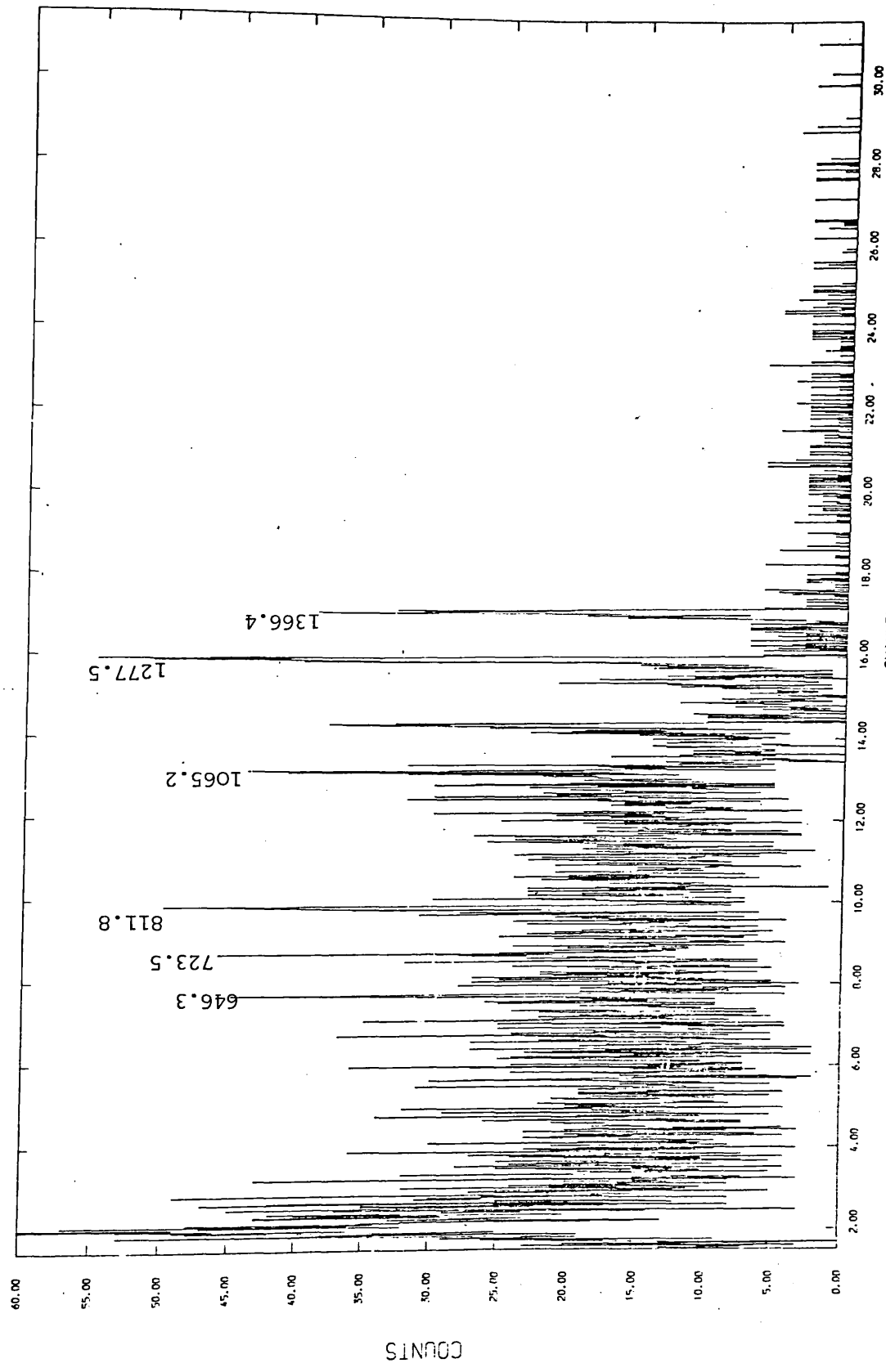

FIG(6.4) SPECTRUM OF 156-EU IN COINCIDENCE WITH 599.5 KEV

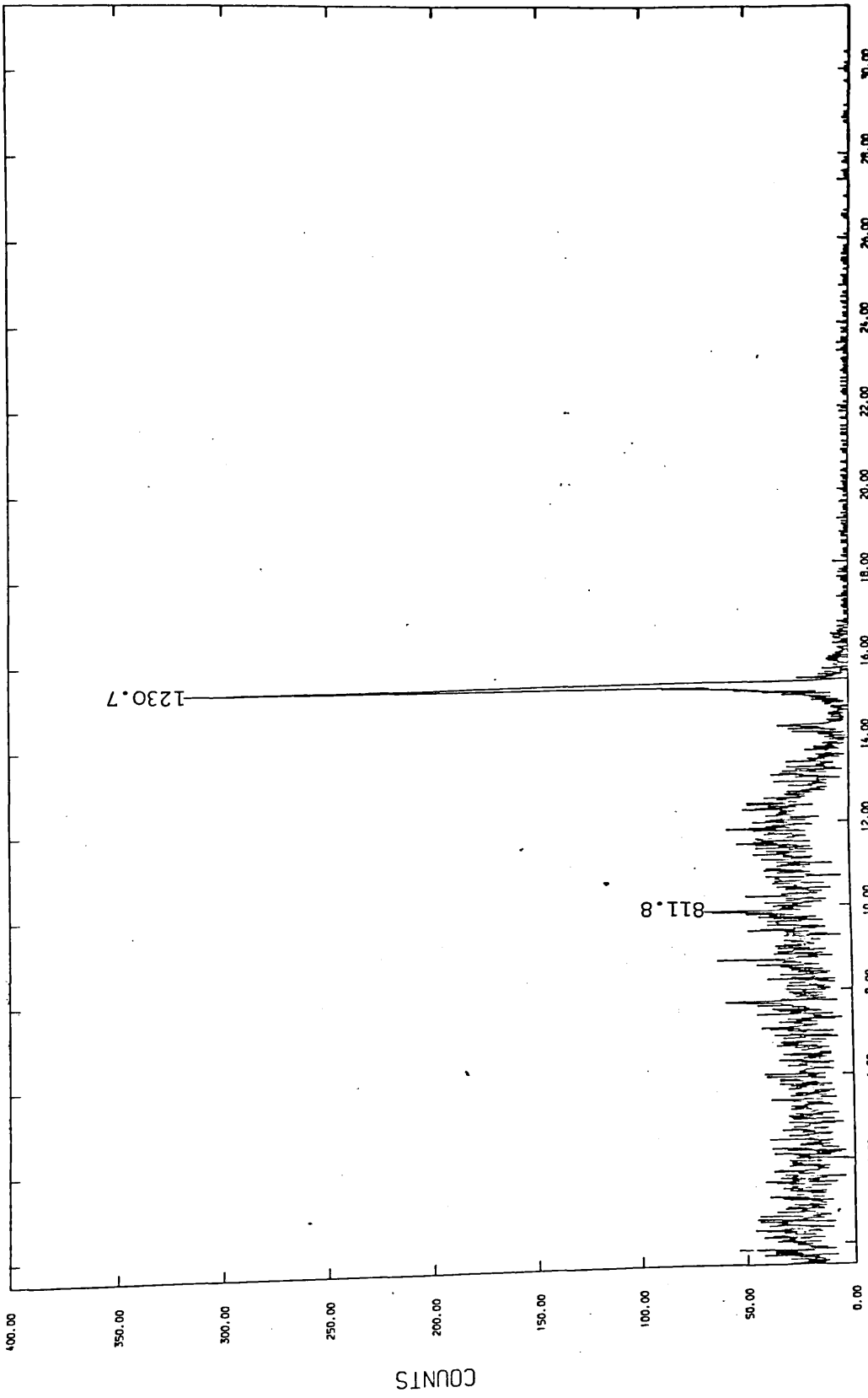

FIG(6.5) SPECTRUM OF 156-EU IN COINCIDENCE WITH 646.2 KEV

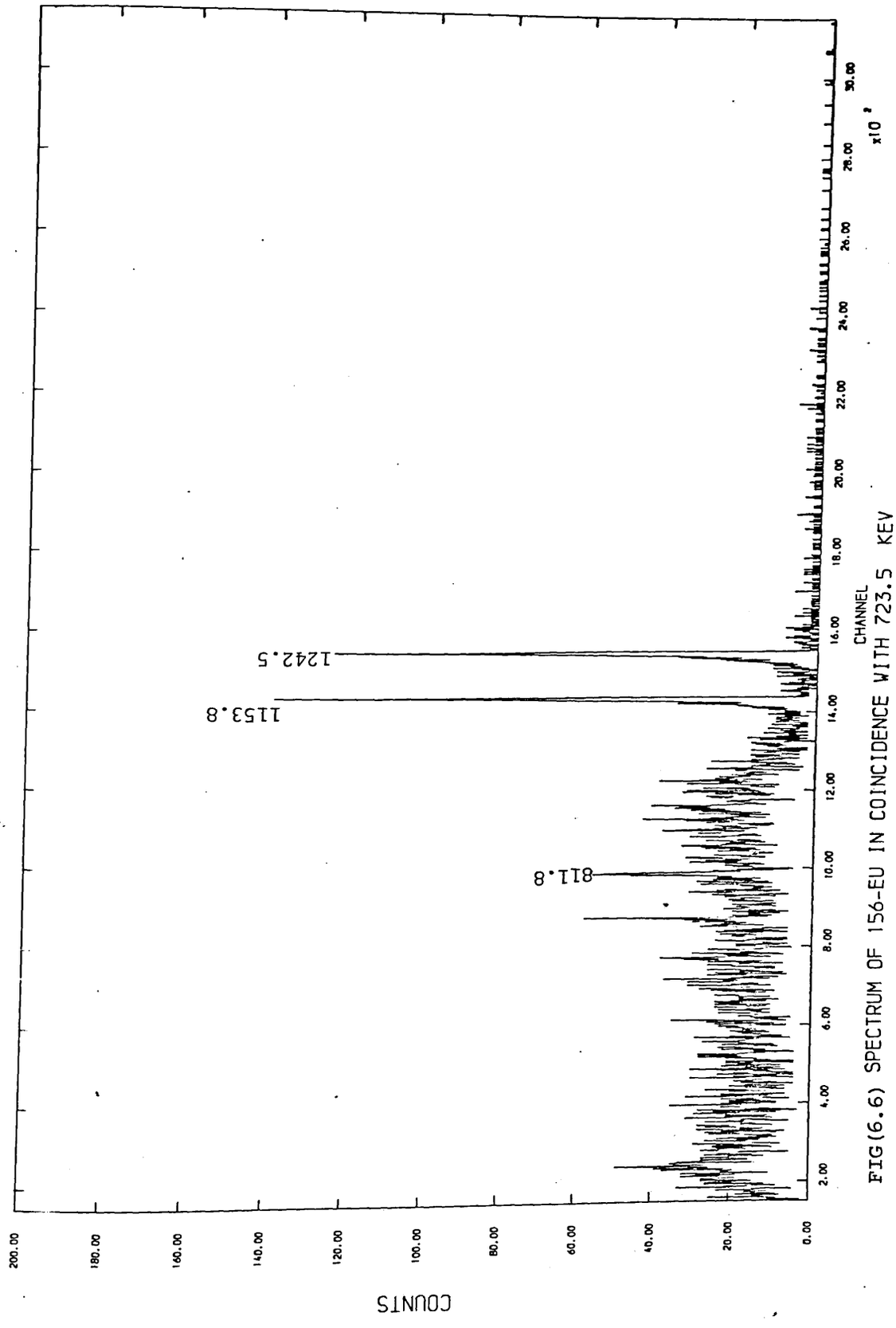

FIG(6.6) SPECTRUM OF 156-EU IN COINCIDENCE WITH 723.5 KEV

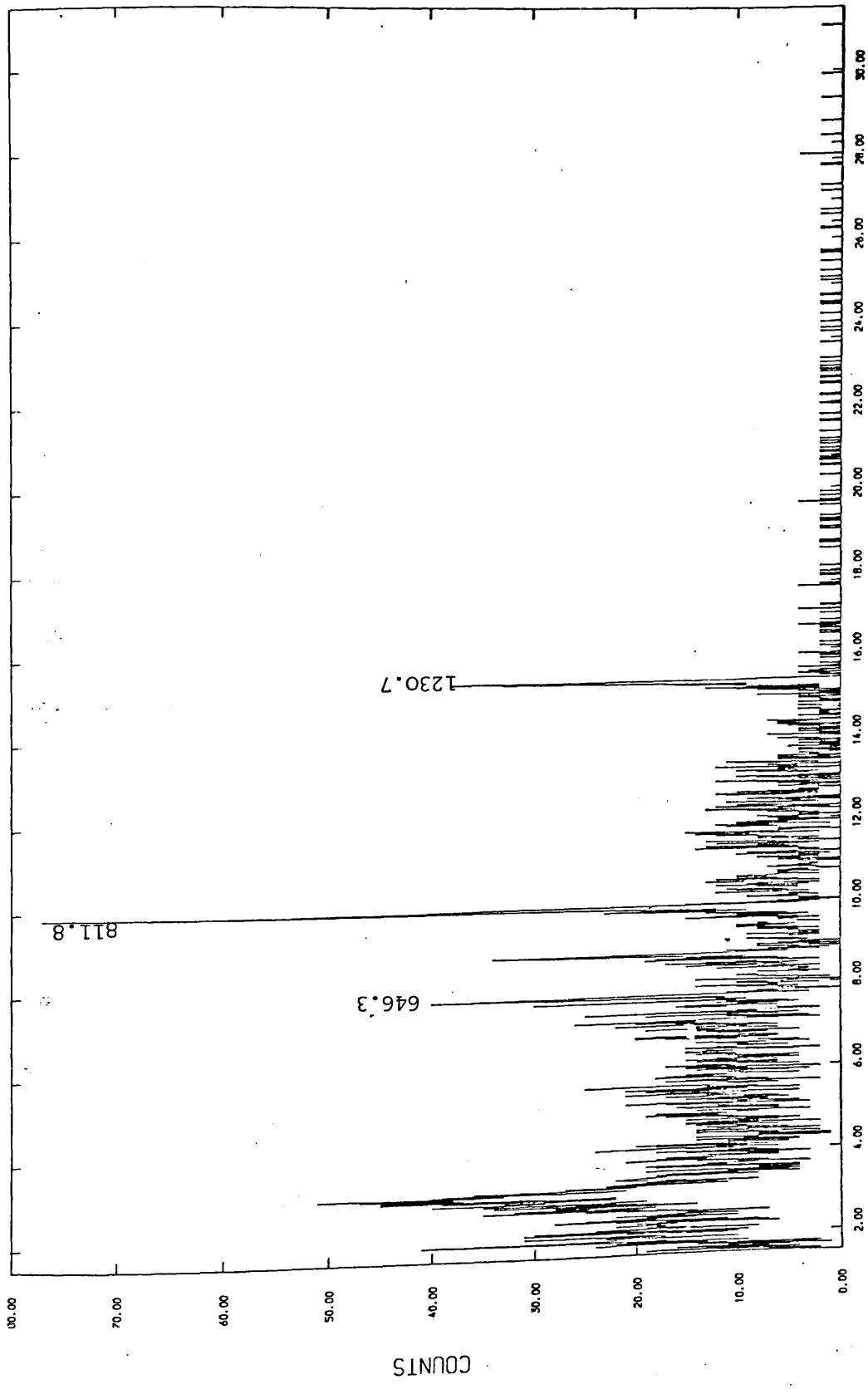

FIG(6.7) SPECTRUM OF 156-EU IN COINCIDENCE WITH 867.0+866-KEV

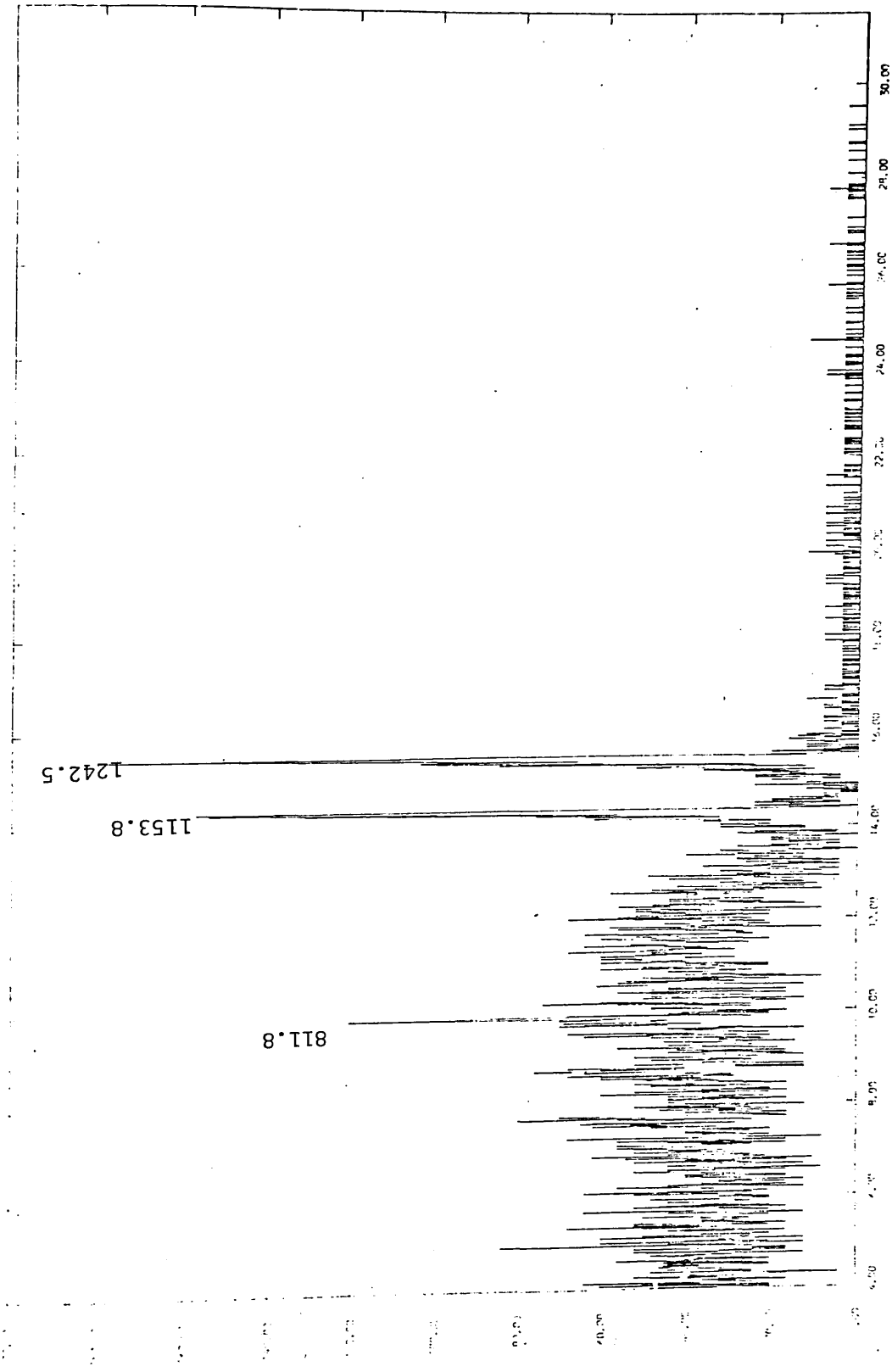

FIG(6.8)

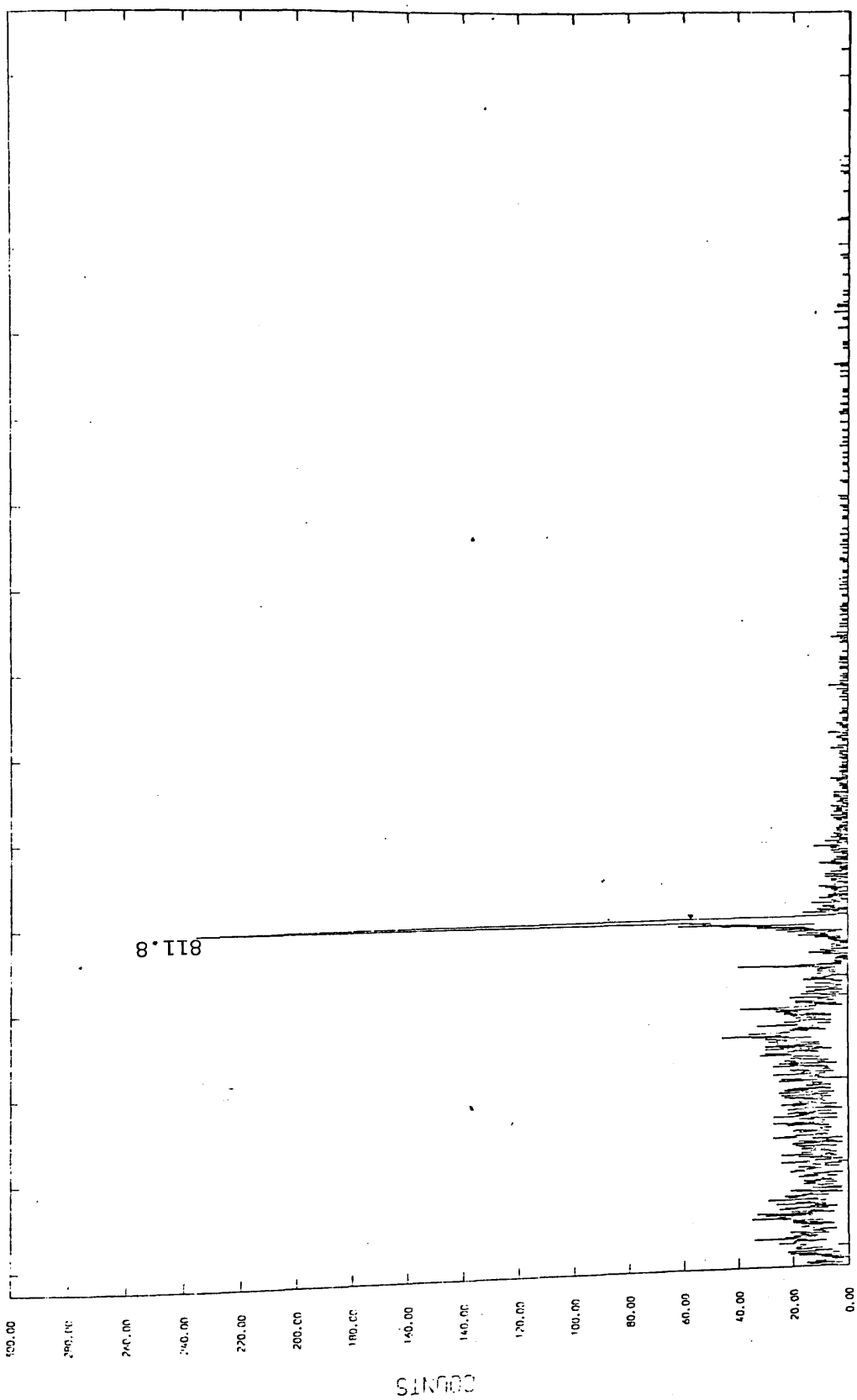

FIG(6.9)SPECTRUM OF 156-EU IN COINCIDENCE WITH 1065.1 KEV

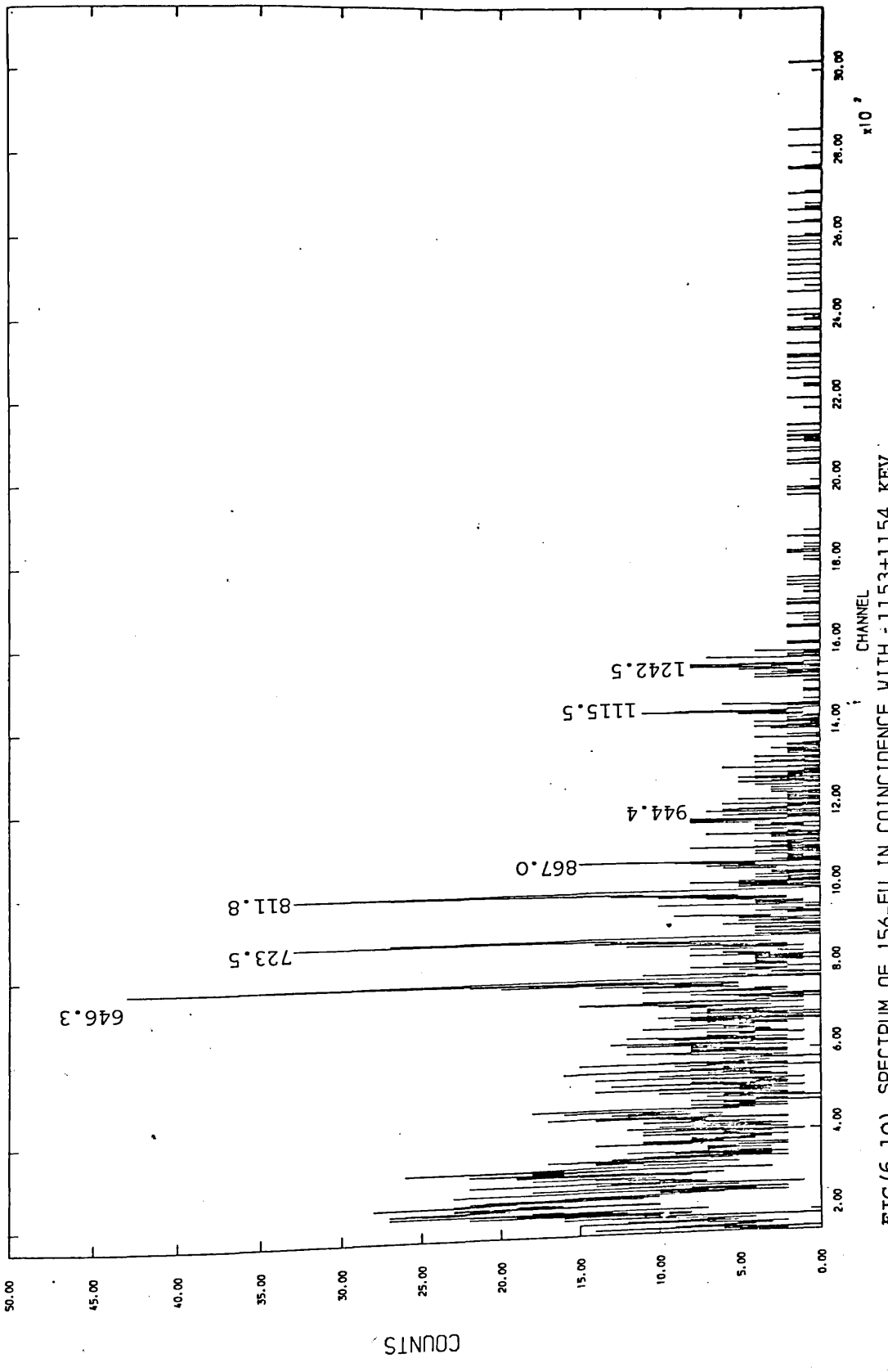

FIG(6.10) SPECTRUM OF 156-EU IN COINCIDENCE WITH 1153+1154 KEV

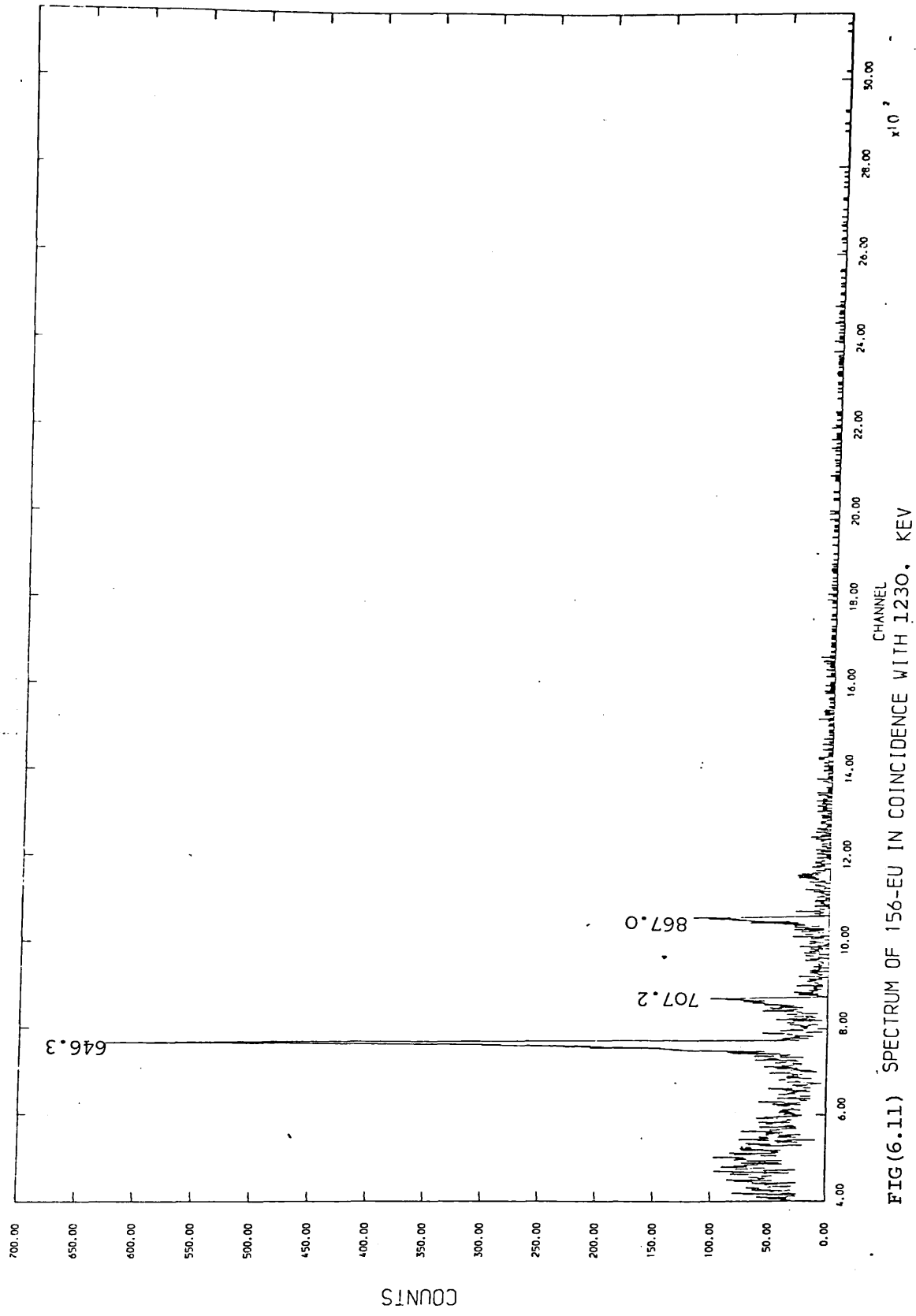

FIG(6.11) SPECTRUM OF 156-EU IN COINCIDENCE WITH 1230. KEV

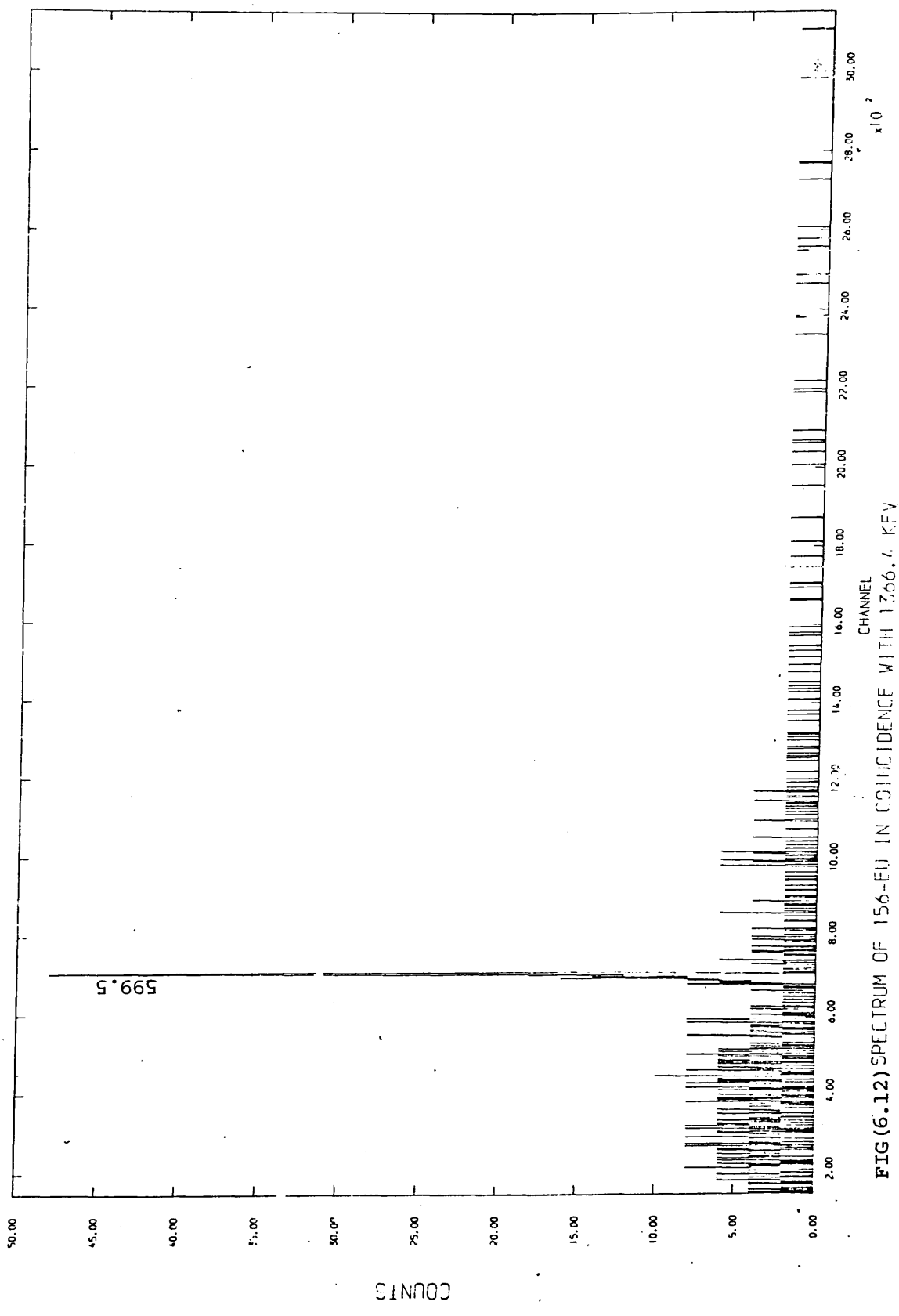

FIG(6.12) SPECTRUM OF 156-EU IN COINCIDENCE WITH 1366.4 KEV

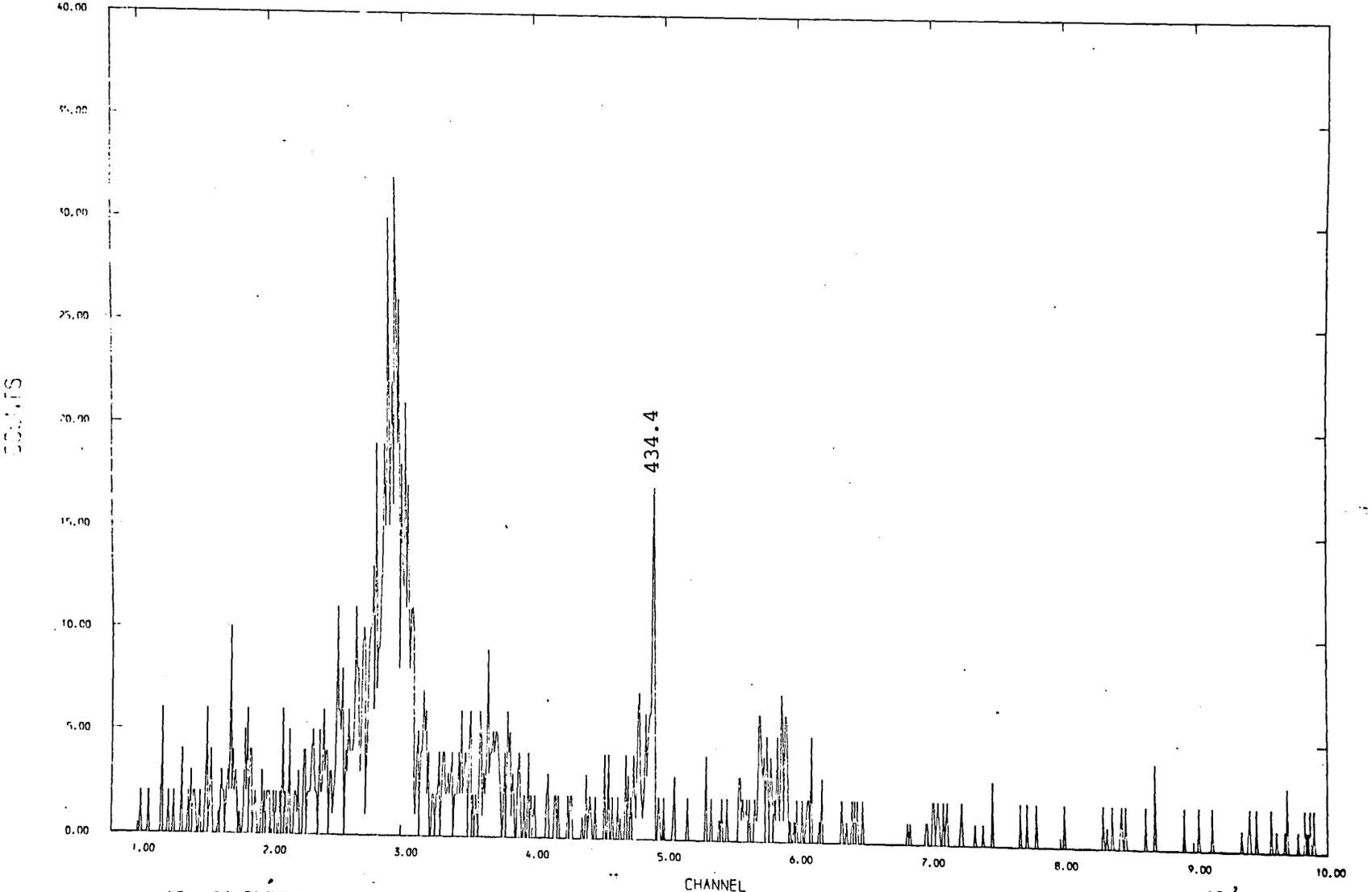

FIG(6.13) SPECTRUM OF 156-EU IN COINCIDENCE WITH 1682.1 KEV

Eγ Crate (keV)	599	646	723	866 + 867	944	1065	1153 + 1154	1230	1366	1682
190.2										
199.2										
317.3										
434.4										VS
472.7										
490.3										
599.5									VS	
646.3	W			W				VS		
707.2								VS		
723.5	W			W						

Table (6.4) A summary of the coincidence results

E_γ Crate (keV)	599	646	723	866 + 867	944	1065	1153 + 1154	1230	1366	1682
768.5										
797.7										
811.8	W		VW	VS	VW	VS	S			
820.4										
836.6										
841.1										
858.4										
866.0										
867.0							S	VS		
872.5										
944.4							VS			

Table (6.4) A summary of the coincidence results, continued (2)

Eγ Crate (keV)	599	646	723	866 + 867	944	1065	1153 + 1154	1230	1366	1682
947.4										
960.5										
961.0										
969.8										
1011.9										
1027.4										
1040.4										
1065.2										
1076.0										
1079.2										
1115.5							VS			

Table (6.4) A summary of the coincidence results, continued (3)

E Crate (keV)	599	646	723	866 + 867	944	1065	1153 + 1154	1230	1366	1682
1140.5										
1153.8			VS		VS					
1154.2										
1156.0										
1169.1										
1230.7		VS		VS						
1242.5			VS		VS		W			
1258.1										
1277.5	VS									
1366.4										
1682.1										

Table (6.4) A summary of the coincidence results, continued (2)

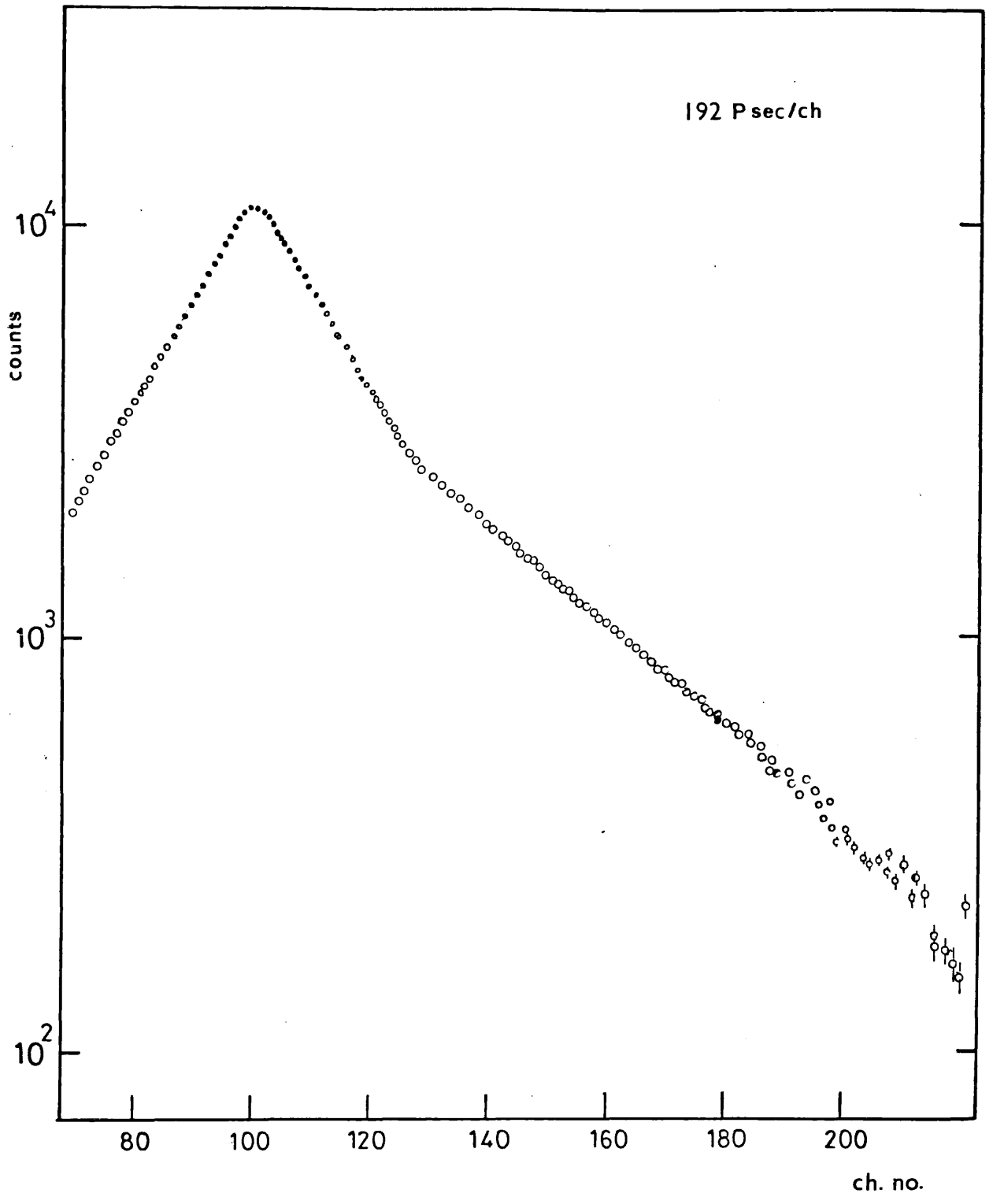

Fig(6.14) The 89 keV level lifetime spectrum

represent Very Strong, Strong, Weak, Very Weak and Probable (within the error limits of the coincidence data), respectively.

6.4 The lifetime measurement

The ^{156}Gd energy level of 88.95 keV has a lifetime in the nanosecond range, so the full use of the Dual-Parameter Energy-Time spectrometer (described in Chapter 3) can provide this lifetime measurement together with the gamma-gamma coincidence. The fast-part spectrum (the spectrum from the TPHC) was gated by the 89 keV photopeak taken from the gating (stop Ge(Li)) detector.

The 89 keV level lifetime spectrum is shown in Fig.(6.14). The analysis of the spectrum was done using the slope method[100]. The experimental errors were <2.8% which is respectively small due to the good linear response of the TPHC (Section 3.4) over the range of approximately 20 n.sec. Table (6.5) shows the result of the lifetime measurement together with those of previous workers.

Table (6.5) The 89 keV level lifetimes (n.sec)

Present work	Meiling et al.[122]	Fossan et al.[123]
2.21 ± 0.05	2.19 ± 0.06	2.16 ± 0.06

This result with slightly improved accuracy is in excellent agreement with the value reported by Meiling et al.[122]. Also the agreement with value reported by Fossan et al.[123] is very good.

6.5 Decay scheme and discussion

Based on the coincidence results, gamma-ray energies and energy sum relations the decay scheme of ^{156}Gd was obtained and is shown in Fig.(6.15). The energy sum relations are given in Table (6.6). The log ft values,

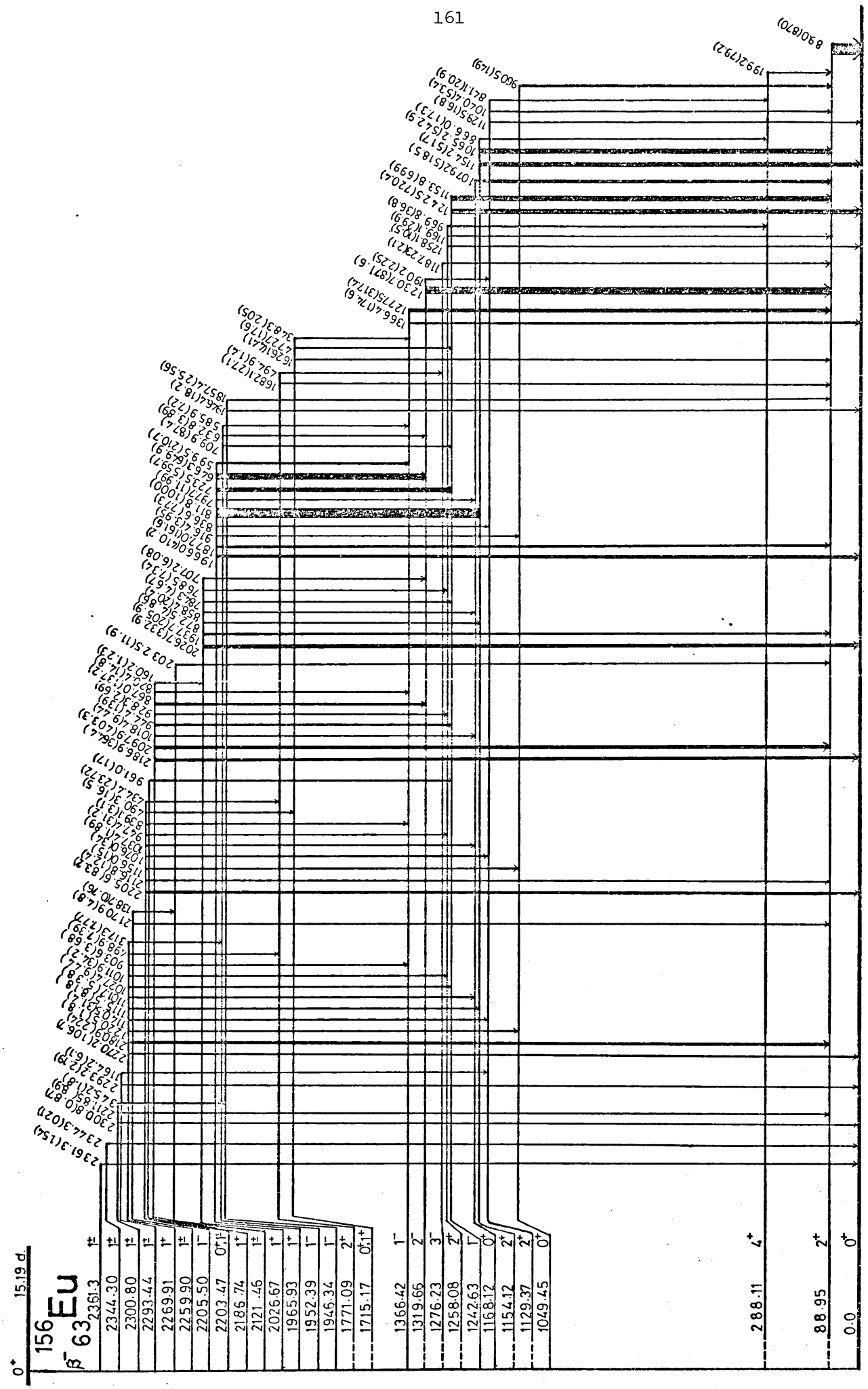

Fig(6.15) Level scheme of ^{156}Gd

Table (6.6) Energy sum relations

Energy Sum (keV)	Mean	Energy level (keV)
88.95		88.95
199.16 + 88.95		288.11
960.50 + 88.95		1049.45
1129.49	1129.49	1129.37
1040.46 + 88.95	1129.41	
841.11 + 199.16 + 88.95	1129.22	
1154.12		1154.12
1065.19 + 88.95	1154.14	
865.99 + 199.16 + 88.95	1154.10	
1079.17 + 88.95		1168.12
1242.47	1242.47	1242.63
1153.84 + 88.95	1242.79	
1258.08	1258.08	1258.08
1169.28 + 88.95	1258.23	
969.82 + 199.16 + 88.95	1257.93	
1187.28 + 88.95	1276.23	1276.23
1366.42	1366.42	1366.42
1277.46 + 88.95	1366.41	

Table (6.6) continued (2)

Energy Sum (keV)	Mean	Energy level (keV)
1626.05 + 88.95	1715.00	1715.17
472.70 + 1242.63	1715.33	
1682.14 + 88.95		1771.09
1946.36	1946.36	1946.34
1857.37 + 88.95	1946.32	
709.86 + 1242.47	1952.33	1952.39
632.78 + 1230.71 + 88.95	1952.44	
585.99 + 1366.42	1952.41	
1965.98	1965.98	1965.93
1876.97 + 88.95	1965.92	
916.41 + 960.50 + 88.95	1965.86	
836.57 + 1129.49	1966.06	
811.75 + 1154.15	1965.90	
797.65 + 1079.17 + 88.95	1965.77	
723.48 + 1242.47	1965.95	
646.29 + 1230.71 + 88.95	1965.35	
599.53 + 1366.42	1965.95	

Table (6.6) continued (3)

Energy Sum (keV)	Mean	Energy level (kev)
202.74	2026.73	2026.67
1937.74 + 88.95	2026.69	
872.49 + 1154.15	2026.64	
858.35 + 1079.17 + 88.95	2026.57	
784.32 + 1242.47	2026.79	
768.49 + 1258.08	2026.57	
767.1 + 1230.71 + 88.95	2026.76	
2032.51 + 88.95		2121.46
2186.91	2186.91	2186.74
2097.93 + 88.95	2186.88	
1018.42 + 1079.17 + 88.95	2186.54	
944.43 + 1242.47	2186.80	
928.34 + 1258.08	2186.42	
867.01 + 1230.71 + 88.95	2186.67	
160.2 + 2026.73	2186.93	
961.0 + 1242.47		2203.47
2205.56	2205.56	2205.50
2116.8 + 88.95	2205.75	
1155.95 + 960.5 + 88.95	2205.40	
1075.98 + 1129.49	2205.47	
1037.38 + 1079.17 + 88.95	2205.50	
947.43 + 1258.08	2205.51	
839.08 + 1366.42	2205.50	
490.34 + 1626.05 + 88.25	2205.34	
434.40 + 1682.14 + 88.95	2205.49	

Table (6.6) continued (4)

Energy Sum (keV)	Mean	Energy level (keV)
2170.95 + 88.25		2259.90
2270.17	2270.17	2269.91
1027.38	1242.47	2269.85
2180.89 + 88.95	2269.84	
1220.5 + 960.5 + 88.95	2269.95	
1140.46 + 1129.49	2269.95	
1101.70 + 1079.17 + 88.95	2269.82	
1011.87 + 1258.08	2269.92	
903.61 + 1366.42	2270.03	
317.3 + 709.86 + 1242.47	2269.63	
2293.19	2293.19	2293.44
1164.2 + 1129.49	2293.69	
2300.8	2300.80	3200.80
2211.85 + 88.95	2300.80	
2344.3		2344.3
2361.3		2361.3
1230.71 + 88.95	1319.66	1319.66
190.16 + 1129.49	1319.65	

spin and parity assignments together with the β^--feeding branching ratios to each level are given in Table (6.7). The β^- energies were obtained from the energy levels determined and considering the Q-value of 2452 keV given by Burrows[124]. The log ft was evaluated using the Mozkowaki[74] momograms. The multipolarity of the γ-ray transition determined were also useful in spin-parity assignments for the ^{156}Gd levels, so that the experimental K-shell internal-conversion coefficient values were calculated from the gamma-ray intensities reported here (Table 6.2) and the K-electron intensities I(K) of H. Yamada et al.[121]. The experimental α(K) for transitions in ^{156}Gd are compared with the theoretical values corresponding to E1, E2 and M1 multipolarity in Table (6.8). The theoretical values were taken from Hamilton et al.[125] for transitions below 1.5 MeV and from Trusov[77] for those above 1.5 MeV.

The ^{156}Eu ground state spin-parity of 0^+ (Ref. 124) allows a high β^- feeding ratio of 29.5% (Ref. 107) to the 0^+ ground state of the even even nucleus of ^{156}Gd.

The 288.11 keV level (log ft > 11.8) is observed to decay to the first excited state at 88.95 keV (2^+) via the 199.19 gamma-ray which appears to be a pure (E2) transition (Table 6.8) so that the established spin and parity assignment of 4^+ is verified.

The 1049.45 keV level (log ft 10.3) is observed to decay to the first excited (2^+) state 88.95 keV via the pure (E2) transition of 960.5 keV energy which indicates possible spin-parity values of 0^+ or 4^+. However, from the log ft value the spin-parity assignment (in Table (6.7)) of 0^+ is the most probable value.

The 1129.37 keV level (log ft > 10.9) is observed to decay to the 88.95 keV (2^+) level via the 1040.42 keV which appears to be (E0/E2). It is also observed to decay to the 288.11 keV (4^+) level via the pure (E2) 841.11 keV transition, so that the only possible spin-parity assisgnment is 2^+.

Table (6.7) Log ft values for β^- decay of ^{156}Eu.

Energy level (keV)[a]	β^--feeding %	Log ft value	Spin-Parity[c]
0.0	29.5[b]	9.9	$0^+, 1^+, 1^-$
88.95	< 0.18	> 12.2	$1^+, 2^+, 3^+, 4^+$
288.11	< 0.16	> 11.8	$1^+, 2^+, 3^+, 4^+$
1049.45	1.42	10.3	$0^+, 1^+, 1^-$
1129.37	< 0.09	> 10.9	$1^+, 2^+, 3^+$
1154.12	< 0.16	> 10.8	$1^+, 2^+, 3^+$
1168.12	4.18	9.8	$0^+, 1^+, 1^-$
1242.63	6.0	9.4	$0^+, 1^+, 1^-$
1258.08	< 0.01	> 10.1	$1^+, 2^+, 3^+$
1276.23	< 0.51	> 10.0	$1^+, 2^+, 3^+$
1319.66	< 0.49	> 9.9	$1^+, 2^+, 3^+$
1366.42	2.49	9.7	$0^+, 1^+, 1^-$
1715.17	< 0.04	> 9.2	$0^+, 1^+, 1^-$
1771.09	< 0.01	> 9.8	$1^+, 2^+, 3^+$
1946.34	0.48	9.0	$0^+, 1^+, 1^-$
1952.39	1.01	8.7	$0^+, 1^+, 1^-$
1965.93	32.8	7.4	$0^+, 1^+, 1^-$
2026.67	6.4	7.5	$0^+, 1^+, 1^-$
2121.46	0.14	8.9	$0^+, 1^+, 1^-$
2186.74	11.4	6.8	$0^+, 1^+$
2203.47	0.19	8.3	$0^+, 1^+, 1^-$
2205.50	3.12	6.9	$0^+, 1^+, 1^-$
2259.90	0.09	8.2	$0^+, 1^+, 1^-$
2269.91	4.88	6.5	$0^+, 1^+$
2293.44	0.09	8.0	$0^+, 1^+, 1^-$
2300.80	0.11	7.6	$0^+, 1^+, 1^-$
2344.30	0.01	8.2	$0^+, 1^+, 1^-$
2361.3	0.02	7.6	$0^+, 1^+, 1^-$

Table (6.7) Log ft values for β^- decay of ^{156}Eu, continued (2)

a - The error in the reported energy level values ranges from 0.01 to 0.05 keV for levels less than 2 MeV and from 0.04 to 0.5 keV for levels above 2 MeV, and hence leads to error in determining the β^- energy feeding for these levels.

b - The ground state β^- decay feeding ratio of 29.5% is taken from Peak et al.[107].

c - This spin-parity assignment is based on the log ft value only. The spin parity for the ^{156}Gd level indicated in the decay scheme is based on more information (the transitions multipolarity) discussed in Section (6.5).

E_γ (keV)	$I_i^{\pi_i} \rightarrow I_f^{\pi_f}$	Experimental $\alpha_K \times 10^4$						Theoretical $\alpha_K \times 10^4$			Adopted multipolarity
		Present Work		Kluk et al.		Peek et al.		E1	E2	M1	
88.95	$2^+ \rightarrow 0^+$	15340	(180)	14340	(1360)			3370	15800	24300	E2
199.19	$4^+ \rightarrow 2^+$	1396	(78)	1340	(104)			390	1580	2490	E2
434.5	$1^- \rightarrow 1^+$	52.7	(28)					55.5	164.4	312.9	E1
472.7	$0^+ \rightarrow 1^-$	38.5	(89)					45.7	131.5	252	E1
490.3	$1^- \rightarrow 0^+$	40.3	(85)					42.1	119.7	229.9	E1
499.0	$1^+ \rightarrow 1^+$	188.2	(957)					40.5	114.4	219.9	M1/E2
585.99	$1^- \rightarrow 1^-$	121.8	(511)	144	(90)			28.4	76.7	146.9	M1/E2
599.5	$1^+ \rightarrow 1^-$	31.3	(38)	25.4	(20)	35	(11)	27.1	72.5	138.7	E1
646.3	$1^+ \rightarrow 2^-$	22.0	(16)	23.6	(18)			23.1	60.7	115	E1
709.86	$1^- \rightarrow 1^-$	99.6	(15)	97	(8)			19	48.8	91.2	M1
723.5	$1^+ \rightarrow 1^-$	17.4	(14)	19.6	(15)	15	(2)	18.3	46.8	87	E1
797.7	$1^+ \rightarrow 0^+$	50	(11)	57	(12)			15	37.6	68.5	M1/E2
811.7	$1^+ \rightarrow 2^+$	59.4	(30)	67.4	(50)			14.5	36.2	65.7	M1
836.4	$1^+ \rightarrow 2^+$	58.9	(167)					13.7	33.9	61.1	M1
841.2	$2^+ \rightarrow 4^+$	32.9	(57)					13.5	33.5	60.2	E2

Table (6.8) K-Shell Internal-Conversion Coefficients

E_γ (kev)	$I_i^{\pi_i} \rightarrow I_f^{\pi_f}$	Experimental $\alpha_K \times 10^4$						Theoretical $\alpha_K \times 10^4$			Adopted multipolarity
		Present Work		Kluk et al.		Peek et al.		E1	E2	M1	
858.4	$1^+ \rightarrow 1^+$	43.9	(94)	78	(48)			13	32	57.4	M1/E2
865.99	$2^+ \rightarrow 4^+$	35.1	(50)	37.4	(70)			12.8	31.4	56.2	E2
867.2	$1^+ \rightarrow 2^-$	11.4	(20)	15.0	(19)			12.8	31.3	56	E1
944.2	$1^+ \rightarrow 1^-$	8.2	(32)					10.8	26.1	45.6	E1
960.5	$0^+ \rightarrow 2^+$	26.1	(19)	24.8	(22)	12	(5)	10.5	25.2	43.8	E2
969.82	$2^+ \rightarrow 4^+$	29.3	(40)					10.3	24.7	42.8	E2
1011.9	$1^+ \rightarrow 2^+$	44.9	(105)	43	(5)			9.5	22.6	38.7	M1
1018.5	$1^+ \rightarrow 0^+$	49	(10)	60	(12)			9.4	22.4	38.1	M1
1040.5	$2^+ \rightarrow 2^+$	108.8	(95)	12.6	(10)			9.	21.4	36.2	E0/E2
1065.19	$2^+ \rightarrow 2^+$	18.5	(18)	23.6	(18)	26	(9)	8.7	20.4	34.2	E2
1079.2	$0^+ \rightarrow 2^+$	18.4	(17)	20.1	(16)	16	(4)	8.5	19.9	33.2	E2
1140.5	$2^+ \rightarrow 2^+$	28.1	(77)					7.6	17.8	29.1	M1
1153.84	$1^- \rightarrow 2^+$	8.0	(7)	6.9	(7)	5.3	(13)	7.5	17.4	28.3	E2
1154.1	$2^+ \rightarrow 0^+$	16.7	(19)	18.4	(18)			7.5	17.4	28.3	E2
1168.8	$2^+ \rightarrow 2^+$	22.5	(34)					7.3	17	27.4	M1/E2
1230.7	$2^- \rightarrow 2^+$	6.6	(4)	6.2	(5)	4.9	(8)	6.7	15.4	24.3	E1

Table (6.8) K-Shell Internal-Conversion Coefficients, continued (2)

E_γ (kev)	$I_i^{\pi_i} \rightarrow I_f^{\pi_f}$	Experimental $\alpha_K \times 10^4$						Theoretical $\alpha_K \times 10^4$			Adopted multipolarity
		Present Work		Kluk et al.		Peek et al.		El	E2	M1	
1242.47	$1^- \rightarrow 0^+$	6.3	(4)	6.3	(5)			6.6	15.1	23.8	E1
1258.08	$2^+ \rightarrow 0^+$	13.5	(34)					6.4	14.7	23.1	E2
1277.4	$1^- \rightarrow 2^+$	5.5	(7)	5.6	(15)			6.2	14.5	22.1	E1
1366.8	$1^- \rightarrow 0^+$	6.6	(17)	5.5	(17)			5.5	12.5	19.1	E1
1682.14	$2^+ \rightarrow 2^+$	14.7	(52)					4	8.6	11.5	M1
1857.4	$1^+ \rightarrow 2^+$	2.3	(12)					3.4	7.9	9.2	E1
1876.6	$1^+ \rightarrow 2^+$	8.5	(8)	10.7	(12)			3.3	6.9	9.1	M1
1937.5	$1^+ \rightarrow 2^+$	8.5	(4)	9.3	(9)			3.2	6.5	8.5	M1
1946.1	$1^- \rightarrow 0^+$	5.3	(29)					3.2	6.4	8.3	M1/E2 or E1
1965.8	$1^+ \rightarrow 0^+$	8.6	(3)	9.3	(7)			3.1	6.3	8.1	M1
2026.6	$1^+ \rightarrow 0^+$	7.9	(5)	7.9	(7)	10	(8)	3.0	6.0	7.8	M1
2097.9	$1^+ \rightarrow 2^+$	6.8	(5)	7.4	(6)	6.6	(8)	2.8	5.6	7.1	M1
2180.6	$1^+ \rightarrow 2^+$	6.6	(3)	6.2	(6)	5.6	(3)	2.6	5.3	6.5	M1
2186.6	$1^+ \rightarrow 0^+$	6.7	(4)	8.1	(6)	7.6	(14)	2.6	5.2	6.4	M1
2205.2	$1^- \rightarrow 0^+$	2.9	(3)					2.6	5.1	6.3	E1
2270.1	$1^+ \rightarrow 0^+$	5.1	(14)					2.4	4.9	6	M1/E2

Table (6.8) K-Shell Internal-Conversion Coefficients, continued (3)

The 1154.12 keV level (log ft > 10.8) is observed to decay to the 88.95 keV (2^+) level via the 1065.19 keV (E2) transition and via the 865.99 keV gamma-ray which also appears to give a pure (E2) transition to the (4^+) 288.11 keV level. From the possible spin-parity assignments for this level in Table (6.7) it is concluded that spin-parity assignment is 2^+.

The energy level at 1168.12 keV (log ft = 9.8) is observed to decay to the first excited state at 88.95 keV (2^+) via the 1079.17 keV (E2) transition and is fed by the 1101.70 keV pure (M1) transition from the 2269.91 keV (1^+) level. Again, these data along with log ft value indicate $I^\pi = 0^+$.

The 1242.63 keV level (log ft 9.4) yields a pure (E1) transition of 1242.47 keV and an (E1) transition of 1153.84 keV to the (0^+) ground state and the 88.95 keV (2^+) level, clearly indicate a spin parity assignment of 1^-.

The energy level at 1258.08 keV (log ft > 10.1) is observed to decay to the ground state via 1258.08 keV (E2) transition and also to the 288.11 keV (4^+) level via the 969.82 keV transition which appears to be pure (E2) so that the established spin and parity assignment of 2^+ is verified.

The new suggested level at 1276.1 keV (log ft > 10.0) is not shown in the last proposed ^{156}Gd level scheme[109] from ^{156}Eu decay. This level is mainly fed by the new 494.9 kev γ-ray (identified in Table (6.3)) from the 1771.17 keV level, and observed to decay to the 88.95 keV level via the new 1187.28 keV transition; the possibility of β^--feeding is very poor so that the probable value of spin-parity from log ft value 3^+, 2^+, 1^+, but in the ^{155}Gd (n,γ) ^{156}Gd studies[115] this level has been observed and a spin-parity assignment of 3^- was reported. Both 494.9 keV and 1187.28 keV transitions, which feed and depopulate this level respectively, were adopted as pure E1 transitions in the studies of Ref.[115]. In the present work the additional information that transitions arise from (2^+)

1771.08 keV level to the 1276.1 keV level and from 1276.1 keV level to the (2^+) 88.95 keV level leads to a spin-parity assignment of 3^-.

The 1319.66 keV level (log ft > 9.9) is established from the strong coincidence between the 1230.71 keV gamma-ray arising by a pure (E1) transition from this level to the first excited state 88.95 keV (2^+) and the 646.29 gamma-ray (E1) transition which is mainly feed this level and coming from the (1^+) 1965.93 keV level this led to an odd parity assignment and spin value of 2 which was also indicated by the log ft value.

The 1366.42 keV level (log ft = 9.7) is observed to decay to ground state (0^+) by the 1366.42 keV gamma-ray which appears to be a pure (E1) transition, so that the possible spin-parity assignment is 1^-, which is also indicated by the log ft value.

The 1715.17 keV level (log ft > 9.2) has been placed for the first time in the last proposed ^{156}Gd level scheme [109], and I^π assignment of 0^+ or 1^+ or 1^- was made. In the present work this level is observed to decay to the 88.95 keV (2^+) level via 1626.05 keV transition and also via 472.70 keV gamma-ray to the 1242.63 keV level (1^-) which appears to be a pure (E1) transition. This information along with the log ft value indicates a probable spin-parity assignment of 0^+ or 1^+.

The 1771.09 keV level (log ft > 9.2) is observed to decay to the 88.95 keV (2^+) level via the 1682.14 keV gamma-ray which indicate a pure (M1) transition, also to decay to the (3^-) 1276.1 keV level via 494.9 keV gamma-ray (E1) transition, so that the spin and parity assignment of (2^+) for this level is the most probable value.

The 1946.34 keV level (log ft = 9.0) has been placed for the first time in the level scheme proposed by Kluck et al.[109] and a I^π assignment of 1^+ or 1^- was made. From the data reported here this level is seen to decay to the (0^+) ground state by the 1946.36 keV gamma-ray in a (M1/E2 or E1) transition, and it also decays to the 88.95 keV (2^+) level via the

1857.37 keV gamma-ray which appears to be pure (E1) transition. These data along with log ft value clearly indicate a spin-parity assignment of 1^- for this level.

The 1952.39 keV level (log ft 8.7) again has been proposed for the first time in the last established level scheme[109]. This level is observed to decay to the 1242.63 keV level (1^-) via 709.86 keV (M1) transition, and also to decay to the 1366.42 keV level (1^-) via 585.99 keV (M1/E2) transition. These data along with the calculated log ft value verified the suggested spin-parity assignment of 1^-.

The 1965.93 keV level (log ft 7.4) is established from the strong coincidence between the 1366.42 keV gamma-ray and the 646.29 gamma-ray and also the strong coincidence between the 811.75 keV gamma-ray and the 1065.19 keV gamma-ray. The resulting 646.29 keV and 811.75 keV gamma-rays from this level to the 1319.66 keV (2^-) level and the 1154.12 keV level (2^+), indicate pure (E1) and pure (M1) respectively. These considerations, along with log ft values, lead to spin-parity assignments of 1^+ for this level.

The 2026.67 keV level (log ft = 7.5) is established from the coincidence between the 1230.71 keV gamma-ray and 707.18 keV gamma-ray. It is observed to decay to the (0^+) ground state via the 2096.73 keV gamma-ray (M1) transition and also to the 88.9 keV level (2^+) via the 1937.74 keV gamma-ray (M1) transition; these results, along with log ft value, lead to spin-parity assignemtn of 1^+.

The 2121.46 keV level (log ft $\doteq$ 8.9) was observed for the first time in the Kluck et al.[109] studies. This level is observed from the data reported here to decay to the first excited (2^+) state at 88.95 keV via the 2032.51 keV transition. No evidence was found for the 2121.3 keV gamma-ray transition from this level to the ground state more than 5×10^{-5} relative to the 811.75 keV gamma-ray intensity. However, the log ft value suggest a spin-parity assignemtn of 1^+ or 1^-.

The 2186.74 keV level (log ft = 6.8) is established from the strong coincidence between the 944.4 keV gamma-ray transition and the 1242.47 keV gamma-ray transition. It is observed to decay to the (0^+) ground state via the 2186.91 keV gamma-ray (M1) transition which indicates the I^π of 1^+. In addition the pure (M1) 2097.93 and 1018.42 keV transitions to the 88.95 keV (2^+) and 1168.12 keV level (0^+) respectively give a definite indication of 1^+.

The 2203.47 keV level (log ft = 8.3) is observed to decay to the 1242.47 keV level via the 961.0 keV gamma-ray transition. The log ft value gives the probable spin-parity assignment of 0^+ or $1^\pm$.

The 2205.50 keV level (log ft = 6.9) is a well established level in the previous investigation with I^π assignment of 1^+ or 1^-. In the results reported here, this level is observed to decay to the 0^+ ground state via the 2205.56 keV gamma-ray which appears to be a pure (E1) transition which leads to a spin-parity assignment of 1^-. Also, the 434.40 keV gamma-ray (E1) transition to the 1771.08 keV (2^+) level indicates the same assignment 1^- for this level.

The 2259.90 keV level (log ft = 8.2) is placed for the first time in the decay scheme proposed in [109]. In the present investigation this level is observed to decay to the 88.95 keV (2^+) level via the 2170.95 keV gamma-ray transition and also to the 2121.46 keV (1^-) level. Again, these data along with the log ft value indicate a spin-parity assignment of 1^+ or 1^-.

The 2269.91 keV level (log ft = 6.5) is observed to decay to the ground state (0^+) via the 2270.17 keV transition which appears to be (M1/E2) and also decays to the 1258.08 keV level (2^+) by the pure (M1) 1011.87 keV transition. These data along with the log ft value indicate a spin-parity assignment of 1^+ is the most probable value.

The 2293.44 keV (log ft = 8.0) is reported for the first time in Ref.[109] and from the data reported here this level is observed to decay to the ground

state (0^+) via the 2293.19 keV gamma-ray transition, and also via 1164.2 keV transition to the (2^+) 1129.37 keV level with log ft value indicate a spin value of 1 with odd or even parity.

The 2300.80 keV (log ft = 7.6) is also reported for the first time in the investigation of Kluck et al.[109]. From the present study this level is observed to decay to the ground state (0^+) via the 2300.80 keV transition and also via the 2211.85 keV gamma ray transition to the 88.95 keV (2^+) level. Along with the log ft value this leads to a spin assignment of 1 with odd or even parity.

The 2344.3 keV level (log ft = 8.2) is also reported for the first time in Ref.[109]. From the data reported in here this level is observed to decay to the ground state (0^+) via the 2344.3 keV transition. No evidence for the 2255.5 keV transition from this level to the first excited state at 88.95 was found. This, with the log ft value, indicates the spin assignment of 1 with odd or even parity.

The 236.13 keV level (log ft = 7.6) is observed to decay to the ground state (0^+) via the 2361.3 keV transition, thus suggesting a spin of 1 with either odd or even parity.

6.6 A comparison with theory

The rotational model of Bohr and Mottelson[126] provides a good starting point for analysing and studying most nuclear spectra. However, this model, which makes small amplitude vibrations, fails to explain the decay characteristics of the low lying energy levels in the ^{156}Gd nucleus. A microscopic treatment by Gupta et al.[127] for this problem is therefore considered in order to gain more insight into the structure of this nucleus, the two-body interactions coming from the long range quadrupole force and the short range pairing force being taken into account. Thus the Hamiltonian was written as

$$H = H_{SS} + H_Q + H_P$$

vibration Band	level I	Energy level (MeV) Present work expt.	Theory Ref (127)
g	0	0.0	0.0
	2	0.089	0.087
	4	0.288	1.283
β	0	1.049	1.234
	2	1.129	1.149
γ	2	1.154	1.531
0^+	0	1.168	2.275
	2	1.258	2.586

Table (6.9) Experimental and theoretical energy values for even parity levels in ^{156}Gd.

level I	Energy level (keV) Present work expt.	Theory ref (128)
1^-	1242.63 (6)	1242.5
3^-	1276.23 (20)	1276.0
2^-	1319.66 (6)	1328.6
1^-	1366.42 (3)	1370.4

Table (6.10) Experimental and theoretical energy values for odd parity levels in ^{156}Gd.

Vibration B and	Transitions $I_i \rightarrow I_f/I'_f$	E_γ (keV)	B(E2) branching ratios	
			Present work expt.	Theory Ref(127)
$\beta \rightarrow g$	$2^+ \rightarrow 0^+/2^+$	1129.5/1040.4	0.209 ± 0.008	0.12
	$2^+ \rightarrow 4^+/2^+$	841.1/1040.4	1.11 ± 0.12	2.1
	$2^+ \rightarrow 0^+/4^+$	1129.5/841.1	0.18 ± 0.02	0.05
$\gamma \rightarrow g$	$2^+ \rightarrow 0^+/2^+$	1154.2/1065.2	0.64 ± 0.03	0.64
	$2^+ \rightarrow 4^+/2^+$	866.0/1065.2	0.089 ± 0.003	0.20
	$2^+ \rightarrow 0^+/4^+$	1154.2/866.0	7.1 ± 0.3	3.22
second $0^+ \rightarrow g$	$2^+ \rightarrow 0^+/2^+$	1258.1/1169.1	0.243 ± 0.026	0.44
	$2^+ \rightarrow 4^+/2^+$	969.8/1169.1	3.13 ± 0.35	1.82
	$2^+ \rightarrow 0^+/4^+$	1258.1/969.8	0.078 ± 0.004	0.24

Table (6.11) The B(E2) branching ratios for transition in ^{156}Gd

where H_{SS} is the spherical-shell Hamiltonian, H_Q is a Q-Q interaction with I = 2, and H_P is a pair-pair interaction with I = 0. The parameters of the collective Hamiltonian were derived from a microscopic theory, instead of being taken from experiment. These calculations gave the energy values of even parity levels in ^{156}Gd which are compared with the experimental energy level values from the data reported here in Table (6.9). These values are comparable for the ground state band, but large differences are seen for the other vibrational bands.

The theoretical energy values calculated by Koniju et al.[128] for odd parity levels are given in Table (6.10) along with the measured values.

This calculation is based on the Interacting Boson Approximation (IBA)[129] in which the ^{156}Gd even-even nuclei are described as a system of bosons, where a boson is seen as a collective two-nuclean pair[130].

The agreement of IBA model of odd parity states is so much better than the two-body interactions calculation by Gupta et al.[127] of even-parity states.

Table (6.11) compares the theoretical (from Ref.[127]) reduced transition probability branching ratios and the experimental values calculated from the results reported in this work. In general the B(E2) branching ratios for transition to the (0^+) ground state and the (2^+) first excited state are the most comparable values with the theoretical results, and large differences are seen for those calculated from levels to the (4^+) second excited state and (0^+) ground state.

6.7 Conclusions

The level scheme of ^{156}Gd has been investigated with Ge(Li) detectors using a Dual-Parameter Energy-Time spectrometer. Support is found for the seven new levels reported in the last proposed level scheme for this nucleus. A new level is proposed at 1276.23 keV and identification for five gamma-rays to be placed in the ^{156}Gd level scheme.

No evidence for the weak gamma-ray transitions at 2121.3 keV, 2259.8 keV and 2255.5 keV was found. The measured value of 2.21 ± .05 n.sec for the lifetime of the 88.95 keV level shows good agreement with the previous measurements. More definite spin-parity assignments have been reported here than in the last proposed level scheme of Kluck et al. Notably the 1715.17 keV, 1771.09 keV, 1946.34 keV and 2205.50 keV levels are found to be 0^+ or 1^+, 2^+, 1^- and 1^- respectively.

REFERENCES

1. J.H. Hamilton and J.C. Manthuruthil, Radioactivity in Nuclear Spectroscopy, Vol. 1 (Gordon & Breach, Science Publishers, 1969).

2. W.D. Hamilton, The Electromagnetic Interaction in Nuclear Spectroscopy (North-Holland Publishing Company, 1975).

3. B. Burde, V. Richter, Nucl.Instr. and Meth. 151, 961 (1978).

4. A. Hamilton, Radioactivity in Nuclear Spectroscopy, Vol. 1 (1972) Gordon & Breach, London.

5. D. Gardner and J. Gardner, Chem.Phys. 31, 178 (1959).

6. W. Nervik, Application of Computers to Nuclear and Radiochemistry, Washington, NAS-NS 3107, 1963, P.9.

7. H. Bateman, Proc.Cambridge Phil.Soc. 15, 423 (1910).

8. W.J. Rubinson, Chem.Phys. 17, 542 (1949).

9. J.M. Blatt and W.F. Weisskoph, Theoretical Nuclear Physics (John Wiley & Sons, New York, 1952).

10. H. Morinaga and T. Yamazaki, In-Beam Gamma-Ray Spectroscopy (North-Holland Pub.Co. 1976).

11. N. Tralli and G. Goertzel, Phys.Rev. 83, 399 (1951).

12. M.H. Hebb and E. Nelson, Phys.Rev. 58, 486 (1940).

13. T.A. Green and M.E. Rose, Phys.Rev. 110 (1958) 105.

14. K. Umeda, J.Fac.Sc. Hokkaido Imp. Univ. II, 3 (1949).

15. M.E. Rose, Phys.Rev. 91, 610 (1953).

16. L.A. Sliv and I.M. Band, α, β and γ-ray spectroscopy App.5. ed. K. Siegbahn (North Holland Publishing Co., 1965).

17. E.L. Church and J. Wenesen, Phys.Rev. 163, 1035 (1956).

18. S.G. Nilsson, Math.Fys.Medd. 29, 16 (1955).

19. V.F. Weisskoph, Phys.Rev. 83, 1073 (1951).

20. Townes et al. Phys.Rev. 76, 1415 (1949).

21 M. Goldhaver and A. Sunyar, Phys.Rev. 83, 906 (1951).

22. J. Rainwater, Phys.Rev. 79, 432 (1950).

23. A. Bohr, Rotational States of Atomic Nuclei (E. Munksgaard, Copenhagen, 1954).

24. A. Bohr and B. Mottelson, Mat.Fys.Medd. 27, No.16 (1953).

25. J.B. French and B.J. Raz, Phys.Rev. 104, 1411 (1956).

26. D.M. van Patter, Bull.Am.Phys.Soc. Ser.II, 3, 212 and 360 (1958).

27. V.K. Thankappan, Phys.Lett. 2, 122 (1962).

28. V.K. Thankappan and S.P. Pandya, Nucl.Phys. 19, 303 (1960).

29. V.K. Thankappan and S.P. Pandya, Nucl.Phys. 39, 394 (1962).

30. B. Castel, Nucl.Phys. A162. 273 (1971).

31. B. Castel et al. Can.J.Physics, 51. 2403 (1973).

32. J.B. McGrory and S. Raman, Phys.Rev.C 20, No. 2 (1979) 830.

33. K. Ogawa and H. Horie, Nucl.Phys. A216, 406 (1973).

34. K. Debertin and U. Schötzig, Nucl.Instr. and Meth. 158 (1979) 471.

35. The chemical standards sources are standard reference radioactive materials available from the Radiochemical Centre, Amersham, Buckinghamshire, U.K.

36. U.S.A. Atomic Energy γ-ray Spectrum Catalogue (3rd Edition), Aerojet Nuclear Company, U.S.A. Energy Research & Development Administration.

37. U. Schötzig et al., Int.J.Appl.Rad.Isotopes, 28 (1977) 503.

38. R.L. Auble, Nucl.Data Sheets 20 (1977) 327.

39. J.T. Routti, Lawrence Berkeley Laboratory Report UCRL 19452 (1969).

40. J.T. Routti and S.G. Brussin, Nucl.Instr. and Meth. 72 (1969) 125.

41. P.M. Endt, Nucl.Phys. A214, 388 (1973).

42. P.M. Endt and C. Vanddeleum, Nucl.Phys. A214 80 (1973).

43. R.L. Buntind and J.J. Kraushaar, Nucl. Data Sheets, 18. 87 (1976).

44. J. Braunsfurth and J.H. Korner, Nucl.Inst. and Meth., 34 202 (1965).

45. D.A. Gedck and W.J. McDonald, Nucl.Instr.Meth., 55, 377 (1967).

46. B. Bengston and M. Moszynski, Nucl.Instr. and Meth., 81, 109 (1970).

47. M.R. Maier and D.A. Landis, Nucl.Instr.Meth., 117, 245 (1974).

48. U. Baverstam and M. Hojeberg, Nucl.Instr. and Meth., 95, (1971) 611.

49. M. Yousf Sulaiman and R.N. Thomas, Nucl.Instr. and Meth., 166, 305 (1979).

50. M.H.B. Sulaiman, Ph.D. thesis, Bedford College, University of London (1977).

51. A.H. Wapstra, α, β and γ-ray spectroscopy, Vol.I (North-Holland Pub. Co. (1965)).

52. J.B. Birks, The Theory and Practice of Scintillation Counting, (North-Holland Pub.Co. 1959)).

53. M. Theim, Ph.D. Thesis, University of London (1977).

54. R. Fisi and A. Gainotti, Phys.Rev. 175 (1968) 383.

55. M. Groxeclose and Sappa, L. Nuovo Cim 50 (1967) 256.

56. B. Wilson and L. Bostrom, Nucl.Instr. and Meth., 44 (1966) 65.

57. R.L. Auble, Nucl.Data Sheets, 20, 259 (1977).

58. P. Kienle, R.E. Segel, Phys.Rev., 114, 1554 (1959).

59. J. Kerm, Gamma-ray standards in charged-particle-induced radioactive capture, pp. 345, Vienna: IAEA 1974.

60. D. Camp and J. Gerald, Nucl.Phys. A166, 349 (1971).

61. R.J. Gehrk, R.G. Helmer and R.C. Greenwood, Nucl.Inst. and Meth. 150, 599 (1978).

62. M. Hautala, A. Anttila and J. Keinonem, Nucl.Inst. and Meth. 147, 405 (1977).

63. G.J. McCallum and G.E. Coote, Nucl.Instr. and Meth. 124, 309 (1975).

64. H.W. Taylor and B. Singh, Nucl.Phys., A172, 227 (1971).

65. B.K. Armitage, A. Ferguson and G. Neilson, Nucl.Phys., A133, 241 (1969).

66. Y.K. Agarwal and S. Hofmann, Nucl.Phys.A176, 142 (1971).

67. S. Hofmann, Z.Physik 270, 133 (1974).

68. D. Wells and W. Meyerhof, Phys.Rev. 130, 1961 (1963).

69. H. Ohnuma and I. Tomita, Nucl.Phys. 66, 337 (1965).

70. A.H. Sher and B.D. Pate, Nucl.Phys. A112, 85 (1968).

71. H. Pettersson, O. Bergman, C. Bergman, Arkiv.Fysik 28, 423 (1965).

72. P.Y. Meskvarishvili and M.A. Elizbarashvili, 26th Soviet meeting on Nucl. Spectroscopy, Baku, Academy of Science, U.S.S.R., pp.48 (1976).

73. R.C. Greenwood, R.C. Helmer, R.G. Gehrke, R.J.Nucl.Instr.and Meth. 159 (1979) 465.

74. A. Moszkowaki, Table of Isotopes, C.M. Lederer et al. 6th Ed. (John Wiley & Sons, 1967).

75. Table of Isotopes (John Wiley & Sons, 1978).

76. M.E. Rose, Internal Conversion Coefficients, North-Hall & Pub.Co. Amsterdam (1958).

77. V.T. Trusov, Nucl. Data Tables, 10, 481 (1972).

78. R.L. Auble, Nucl.Data Sheets 20, 253 (1977).

79. N. Bendjabala, J. Delannay and K. Ogawa, Nucl.Phys. A284, 513 (1977).

80. M. Lederer, Table of Isotopes (John Wiley & Sons, Inc., New York (1978)).

81. W.S. Cowart and M.L. Pool, Physical Rev. 73 (1948) 12.

82. W. Pratt, Nucl.Phys., A147 (1970) 601.

83. N. Imanishi et al. Nucl.Phys. A125 91 (1969) 616.

84. W. Schölz and F.B. Malik, Phys.Rev. 176 (1968) 355.

85. Mathilde de Croës et al., Arkiv für Physik, 16 (1960) 567.

86. W.F. Edwards et al., Nucl.Phys. 26 (1961) 649.

87. E.P. Grigoriev et al., Nucl.Phys. 14 (1960) 449.

88. P. Jahn et al., Zeit.Phys. 210 (1968) 245.

89. J. Varma and M.A. Eswaran, Phys.Rev. 125 (1962) 656.

90. P. Venngopala Rao et al., Nucl.Phys. 81 (1966) 296.

91. D.E. Raeside et al., Nucl.Phys. A130 (1969) 677.

92. T. Paradellis et al., Nucl.Phys. A131 (1969) 378.

93. R.L. Robinson et al., Nucl.Phys. A104 (1967) 401.

94. W. Pratt, Nucl.Phys. A170 (1971) 223.

95. R.N. Thomas and R.V. Thomas, J.Phys.A. Math, Nucl, Gem, Vol.6 July (1973).

96. J.L. Campbell, J.Phys.A. Math, Nucl, Gem, Vol.7 No. 12 (1974).

97. H.S. Shahota et al., J.Phys.G.Nucl.Phys. Vol.3, No. 9 (1977) 1261.

98. Y. Ellis, Nucl.Data Sheets 16, 128 (1975).

99. R.L. Auble, Nucl.Data Sheets 20, 125 (1977).

100. W. Meiling and Fstary, Nano-second pulse Technique (North-Holland Publ. Co. (1965).

101. Y. Ellis, Nucl.Data Sheets 16, 36 (1975).

102. Table of Isotopes, 6th Ed. (John Wiley & Sons (1967)).

103. M. Höjerberg and S. Malmskag, Nucl.Phys. A133 (1969) 691.

104. W.F. Edwards and C.J. Gallagher, Nucl.Phys. 26 649 (1961).

105. Y. Ellis, Nucl. Data Sheets 16, 30 (1975).

106. G.T. Ewan, R.L. Graham and J.S. Geiger, Nucl.Phys. 29, 153 (1962).

107. N.F. Peek, J.A. Jungerman, and C.G. Patten, Phys.Rev. 136, B330 (1964).

108. R.J. Bower and G.T. Ewan, Bull.Am.Phys.Soc., 11, 11 (1966).

109. A.F. Kluk, N.R. Johnson and J.H. Hamilton, Phys.Rev., C10. 1966 (1974).

110. L.V. Groshev, A.M. Demidov, V.A. Ivanov, V.N. Lutsek and K.K. Pelekhov, Izv.Akad.Nank, SSSR (1962).

111. A. Backlin, B. Fogelberg, G. Hedin and R.C. Greenwood, International Atomic Energy, Vienna, Austria, 1969, p.147.

112. L.M. Bollinger and G.E. Thomas, Phys.Rev. C2, 1951 (1970).

113. B.S. Dzhelepov, A.G. Dmitriev, N.N. Zukovskii and A.G. Malyan (transl. Bull.Acad.Sci. USSR, Phys.Ser. 30, 401 (1966).

114. T.A. Siddiqi, F.P. Cranston and D.H. White, Nucl.Phys. A179, 609 (1972).

115. Wolfganstöffl, Ph.D. thesis, Technischen Universität, München.

116. D.J. McMillan, J.H. Hamilton and J.J. Pinajian, Phys.Rev. C4, 542 (1971).

117. P.F. Kenealy, E.G. Funk and J.W. Mihelich, Nucl.Phys. A105, 522 (1967).

118. M. Fujioka, Nucl.Phys. A153, 337 (1970).

119. J.H. Hamilton, M. Fujioka and D.J. McMillan, Phys.Rev. C5 1800 (1972).

120. J.H. Hamilton, A.V. Ramayya, Phys.Rev., C3 313 (1971).

121. H. Yamada, T. Katoh and N.R. Johnson, J.Phys.Soc. of Japan, Vol.41, No. 6, Dec. (1976).

122. W. Meiling and F. Story, Nucl.Phys. 74, 113 (1965).

123. D.B. Fossan and B. Herskind, Nucl.Phys. 40 (1963) 24.

124. T.W. Burrows, Nucl. Data Sheets 18, 553 (1976).

125. J.H. Hamilton, P.E. Little, A.V. Rannayya, E. Collis, N.R. Johnson, J.J. Pinajian and A.F. Kluck, Phys.Rev. C5, 899 (1972).

126. A. Bahr and B. Mattelson, Mat.Fys.Medd. 26, 16 (1953).

127. J.B. Gupta, Krishna Kumar and J.H. Hamilton, Phys.Rev. C16, No. 1 (July 1977).

128. J. Konijn, H. Verheul and O. Scholten, Nucl.Phys. meeting, New Orleans, U.S.A., Feb. (1980).

129. A. Arima and F. Iachello, Phys.Rev.Lett., 35 106((1975).

130. A. Arima, T. Ohtsuka and F. Iachello, Phys.Lett. 66B, 205 (1977).

ACKNOWLEDGEMENTS

It is a great pleasure to express my utmost gratitude to Dr. N.M. Stewart for his supervision, advice and assistance rendered during the course of this work.

The interest of Professor E.R. Dobbs and Dr. P. Rice-Evans are gratefully acknowledged. Thanks are also given to the technical staff of the Physics Department at Bedford College, noteably Messrs. W.A. Baldock, A.K. Betts, J. Sales, and in addition to Mrs. S. Pearson for their services and help.

I am deeply grateful to Dr. T.D. MacMahon for his valuable advice and assistance during the course of this work at the University of London Reactor Centre. I also thank Mr. M. Kerridge for his cooperation in helping to make full use of the facilities there. Thanks are also given to all University of London Reactor Centre staff members, noteably Dr. J. Williams, Mr. G. Burholt and Mr. E. Ceaser for their hospitality, assistance and help.

Thanks are due to Mr. R.N. Thomas for his assistance and design work concerning the dual-parameter data collection system used in part of this work.

I wish to thank the British Council for assistance from the Research Student Support Scheme.

I am very grateful to the Egyptian Government for study leave and full grant support in the last year of the course of this work, noteably the Minister of Education, Professor K. Hellemy, and the Director of the Education Bureau, Professor M.A. Sarhan.

Z. Physik A

Zeitschrift für Physik A Atoms and Nuclei

NUCLEAR INSTRUMENTS AND METHODS 165 (1979) 109-112; © NORTH-HOLLAND PUBLISHING CO.

RELATIVE INTENSITIES OF GAMMA TRANSITIONS IN THE DECAY OF ^{56}Co

A. M. SHABAN, N. M. STEWART

Bedford College, University of London, Regent's Park, London NW1 4NS, England

and

T. D. MACMAHON

University of London Reactor Centre, Silwood Park, Sunninghill, Ascot, Berkshire, SL5 7PY, England

Received 5 March 1979

The transition intensities of ^{56}Co have been determined using Ge(Li) detectors and uncertainties between previously measured values of different authors clarified.

1. Introduction

In view of the importance of ^{56}Co as a standard source several intensity measurements have been carried out on its decay scheme, see Marion[1]) and Kern[2]). The most recent work of Hautala et al.[3]) provides a valuable comparison with that of McCallum and Coote[4]), both employing the known decay schemes of (p, γ) reaction resonances, and also the gamma–gamma directional correlation measurements of Hofmann[5]) on the decay scheme of ^{56}Fe. McCallum and Coote[4]) endeavoured to prove the existence of systematic errors of over 10% in the intensities of the higher energy gamma-rays, greater than 2 MeV, but Hautala et al.[3]) were able to point out some defects of this work in connection with the construction of the efficiency curve. Hautala et al.[3]) were able to measure thirty-nine transitions, and found that their relative intensities were generally lower than those of Hofmann[5]) below 2.2 MeV gamma-ray energy, and greater above this energy. In contrast eight of the ten transitions that could be compared with McCallum and Coote[4]) above 2 MeV were of lower relative intensities. We suggest the correction factor[4])

$$f(E) = 1, \qquad E < 2,$$

$$= 1.053 - 0.079E + 0.036E^2, \qquad 2 \leqslant E < 5,$$

where E is the gamma energy in MeV, deduced from a comparison with published intensity values for both ^{56}Co [2]) and ^{66}Ga [6]) leads to an overestimation when applied to ^{56}Co alone. Below 2 MeV Hautala et al.[3]) report a lower intensity for five of the eight transitions which were measured by McCallum and Coote[4]). There is a large discrepancy of nine times the quoted error, for the line at 1238 keV. In addition, Hofmann[5]) reports intensities for five transitions not seen by Hautala et al.[3]) including the first observance of a 674.7 keV gamma-ray from the decay of ^{56}Co.

In order to further establish the relative intensities of this important calibration source and to further investigate the possibility of systematic differences with data based on (p, γ) reactions, the results of measurements taken with two high efficiency, high resolution Ge(Li) detectors are reported here.

2. Experimental set-up and instrumental calibration

A cylindrical Ge(Li) detector drifted coaxially with an active volume of about 70 cm^3 was positioned at 25 cm from an 8 μCi point source of ^{56}Co obtained from the Radiochemical Centre, Amersham, in the form of a standard source suitable for immediate use. Low activities and an avoidance of a short source-to-detector distance enabled the total counting rates to be kept below 2000 s^{-1} so that pile-up effects were minimised and the coincidence summing corrections suggested by Debertin and Schötzig[6]) need not be applied. Soft photons with energies less than 80 keV were excluded from the spectra by a lower level discriminator.

The output signals for the Ge(Li) detector were fed into a charge sensitive preamplifier and then through an Ortec (Model No. 472) spectroscopy amplifier to a Northern Scientific ADC (Model 626) and thence into a Northern Scientific memory unit (Model No. 630). Pulse height spectra were recorded in 4096 channels and analysed off-line on the University of London CDC-6600 computer.

The system was initially run and tested with a 10% efficient Ortec Ge(Li) detector with a resolution of 2.2 keV fwhm at 1.3 MeV. A second set of measurements was made with a 12% efficient Ortec Ge(Li) detector, with a resolution of 1.9 keV fwhm at 1.3 MeV, and consistent results were obtained with the first measurements, but with a greatly improved accuracy.

2.1. Efficiency calibration

Monte Carlo calculations[7,8]) for the relative efficiency of Ge(Li) detectors have limited usefulness[9]) owing to difficulties in defining accurately the active volumes of these detectors, and differences 10% or more[10]), are found from measured values of relative efficiency. Our efficiency curve was constructed using gamma-ray sources over the energy range 81.0 keV to 4.071 MeV. Up to 1.836 MeV the Chemical Standards Source Set[11]), consisting of the sources ^{133}Ba, ^{137}Cs, ^{57}Co, ^{60}Co, and ^{88}Y, whose details are given in table 1a, was used for the calibration. The calibration was extended to higher energies by using the five isotopes ^{56}Mn, ^{38}Cl, ^{24}Na, ^{88}Rb and ^{49}Ca, which were prepared using the University of London Reactor irradiation facilities.

Table 1 (a, b)

Details of the gamma-ray calibration sources.

Nuclide	Calibration energy E (keV)	Intensity No. of γ-rays/100 disintegrations
^{133}Ba	81.0	34.7
^{57}Co	121.97	87.7
^{57}Co	136.33	12.2
^{133}Ba	302.87	18.3
^{133}Ba	356.03	62.3
^{133}Ba	383.87	8.9
^{137}Cs	661.6	85.3
^{88}Y	898.0	91.4
^{60}Co	1173.1	99.9
^{60}Co	1332.4	100.0
^{88}Y	1836.1	99.4

Nuclide	Calibration energy E (keV)	Reference energy R (keV)	Intensity ratio $I(E)/I(R)$
^{56}Mn	2112.8	1810.7	0.537
^{38}Cl	2166.8	1642.0	1.316
^{24}Na	2753.6	1368.4	0.986
^{88}Rb	3218.0	898.1	0.0176
^{49}Ca	4071.0	3083.0	0.0868

The energies of the most prominent gamma-rays along with reference peak energies needed for the five non-standard sources are given in table 1b. The relative intensities were obtained from refs. 12, 15 and 16.

The efficiency ε of a Ge(Li) detector was taken as a function of energy E to be[13]):

$$\varepsilon = P_1 [E^{P_2} + P_3 \exp(P_4 E)],$$

and the parameters P_1, P_2, P_3 and P_4 were found by a least-squares minimisation procedure carried out by the program SAMPO[14]), modified to run on the University of London CDC-6600 computer. The efficiency curve as a function of energy is shown in fig. 1 for the 12% efficient detector. Fig. 1a shows the relative efficiency as a function of energy

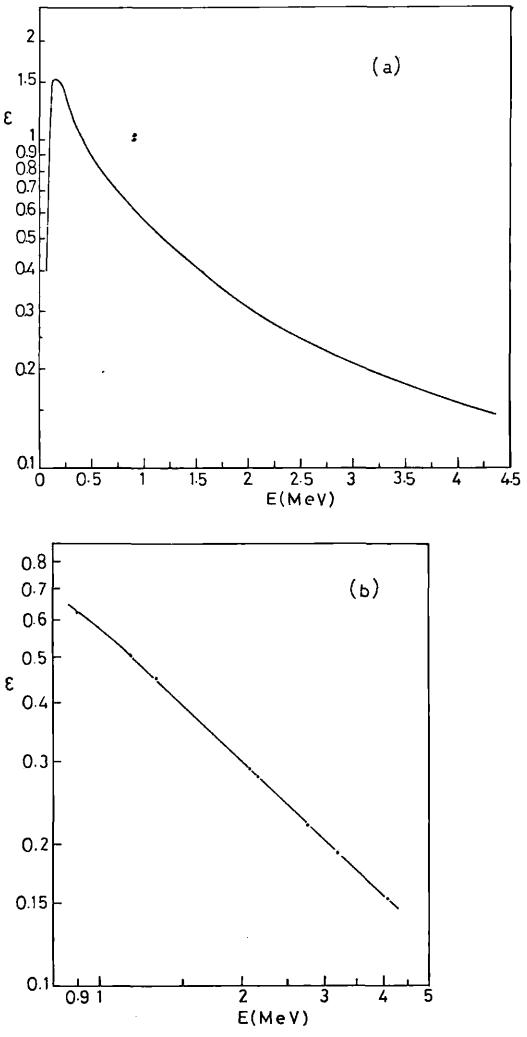

Fig. 1. The relative efficiency ε of the 12% efficient coaxial Ge(Li) detector as a function of gamma-ray energy E.

Z. Physik A

Zeitschrift für Physik A Atoms and Nuclei

over the full energy range, and fig. 1b shows the expected linearity when plotted as a function of log E in the range 800 keV to 5 MeV.

2.2. Lineshape

The shape of any gamma ray photopeak is taken by SAMPO [14]) to be the sum of a Gaussian smoothly joined on to two independent exponentials forming the leading and trailing edges respectively. In this manner any photopeak can be specified by four lineshape parameters, the centre of the Gaussian, its width, and the two distances from the centre to where the exponentials join the Gaussian. These four parameters are found by the least squares fitting routine in SAMPO.

3. Single spectra

The spectra obtained from the Ge(Li) detectors were analysed using the computer program SAMPO, and as the details of this program are well

Table 2

Relative intensities of gamma-rays emitted in the decay of ^{56}Co. Energies are from ref. 5.

Energy (keV)	Intensity related to $I(847) = 1000$			
	Present work	Ref. 3	Ref. 5	Ref. 4
263.34	0.22±0.04		0.20±0.06	
410.94	0.31±0.04		0.25±0.09	
485.2	0.69±0.07		0.7 ±0.02	
674.7	0.38±0.07		0.3 ±0.1	
733.6	1.95±0.14	1.43±0.13	1.65±0.08	
787.77	3.2 ±0.07	3.4 ±0.3	2.9 ±0.3	3.3±0.3
846.78	1000	1000	1000	1000
896.55	0.63±0.06	0.77±0.1	0.62±0.06	
977.39	14.1 ±0.2	13.8 ±0.4	13.7 ±0.04	14.5±0.7
996.48	0.92±0.14	1.7 ±0.14	1.7 ±0.5	
1037.85	141.1 ±1.9	135.0 ±2	142.4 ±1.4	133.4±2.5
1089.31	0.5 ±0.07	0.6 ±0.2	0.7 ±0.2	
1140.52	1.25±0.06	1.17±0.13	1.3 ±0.02	
1160.0	0.74±0.08	0.8 ±0.1	0.78±0.07	
1175.06	23.0 ±0.32	21.1 ±1.0	22.5 ±1.1	21.2±1.2
1198.77	0.4 ±0.1	0.44±0.08	0.28±0.09	
1238.29	684.7 ±8.7	651.0 ±4	676.4 ±6.8	686.0±4
1272.20	0.38±0.06	0.35±0.04	0.22±0.03	
1335.56	1.28±0.06	1.2 ±0.2	1.2 ±0.12	
1360.25	43.2 ±0.6	42.4 ±1.5	43.5 ±1.2	42.7±0.4
1442.65	1.73±0.07	1.95±0.1	1.77±0.09	
1462.28	0.91±0.13		0.65±0.12	
1640.38	0.62±0.07	0.5 ±0.1	0.63±0.06	
1771.33	155.0 ±4.0	152.6 ±1.5	157.8 ±1.6	157.2±2.0
1810.75	6.2 ±0.2	5.9 ±0.3	6.3 ±0.3	
1963.75	7.19±0.15	7.0 ±0.2	7.1 ±0.3	7.0±0.3
2015.33	31.82±0.66	29.7 ±0.3	30.95±0.31	29.8±0.5
2034.90	81.4 ±1.7	76.4 ±0.6	79.5 ±0.8	77.7±2.0
2113.33	3.75±0.14	3.4 ±0.2	3.7 ±0.2	3.8±0.1
2213.07	4.2 ±0.2	3.9 ±0.2	3.6 ±0.2	
2276.09	1.17±0.09	1.5 ±0.2	1.28±0.08	
2373.71	0.97±0.12	0.5 ±0.06	0.59±0.12	
2523.0	0.79±0.11	0.84±0.09	0.44±0.1	
2598.57	174.0 ±3.8	171.9 ±1.5	168.5 ±1.7	175.1±2.0
2657.4		0.29±0.04	0.16±0.05	
3009.82	8.4 ±0.4	10.5 ±0.3	9.8 ±0.9	9.9±0.5
3202.18	30.3 ±0.7	32.4 ±0.3	30.3 ±0.3	33.6±0.5
3253.61	76.0 ±1.5	79.7 ±1.1	73.9 ±0.75	81.2±0.9
3273.16	18.15±0.36	18.4 ±0.3	17.55±0.18	18.2±0.4
3369.67	0.11±0.02	0.1 ±0.01	0.08±0.02	
3451.29	9.0 ±0.2	9.5 ±0.2	8.9 ±0.4	9.6±0.2
3548.27	1.96±0.06	1.96±0.05	1.78±0.09	2.0±0.1
3600.85	0.15±0.02	0.12±0.03	0.16±0.02	
3611.90	0.10±0.02	0.05±0.02	0.08±0.02	

documented i.e. refs. 13 and 14, only an outline of its main features are given here.

The calibration parameters are read in and then the program carried out the following operations on each spectrum. All the peaks in the spectrum are identified by PEAKFIND, and FITDO fits the previously calibrated lineshape functions to each peak. Finally peak acceptance criteria are applied and those peak areas which survive are output by RESULTS. We also utilised the option of generating a smoothly varying polynomial-type background continuum, which greatly improved the lineshape fitting.

The peak search algorithm is based on the method of second differences and after an assessment is made of the statistical significance of a potential peak it must then satisfy a peak shape test before being entered into an array to be least squares fitted.

The different periods of counting with each detector were analysed separately, and then the resulting intensities combined statistically below 1.7 MeV. For the 10% efficient detector the measurements above 1.7 MeV were not used as the extended calibration was not carried out for this detector.

The relative intensities obtained were normalised to 1000 for the gamma-ray at 847 keV and are given in the second column of table 2. The results of earlier work[3-5]) are also given in table 2 for comparison, those in column three being the most recent. The energy values are taken from ref. 5.

4. Conclusions

We have measured, with generally improved accuracy, the relative intensities of forty-three gamma-rays from the decay of ^{56}Co, and good agreement is obtained with previous measurements[3-5]) of other workers. Support is found for the five transitions reported by Hofmann[5]) and not observed by Hautala et al.[3]). Of these, the relative intensities at the four lowest energies of 263.3, 410.9, 485.2, and 674.7 keV, the last proposed for the first time by Hofmann[5]), are in very good agreement. For the fifth at 1462.3 keV our value is higher, but agrees within the quoted errors.

The intense lines at 2.599 and 1.771 MeV have relative intensities closest to those of McCallum and Coote[4]), and the excellent agreement of the very intense measurement at 1.238 MeV with these authors discriminates against the low value reported by Hautala et al.[3]). It is also of interest that Hautala et al.[3]) find an intensity nearly twice that of Hofmann[5]) for the line at 2.523 MeV and that we clearly favour the value of the former authors.

A comparison of our relative intensity measurements with those of Hautala et al.[3]), based on (p, γ) reactions, does not show a systematic high variation for energies above 2.5 MeV, as might have been expected from the work of McCallum and Coote[4]), but would rather indicate this possibility between 1.5 and 2.5 MeV, as do the results of Hofmann[5]).

The present work provides a further independent measurement of the relative intensities over the full energy range of gamma transitions in the decay of the important calibration source ^{56}Co, and will help to improve precision and reduce the possibility of systematic errors.

We thank the Director and staff at the University of London Reactor Centre for their co-operation in helping to make full use of the facilities there. Dr. N. M. Stewart is grateful to the Central Research Fund of the University of London for provision of some of the apparatus used in this work. Mr. A. M. Shaban wishes to thank the British Council for assistance from the Research Student Support Scheme.

References

1) J. B. Marion, Nucl. Data **A4** (1968) 301.
2) J. Kern, *Gamma ray standards in charged-particle-induced radiative capture* (IAEA, Vienna, 1974) p. 345.
3) M. Hautala, A. Anttila and J. Keinonen, Nucl. Instr. and Meth. **150** (1978) 599.
4) G. J. McCallum and G. E. Coote, Nucl. Instr. and Meth. **124** (1975) 309.
5) S. Hofmann, Z. Physik **270** (1974) 133.
6) K. Debertin and U. Schötzig, Nucl. Instr. and Meth. **158** (1979) 471.
7) K. M. Wainro and G. F. Knoll, Nucl. Instr. and Meth. **44** (1966) 213.
8) V. J. Orphan and N. C. Rasmussen, IEEE Trans. Nucl. Sci. **NS-14**, no. 1 (1967) 544.
9) B. P. Singh and H. C. Evans, Nucl. Instr. and Meth. **97** (1971) 475.
10) J. E. Cline, IEEE Trans. Nucl. Sci. **NS-15** no. 3 (1968) 198.
11) The T.R.C. set is standard reference material available from the Radiochemical Centre, Amersham, Buckinghamshire, U.K.
12) U.S.A. Atomic Energy γ-ray spectrum catalogue (3rd edition), Aerojet Nuclear Company, U.S.A. Energy Research and Development Administration.
13) J. T. Routti, Lawrence Berkeley Laboratory Report UCRL 19452 (1969).
14) J. T. Routti and S. G. Prussin, Nucl. Instr. and Meth. **72** (1969) 125.
15) U. Schötzig et al., Int. J. Appl. Rad. Isotopes **28** (1977) 503.
16) R. L. Auble, Nucl. Data Sheets **20** (1977) 327.

Z. Physik A

Zeitschrift für Physik A Atoms and Nuclei

Low Lying Energy Levels of ^{56}Fe from $\gamma-\gamma$ Coincidences

N.M. Stewart and A.M. Shaban
Bedford College, University of London, London, England

Received March 12, 1980

The level scheme of ^{56}Fe was built up from $\gamma-\gamma$ coincidence measurements using Ge(Li) detectors and a Dual Parameter data collection system. The previously suggested γ-transitions [8] of 263.3, 410.9, 485.2, 674.7 and 1,462.3 keV were confirmed and evidence found for a new 655.0 keV γ-transition between the levels at 4,100.32 and 3,445.32 keV. No evidence was found for the transition of 2,657.4 keV and the previously proposed β^+-feeding of the level at 3,600.3 keV is ruled out, while the existence of a level at 4,447.5 keV is suggested. The relative intensities and branching ratios of 44 transitions were determined. A calculation of experimental K-shell internal conversion coefficients $\alpha(K)$ showed large discrepancies from previous studies for the 3,009.6 and 3,451.2 keV transitions, the latter being assigned a different multipolarity. Log ft values were calculated and spins and parities of the levels deduced. In particular the assignment of 3^+ is verified for the level at 4,297.97 keV.

1. Introduction

Several investigations of the γ rays of ^{56}Co, which populate the levels of ^{56}Fe, have been carried out in the last ten years [1-4]; the relative intensity measurements being widely required for calculations of the efficiency of Ge(Li) detectors. However, extensive studies [5-7] of the ^{56}Fe level scheme have only been done with Ge(Li)–NaI(Tl) detectors employed in $\gamma-\gamma$ directional correlation measurements. The most recent experimental studies on the even-even ^{56}Fe nucleus using this technique were performed by Hofmann [8] in 1974, and the 674.7 and 2,657.4 keV γ-rays were observed for the first time in his work. Several weak γ-rays from the transitions in 56Fe were confirmed and added to the decay scheme. No further studies of the decay scheme of this important nucleus have been undertaken since.

The simple ^{56}Fe level scheme of 23 γ-ray transitions between 14 levels proposed by Sher et al. [9] in 1968 was based on $\gamma-\gamma$ coincidence measurements using a NaI(Tl) detector together with a small volume (0.85 cm^3) Ge(Li) detector. No subsequent $\gamma-\gamma$ coincidence measurements have been made in the intervening 12 years during which time the performance of Ge(Li) detectors has been greatly improved.

Clearly there is a need for further studies using high efficiency, high resolution Ge(Li) detectors in $\gamma-\gamma$ coincidence measurements to give a more realistic comparison with recent $\gamma-\gamma$ directional correlations results.

2. Instrumentation and Experimental Procedure

Radioactive sources for the γ-rays were produced by the ^{56}Fe(p, n) reaction at the Radiochemical Centre Amersham and obtained in the form of standard point sources.

Singles, Compton suppression or coincidence spectra have been taken using three Ge(Li) detectors having efficiencies of 10, 11 and 12% together with resolutions of 2.2, 2.4 and 1.9 keV respectively for the 1.33 MeV ^{60}Co line. The 10% and 12% efficient detectors were used to obtain the singles spectra and were arranged together in the coincidence measurements.

In order to obtain singles spectra the signals from a Ge(Li) detector were fed into an Ortec (Model 472) spectroscopy amplifier and pulse height information

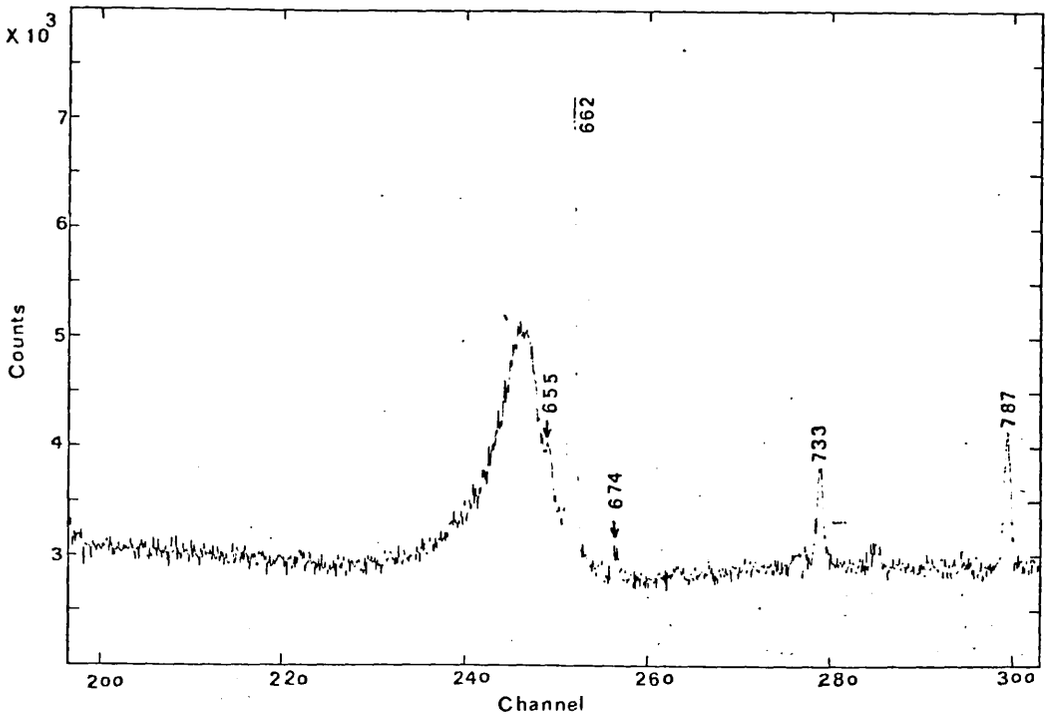

Fig. 1. ^{56}Co Compton suppression spectrum between 550 and 800 keV

recorded by a Northern Scientific (Model NS 630) 4,096 multichannel analyser.

The Compton suppression system consisted of the 11% efficient detector and a 20 cm diameter × 20 cm long NaI(Tl) crystal viewed by four photomultipliers. A photopeak to Compton ratio of 270:1 for the 1.33 MeV ^{60}Co gamma-ray photopeak was obtained with a dual sum Ortec (Model 433A) unit and a Harshaw (NC 26) time analyser.

Coincidence experiments were performed with two large-volume (approximately 70 cm^3) Ge(Li) detectors coupled to a 4,096 × 4,096 Dual-parameter data collection system [10]. Gating pulses were generated with a time-to-pulse height converter (TPHC) for which constant fraction timing discriminators Ortec (Model 473) provided the start and stop pulses. The resolution of the pulse distribution from the TPHC was 40 ns. The gating and spectrum analog-to-digital converters (ADCs) connected to a write interface enabled data to be recorded on magnetic tape. The coincidence data written on magnetic tape was analysed at a later time after the data collection by setting digital windows on a particular region of interest (a coincidence gate) in the spectrum from the 10% efficient detector. Coincidence windows were separately set on all full-energy peaks of interest to include the immediate background just above or below the peaks. Corrections for background and chance (accidental) coincidences were made using the subtract mode of the NS 630 analyser and by switching in the chance mode of the read unit in the magnetic tape interface.

All the data collected as singles or coincidence spectra were analysed with the program SAMPO [11, 12] on the University of London CDC 6600 Computer.

3. Singles Spectra

Singles spectra measurements over the energy range from 200 keV up to 4 MeV were made using the 10% and 12% efficient detectors; the 11% efficient detector was used in a Compton suppression spectrometer in the same energy region. The spectra taken using this spectrometer were very useful as there were several low intensity γ-ray lines located in the Compton scattering region, these low energy transition photopeaks being shown in Fig. 1.

The efficiencies of the detectors were obtained using gamma-ray sources over the energy range from 81 keV up to 4.07 MeV. Below 1.84 MeV the isotopes ^{133}Ba, ^{137}Cs, ^{57}Co, ^{60}Co and ^{88}Y were obtained from the chemical standards source set [13]. These efficiency calibrations were extended to higher energies by using the five isotopes ^{56}Mn, ^{38}Cl, ^{24}Na, ^{88}Rb and ^{49}Ca, whose photopeak energies together with those of the standards source set are given in Table 1. The five higher energy isotopes were prepared using the University of London Reactor irradiation facilities. More details of the method for obtaining the efficiencies of these detectors over a

Table 1. Energies of the γ-ray calibration sources from [15-18]

Nuclide	Calibration Energy E_γ (keV)
^{133}Ba	81.0
	302.87
	356.03
	383.87
^{57}Co	121.97
	136.33
^{60}Co	1,173.23
	1,332.52
^{88}Y	898.02
	1,836.01
^{56}Mn	2,113.05
^{38}Cl	2,167.45
^{24}Na	2,753.98
^{88}Rb	3,218.48
^{49}Ca	4,071.9

wide energy range were discussed in a previous publication [14].

The energy calibration was determined by a least-squares fit to an n^{th} degree polynomial to the γ-rays from several standard sources. The peak positions for this fit were corrected for nonlinearity which was ± 0.55 channels over 90% of the ADC range as measured with a precision pulser. This nonlinearity correction was estimated to give 0.05 and 0.1 channels uncertainty in determining the photopeak centroid and was folded into the peak position error. A third order polynomial was found to give the best fit.

The energies of the transitions observed in the decay of ^{56}Co are listed in Table 2. The errors assigned to these energies, as determined by SAMPO, range from 50 eV for the most intense gamma-ray transitions, to 0.8 keV for the weak high-energy transitions. The energies of the 18 high intensity γ-rays given with the highest precision in Table 2 are taken from [19]. The relative intensities of the gamma-rays following the decay of ^{56}Co compared with the most recently published intensity values are also given in Table 2. A total of forty-four γ-ray transitions were found in all the singles spectra collected.

Table 2. Relative intensities of γ-rays emitted from the decay of ^{56}Co

Energy	Intensity related to $I(847)=1{,}000$		
(keV)	Present work	Ref. 4	Ref. 8
263.34	0.22 ±0.04		0.20 ±0.06
410.94	0.31 ±0.04		0.25 ±0.09
485.2	0.69 ±0.07		0.7 ±0.02
655.0	0.38 ±0.08		
674.7	0.38 ±0.07		0.3 ±0.1
733.6	1.95 ±0.14	1.43 ±0.13	1.65 ±0.08
787.77	3.2 ±0.07	3.4 ±0.3	2.9 ±0.3
846.764	1,000	1,000	1,000
896.55	0.63 ±0.06	0.77 ±0.1	0.62 ±0.06
977.39	14.1 ±0.2	13.8 ±0.4	13.7 ±0.04
996.48	0.92 ±0.14	1.7 ±0.14	1.7 ±0.5
1,037.844	141.1 ±1.9	135.0 ±2	142.4 ±1.4
1,089.31	0.5 ±0.07	0.6 ±0.2	0.7 ±0.2
1,140.52	1.25 ±0.06	1.17 ±0.13	1.3 ±0.02
1,160.0	0.74 ±0.08	0.8 ±0.1	0.78 ±0.07
1,175.099	23.0 ±0.32	21.1 ±1.0	22.5 ±1.1
1,198.77	0.4 ±0.1	0.44 ±0.08	0.28 ±0.09
1,238.287	684.7 ±8.7	651.0 ±4	676.4 ±6.8
1,272.20	0.38 ±0.06	0.35 ±0.04	0.22 ±0.03
1,335.56	1.28 ±0.06	1.2 ±0.2	1.2 ±0.12
1,360.206	43.2 ±0.6	42.4 ±1.5	43.5 ±1.2
1,442.65	1.73 ±0.07	1.95 ±0.1	1.77 ±0.09
1,462.28	0.91 ±0.13		0.65 ±0.12
1,640.38	0.62 ±0.07	0.5 ±0.1	0.63 ±0.06
1,771.350	155.0 ±4.0	152.6 ±1.5	157.8 ±1.6
1,810.722	6.29 ±0.13	5.9 ±0.3	6.3 ±0.3
1,963.714	7.19 ±0.15	7.0 ±0.2	7.1 ±0.3
2,015.179	31.82 ±0.66	29.7 ±0.3	30.95 ±0.31
2,034.159	81.4 ±1.7	76.4 ±0.6	79.5 ±0.8
2,113.107	3.75 ±0.14	3.4 ±0.2	3.7 ±0.2
2,212.921	4.2 ±0.2	3.9 ±0.2	3.6 ±0.2
2,276.09	1.17 ±0.09	1.5 ±0.2	1.28 ±0.08
2,373.71	0.97 ±0.12	0.5 ±0.06	0.59 ±0.12
2,523.0	0.79 ±0.11	0.84 ±0.09	0.44 ±0.1
2,598.460	174.0 ±3.8	171.9 ±1.5	168.5 ±1.7
2,657.4	<0.05	0.29 ±0.04	0.16 ±0.05
3,009.596	8.4 ±0.4	10.5 ±0.3	9.8 ±0.9
3,201.954	30.3 ±0.7	32.4 ±0.3	30.3 ±0.3
3,253.417	76.0 ±1.5	79.7 ±1.1	73.9 ±0.75
3,272.998	18.15 ±0.36	18.4 ±0.3	17.55 ±0.18
3,369.97	0.11 ±0.02	0.1 ±0.01	0.08 ±0.02
3,451.154	9.0 ±0.2	9.5 ±0.2	8.9 ±0.4
3,548.27	1.96 ±0.06	1.96 ±0.05	1.78 ±0.09
3,600.85	0.15 ±0.02	0.12 ±0.03	0.16 ±0.02
3,611.80	0.10 ±0.02	0.05 ±0.02	0.08 ±0.02

4. Coincidence Results

A summary of the results of the gamma-gamma coincidence experiments is given in Table 3. Coincidence gates for all the prominent gamma-rays which are necessary to establish the features of the ^{56}Fe level scheme are listed in the first row. The observation of a γ-ray in the spectrum in coincidence with a gating gamma-ray is indicated in the table by one of the following entries: VS, S, W, VW or P. These entries give the strength of the observed gamma-ray relative to the other γ-rays in the coincidence spectrum and they represent Very Strong, Strong, Weak, Very Weak and Probable, respectively. The last entry (P) represents a coincidence relationship which within the error limits of the coincidence data is probable, yet not conclusive. In the decay of ^{56}Co the coincidence relationships could be thoroughly investigated using 12 prominent gamma-rays in the energy range from 788 keV to 3.2 MeV, and a typical coincidence spectrum is shown in Fig. 2.

Table 3. $\gamma-\gamma$ coincidence results from the decay of ^{56}Co

E_γ	Gate (keV)											
	788	846	1,038	1,175	1,238	1,335	1,771	1,810	2,034	2,113	2,598	3,202
263.34							P					
410.94												
485.2			S									
655.0											W	
674.7												
733.6												
787.77								VS				
846.77	S		VS	S	VS	S	S	VS	S	S	VS	VS
896.55										P		
977.39			P									
996.48			P									
1,037.85	W			VS		VS	VW					
1,089.31										P		
1,140.52										W		
1,160.00										W		
1,175.09												
1,198.77								S				
1,238.28	W	VS		S		S	VS	S	VS	VW		
1,272.2												
1,335.56				VS								
1,360.20				W								
1,442.62								S				
1,462.28								W				
1,640.38								VW				
1,771.33	W			W								
1,810.72	VS	VS										
1,963.71												
2,015.18	W											
2,034.76	W											
2,113.10		S			VW							
2,212.92												
2,276.09		S										
2,373.71												
2,523.0		W										
2,598.26		VS										
2,657.7												
3,009.59		VS										
3,201.96		VS										
3,253.42		VS										
3,273.00		VS										
3,369.97												
3,451.15		S										
3,548.27		S										
3,600.85		S										
3,611.8		S										

5. Decay Scheme and Discussion

Based on the coincidence results and energy sum relations the decay scheme of ^{56}Fe was obtained and is shown in Fig. 3. The experimental K-shell internal-conversion coefficients $\alpha(K)$ for transitions in ^{56}Fe are compared with the theoretical values corresponding to $E1$, $E2$ and $M1$ multipolarity in Table 4a. The experimental $\alpha(K)$ were calculated using our γ-ray intensities and the K-electron intensities $I(K)$ of Pettersson et al. [21]. The quoted errors would be reduced by up to a factor of six if the most probable values of $I(K)$ were used with our relative intensity errors only. The theoretical results were taken from Rose [22] for transitions <1 MeV and from Trusov [23] for transitions above 1 MeV. A Q value of 4,567.9 keV for the β^+, EC was taken from [24]. In Table 4b a comparison with $\alpha(K)$ calculated from the more recent $I(K)$ values of Metskvarishvili et al. [25] shows very large discrepancies for both the 3,009.6 and 3,451.2 keV transitions and indicates a ($M1/E2$) multipolarity.

An inspection of Table 3 shows that most of the gamma-rays are in coincidence with the 846.8 keV line. This result is to be expected because the spin of the ground state level of the ^{56}Co nucleus as given by Auble [24] is 4^+ and therefore the β^+ decay will primarily populate levels with spins and parities 3^+ od 4^+. Levels of such high spin would be expected to decay primarily to the 2^+ first excited state rather than decay to the 0^+ ground state.

The level at 3,600.8 keV previously suggested by Hofmann [8] on the basis of a transition from this β^+-fed level to the ground state is ruled out. We find a definite coincidence between the 3,600.8 keV and the 846.6 keV γ-rays which would suggest a level in ^{56}Fe at 4,447.6 keV which was not shown in the decay scheme proposed by Hofmann [8]. This level was previously placed in a decay scheme proposed by Taylor et al. [5] based on their results from $\gamma-\gamma$ directional correlation measurements, but no definite evidence for its existence was forthcoming so the origin of the 3,600 keV γ-ray line was not certain. However, we now feel the existence of the 4,447.5 keV level has been established.

A new 655.0 keV gamma-ray seen for the first time in this work in singles, coincidence and Compton suppression spectra was placed in the decay scheme arising from the gamma-transition between the (3^+) 4,100.22 keV level and the (3^+) 3,445.22 keV level.

The 2,085.04 keV level ($\log ft = 8.6$) is observed to decay to the 846.76 keV (2^+) level via the 1,238.28 keV transition which appears to be a pure ($E2$) transition so that the established spin and parity assignment of 4^+ is verified.

The 2,657.48 keV level ($\log ft > 10.4$) is observed to decay to the 846.76 keV (2^+) level by the 1,810.72 keV transition. This level is mainly fed by the 787.65 keV ($M1/E2$) transition and the possibility of β^+, EC feeding is very poor so that the possible value of spinparity is 3^+. The γ-ray transition of 2,657.7 keV from this level to the 0^+ ground state level is not seen in the coincidence spectrum, or in any of the singles

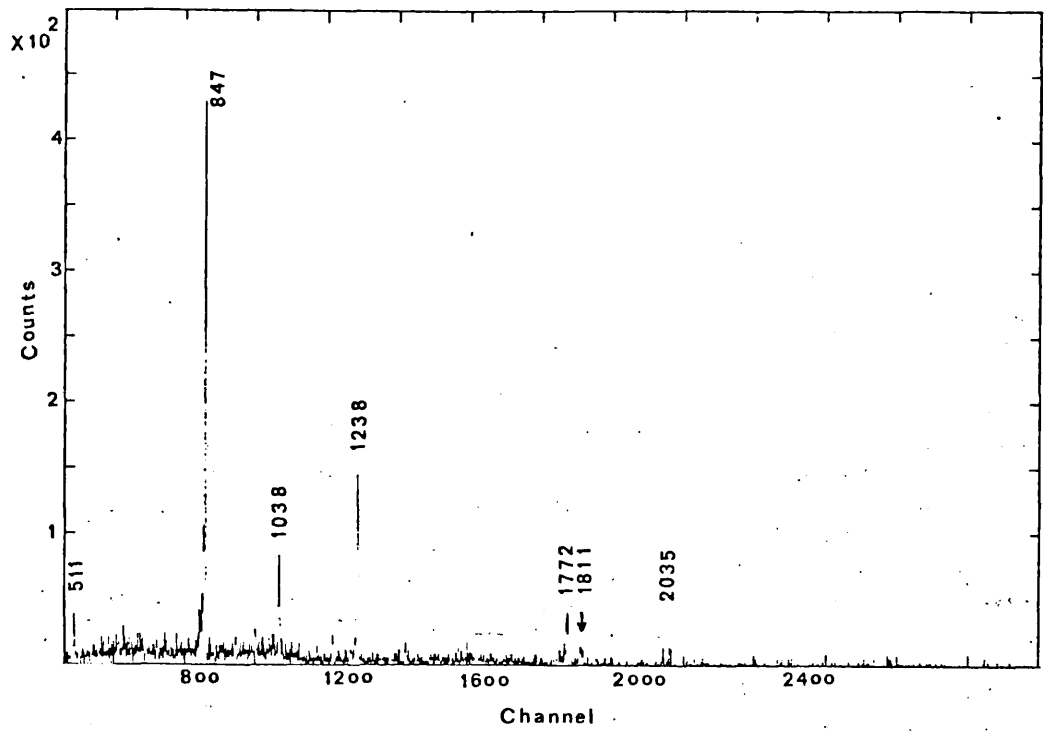

Fig. 2. ^{56}Co spectrum in coincidence with the 788 keV γ-ray

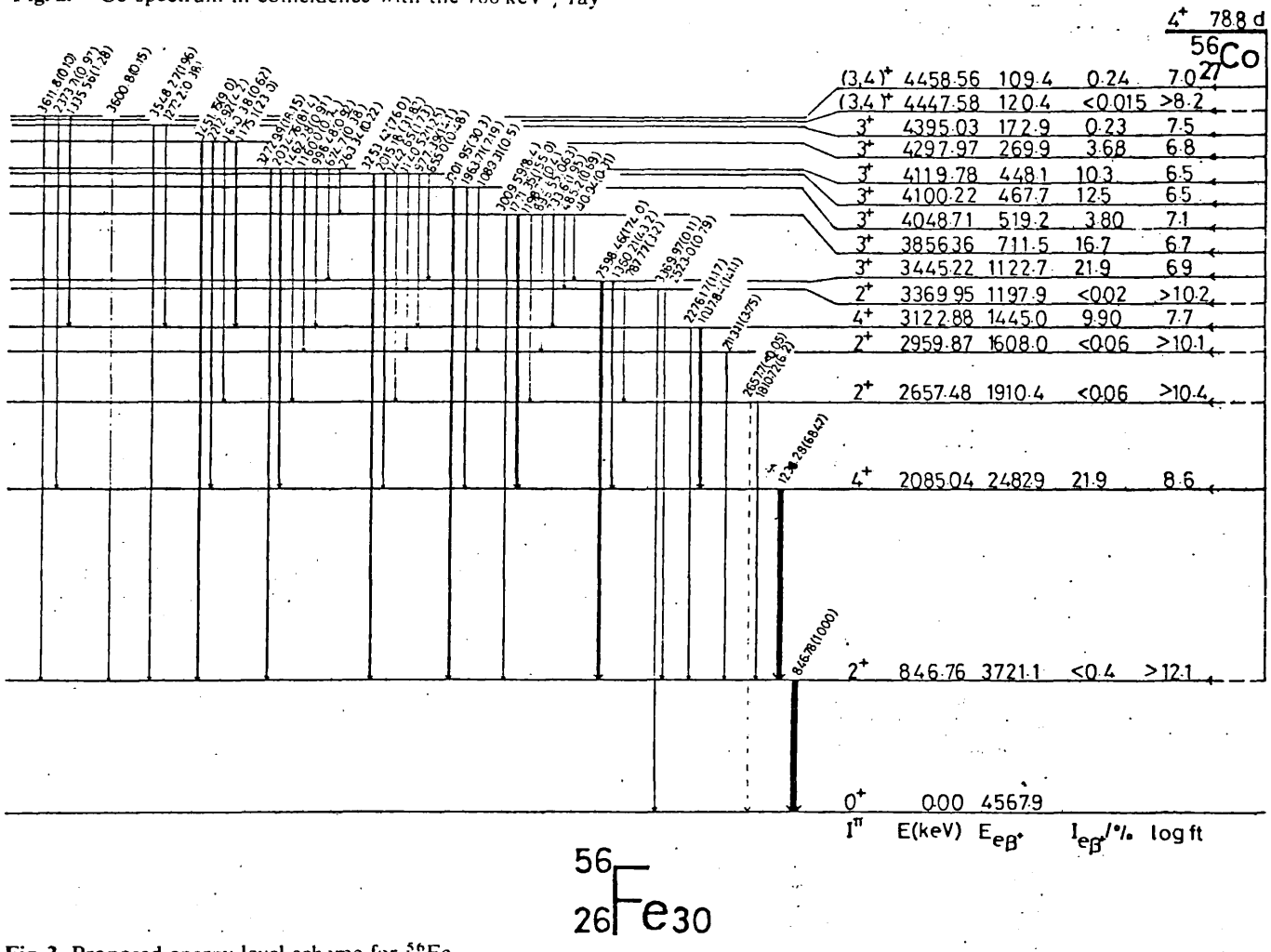

Fig. 3. Proposed energy level scheme for ^{56}Fe

Table 4. *K*-shell internal-conversion coefficients for ^{56}Fe transitions. (a) Comparison with theory. (b) Dependence on experimental *K*-electron intensities

E_γ (keV)	$I_i^\pi \to I_f^\pi$	Experimental $\alpha(K)\times10^4$	Theoretical $\alpha(K)$			Adopted Multipolarity
			*E*1	*E*2	*M*1	
733.6	$3^+\to4^+$	2.51 (54)	1.30	3.78	2.58	*M*1
787.77	$3^+\to2^+$	2.66 (26)	1.18	3.08	2.28	*M*1/*E*2
846.76	$2^+\to0^+$	2.6	1.22	2.60	1.97	*E*2
977.39	$3^+\to4^+$	1.39 (5)	0.81	1.88	1.45	*M*1
1,037.84	$4^+\to4^+$	1.33 (10)	0.72	1.66	1.30	*M*1
1,175.10	$3^+\to4^+$	0.94 (21)	0.57	1.22	0.99	*M*1
1,238.28	$4^+\to2^+$	1.012 (18)	0.518	1.048	0.915	*E*2
1,360.21	$3^+\to4^+$	0.764 (16)	0.445	0.902	0.768	*M*1
1,771.33	$3^+\to4^+$	0.472 (18)	0.270	0.480	0.460	*M*1/*E*2
1,963.71	$3^+\to4^+$	0.389 (17)	0.248	0.430	0.388	*M*1
2,015.18	$3^+\to4^+$	0.389 (20)	0.236	0.405	0.374	*M*1/*E*2
2,034.76	$3^+\to4^+$	0.372 (13)	0.232	0.400	0.370	*M*1
2,598.46	$3^+\to2^+$	0.260 (8)	0.168	0.264	0.248	*M*1/*E*2
3,009.60	$3^+\to2^+$	0.262 (72)	0.136	0.212	0.200	*M*1/*E*2
3,201.96	$3^+\to2^+$	0.209 (11)	0.127	0.189	0.183	*M*1/*E*2
3,253.42	$3^+\to2^+$	0.195 (9)	0.124	0.186	0.178	*M*1/*E*2
3,273.00	$3^+\to2^+$	0.191 (17)	0.122	0.181	0.176	*M*1/*E*2
3,451.15	$3^+\to2^+$	0.113 (20)	0.114	0.167	0.164	*E*1

E_γ (keV)	$\alpha(K)\times10^4$	
	I(*K*) from [21]	*I*(*K*) from [25]
2,598.46	0.260 (8)	0.260
3,009.60	0.262 (72)	0.174 (29)
3,201.96	0.209 (11)	0.206 (22)
3,253.42	0.195 (9)	0.186 (19)
3,273.00	0.191 (17)	0.185 (19)
3,451.15	0.113 (20)	0.143 (16)

spectra. Additional data taken using a Compton suppression spectrometer in a special investigation to look for this transition did not show any evidence at more than 10^{-5} relative to the intensity of the 846.76 keV line.

The 2,959.87 keV level ($\log ft = 10.1$) is established from the strong coincidence between the 846.76 keV γ-ray arising by a pure *E*2 transition from the first excited state to the ground state and the 2,113.11 keV γ-ray from this level to the first excited state. The $\log ft$ value suggests a spin parity assignment of 2^+.

The γ-ray observed at 1,037.85 keV suggests an *M*1 transition between the 3,122.88 keV level ($\log ft = 7.7$) and the second excited 4^+ state at 2,085.04 keV and provides a spin-parity assignment of either 4^+ or 3^+ for the former level, but the calculated $\log ft$ value clearly indicates a spin-parity of 4^+.

The 3,445.22 keV level ($\log ft = 6.9$) is established from the strong coincidence between the 846.76 keV γ-ray and the 2,598.54 keV γ-ray in an (*M*1/*E*2) transition. The 1,360.22 keV (*M*1) transition from this level to the 4^+ 2,085.04 keV level and the $\log ft$ value verify the established spin and parity assignment of 3^+.

The 3,856.36 keV level ($\log ft = 6.7$) is established from the coincidence between the 3,009.6 keV and the 846.7 keV γ-rays and from another coincidence between the 1,171.4 keV and 1,238.3 keV γ-rays. The γ-rays of 733.6, 1,772.5 and 3,009.6 keV from this level cause transitions to the levels at 3,122.8, 2,085 and 846.7 keV which appear to be *M*1 transitions so the spin parity assignment of the 3,856.36 keV level is taken to be 3^+.

The energy level at 4,100.22 keV ($\log ft$ 6.5) yields pure (*M*1) transitions of 977.5 keV and 3,253.63 keV to the 3,122.88 keV (4^+) and 846.8 keV (2^+) levels respectively, which suggests a spin parity assignment of 3^+.

The 4,297.97 keV level ($\log ft = 6.8$) gives rise to an apparent *E*1 γ-ray transition to the first excited state. This leads to a spin-parity assignment of 3^- which is in agreement with Pattersson et al. [21]. However, as is seen from Table 4b the work of Metskvarishvili et al. [25] leads to a different value for $\alpha(K)$, which indicates an (*M*1/*E*2) multipolarity, and suggests a spin parity assignment of 3^+. Also, the γ-ray transition of 1,175.1 keV from this level to the 3,122.88 keV (4^+) level appears to be a pure (*M*1) transition which leads to a spin-parity assignment of 3^+. We therefore suggest that a spin of 3 with an even parity is the most probable for the $\log ft$ value of 6.8.

Thanks are due to Dr. T.D. Macmahon, the Director, and staff at the University of London Reactor Centre for their assistance in making full use of the facilities there. Dr. N.M. Stewart wishes to acknowledge the provision of a grant from the Central Research Fund of the University of London. Mr. A.M. Shaban would like to thank the British Council for assistance from the Research Student Support Scheme. We are grateful to Professor Dobbs who, as Head of the Physics Department, provided additional funds and encouragement for this work.

References

1. Kerm, J.: Gamma-ray standards in charged-particle-induced radiative capture. pp. 345. Vienna: IAEA 1974
2. Camp, D., Gerald, ..: Nucl. Phys. A 166, 349 (1971)
3. Gehrke, R.J., Helmer, R.G., Greenwood, R.C.: Nucl. Instrum. Methods 147, 405 (1977)
4. Hautala, M., Anttila, A., Keinonem, J.: Nucl. Instrum. Methods 150, 599 (1978)
5. Taylor, H.W., Singh, B.: Nucl. Phys. A 172, 337 (1971)
6. Armitage, B.H., Ferguson, A.T.Q., Neilson, G.C.: Nucl. Phys. A 133, 241 (1969)
7. Agarwal, Y.K., Hofmann, S., Wien, K.: Nucl. Phys. A 176, 142 (1971)
8. Hofmann, S.: Z. Physik 270, 133 (1974)

9. Sher, A.H., Pate, B.D.: Nucl. Phys. A **112**, 85 (1968)
10. Sulaiman, M.J.: Ph.D. thesis, University of London, 1977
11. Camp, D.C.: Nucl. Phys. A **121**, 561 (1968)
12. Rautti, J.T., Prussin, S.G.: Nucl. Instrum. Methods **72**, 125 (1969)
13. The T.R.C. set is standard reference material available from the Radiochemical Centre, Amersham, Buckinghamshire, U.K.
14. Shaban, A.M., Stewart, N.M., Macmahon, T.D.: Nucl. Instrum. Methods **165**, 109 (1979)
15. Auble, R.L.: Nucl. Data Sheets **20**, 327 (1977)
16. Bunting, R.L., Kraushaar, J.J.: Nucl. Data Sheets **18**, 87 (1976)
17. Halbert, M.L.: Nucl. Data Sheets **24**, 175 (1978)
18. Scholzig, V., et al.: Int. J. Appl. Radiat. Isot. **28**, 503 (1977)
19. Greenwood, R.C., Helmer, R.G., Gehrke, R.J.: Nucl. Instrum. Methods **159**, 465 (1979)
20. Ewbank, W.B., Raman, S.: Nucl. Data B3, No. 4, 187 (1970)
21. Pettersson, H., Bergman, O., Bergman, C.: Arkiv Fysik **28**, 423 (1965)
22. Rose, M.E.: Internal Conversion Coefficient, pp. 4. Amsterdam: North-Holland Pub. 1958
23. Trusov, V.T.: Nucl. Data Tables **10**, 481 (1972)
24. Auble, R.L.: Nucl. Data Sheets **20**, 253 (1977)
25. Metskvarishvili, P.Y., Elizbarashvili, M.A.: 26th Soviet meeting on Nucl. Spectroscopy and Atomic Nucl. Structure, Baku. Academy of Science, U.S.S.R. Moscow, pp. 48 (1976)

N.M. Stewart
A.M. Shaban
Bedford College
University of London
Regent's Park
London NW1 4NS
England